Quantitative in vivo analysis of ligand-receptor interactions in the Wnt signalling network

Submitted by Michael Dawes

To the University of Exeter as a thesis for the degree of

Doctor of Philosophy in Biological Sciences

October 2023

This thesis is available for Library use on the understanding that it is copyright material and that no quotation from the thesis may be published without proper acknowledgement.

I certify that all material in this thesis which is not my own work has been identified and that any material that has previously been submitted and approved for the award of a degree by this or any other University has been acknowledged.

Abstract

The Wnt family of proteins are secreted glycoproteins with significant palmitoleate post-translation modification that renders each Wnt protein hydrophobic. Wnt proteins are a class of morphogens whose role is to be secreted and dispersed within the tissue to elicit a wide range of cellular responses based on the concentration of the ligand. However, as Wnt proteins are hydrophobic, standard diffusion through the aqueous extracellular environment is severely reduced. Indeed, alternative methods are required to aid dispersal and prevent aggregation. One such method involves active extension and protrusion of cell surface membrane by actin rich structures called cytonemes. These cytonemes have been characterised in the literature and several proteins are known to play an important role in their function and regulation. Indeed, Wnt protein over-expression and reception directly modulates cytoneme number, length and polarity of the cell to bias cytoneme direction in growth. However, to date, there has been no unbiased identification of the proteome surrounding cytoneme mediated Wnt handover. To address this, I developed a novel GFP-binding nanobody-directed biotin ligase system to extract and identify proteins specifically on cell surface membrane and cytoneme protrusions involved in the Wnt handover. I generated this assay from the ground up; exploring different cell cultures, biotin ligase constructs, methods of application and optimisations. This methods development was subject to a series of mass spectrometry analyses, which culminated in the identification of Caveolin1 as a protein hit to Wnt5a. Further protein hits were also suggested and investigated for possible co-localisation to Wnt5a, demonstrating the success of the assay. While further improvements are necessary, this thesis demonstrates the success of the novel nanobody-biotin ligase assay and its applicability to a wide range of proteins of interest.

Acknowledgments

I would like to thank my supervisor, Prof. Steffen Scholpp, for the invaluable tutoring, guidance and training during the course of this PhD, and the opportunity to work in his lab group. Steffen has always provided guidance and support at every opportunity while allowing me the independence to explore my scientific inspirations. It has been a pleasure to work under Steffen and with his lab, an experience I will hold dearly.

I also want to thank two very important colleagues who have both inspired and mentored me during my PhD. I want to thank Dr. Sally Rogers and Dr. Daniel Routledge. Together, I have been blessed with their warm encouragement and support during the highs and lows of a PhD. Dr Sally Rogers took me under her wing from start to finish of my PhD and Dr Daniel Routledge travelled the same journey with me and provided immense help in the editing of this thesis.

I want to thank the other members of the Scholpp lab equally, who each have provided encouragement and support throughout, both in technical and social help. Thank you to Dr. Lucy Brunt, Dr. Thomas Piers, Dr. Yosuke Ono, Dr. Agnieszka Kaczmar, Dr. Ashish Bhandari, Dr. Kelly Sanders, Gemma Sutton, Kevin Fang and Emma Cooper.

This work was supported by the SWBio BBSRC DTP and Leica Microsystems.

Table of Contents

List of Figures

List of Abbreviations

AGS – Primary gastric adenocarcinoma

APC – Adenomatous polyposis coli

AP2 – Clathrin adapter protein 2

ARP2/3 – Actin-related proteins 2/3

Cav1 – Caveolin 1

Cdc42 – Cell division control protein 42 homologue

CK1 – Casein kinase 1

Copb – Coatomer subunit beta

DAAM1 – Dishevelled associated activator of morphogenesis 1

DMSO – Dimethyl sulfoxide

Dvl – Dishevelled

ECM – Extracellular matrix

ER – endoplasmic reticulum

Evi/Wls – Evenness interrupted / Wntless

Flot1/2 – Flotillin-1/2

Fzd – Frizzled

GSK3 – Glycosylphosphatidylinositol

HEK – Human embryonic kidney

HeLa – Henrietta Lacks cervix epithelioid carcinoma

Hh – Hedgehog

HSPG – Heparan sulphate proteoglycan

IRSp53 – Insulin receptor tyrosine kinase substrate 53

JNK – C-jun N-terminal kinase

LC – Liquid chromatography

LDL – Low-density lipoproteins

Lef – Lymphoid enhancer factor

Lrp – Low-density lipoprotein receptor related protein

MBOAT – Membrane-bound O-acyl transferase

MEF – Mouse embryonic fibroblast

mRNA – messenger ribonucleic acid

MyoX – Myosin X

PAC2 – 24-h post-fertilization zebrafish embryo fibroplast

PCP – Planar cell polarity

PCR – Polymerase chain reaction

PFA – Paraformaldehyde

Porcn – Porcupine

Rho – Ras homologue gene family

Ror2 – Receptor tyrosine kinase-like orphan receptor 2

Ryk – Related to receptor tyrosine kinase

SCD – Stearoyl-CoA desaturase

sFRP – secreted frizzled-related protein

Shh – Sonic hedgehog

TCF – T-cell factor

Vangl2 – Vangl planar cell polarity protein 2

Wg – Wingless

Wnt – Wingless-intergrated

1. Introduction

1.1 Cell-to-cell communication

Intercellular signalling is a fundamental and essential aspect of all metazoan biology at all stages of life. Multicellular organisms must communicate at a paracrine level to achieve a multitude of tasks during development, tissue homeostasis and repair. These intercellular communications are facilitated through biomechanical, electrical or the precise spatiotemporal distribution of diffusive chemicals and/or peptides that elicit a specific response in recipient cells. Intercellular communication is a fundamental pillar of multicellular biology that these systems are extremely conserved across different species. Indeed, various pathological conditions, such as cancer and developmental disorders, result from disruptions in these communications. Cellular communication is required for each cell to understand its position, purpose, and function to generate a functional tissue (Ahmed & Xiang, 2011).

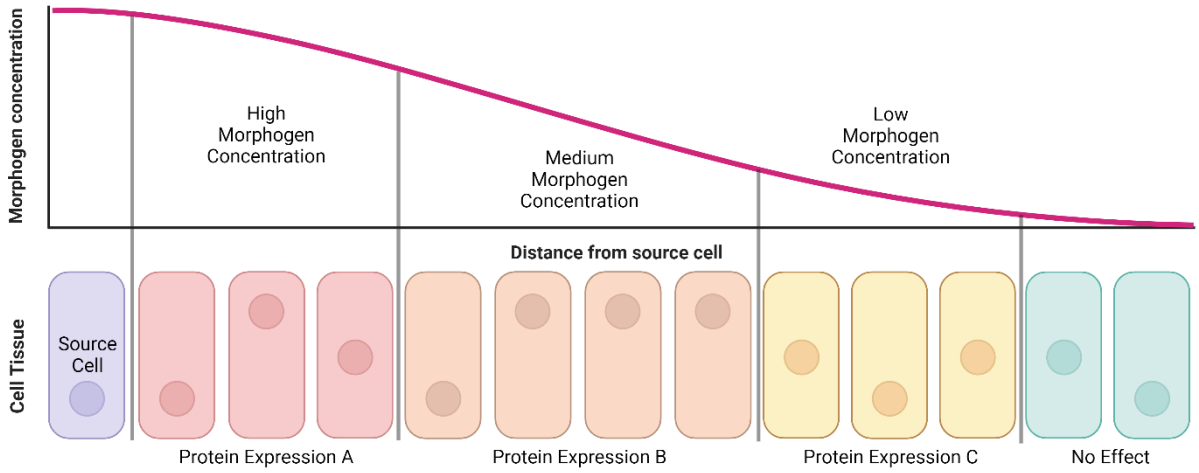

Figure 1. The Morphogen Gradient. *Cartoon representation of morphogen gradient across a tissue that causes unique protein expression in target cells depending on morphogen concentration. Created with BioRender.com.*

Furthermore, intercellular communication allows for the coordination of cellular differentiation and proliferation, ensuring the organised development of the organism. Many models of action allow a cell to communicate with its

neighbouring cells and/or tissues. These take the form of paracrine (distribution of signal peptide), juxtacrine (contact between cells), endocrine (long-range signalling via the bloodstream) and autocrine (self-signalling). Whilst many signalling molecules and peptides exist, one class is the family of form-giving molecules known as morphogens (Fig 1). Morphogens are secreted molecules that have differential effects on the target cells based on the cell type and the distance from the source cell as recipient cells respond to morphogens in a concentration-dependent manner (Sagner & Briscoe, 2017). Morphogens are signalling proteins which orchestrate tissue development during embryogenesis, regeneration and homeostasis. Tissue patterning is the functional goal of a morphogen gradient, as cells receive spatial awareness due to the concentration of a morphogen from a source cell. Cells within a tissue are likewise informed of their function and role due to morphogens. Many families of morphogens exist, such as the Wnt/Wingless, BMP/TGFβ, and Hedgehog families (Ayers et al., 2010). In this thesis, I will focus on and describe the family of Wnt proteins.

1.2 Wnt proteins and the Wnt signalling network

The Wnt signalling network is a highly conserved and diverse signalling pathway that elicits a wide range of cellular processes. These processes include but are not limited to cell survival, proliferation, differentiation, polarity and migration. To date, the Wnt gene family consist of 19 different human Wnt genes, which share 27-83% amino-acid sequence identity, each possessing a highly conserved 23 or 24 cysteine residues responsible for receptor binding (Miller, 2002). Humans and mice have 19 Wnt proteins, zebrafish up to 23 due to the teleost-specific whole-genome duplication (Duncan et al., 2015; Ruzicka et al., 2019), and *Drosophila* 7 (Wodarz & Nusse, 1998). Wnt proteins bind to a broad range of receptors such as Frizzled (Fzd), LRP5/6, Ror2, Ryk and Vangl, generating a unique cellular response (Routledge et al., 2022). Co-ligands such as R-spondins further potentiate the signal or even alter the signal outcome entirely. This enormous diversity of both Wnt ligands and their cognate receptors is responsible for the complexity of the Wnt signalling network. Although such a system has several redundant properties, disruption of the Wnt signalling pathway is responsible for conditions such as William's syndrome,

Congenital Hypothyroidism and various forms of cancer (Chiurillo, 2015; Flanagan et al., 2017; Zhan et al., 2017; Zhao et al., 2005). Such a diverse and crucial signalling pathway as Wnt has been the subject of extensive research for over 40 years.

1.3 Wnt protein expression and post translational modification

Wnt proteins are approximately 300-400 amino acids in length, each containing a highly conserved cysteine-rich residue located N-terminally and an N-terminal signal peptide responsible for secretion (Takada et al., 2006; Willert et al., 2003) (Fig 2.D+E). The first discovery of Wnt was in *Drosophila*, termed Wingless (Wg) by Nüsslein-Volhard, which, upon its knockout was observed to ablate wing development completely, hence the name (Nüsslein-Volhard & Wieschaus, 1980). The first homologue found in mammals being the Int1-like Wingless homologue (Wnt1), discovered by Roel Nusse, by infecting mice with mouse mammary tumor virus which identified the proto-oncogene that promoted cancer (Nusse et al., 1984). Finally, the first Wnt protein purified and analysed was the murine Wnt3a for its high secretion efficiency in cell culture (Willert et al., 2003). Upon translation, Wnt proteins are shuttled to the endoplasmic reticulum (ER) for post-transcriptional modification, namely glycosylation and fatty acylation (Hausmann et al., 2007; Takada et al., 2006; Willert et al., 2003). This translocation to the ER results in cleavage of the N-terminal signal sequence. The lipid modification (C16:1Δ9), a palmitoleate, is linked to a conserved serine on the Wnt protein via an oxyester bond. In murine Wnt3a, this is serine 209 (Takada et al., 2006) (Fig 2.D). The enzyme responsible for this acylation is Porcupine (PORCN), which facilitates this process (Hofmann, 2000; Willert et al., 2003; Zhai et al., 2004). PORCN is a member of the membrane-bound O-acyl transferase (MBOAT) family, and it palmitoleates Wnt in two steps. The first step generates a monosaturated fatty acid from a different protein, stearoyl-CoA desaturase (SCD), to be used as a substrate for PORCN. SCD generates a cis-double bond at position 9 in palmitoyl-CoA and stearoyl-CoA to generate ‘kinked’ monounsaturated fatty acyl-CoA. However, this process does not generate monounsaturated fatty acyl-CoA at a fixed length, and PORCN is biased to using monounsaturated fatty acyl-CoA with a length shorter than, but not longer than, 16 carbons. PORCN

links this cis-Δ9-monounsaturated fatty acyl-CoA to the conserved serine on all Wnts. This renders the Wnt protein highly hydrophobic but otherwise necessary for binding to transport proteins for secretion (Rios-Esteves & Resh, 2013; Takada et al., 2006). A second palmitate-based modification of Wnt is performed on a separate yet equally conserved cysteine residue, cysteine 77 on murine Wnt3a (Willert et al., 2003) (Fig 2.D). Unlike palmitoylation of serine 209, which is necessary for export from the ER, palmitoylation of cysteine 77 is necessary for β-catenin activation by recognising cognate cell surface receptors (Fig 2.D). Wnts are further modified by adding glycosylation groups, which may be necessary for an appropriate exocytic route (Komekado et al., 2007; Tanaka et al., 2002). Glycosylation of Wnts is less well understood; however, it is interpreted that glycosylation of Wnt precedes palmitoleation and that interruption of glycosylation significantly impedes Wnt's ability to both secrete and signal through the Wnt signalling pathway (Hausmann et al., 2007).

Once the mature Wnt protein has been modified, it is rendered severely hydrophobic, requiring multiple unique modes of transport to prevent aggregation and aid the mobility of the protein. Post-modified Wnts are transported to the Golgi apparatus, where they encounter the Wnt chaperone protein Wntless (Wls). Otherwise known as Evenness Interrupted (Evi) in Drosophila (Hausmann et al., 2007), Wls is crucial to the secretion of Wnt. Wls is a multi-pass transmembrane protein (debated to contain 4 to 8 transmembrane regions (Wolf & Boutros, 2023)) that is localised to the Golgi apparatus where it binds to and packages Wnt into vesicles for transport to the cell surface membrane. Wls binds to the lipid moiety of Wnt, and the two are transported by protein complex-II (Cop2) assembled vesicles for export from the ER (Sun et al., 2017). A single-pass transmembrane protein TMEM132A is recruited *en route*, which binds to and supports the Wnt/Wls complex (Li & Niswander, 2020). In *Drosophila*, additional transport proteins such as p24 cargo proteins Emp24, Eclair, Baiser, CHOp24 and Opossum are also required for Wg secretion, either for different contexts or in replacement to Evi (Buechling et al., 2011; X. Li et al., 2015; Port et al., 2011). Such an example is the cargo adaptor Opossum, which transports translated Wg from the ER to Golgi but no further. Indeed, the human orthologue of opossum 'TMED3' has also been shown to regulate human Wnt3a signalling (Duquet et al., 2014).

Once Wnt/Wls reaches the cell surface membrane, Wnt is released, and Wls is re-endocytosed (Nygaard et al., 2021). How Wnt and Wls dissociate is still under investigation, however, its transfer is thought to be Wls protein conformational change dependant (Nygaard et al., 2021). There remain several modes of transport of Wnt beyond the plasma cell surface membrane, and so its release from Wls is far from understood. Once Wnt is secreted, Wls is re-endocytosed and destined for either re-cycling back to the Golgi apparatus to repeat the process or sent to lysosomes for degradation (Yu et al., 2014). The conserved endocytosis motif on Wls is recognised by Clathrin adapter protein 2 (AP2) on the cell surface membrane, which triggers a Clathrin-mediated internalisation (Gasnereau et al., 2011). The early endosome containing Wls is thought to be deterred from lysosomal degradation by the involvement of the retromer complex VPS26/VPS29/VPS35, which sorts Wls into recycling endosomes that eventually fuse to the Golgi apparatus (Yang et al., 2008).

1.4 Wnt protein signal transduction

Once secreted, Wnt ligands are spread through the tissue in a radius from the source cell(s) (Fig 1) (Sagner & Briscoe, 2017). As the range increases, the concentration of Wnt ligands decreases. Characteristically of morphogens, the concentration of Wnt on the receiving cell can cause completely different Wnt target gene expression. However, more than just concentration regulates the resulting Wnt target genes expressed. Indeed, Wnt peptides activate various signalling pathways, the best characterised being the canonical Wnt pathway. This pathway involves stabilising and retaining of free intracellular β-catenin upon Wnt binding to a cell surface receptor-like Fzd. Within the nucleus, β-catenin is a transcription factor that binds with the T-cell factor (TCF)/lymphocyte enhancer factor (LEF) family of transcription factors to promote transcription of canonical Wnt target genes (MacDonald et al., 2009). Levels of nuclear and cytosolic β-catenin are tightly controlled by the β-catenin destruction complex, a cluster of proteins consisting of Axin, adenomatosis polyposis coli (APC), protein phosphatase 2A (PP2A), glycogen synthase kinase 3 (GSK3) and casein kinase 1α (CK1α) (Komiya & Habas, 2008). This constitutively active complex labels free intracellular β-catenin by phosphorylation from CK1α and GSK3 for degradation (Fig 2.A). ‘Canonical’

Wnt ligands such as Wnt1, Wnt3, Wnt3a, Wnt8a, Wnt8b and Wnt10 (Ackers & Malgor, 2018) bind to receptors such as Fzd and co-receptors LRP5/6 which leads to the recruitment of cytoplasmic phosphoprotein Dishevelled (Dsh, Dvl in mammals). Active Dvl inactivates the β-catenin destruction complex by recruitment of Axin, APC and CK1α, preventing phosphorylation of β-catenin. The increased levels of β-catenin result in nuclear import, where β-catenin binds to and activates TCF/LEF transcription factor families (Fig 2.B) (Clevers & Nusse, 2012). These genes mainly promote cell survival and growth, expressing genes such as Cyclin D1 and c-myc, but also genes responsible for inhibiting 'canonical' Wnt signalling such as Axin2 (Lecarpentier et al., 2019).

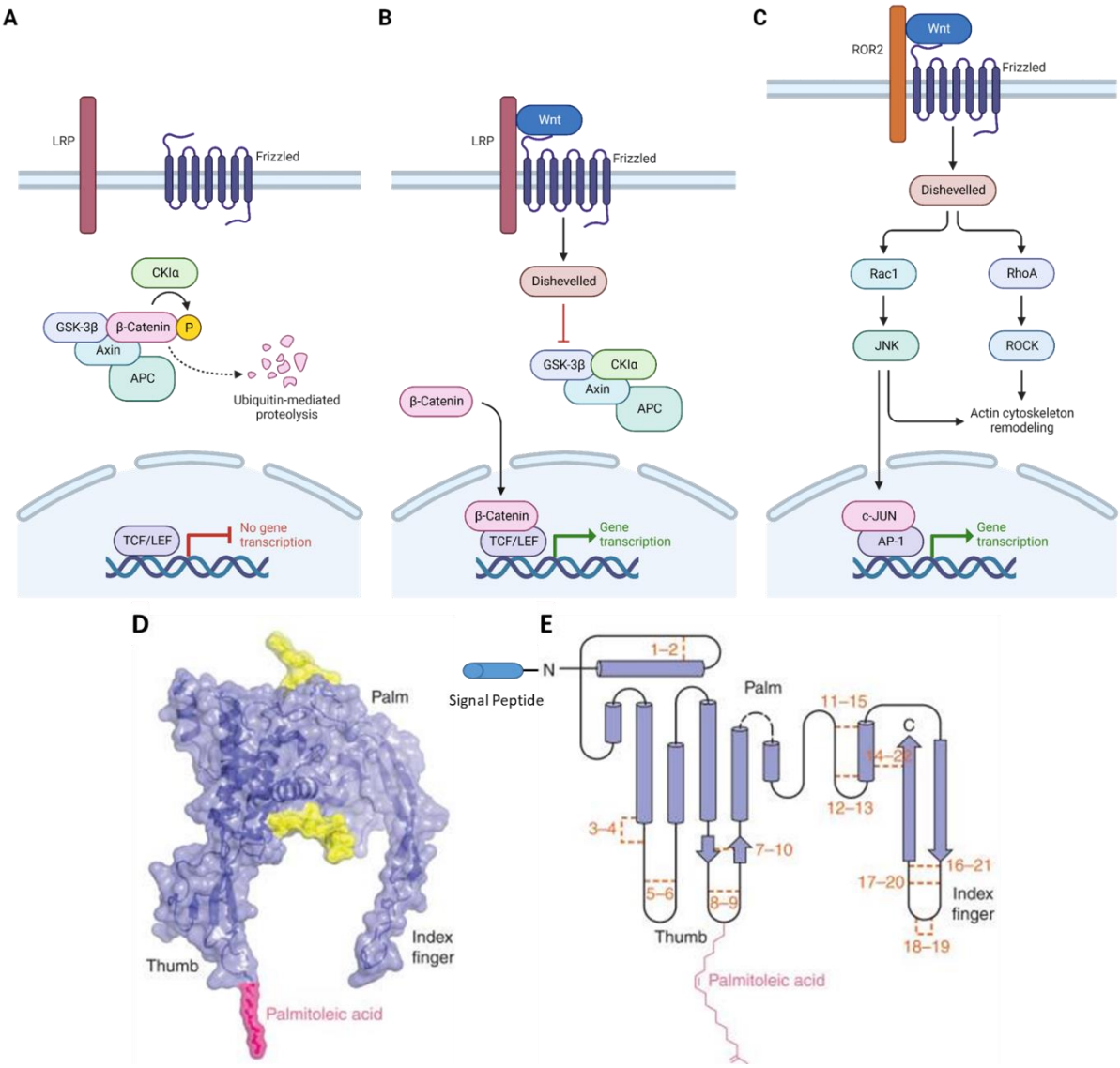

Figure 2. Canonical vs Non-Canonical Wnt Signalling Pathway. *(A-C) Cartoon representation of the Wnt signalling pathway. (A) Inactive canonical*

Wnt signalling due to β-catenin degradation. (B) Active canonical Wnt signalling due to stabilisation and retention of β-catenin. (C) Active non-canonical Wnt signalling through Rac1 and RhoA activation. Created with BioRender.com using pre-made template. (D) Cartoon of Xenopus Wnt8 crystal structure with Frizzled CRD domain removed. Palmitoleic acid (pink) and glycosylation (yellow) residues highlighted. (E) Secondary structure of Xenopus Wnt8 highlighting conserved 22 cysteine residues (orange) and palmitoleic acid residue. Figure adapted from (Willert & Nusse, 2012) 'Wnt Proteins', 2012.

Alternative Wnt signalling occurs independently of β-catenin in a pathway termed 'non-canonical' or Wnt/PCP signalling pathway. The β-catenin independent pathway comprises two separate signalling networks that could be categorized in a Calcium-dependent or a Calcium-independent branch (Komiya & Habas, 2008). Typically, non-canonical Wnt proteins comprise of ligands Wnt4, Wnt5a, Wnt5b, Wnt6, Wnt7a, Wnt7b and Wnt11; however, there are instances where these ligands can promote canonical signalling, such as Wnt7a (Ackers & Malgor, 2018). These ligands are capable of binding to Fzd receptors similarly to canonical Wnts, but compete with the canonical pathway and inhibit intracellular β-catenin accumulation in favour of a PCP phenotype. Indeed, canonical and non-canonical bias is defined by the co-receptors associating to Wnt-Fzd complexes, such as Ror1, Ror2, Ryk and Vangl2 (Ackers & Malgor, 2018). The Calcium dependant non-canonical Wnt pathway stimulates the generation of inositol trisphosphate (IP3) and diacyl glycerol (DAG) through the activation of phospholipase C following Wnt binding. This subsequently promotes intracellular Calcium release via IP3 and activation of protein kinase C (PKC) via DAG release (De, 2011). Alternatively, the non-canonical Wnt pathway can occur through the activation of the planar cell polarity (PCP) pathway, a calcium independent pathway, which recruits and activates the Rac/JNK signalling cascade and DAAM1/Rho GTPase family of proteins which are both essential in actin cytoskeletal modification (Fig 2.C) (Yang & Mlodzik, 2015). The PCP pathway is highly important in cellular polarity, mobility and adhesion among others that are critical in both development and homeostasis. Indeed, neural tube defects such as spina bifida affect 1 in 2,500 births within the US every year because of abnormalities within the PCP pathway (Williams

et al., 2005). Despite this, non-canonical Wnt signalling is less characterised than its canonical counterpart within the literature but has an ever increasing importance in many aspects of animal biology.

1.5 Mechanisms of Wnt transport

Wnt proteins have various levels of regulation that ensure strict control of their expression for appropriate signalling. As mentioned previously, Wnts are heavily post-translationally modified with glycosylation and palmitoleation. These are to ensure both intra/intercellular transport and cellular recognition as a morphogen in receiving cells (Galli et al., 2007). This palmitoyl residue renders the Wnt protein hydrophobic, preventing diffusion of the protein through an aqueous medium. However, Wnt ligands generate morphogen gradients *in vivo*, thus they are transported despite this. To circumvent this issue, cells have been observed to transport Wnt through four methods: protein assisted (Hoang et al., 1996), vesicular (Korkut et al., 2009), lateral diffusion (Farin et al., 2016) and membrane protrusion (Stanganello et al., 2015). Many chaperone proteins exist to shield the lipid moiety of Wnt from the hydrophilic extracellular environment to allow free diffusion. These include secreted Frizzled-related protein (sFRP), Wnt inhibitory factor (WIF), Afamin and glypican family of proteins (Baeg et al., 2001; Hoang et al., 1996; Hsieh et al., 1999; Mihara et al., 2016). Many secreted Wnt binding proteins act in an antagonist fashion, for example, sFRP1-3 or WIF1 that bind to and prevent Wnt binding to Fzd and LRP5/6 (Kawano & Kypta, 2003). However, for sFRP's this is highly debated, as in certain context and concentrations it can act to augment Wnt signalling instead (Houart et al., 2002; Üren et al., 2000; Xavier et al., 2014). Indeed in Drosophila, the secreted Wg interacting molecule (Swim), or in *Xenopus* embryos, sFRPs, have been shown to improve Wg and Wnt8/Wnt11 diffusion respectively by enhancing solubility (Mii & Taira, 2009; Mulligan et al., 2012). Vesicles are another form of Wnt transport observed to be necessary for certain contexts of Wnt signalling. Wnt3a associates to lipoproteins in the media of *in vitro* mouse fibroblasts, the importance of which is highlighted by an ablation of Wnt3a presence in the media when lipoproteins are silenced (Neumann et al., 2009). However, Wnt does not always require secretion into the extracellular matrix to activate the Wnt pathway in receiving cells. Indeed, intestinal

organoids with non-diffusible Wnt3 demonstrated canonical Wnt activation through Frizzled-bound Wnt3 migration from one cell membrane to another (Farin et al., 2016).

The final known method of Wnt transport requires an intentional and active form of transport by the extension of the cell surface membrane to physically contact neighbouring cells and deposit Wnt (Fig 3). These membrane protrusions are filopodia and are actin-stabilized structures typically associated with various cellular phenotypes such as environmental sensing and migration (Mattila & Lappalainen, 2008). Specialised filopodia, known as cytonemes, have been observed to contain packages of morphogens such as Wnt to facilitate cell-cell communication (Mattes & Scholpp, 2018; Stanganello et al., 2015). Thomas B Kornberg first discovered Cytonemes in the imaginal wing disc of drosophila in 1999 (Ramírez-Weber & Kornberg, 1999). In this paper, long thin cellular protrusions were observed growing in the direction of a Fibroblast Growth Factor (FGF) source and were speculated to be responsible for distributing morphogens within the imaginal disc. Since the publishing of this paper, cytonemes have demonstrated to be responsible for shuttling of a wide range of signalling proteins such as Notch, Spi/EGF, Branchless (Bnl)/FGF, Dpp/BMP, Wg/WNT, and hedgehog (Hh)/ Sonic (S)hh (Casas-Tintó & Portela, 2019). Indeed, cytonemes are crucial in the delivery of certain Wnts in zebrafish and Dpp in the Drosophila wing disc (Mattes & Scholpp, 2018; Stanganello et al., 2015). Cytonemes demonstrate both delivery of and receiving of signals from neighbouring cells. For instance, Hh signal requires the protrusion of both receiving and sending cells to contact halfway and handover Hh ligands (Kornberg & Roy, 2014), whereas the majority of Wnt cytonemes appear on producing cells (Stanganello et al., 2015).

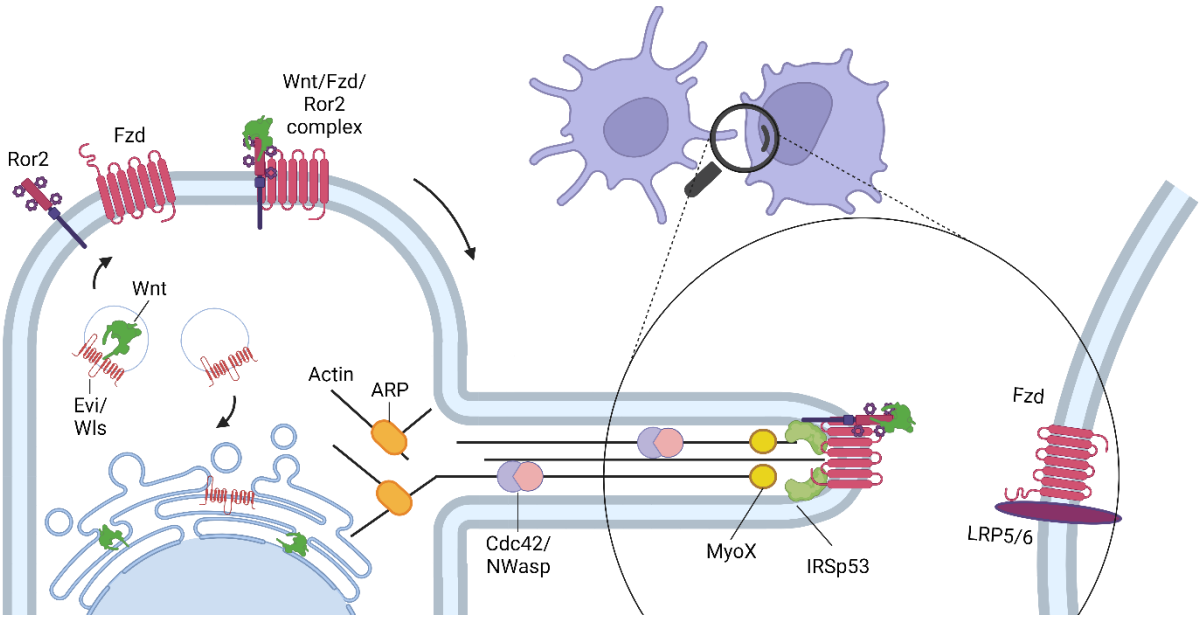

Figure 3. Cytoneme Mediated Wnt Handover. *Cartoon representation of the cytoneme mediated process of Wnt handover to recipient cell. Wnt with post-translational palmitoleated modification is bound by Evi/Wls in the Golgi to be transported to cell surface membrane where it is shuttled to cytoneme tips. Created with BioRender.com.*

Cytonemes are actin rich structures that host a plethora of cytoskeletal related proteins critical for all forms of membrane protrusions such as lamellipodia and filopodia (Mattila & Lappalainen, 2008). Much like filopodia, cytonemes are generated via the outgrowth of the lamellipodia actin network through the convergence of uncapped or formin-nucleated actin filament barbed ends (Yang et al., 2007). ARP2/3 proteins generate an outgrowth of novel actin filaments following activation of CDC42. This leads to ENA/VASP and Dia2 mediated elongation of the actin barbed ends which drives the protrusion of the actin cytoskeleton (Krause et al., 2003). This protrusion generates tension on the cell surface membrane, distorting the membrane by generating a curvature that the nascent filopodia elongates from. The insulin-receptor substrate p53 (IRSp53) is an inverse BAR domain-containing protein that functions as a membrane attached scaffold and has been observed to directly affect the frequency and length of filopodia (Yamagishi et al., 2004). IRSp53 might further enhance the outward curvature of the surface membrane to aid the actin filament elongation and/or may sense the deformation of the membrane and recruit various filopodia related components (Yamagishi et al., 2004). As the membrane

filopodia extends, unconventional myosin protein 10 (MyoX) shuttles various filopodial related proteins to the elongating tips, stabilising the protrusion (Berg & Cheney, 2002). As with typical filopodia, cytonemes appear to follow the same process. Indeed, in zebrafish embryos, all cytoskeletal proteins mentioned are observed in Wnt bearing cytonemes (Stanganello et al., 2015).

Cytonemes can contain unique markers that are not present on standard filopodia. Specifically, these protein markers are morphogen specific, with accumulations of signal receptors Tkv, Breathless (Btl), Patched (Ptc), and Fibroblast Growth Factor Receptor (FGFR) in drosophila (Casas-Tintó & Portela, 2019). Wnt related proteins are also localised to the tip of cytonemes, such as Evi/Wls, Fzd and LRP5/6 (Stanganello et al., 2015; Stanganello & Scholpp, 2016). Indeed, the unique proteome on cytonemes can be broad yet specialised. An example is the different cytonemes present in specific locations of the drosophila imaginal disc. In the apical side, cytonemes will contain components of Dpp pathway (Tkv), the basal side will contain components of Hh pathway (Hh, Shf/DmWif, Dally, Dlp, Disp, Ihog, and Ptc) and the air sac primordium (ASP) produce cytonemes displaying Btl or Tkv but never both (Casas-Tintó & Portela, 2019). This demonstrates how cytonemes are specialised from typical filopodia, as they possess machinery unique to and necessary for the specific signalling pathway they intend to transmit.

Observed in developing zebrafish embryos, the directionality and length of these cytonemes is biased towards particular poles which accounts for the Wnt signalling gradient. It has been implied that this bias in Wnt gradient generated by cytonemes is critical in coordinating appropriate tissue patterning during this phase (Stanganello et al., 2015). Furthermore, there is evidence that suggests that the other listed methods of Wnt transport are not essential for gradient formation (Beckett et al., 2013). Wnt8a is loaded on these cytoneme tips where it contacts neighbouring cells, facilitating Lrp6/Fzd receptor clustering into the Lrp6 signalosome to stimulate canonical Wnt signalling (Bilić et al., 2007; Gammons et al., 2016). Recent papers highlight how modulating the Wnt pathway directly alters cytoneme number and length (Brunt et al., 2021; Mattes & Scholpp, 2018; Routledge et al., 2022; Stanganello et al., 2015). Clearly, Wnt signalling and cytoneme development are closely intertwined, the most likely candidate for facilitating this relationship being the Wnt PCP-pathway. The PCP

pathway has been well characterised for its pro-migratory effects via activation of either calcium mediated PKC or JNK mediated stimulation of CDC42 (Yang & Mlodzik, 2015). Concurrently, expression levels of key PCP pathway proteins such as Ror2 or Wnt8a directly alter the number and length of filopodia within the source cells (Mattes et al., 2018). However, whilst activation of Ror2 dependant PCP on the receiving cell has been well characterised, the source cell's Wnt8a dependant cytoneme coordination is still not well understood. Wnt, along with associated proteins such as Evi/Wntless, cluster at regions of the cell surface membrane, which later initiate cytonemes (Stanganello et al., 2015). It is unknown the principle signalling cascade responsible for the initiation and transport of Wnt along cytonemes.

1.6 The cytoneme question

Various evidence based mechanisms tie in the PCP pathway to cytoneme development and coordination; however, there is no comprehensive isolation and investigation into the full proteome at work at all stages of cytoneme development. Cytonemes are highly transient structures that develop and transfer Wnt typically in under 10 minutes (Stanganello et al., 2015). Cytonemes are also thin, fragile structures, averaging 1.5 µM wide and 10 µM long (Stanganello et al., 2015). These factors have long presented the field with difficulty observing and isolating cytonemes for component analysis. For example, the fixation of these delicate structures is only possible by using specialised additives such as glutaraldehyde to preserve their fragile appearance (Hall & Ogden, 2018; Rogers & Scholpp, 2020). Therefore, the proteome of these structures is unknown.

Despite this, attempts have been made to investigate filopodial-like structures. Zakaria Ezzoukhry *et al.* isolated filopodia from migratory normal and cancer cells called invadosomes (Ezzoukhry et al., 2018). Invadosomes were isolated using laser microdissection combined with protein isolation and analysis through mass spectrometry. However, a problem persisted with a small protein fraction isolated (too small to measure total protein concentration), which was resolved by using automated identification and harvest via software image analysis. This technique identified the presence of a host of unique proteomes

along the invadosome tips, including translational-related proteins like eEF2 and eEF1A which, upon depletion using siRNA screens resulted in a reduction of invadasome formation. Another group, Yutaka Furutani *et al.*, used a different approach to address the lack of material by forcing filopodial outgrowth in neuronal dendrites by exploiting the specific and high-affinity binding between dendritic filopodial membrane protein, telencephalin, and its extracellular matrix ligand, vitronectin (Furutani & Yoshihara, 2018). Using vitronectin-coated beads, the team could force dendritic filopodial outgrowth around these beads, which were then isolated. This technique successfully identified 319 proteins through mass spectrometry analysis, including several proteins known to be enriched in the filopodia. However, as the protein fraction was increased, it could be argued that the artificial outgrowth would bias the data and disproportionally misrepresent a physiological filopodia proteome. Various alternative approaches to investigating the filopodial proteome were explored through focal adhesion points (Horton et al., 2015; Kuo et al., 2011; Schiller et al., 2011) or differential cell lysis/subcellular fractionation (Attanasio et al., 2011; Cervero et al., 2012; Havrylov & Park, 2015). These proteomic screens on filopodia have shown much success; however, this has not been applied to specialised filopodia for cell-cell signalling, let alone cytonemes. Applying a filopodia enrichment screen for morphogen signalling such as Wnt presents the field with a void of knowledge in the full breadth of molecular entities at work.

A new assay must be produced to truly dive into the mechanisms that tie cytonemes and the Wnt signalling proteome together. Investigating protein markers individually for possible localisation to cytonemes lacks high throughput and risks missing entire sub-proteomes that link the system as a whole due to bias. To assess the proteome of the Wnt-positive cytoneme, three assay conditions must be satisfied. The first condition is to ensure the specificity of the assay – that is, to remove unnecessary proteins identified due to confounding factors such as Wnt-related but not cytoneme specific. The second is to generate an unbiased list that can identify all proteins involved in cytoneme-mediated Wnt transfer, so proteins that would otherwise be discounted are accounted for. For example, even in the most unlikely case, a histone protein played a small but important role. Finally, an assay that can accurately identify proteins even at minimal concentrations.

1.7 Nanobodies are a way to address the first question

1.7.1 The history of protein binders

To address the first condition needed for our future assay, we require a method of explicitly targeting mature Wnt proteins at the stage of cell surface membrane/cytoneme presentation. This requires a technique that does not rely on the expression of the morphogen in question, as that will encompass all aspects of that morphogen. Instead, we need a tool that can localise to the Wnt protein or become active at the correct time and space. The latter could involve an inducible system such as a ligand activatable system. However, without controlling the activatable activity in specific compartments, we would not solve the pan screening aspect. Perhaps a system with a membrane impermeable ligand, such as the Pierce™ Cell Surface Biotinylation and Isolation Kit, for a biotin ligase system to biotinylate and extract only cell surface proteins (Karhemo et al., 2012). As elegant as this kit would appear, it would still lack the intracellular fraction of cytonemes and or the Wnt signalosome necessary for linking cytoneme behaviour to Wnt signalling pathway. Indeed, it appears the former prospect is more likely. We would require a vehicle to localise our identification system to the Wnt protein once it has reached the cell surface membrane to stay with the Wnt ligand and follow its journey to connect Wnt signalling to cytoneme behaviour. Several systems exist that can perform this task such as protein chimeras. However, the class of protein binders fits this role perfectly. Protein binders are synthetic tools developed to address the experimental desire to artificially localise one protein to another in living systems (Aguilar et al., 2019). Protein binders take on many forms, from Design Ankyrin Repeat Proteins (DARPins) to single-chain variable fragments (scFv), Affibodies, Monobodies and nanobodies. Protein binders are the natural evolution in the field from classical immunoglobin based experiments that have provided invaluable tools such as immunofluorescence, immunohistochemistry, immunoprecipitation among many more. Monoclonal or polyclonal antibodies have provided the basis for an extensively wide field of applications that have revolutionised lab research. Fundamentally, these techniques exploit the specific protein epitope affinity that antibodies express to allow localisation/binding to a protein of interest (POI). When applied in extracellular or *in vitro* conditions, antibodies are effective tools. However, production of

these antibodies for the individual researcher is highly limiting. Indeed, generating antibodies from living systems is notoriously difficult; therefore, the vast majority of antibodies used in research are purchased commercially. Full-length, multi domain antibodies require specific conditions to mature properly, along with crucial inter- and intramolecular disulphide bridges that cannot form in the cytoplasm (Helma et al., 2015). This paired with their instability in the intracellular environment and extremely large size highly limits antibody usefulness in functional studies of cultured cells or *in vivo* systems (Aguilar et al., 2019). This drove the desire to 'break down' antibodies into their constitutive parts, producing the functional fragment antigen-binding (Fab) (~50 kD), scFv (~25 kD), and single, variable domain VH or VL fragments (Chothia et al., 1985). However, replacing disulphide bridges with noncovalent inter-domain interactions, along with exposed hydrophobic residues reduced thermodynamic stability and protein solubility of these early designs (Wörn & Plückthun, 2001).

1.7.2 The very small antibodies: the Nanobodies

In 1993, Hamers *et al* discovered the first single domain heavy chain antibodies (hcAbs) from the camelid family (Hamers-Casterman et al., 1993). These functional antigen-binding antibodies were immensely smaller than typical antibodies (~13–14 kD compared to ~150 kD) which increased stability and expression. Moreover, several properties of these hcAbs were more favourable for biotechnological applications such as substitution of hydrophobic to hydrophilic residues, increased overall stability and the ability for functional expression in eukaryotic hosts (Harmsen et al., 2000; Muyldermans et al., 1994; Rothbauer et al., 2006; Vu et al., 1997). Since this discovery, a wide range of protein binders, both immunoglobulin and non-immunoglobulin based, were developed to better serve the functional aspects of typical antibodies in living systems for functional analysis. Non-immunoglobin protein binders, such as Affibodies, Monobodies and Darpins serve as an alternative to immunoglobulin-based proteins with unique traits that make them more suitable in certain experimental contexts. For example, Affibodies are a class of affinity protein based off the immunoglobulin binding protein A from *Staphylococcus aureus*. Affibodies have more limited use due to the relative lack of target-specific binding from random mutagenesis, however, when applicable, can excel due to

their extremely small size of ~6.5 kD (Nord et al., 1997). Monobodies utilise natural protein fold of 10 kD fibronectin protein which, unlike immunoglobulins, do not require a disulphide bond for stabilisation which allows high stability in reducing environments within the cell (Gross et al., 2013; Koide et al., 1998). Darpins are unique from the list of non-immunoglobulin based protein binders as they are not restricted in epitope specificity because of their natural protein fold template. Darpins are based on the ankyrin fold which forms protein-protein interactions (Li et al., 2006). As ankyrin folds consist of β-sheets with antiparallel α-helices, Darpins form concave binding shapes that bind especially well to large conformational epitopes as opposed to the small peptide string epitopes most protein binders prefer (Parizek et al., 2012). All of these non-immunoglobulin proteins share a significantly reduced size and enhanced stability that makes them superior to large, unstable antibodies in cell culture or *in vivo*.

1.7.3 Nanobodies in research

Nanobodies are single heavy chain immunoglobulin units isolated from camelids, which are referred to as VHH (from variable domain of heavy chain antibodies) (Aguilar et al., 2019). Over the past 30 years, nanobodies have been developed and utilised in an extremely wide variety of experiments. From localisation, to POI degradation, translocation, trapping, post translation modifications, scaffolding and cell-cell contact reporters, nanobodies have dramatically advanced the functional and practical applications of epitope affinity-based tools (Aguilar et al., 2019). The greatest strength nanobodies provide when compared to traditional antibodies or non-immunoglobulin based protein binders is its small size, high stability, fast expression time, good solubility, functionality within living systems and comparatively broad range of epitopes partners. Nanobodies boast both a small size and high epitope binding affinity to commonly used tags, allowing for the localisation of various functional tools to POI in live systems (Aguilar et al., 2019). One such tool is the localisation of E3 ubiquitin ligase complex fused to a nanobody to the POI, which in turn marked the POI for degradation and removal by proteasome (Kuo et al., 2011). deGradFP is a nanobody fused to this E3 ubiquitin ligase complex and used in drosophila embryos and larvae to remove GFP-tagged POI (N-

terminal F-box domain of the drosophila Slmb) without the need for genetic or mRNA level of control (Caussinus & Affolter, 2016). Nanobodies have been used for relocalisation of POI by employing the same principles. The GrabFP nanobody system was developed to trap and relocalise GFP tagged POI to defined regions along the apico-basal axis of epithelial cells in drosophila (Harmansa et al., 2017). Indeed, Harmansa *et al* also used the GrapFP system to track Dpp/Bone morphogenetic protein 2/4 diffusion in drosophila imaginal wing disc basolateral compartment (Harmansa et al., 2017). Similarly, GrabFP was used by Ressurreição *et al.* to better understand the role of Dsh in maintaining cell polarity in epithelial tissue of drosophila by relocating EGFP-tagged Dsh to the mitochondria from the cell surface via the Tom70 mitochondrial translocation signal VHH nanobody (Ressurreição et al., 2018). They found that GrabFP sequestered Dsh with extremely high efficiency that led to a loss of Prickle polarity, which resulted in Prickle inhibiting Dsh polarity in neighbouring cells, triggering a cascade loss of polarity within the tissue. Nanobodies have also been used for trapping of POIs, especially morphogens who's diffusion across the tissue is essential for tissue patterning. Morphotrap is a cell surface membrane bound GFP-binding nanobody that has been used to trap Dpp/Bmp2 in drosophila imaginal discs, Wnt in *C. elegans* and Nodal family of proteins in zebrafish with great success (Almuedo-Castillo et al., 2018; Harmansa et al., 2015; Pani & Goldstein, 2018). Indeed, these morphotrap experiments all definitively demonstrated the role of these morphogens without genomic, small molecule inhibition or mRNA alterations to *in vivo* samples. Instead, with the use of inducible trapping of these morphogens, these papers clearly defined the spread and effect of these morphogens directly. Lastly, nanobodies have been implemented in control of post-translational modifications of POI, albeit less thoroughly implemented; this use of nanobodies goes to show the high potential for nanobodies as a toolset. Indeed, *Roubinet et al* was able to fuse a constitutively active minimal kinase domain of Rho kinase to a GFP-binding nanobody ($Rock^{CA}$-VhhGFP4) generate phosphorylation of myosin light chain in drosophila neuroblasts (Roubinet et al., 2017). The results of which caused an ectopic accumulation in the apical cytoplasmic compartment, suggesting that perturbing Myosin clearing during anaphase compromises the correct physical asymmetry of the cell and unequal cortical expansion.

1.7.4 Usage of Nanobodies towards addressing the first question

Taken together, nanobodies have been thoroughly implemented in a surprisingly wide variety of experiments over the past 30 years. Here I highlighted only a small selection of different experiments that have applied nanobodies to various fields, but allow us to appreciate the robustness of such a tool. Indeed, it is with nanobodies that I believe we can solve the first obstacle addressing the cytoneme mediated Wnt proteome. Nanobodies can provide the perfect tool for localising specifically to Wnts presented on the cell surface or cytoneme tip. A secreted nanobody, secVHH, would be ideal as it functions once secreted from the cell. Combined with a GFP tagged Wnt, the two constructs would interact at the cell surface membrane or cytoneme tip. As opposed to using the Wnt proteins themselves for tagging proteins in proximity for identification, we can filter the protein hits to those only available at these specific compartments. Indeed, with either a co-expression or, ideally, an exogenously introduced secVHH nanobody, this provides an elegant solution. Furthermore, with the generalisability of GFP-binding VHH and the enormous library of GFP-tagged ligands used frequently in research, secVHH nanobodies can be applied to multiple different Wnts in many different cell types, organisms or environments.

1.8 Proximity based biotin ligation, the answer to the second question

1.8.1 The history of biotin ligases

To address the second condition needed for our future assay, we require a method of non-biased labelling of all proteins involved in cytoneme mediated Wnt handover efficiently. This can involve any tool that allows for isolation of proteins involved with Wnt by interaction, proximity or subcellular compartment. One method that allows for isolation of proteins that simply exist within proximity of our POI would be using a promiscuous biotin ligase. Biotin ligases are an enzyme that bind and biotinylate target proteins for post-translation biotinylation in various organisms such as *Escherichia coli* (Roux et al., 2012). The biotin ligase generates an ‘active biotin’ molecule by catalysing the oxygen atom of

the biotin carboxylate on Pa of ATP to form biotinoyl-AMP and pyrophosphate. Biotinoyl-AMP is stable and remains in the active site of the biotin ligase until it encounters its target protein. When bound to the target protein, the biotin ligase localises both the biotinoyl-AMP and nucleophilic epsilon-amine lysine on the target protein. This in turn causes the lysine to attack the mixed anhydride carbon atom on the biotinoyl-AMP, resulting in an amide bond between the lysine and biotin, producing an AMP as a product (Chapman-Smith & Cronan Jr, 1999). Biotin is an essential vitamin for all organisms and is produced in plants, fungi and most prokaryotes but not in mammals (Tong, 2013). Regardless, biotin ligases are ubiquitous for all organisms (Chapman-Smith & Cronan Jr, 1999). Also known as holocarboxylase synthetases in eukaryotes, biotin ligases are highly evolutionarily conserved, demonstrating biotinylation even when the biotin ligase and carboxylase originate from different species (McAllister & Coon, 1966). The only protein species that utilise biotin are biotin-dependent carboxylase enzymes that use biotin as a cofactor for activity (Tong, 2013). Biotin ligases have a very small and highly targeted pool of protein targets, typically localised within the mitochondrial matrix in eukaryotes.

1.8.2 BirA*, the first promiscuous biotin ligase

There exists three classes of biotin ligases denoted class I to III. All three classes have a conserved catalytic domain that catalyse the attachment of AMP to biotin and a C-terminal with unknown yet essential function for catalytic activity (Chapman-Smith et al., 2001). The main differences between these classes stem from their N terminal domains. Class I biotin ligases omit the N-terminal domain entirely. Class II have a winged helix-turn-helix DNA-binding domain that binds to DNA as a repressor of the biotin biosynthesis operon, whereas class III have a larger N-terminus that cannot bind DNA entirely. The first biotin ligase implemented in research was a class II biotin ligase originated from *Escherichia coli* termed BirA. BirA was first utilised in research in an elegant design due to its specificity for its substrate ‘AviTag’, a minimum short biotin-acceptor peptide sequence (Beckett et al., 1999). By fusing an AviTag and BirA to two different protein sequences, researchers were able to deduce if the two constructs interact by examining AviTag biotinylation post lysis. (Fernández-Suárez et al., 2008; Kulyyassov et al., 2011). This use of BirA

demonstrates resemblance to the more commonly implemented Two-hybrid screening (or yeast two-hybrid system) that detects protein-protein or protein-DNA interactions (Young, 1998). Similarly, to Two-hybrid screening, this process required the cloning of two individual constructs to determine interaction – a laborious and time intensive task that severely reduced proteomic discovery assays (Samavarchi-Tehrani et al., 2020). However, mutants of BirA and related biotin ligases began to be developed that opened the gateway for biotin ligase mass proteomic assays. The first mutation was made to the BirA protein in 1980 was the BirA91 with the mutation R118G that resulted in both increased affinity for biotin (100-fold greater Kd) and, importantly, a new dissociation rate of activated biotinoyl-AMP (400-fold higher). This new protein (denoted BirA*) now did not rely on an AviTag, but instead would release the active biotinoyl-AMP into the environment, where any proteins within proximity would bind from their outer exposed lysine residues. This mutant was first recognised by Choi-Rhee *et al* in 2004 for its potential, but only became mainstream after 2012 with Roux *et al* (Choi-Rhee et al., 2004; Roux et al., 2012). BirA* was later popularised as BioID by Roux *et al* and has been used to determine proteins localisation in small to large compartments of the cell, such as focal adhesions, cell junctions, centrosome, P-bodies and stress granules all the way to a draft proximity map of a human cell (Samavarchi-Tehrani et al., 2020). BioID works by generating a ‘cloud’ of activated biotinoyl-AMP with a radius of 10nm. This has the strength of biotinylating all proteins surrounding BioID (and therefore the POI ligated to BioID) but also comes with the limitation of ‘localisation by chance’. Indeed, biotinylated proteins may be biotinylated not because of their interaction to the POI, but rather because the protein is localised to a specific but unrelated cellular compartment. This drawback only constitutes a minor proportion of the total biotinylated protein list that do interact with the POI. Extraction of biotinylated proteins work through affinity based pulldown of cell lysate using avidin or streptavidin. Streptavidin is a tetrameric protein derived from the bacteria *Streptomyces avidinni* (Selvaraj et al., 2022) which has an extremely high binding affinity to biotin (Kd $\sim 10^{-14}$ M) regardless of biotin attachment to proteins (Samavarchi-Tehrani et al., 2020). As biotin cannot be removed from proteins, harsh lysis conditions can be applied to cell cultures to maximise protein solubility, combined with the high binding efficiency of streptavidin to

allow high pulldown sensitivity. However, BioID suffered one problem, long incubation periods of optimally 24 hours, and a minimum of 3 hours (Samavarchi-Tehrani et al., 2020). This long incubation period therefore lost any temporal control of the biotin ligase activity, and instead limited its usefulness to constant biological processes.

1.8.3 Peroxidases and APEX

Peroxidases have been employed to promiscuously label proteins within proximity in a similar fashion to biotin ligases. Peroxidases work by catalysing hydrogen peroxide (H_2O_2)-mediated oxidation of molecules that act as hydrogen donors. These molecules include aromatic molecules such as tyrosine, and are catalysed by the generation of an active radical from the peroxidase and H_2O_2. When given a phenolic substrate, such as biotin-phenol (or biotin-tyramide), tyramides are activated by the radical which in turn causes them to attack electron rich molecules like tyrosine (Bobrow et al., 1992). Horse radish peroxidase (HRP) has been used extensively in research and is the most well defined peroxidase to date. When the substrate is coupled to a fluorophore, chemiluminescent molecule or any small molecule, HRP is able to activate and/or conjugate the molecule to target protein tyrosine residues (Veitch, 2004). This process is very fast, only requiring one minute of peroxide incubation for maximal reactivity. Indeed, when using a biotin-phenol substrate, HRP can work identically to BioID, albeat far faster but in toxic (H_2O_2) conditions. However, HRP is natively a secreted glycoprotein, which contains disulphide bonds necessary for activity. While HRP has been shown to catalyse in the ER and cell surface, it cannot operate in low pH conditions within the cytosol, making many experimental conditions inappropriate for HRP (Hopkins et al., 2000; Martell et al., 2012). To address this, a novel enzyme, APEX, was produced based on the pea ascorbate peroxidase. APEX performs the same action as HRP but doesn't possess the disulphide bonds, nor does it require calcium for its activity that HRP is dependant on, that allows APEX to operate in intracellular conditions (Samavarchi-Tehrani et al., 2020). APEX can oxidise substrates like biotin-phenol, which allowed many researchers to investigate proteomes of the mitochondrial matrix, mitochondrial membrane space, stress granule markers in conditions of cellular stress and more (Hung et al., 2014;

Markmiller et al., 2018; Rhee et al., 2013). Overall, APEX provides an alternative tool to biotin ligase BioID which is several orders of magnitude faster, but comes at the drawback of H2O2 incubation for activity, an aspect of design that can have unknown implications on cell culture viability.

1.8.4 Development of BioID

Long incubation times for BioID had been a subject of due improvement in the biotin ligase toolset. Indeed, mutations of different biotin ligases led to the generation of the BioID successor, BioID2. Biotin ligase protein from the thermophilic bacteria *Aquifex aeolicus* was mutated at R40G (an othologous location to the R118G mutation in BioID) (Tron et al., 2009). This mutation, like that from BirA, lowered the affinity of BioID2 to activated biotinoyl-AMP, releasing it into the surrounding environment. However, BioID2 has a higher affinity to biotin than BioID, allowing for less biotin necessary for biotinylation and a faster biotinylation rate, reducing biotin incubation time. Interestingly, BioID2 is based on type I biotin ligases, therefore lacking the bulky N-terminal region BioID possesses. Making BioID2 smaller also removes the possibility of non-specific localisation of the biotin ligase that BioID was susceptible to due to the structural resemblance to histidine proteins (Groft et al., 1998). Overall, BioID2 is smaller, faster and has a higher signal-to-noise ratio than its predecessor.

Further improvements to BioID did not stop there, however, as future iterations would significantly improve both speed and size dramatically. By employing an error-prone PCR of BioID2 sequence, combined with a yeast cell surface display of BioID and FACS sorting to generate directed evolution, the Ting lab was able to develop two new biotin ligase constructs, TurboID and MiniTurboID (Branon et al., 2018). TurboID and MiniTurbo incorporate a total of 14 and 12 mutations, respectively over the BioID2 (with an N-terminal deletion of the first 63 amino in MiniTurboID). These mutations resulted in a 3~6-fold increase in activity over BioID and BioID2 at very short incubation periods and a 15~23-fold increase over 6-18 hours of incubation. Indeed, TurboID and MiniTurboID reduced the minimum incubation period from 3 hours in BioID to just 5-10 minutes (Branon et al., 2018). The Ting lab also generated a successor APEX

construct, termed APEX2, using the same experimental method. APEX2 only received a single new mutation of A134P substitution, which improved its tolerance to inactivation from H_2O_2 (Lam et al., 2015).

1.8.5 Proximity-based biotin ligation, the answer to the second question

Three protein candidates are thus presented to tag and isolate a non-biased list of proteins that exist within proximity to our POI Wnt. These are the peroxidase-based APEX2 or the biotin ligase-based TurboID or MiniTurbo. All three of these proteins can rapidly and efficiently biotinylate proteins that interact with Wnt on the cell surface and filopodia to allow extraction by streptavidin pull down. Each protein comes with its unique benefits and limitations. Speed of the reaction is essential when identifying proteins on cytonemes. As discussed previously, cytonemes are highly dynamic, thin, and transient structures that transfer Wnt in under 10 minutes. APEX2 is the best candidate for speed, as it can capture these proteomes in as little as one minute. However, APEX2 requires the addition of H_2O_2, which could have dire consequences on the integrity of these structures. TurboID boasts the second fastest speed, requiring a minimum of 5-10 minutes of biotin incubation. Conversely, while MiniTurboID has less affinity for biotin than TurboID, it has significantly reduced size (28kD compared to 35kD of TurboID), which would be invaluable when combined with the GFP nanobody required for localising to Wnt. Overall, all three proteins can be used to address the second obstacle outlined in our conditions required to determine the proteome of cytoneme-mediated Wnt handover.

1.9 Mass Spectrometry, the answer to the third question

1.9.1 Mass spectrometry and proteomics

The final obstacle to address in the design of our future assay requires a suitable technique that can identify protein peptides isolated from the assay. Two possible techniques exist to identify protein peptides: Edman Degradation and Mass Spectrometry. The Edman degradation technique works on individual proteins by ‘reading’ the amino acid sequence, similar to Sanger sequencing for DNA. However, unlike Sanger sequencing, Edman degradation works by

labelling the N-terminal amino acid sequence and subsequent cleavage of this amino acid to determine its identity. The process does not interfere with the original peptide sequence. This process is repeated until the entire peptide is sequenced or if the reaction encounters a chemically modified N-terminus (acetylation, for example) or a non-amino acid (such as aspartic acid) (Edman et al., 1950). While helpful in identifying individual proteins (given they do not include the conditions that stop the reaction), Edman degradation cannot work on complex protein mixtures such as a cell lysate. Mass spectrometry is a technique that exploits the mass and charge of protein peptides to filter each protein ion for further analysis and subsequent identification and relative abundance (Pappireddi et al., 2019). Mass spectrometry has been a workhorse for various applications, not limited to biological-based research. Discovered in 1912, mass spectrometry was initially devised as the parabola spectrograph and used to determine the existence of non-radioactive isotopes (Sinha & Mann, 2020). Intended to determine mass-to-charge ratios of ions, the principle of mass spectrometry has evolved and refined enormously over the past century to determine individual protein peptides within the complex environment of biological samples. Modern proteomic analysis is performed using liquid chromatography-mass spectrometry (LC-MS), which combines the separation of complex protein mixtures in liquid chromatography (LC) with the analysis of mass spectrometry. LC is an essential prerequisite of mass spectrometry as it separates the protein mixtures based on size, charge, hydrophobicity and polarity to generate a readout of ion count (observed in the mass spectrometer) against time. Other separation techniques can also be employed (such as SDS-page electrophoresis); however, LC remains the ideal solution. Indeed, the proportion of gaseous peptide ions is proportional to the concentration being ionised before mass spectrometry analysis. Therefore, the slowest rate of flow in LC (and hence, the highest separation of peptides) is necessary.

1.9.2 Mechanism of mass spectrometry

Mass spectrometry requires the digestion of proteins to generate a library of protein-peptide fragments, typically using Trypsin. Trypsin cleaves proteins at known locations with high specificity, generating a library of peptides that start and end in predictable amino acids. As opposed to whole proteins, measuring

peptides can produce outputs of protein mass/charge ratios that can be compared to a peptide database to identify the peptide. These identified peptides can be later reconstituted to identify the original protein. Protein fragmentation occurs before LC, and once the peptides exit LC, they undergo electrospray ionisation. Droplets of protein solution are evaporated by increasing concentration of positively charged peptides overcoming surface tension from the increased coulombic repulsion, resulting in a gas of charged particles (Fenn et al., 1989). An interesting phenomenon of peptide ionisation is that the efficiency can differ by several orders of magnitude, resulting in some peptides being over or under-represented in mass spectrometric analysis (Muntel et al., 2015). This problem singlehandedly results in an inability of mass spectrometry to detect proteins quantitatively. Instead, additional and indirect steps must be taken to generate quantitative data on top of the qualitative data. Ionised peptides in the gas phase are accelerated and enter a deflection chamber that constitutes powerful magnets designed to push the stream of ionised peptides in a bend. This deflection depends on both the charge and mass of the peptide in question, thereby identifying the mass/charge ratio of the peptide. Peptides continue until they collide with a detector that measures the position of the colliding peptide (Fig 4). A chromatogram of the number of ions hitting the detector over time is generated, with each instance of time depicting what is known as an MS1 spectrum. An MS1 spectrum details all intact peptides, and its spectrum is plotted as Ion counts over mass/charge ratio.

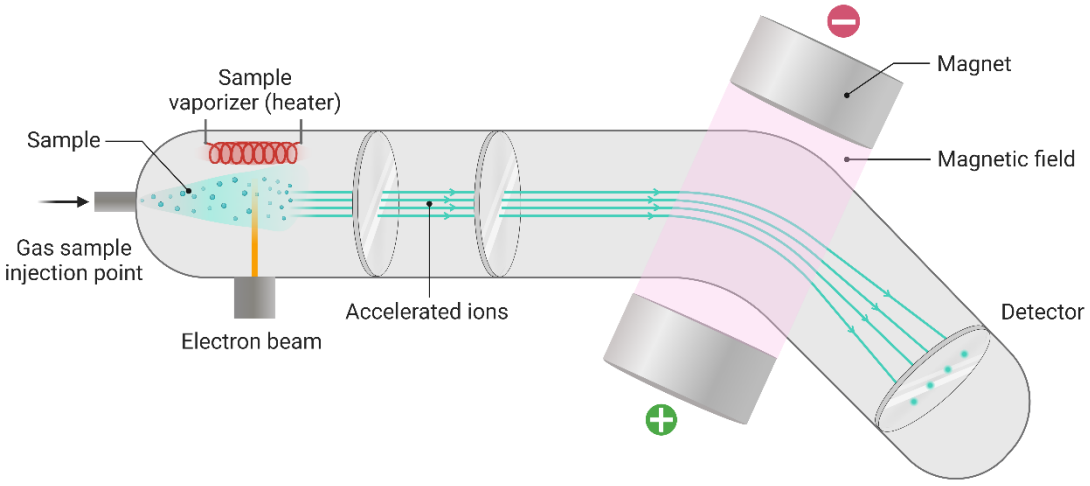

Figure 4. Mass Spectrometry General Principle. *Cartoon representation of mass spectrometry general working principle. Created with BioRender.com*

using pre-made template (https://www.khanacademy.org/science/ap-chemistry-beta/x2eef969c74e0d802:atomic-structure-and-properties/x2eef969c74e0d802:mass-spectrometry-of-elements/v/mass-spectrometry).

Therefore, for any instance of fractionated peptides from the LC, the frequency of all different mass/charge hits identified by the detector can be logged (Chelius & Bondarenko, 2002). Alone, this data cannot determine what the original peptide was or how many of that peptide it detected, as many different peptide fragments can possess identical mass/charge ratios. To address this, the dominant MS1 peaks are further fragmented with colliding inert gasses to break their weakest bonds – the peptide bond between amino acids. These individual amino acids are plotted in another graph of ion count over mass/charge ratio, which can be referenced to an amino acid library to determine which amino acids constituted the whole peptide and their frequency. Combining both the MS1 and MS2 spectrums, along with their time on the original chromatograph, we can infer the original peptide with high accuracy. Further referencing the list of all detected peptides to an organism's protein database, we can determine the whole protein before fragmentation and the number of those proteins detected in the detector (note, not the entire number of proteins in the cell lysate as many are not ionised and so lost) (Pappireddi et al., 2019). This method of proteomic analysis is often called the 'Bottom-up' approach as it requires deconstruction of the protein for identification, whereas the 'Top-down' approach looks at the whole protein first for identification.

1.9.3 Non-labelling mass spectrometry

Mass spectrometry is a potent tool for distinguishing proteins from the complex mixture of the cell lysate; however, it is also used to measure the differences in protein abundance between multiple conditions. The most widely used form of mass spectrometry proteomics uses 'label-free' quantification, as opposed to multiplexed or isobaric labelling. As the title suggests, label-free proteomics does not attempt to alter the peptides before analysis. Instead, each sample is measured separately and consecutively (Ong & Mann, 2005). The MS1 signal

for a given peptide is integrated for all MS1 signals for that peptide observed. This generates a curve where the area under the curve measures the total number of ions for that peptide. This total number of ions count can be directly compared with different samples to develop a relative concentration of that peptide and helps measure differences between samples. A regression model is fitted between the two (or more) curves to determine statistical differences in samples. The main advantage of this technique is the lack of further (and often costly) modifications to the proteins before analysis and the applicability of this approach on thousands of samples for grouped analysis (Pappireddi et al., 2019). However, this approach investigates one sample per run, sometimes for multiple runs, if multiple fractionations of the lysate are performed to increase sensitivity.

Furthermore, there is a risk of poor measurement precision with coefficients of variation ranging from 20% between samples (Cox et al., 2014). This poor consistency is especially prevalent in low-abundance proteins, with some protein fragments not being detected outright. The main culprit is the difficulty in normalising different protein samples before analysis. This risk of protein loss is known as the missing value problem. Increasing concentrations of proteins can reduce the risk of missing values but also increases the risk of losing detection of low-abundance proteins. Many advancements have been made to mitigate all these limitations; however, alternative mass spectrometric techniques may be more applicable.

1.9.4 Multiplexed mass spectrometry

The alternative is multiplexed or isobaric labelling mass spectrometry. Isobaric labelling is based on adding covalently bonded isobaric tags to the fragmented peptides after digestion but before LC. The most common tags are Tandem Mass Tags (TMT) or Isobaric Tags for Relative and Absolute Quantitation (iTRAQ) (Dayon et al., 2008; Ross et al., 2004). These tags are reagents that constitute two groups, the reporter and the compliment ions, covalently bound by a fragile bond designed for fragmentation. These tags are unique by the distribution of heavy isotopes on either the reporter or compliment ions; however, the sum of molecular weights is equal between different tags when

non-fragmented. This allows for multiplexed mass spectrometry, where many different experimental samples are labelled with separate isobaric tags and run through the mass spectrometry simultaneously. Identical peptides from different samples are eluted by LC and loaded into the mass spectrometer, where they are all analysed by the detector simultaneously. As all isobaric tags share identical masses, they do not alter the mass/charge ratio of the peptide. On the MS1 graph, this results in more giant peaks as it detects more of the same peptide. However, the MS1 peak fragmentation can result in either isobaric tag splitting (generating reporter and complimentary reporter ions) or fragment ions (a product of backbone splitting but isobaric tag remaining), giving rise to an MS2 spectrum that can link the peptide sequence to its respective sample (Stadlmeier et al., 2018). This mass spectrometry method improves upon non-labelling techniques, increasing throughput and decreasing time for multiple sample analysis.

Furthermore, it increases reproducibility by reducing coefficients of variation to around 5%. This is due to the massive enrichment of proteins analysed by incorporating more samples. Missing values are also mitigated as protein abundances significantly decreased or not detected for one sample are inferred to be less abundant than the other. Overall, TMT or iTRAQ multiplexed mass spectrometry increases speed, reproducibility and accuracy over non-labelling techniques. There are significant limitations imposed by multiplexed mass spectrometry, principally the problem of multiple peptides with similar mass/charge ratios from the same sample can interfere during MS2 fragmentation (Karp et al., 2010; Ting et al., 2011; Wenger et al., 2011). Many techniques are developed to mitigate this limitation, but it is always a consideration.

1.10 Functionalised nanobody BLITZ line in zebrafish embryos

Functionalising a nanobody with a biotin ligase for mass spectrometry analysis is an elegant solution to the problems outlined previously in understanding cytoneme-mediated Wnt proteome. Together, these three tools would allow for a highly specific assay to biotinylate even transient structures such as cytonemes in standard culture conditions. The most significant aspect of this

toolset would be the generalisability of using GFP-ligated POI to run the assay. Indeed, this assay satisfies all these requirements so well that our lab is not the only one to use it. During the development of my thesis, Zherui Xiong *et al.* implemented a near-identical assay to identify their POI within zebrafish embryos (Xiong et al., 2021). Xiong developed and tested a GFP-binding nanobody-TurboID (called TurboID-GBP) zebrafish line designed to be crossed with any GFP-expressing zebrafish line. Termed BLITZ (Biotin Labelling In Tagged Zebrafish), the team developed and tested BLITZ expression in F0 lines for proper expression and activity. The TurboID-GBP was improved to be 'destabilised' without a GFP binding partner, resulting in rapid degradation (termed TurboID-dGBP). Once the team confirmed stable expression, they crossed this line with various GFP tagged lines such as Cavin1a, Cavin4a, MotoN (motor neurones) and kdrl (cytoplasmic GFP in the vasculature). Indeed, all four GFP constructs tested found streptavidin staining co-localised to GFP only in the presence of TurboID-dGBP and that it can produce proximity-based biotinylation with subcellular specificity. Furthermore, BLITZ lines crossed with cavin1a, cavin4a and cavin 4b were successfully analysed using TMT mass spectrometry. These results provide strong evidence for the success of a biotin ligase fused nanobody toolset for identifying the Wnt proteome with reasonable subcellular specificity.

1.11 Aims of thesis

In this thesis, I aim to explore this novel nanobody-biotin ligase-based assay to observe and optimise its efficacy in mass spectrometry proteomics of the Wnt cytonemes. To this end, I explore the expression and transport of Wnt8a- and Wnt5a/b- GFP within live cell cultures with the secreted nanobody secVHHmCh fused to biotin ligase MiniTurboID. In pursuing method development, I explore various options for the final assay conditions, such as using cytoneme inhibitors, the ideal Wnt ligand for study and maximising biotinylation. My first goal is to deduce the behaviour of Wnt in various cell cultures and their suitability for the secVHHmCh-MT system. Second, I aim to deduce the level and location of biotinylation from this system and attempt extraction of biotinylated proteins. Third, I aim to use this novel assay for mass spectrometry analysis and improve assay conditions. Finally, I develop preliminary

examinations into protein hits generated from the assay to observe co-localisation to Wnt-GFP, especially in the cytoneme tips.

2 Materials and Methods

2.1 Materials

2.1.1 DNA Plasmids

DNA construct	Plasmid Vector	Source
Membrane-Cherry	pCS2+	Scholpp *et al.*, 2019
Membrane-GFP	pCAG-mGFP	Addgene #14757
Membrane-BFP	pCS2+	Replaced GFP from Membrane-GFP with BFP from Ror2BFP
secVHHmCh	pUAS	The Affolter Lab
secVHHmCh	pCS2+	Subcloned from pUAS plasmid
secVHH-13xLinker	pcDNA3.1	secVHH and 13xLinker from BioID2 origional plasmid subcloned and fused into pcDNA3.1
secVHH-MiniTurboID	pcDNA3.1	MiniTurboID subcloned into secVHH-13xLinker plasmid
secVHHmCh-MiniTurboID	pcDNA3.1	mCh subcloned from secVHHmCh and inserted into secVHH-MiniTurboID using Gibson
secVHH-BioID2	pcDNA3.1	BioID2 subcloned into C-terminal of secVHH-13xLinker
Wnt8a-GFP	pCS2+	Stanganello *et al.*, 2015
Wnt5a-GFP	pCS2+	*Xenopus* Wnt5a and eGFP open reading frame fused via

		PCR and subcloned into pCS2+ via XhoI
Wnt5b-GFP	pCS2+	Chengting *et al.*, 2022
Wnt3a-GFP	pCS2+	Cloned into pCS2+ with ClaI and XbaI
MyoX-GFP	EGFPC1	Addgene #47608
Ryk-mCh	pCS2+	Max Fuerthauer Lab
ΔN-Ryk-mCh	pCS2+	Max Fuerthauer Lab
IRSp534K	Unkown	Meyen *et al.*, 2015
MiniTurboID	pSBbi	Estell *et al.*, 2023
Apex2	pcDNA3.1	Addgene #49386
BioID2	pcDNA3.1	Addgene #92308
Rab5-GFP	pCS2+	Zerial Lab
Rab7-RFP	pCS2+	Rudiger Rudolf Lab
Flotillin 1a-GFP	pCS2+	cDNA subclone into pCS2+ using BamHI and XbaI
Flotillin 2-GFP	pCS2+	Routledge *et al.*, 2022
Caveolin 1-GFP	pCS2+	cDNA subclone into pCS2+ using ClaI
Evi-mCh	pCS2+	Chengting *et al.*, 2022
Ror2-mCh	pCS2+	Rogers *et al.*, 2022

2.1.2 Antibodies

Antibody	Working Dilution	Source
Streptavidin conjugate-555	1:5000	Invitrogen S21381
Anti-Flag M2	1:100	Sigma-Aldrich F1804-50UG
Anti-Myc	1:100	Abcam ab32
Anti-GAPDH	1:1000	Sigma-Aldrich MAB374
Polyclonal Anti-GFP	1:1000	Abcam ab290
Anti-Ror2	1:100	Cell Signalling D3B6F (88639S)
Phalloidin i-Fluor 405 reagent	1:1000	Abcam ab176752
Phalloidin i-Fluor 594 reagent	1:1000	Abcam ab176757
Goat Anti-Rabbit AlexaFluor®488	1:1000	Abcam ab150077
Goat Anti-Rabbit AlexaFluor®568	1:1000	Abcam ab175471
Goat Anti-Mouse IRDye®800CW	1:5000	Abcam ab216772
Donkey Anti-Rabbit AlexaFluor®680	1:5000	Abcam ab175772
Donkey Anti-Goat AlexaFluor®647	1:1000	Abcam ab150135
Donkey Anti-Rabbit AlexaFluor®488	1:1000	Abcam ab150073
Donkey Anti-Mouse AlexaFluor®568	1:1000	Abcam ab175472

2.1.3 Primers

Primer	Protocol	Sequence (5' → 3')
secVHH F	Cloning	AAA AGC TAG CCA CCA TGG CCT CAC CGT TGA CC
secVHH R	Cloning	AAA AAT CGA TGC TGG AGA CGG TGA CCT G
13x Linker F	Cloning	AAA AAT CGA TTT TTC GGA ATT CGG ATC CGG TGG AGG C
13x Linker R	Cloning	AAA AGG CGC GCC GAT CCA CCG C
BioID2 F	Cloning	AAA AGG CGC GCC GTG AAC AAA AAC TCA TCT CAG AAG AG
BioID2 R	Cloning	AAA ACT CGA GGC TTC TTC TCA GGC TGA A
Apex2 F	Cloning	AAA AGG CGC GCC GTG AAC AAA AAC TCA TCT CAG AAG AG
Apex2 R	Cloning	AAA ACT CGA GGG CAT CAG CAA ACC CA
MiniTurboID F	Cloning	AAA AGG CGC GCC GTG ACT ACA AAG ACG ATG ACG ACA AGG
MiniTurboID R	Cloning	AAA ACT CGA GCT TTT CGG CAG ACC GCA G
secVHHmCh F	Cloning	AAA AGC TAG CAA TGG CCT CAC CGT TGA C
secVHHmCh R	Cloning	AAA AAC CGG TAT TAC TTG TAC AGC TCG TCC A
MiniTurboID (Wnt8a) F	Cloning	AAA AGG TAC CGG AAT CCC GCT GCT GAA CG

MiniTurboID (Wnt8a) R	Cloning	AAA AGC GGC CGC CTT TTC GGC AGA CCG CAG
Zebrafish Ubiquitin B Promoter F	Cloning	AAA ACA ATT GAC CAG CAA AGT TCT AGA ATT TGT CG
Zebrafish Ubiquitin B Promoter R	Cloning	AAA CGA TCG CTG TAA ACA AAT TCA AAG TAA GAT TAG C
secVHHmCh-MT Gibson F1	Gibson	TAT AGG GAG ACC CAA GCT GGC TAG CCA CCA TGG CCT CAC CGT TGA CCC G
secVHHmCh-MT Gibson R1	Gibson	CCG AAT TCC GAA AAA TCG ATC TTG TAC AGC TCG TCC ATG C
secVHHmCh-MT Gibson F2	Gibson	GCA TGG ACG AGC TGT ACA AGA TCG ATT TTT CGG AAT TCG G
secVHHmCh-MT Gibson R2	Gibson	CAG ATA TCC AGC ACA GTG GC
MiniTurboID (Wnt5bGFP) F	Gibson	AGA CCA GTT TGT GTG CAA GTC TAG AGA CAC GGA CTA CAA AGA CGA TGAC GA
MiniTurboID (Wnt5bGFP) R	Gibson	CGC CCT TGC TCA CCG TGT CTC TTT TCG GCA GAC CGC AGA C

2.2 Methods

2.2.1 Cell Culture

Cells were cultured in media and incubation conditions respective to their cell line. HeLa, MEF and AGS cells were cultured in 37°C, 5% CO2. PAC2 cells were cultured in 28°C, normal atmosphere. HeLa and MEF cells were cultured in DMEM media supplemented with 10% FBS and 1% Penicillin/Streptomycin. AGS cells were cultured in RPMI media supplemented with 10% FBS and no antibiotics. PAC2 cells were cultured in Leibovitz L15 media supplemented with 10% FBS and no antibiotics. Depending on speed of cell growth, cells were passaged once or twice a week using 0.05% Trypsin-EDTA once cell confluence reached 80-90%.

2.2.2 Transfection

Cells were digested using 0.05% Trypsin-EDTA and seeded in 6-well plates at $2_{x10}5$ and $1.5_{x10}5$ for HeLa/MEF/AGS and PAC2 cell cultures respectively. Cells were left to incubate for 24 hours in respective incubation conditions before transfection. Immediately prior to transfection, fresh media was given to the culture. Transfection was performed using Optimem, DNA and Fugene at a ratio of 100:1:3 respectively, using 100µL of Optimem for each cell culture. Assembled transfection mixture was left to incubate for 15 minutes in RT, then placed directly to cell culture. Following experiments were performed 24 or 48 hours post transfection. Cells were washed with fresh media to remove dead cells using standard/phenol free media. In the case of secVHHmCh co-cultured samples, either the last step was excluded or washed using secVHHmCh-MT conditioned media to preserve free secVHHmCh concentration.

For co-culture assays, cells were digested using 0.05% Trypsin-EDTA 24 hours post transfection and collected. Cells were spun down at 300G for 3 minutes 30 seconds at room temperature and re-suspended in fresh media. Total cell count was not measured; instead, half of both cell suspensions were placed into a fresh relevant culture container together. The new ‘co-culture’ assay contains an equal quantity of each transfected cell cultures. Co-cultured cell cultures left to incubate in appropriate conditions for 24 hours before experiment. For co-

cultures containing a mix of PAC2 and AGS cells, the new co-culture produced from mixing was incubated in Leibovitz L15 media supplemented with 10% FBS and no antibiotics and incubated in 28°C, normal atmosphere.

For conditioned media samples, transfection of cell culture was standard. The cell culture used to generate the conditioned media was incubated in fresh media for 24 hours and then collected. The conditioned media was filtered using 0.22μM filter and stored in 4°C to be used within the week. 24 or 48 hours post transfection of receiving cell cultures were washed in PBS and given relevant conditioned media. These samples were incubated in the conditioned media for 24 hours before imaging or protein lysate collection. When applying AGS conditioned media to PAC2 cells, both cells are incubated in fresh Leibovitz L15 media supplemented with 10% FBS and no antibiotics and incubated in 28°C, normal atmosphere.

2.2.3 Stable Cell Generation

Stable cells were generated following standard cell culture and passaging methods outlined previously. Stable cell specific plasmids were generated using pcDNA3.1 vectors. pcDNA3.1 secVHHmCh-MT maxi-prepped plasmids were linearized prior using ScaI restriction enzyme. AGS cells were transfected using linearized plasmids following previously described protocol. Cells were left to incubate at 37°C 5% CO_2 for 48 hours. Cell media was then supplemented with 'low' (400μg/μL), 'optimal' (700μg/μL) and 'high' (900μg/μL) G418 for 10 days, ensuring multiple media changes to remove dead cells. Cells were then passaged and diluted to one cell per 10μl of media and placed into 96wp at 1 cell per well. Cells were cultured as standard without G418 supplement until colony-forming units were observed. Wells that contain a single colony were marked and tracked. Once colony grows to 50% confluence and shows fluorescent expression, cells were passaged into 24wp, then 6wp until finally a standard culture flask (T25 or T75). Stable cells were cultured as standard, and multiple sample freeze downs were made for stock.

2.2.4 Antibody Staining

Cells were passaged as described previously but were plated onto glass cover slips on 6-well plates. Transfection of the cells was also performed as described previously. 24 to 48 hours post transfection, cell cultures were washed with PBS and then incubated in either 4% PFA for 20 minutes room temperature, methanol for 10 minutes at room temperature or with chilled Memfix (4% formaldehyde, 0.25% glutaraldehyde and 0.1M Soren's phosphate buffered solution) for 7 minutes at 4°C. For PFA and methanol fixation, cover slips were incubated in permeabilisation buffer (0.1% Triton-X, 5% serum in Soren's buffer) for 1 hour at room temperature. Memfixed cover slips were instead incubated in 0.1% $NaBH_4$ in Soren's buffer for 7 minutes. The cover slips were then washed 3 times using 50mM glycine in Soren's buffer for 10 mins at room temperature. Cover slips were never rocked during washing stages to preserve fragile cytoneme structures. Memfixed cover slips were then incubated in permeabilisation buffer identical to PFA or methanol fixed slides. Cover slips were then incubated in incubation buffer (0.1% Tween-20, 5% serum in Soren's buffer) containing diluted primary antibodies over night at 4°C. Cover slips were then washed 3 times in Soren's buffer for 5 mins each, then incubated in incubation buffer containing diluted secondary antibodies for 1 hour at room temperature. Cover slips were then washed 5 times in Soren's buffer for 10 mins each, then mounted on glass slides using ProLong Diamond anti-fade mountant (Invitrogen) and sealed using translucent clear nail varnish. Slides were imaged 24 hours post mounting.

Multiple imaging systems were implemented for various advantages respective to each system. For standard imaging of live or fixed cells, the Leica SP8 confocal microscope was utilised for its fast and reliable imaging. The Leica Hyvolution was used as an alternative. Alternative imaging mechanisms to confocal microscopy was used, such as the ZEISS Elyra 7 super-resolution lattice sim microscope. The Elyra was utilised for its super-resolution properties when identifying exact spatial resolution was necessary.

2.2.5 Western Blotting

Cell lysates were generated by one of two methods of collection using Pierce RIPA buffer (ThermoFisher) supplemented with 1X cOmplete protease inhibitor cocktail (Merk). The different collection methods were dictated as to whether preservation of membrane proteins was necessary. Non-membrane protein lysates were collected by incubating the cell culture in Trypsin-EDTA, then spun down to re-suspend cell pellet directly into RIPA buffer. Membrane protein lysates were collected by washing the cells in PBS, then adding RIPA buffer directly to the cell culture well. The culture was incubated in RIPA buffer for 10 mins at 4°C and rocked to ensure the RIPA buffer covered the whole plate. Using a cell scraper, the cell lysate was collected. Lysate was agitated on ice for 30 mins and sonicated. Lysates were spun down at 13000RPM for 20 mins at 4°C. The pellet was discarded and the protein concentration of the supernatant was measured using a Pierce BCA assay kit (according to manufacturer's protocol).

Sample preparation for SDS-Page gel electrophoresis was performed by adding 15-30µg protein to 5µl of 4x Laemmli buffer (containing 10% β-mercaptoethanol) to create a final volume of 20µl. The mixture was boiled at 95°C for 5 mins, spun down, then loaded into the BIORAD Mini-PROTEAN pre-cast SDS-Page gel (12% acrylamide) along with Spectra^{TM} Multicolour Broad Range Protein Ladder. Gels were run at 100V for 75 mins. Gels were transferred to nitrocellulose using Wet transfer at 70V for 1 hour. Nitrocellulose blots were then blocked in 5% BSA (for streptavidin blots) or 5% milk powder (for general blots) in TBST for 1 hour on roller. Blots were incubated overnight at 4°C in TBST containing primary antibody dilutions. Blots were then washed 3 times in TBST, then placed in TBST containing secondary antibody dilutions for 2 hours at room temperature. Blots were then washed twice in TBST, then 3 times in TBS. Blots were then imaged using BioRad ChemiDoc MP Imaging System and image processing was performed in ImageJ.

2.2.6 Streptavidin Pulldown

PAC2 cells were transfected with the POI fused to a GFP and incubated for 24 hours at 28°C. Transfected PAC2 cells were then either co-cultured with

secVHHmCh-MT stable expressing AGS cells or cultured in secVHHmCh-MT conditioned media for a further 24 hours at 28°C. For conditioned media, cell culture media was replaced with fresh conditioned media 24, 5 and 1 hour before collection. One hour prior to collection, cell culture was treated with 500μM biotin. Cells were then washed with PBS twice and collected in RIPA buffer supplemented with 1x protease inhibitor. Cell lysates were sonicated and spun down at 12,000RPM for 20 minutes at 4°C. Cell lysate pellet was discarded and lysate protein concentration was measured using Pierce BCA assay following manufacturer's protocol. Streptavidin bead slurry was washed twice in RIPA buffer using magnetic rack to precipitate beads from solution. 360μg of protein was mixed with 30μl of washed streptavidin beads and volume of RIPA buffer was increased to minimum of 500μl to ensure mixing. Streptavidin beads were then placed in rocking wheel to mix overnight at 4°C. Using a magnetic rack, RIPA buffer was collected from the streptavidin beads and placed into different eppindorf to be used as flow-through fraction. The streptavidin beads were then subject to a series of washes. The beads were washed twice in RIPA buffer, then 1M KCL in water, 0.1M Na_2CO_3 in water, 2M Urea in 10mM Tris-HCL pH 8.0, and finally two more washes of RIPA buffer. Streptavidin beads were then boiled in 30μl 3x protein loading buffer (Laemmli) supplemented with 2mM biotin and 20mM DTT for 10 minutes. Streptavidin beads were vortexed, spun down and then quickly cooled on ice. Using magnetic rack, the eluates were collected and the beads discarded. For western blot, 10μl of eluate was loaded into SDS poly-acrylamide gel. For mass spectrometry analysis, beads were frozen down on beads instead of being eluted and shipped to the University of Bristol Proteomics Facility for further processing and mass spectrometry.

2.2.7 Mass Spectrometry Analysis and Bioinformatics.

Mass spectrometry report was received from the University of Bristol Proteomics Facility which includes false discovery rate (FDA) confidence, protein Uniprot accession number, Identifier of general contaminants, organism of origin, percentage peptide coverage, number of peptide hits, number of peptide spectrum matches, number of unique peptides hit, peptide abundance and abundance counts along with ratios between samples and their standard

error. Initial analysis began with identifying statistically significant protein hits using unpaired T-test with Welch's correction. An Rstudio script was used to automate statistical analysis for every peptide comparing the means between experimental and control samples. Peptides that show significant enrichment in the experimental group were appended to a separate file where a Python script extracts the Uniprot accession for further bioinformatics analysis. Online Bioinformatic resources used include String.db for peptide clustering based on various factors including literature text mining, biochemical and experimental correlation, co-expression and associations in various curated databases. Database for Annotation, Visualization and Integrated Discovery (DAVID) and Gene Ontology/Panther resource were used to identify gene enrichment in biological processes, molecular functions and cellular components.

2.2.8 DNA Preparation and Cloning

Where applicable, DNA plasmid constructs were either generously gifted to us or purchased from Addgene.com. PCR amplification of DNA was performed using the following reaction mix:

10µl 2x CloneAmp, 0.5µl of each primer, 2µl of vector and 5µl of H_20.

Accounting for size of DNA length to be cloned, the thermocycler was set to 35 repeats of 95°C, the primer annealing temperature and then 72°C. PCR products were then separated by agarose gel electrophoresis at 0.7% for 30-45 mins at 100V. DNA bands were excised and extracted using GeneJET Gel Extraction Kit following the manufacturer's protocol.

Restriction enzyme cutting of DNA was performed using New England Biolab (NEB) restriction enzymes using the following reaction mix:

Plasmid digest: 2µl 10x reaction buffer, 2µl of each enzyme, 2µl of plasmid and 14µl of H_20.

PCR digest: 2µl 10x reaction buffer, 2µl of each enzyme, 10µl of PCR product and 11µl of H_20.

Two methods were employed in the generation of novel DNA plasmid constructs. These are T4 DNA ligase or Gibson reaction cloning. T4 DNA ligase

cloning involved the generation of PCR products with overhanging restriction sites complimentary to restriction sites on the desired plasmid for insertion. PCR product(s) were then digested with respective restriction enzymes, cleaned up using gel electrophoresis described previously, then ligated together. Gibson cloning involved PCR of each fragment, followed by ligation using NEBuilder® HiFi DNA Assembly Master Mix for one hour at 50ºC.

2.2.9 Computational Scripts

Below is the Rstudio script used for performing statistical T-test between experimental and control samples for each protein abundance:

```
# Install the readxl and t.test packages if they are not already installed
install.packages("readxl")
install.packages("t.test")
install.packages("openxlsx")
install.packages("dplyr")
# Load the packages
library(readxl)
library(t.test)
library(openxlsx)
library(dplyr)
# Read the data from the Excel file into a data frame - change directory info to find file
                    properly
data <- read_excel("Input_File_Here.xlsx")
# Specify the columns of data for the first and second samples - will change these to fit
                    my real data columns
sample1_cols <- c("Abundance_Control_Repeat1", "Abundance_Control_Repeat2",
              "Abundance_Control_Repeat3", "Abundance_Control_Repeat4")
sample2_cols <- c("Abundance_Experimental_Repeat1",
                    "Abundance_Experimental_Repeat2",
              "Abundance_Experimental_Repeat3", "Abundance_Experimental_Repeat4")
# Create a new data frame to store the results
results <- data.frame(Accession = data$Accession, stringsAsFactors = FALSE)
# Add the Abundance Ratio column to the results data frame - again, change this
                    column name if needed
results$`Abundance Ratio: (Experiment) / (Control)` <- data$`Abundance Ratio:
                    (Experiment) / (Control)`
# Loop through each row of the data
for(i in 1:nrow(data)) {
  # Extract the data for the first and second samples
  sample1 <- data[i, sample1_cols]
  sample2 <- data[i, sample2_cols]

  #transpose these data sets so they are compatible for a t-test
  data_transpose <- t(sample1)
  data_transpose2 <- t(sample2)
  # Run a t-test between the two samples
  t_test_result <- t.test(data_transpose, data_transpose2)
    # Store the p-value in the results data frame
  results[i, "p.value"] <- t_test_result$p.value
  #print results for proof reading script
  #print(c(data_transpose,data_transpose2))
}
```

```
# Order the results data frame by the Abundance Ratio column - helps to see what data
        is increased or decreased as a result of treatment
results <- results %>% arrange(desc(`Abundance Ratio: (Experiment) / (Control)`))
# Output the results to an Excel file - choose the output directroy, at the moment its for
        my practice data
write.xlsx(results, "Output_File.xlsx")
```

Below is the python script used to identify unique protein peptides from the ‘Test’ mass spectrometry data set that is not in the first or second mass spectrometry data sets:

```
import pandas as pd
# Open the 'Test' dataset and the dataset used to compare it against
df1 = pd.read_excel('Test_DataSet.xlsx', usecols=['Accession'])
df2 = pd.read_excel('1st_or_2nd_Mass_Spectrometry_DataSet.xlsx',
        usecols=['Accession'])
# Iterate through each Accession number and drop it from list if it exists in other dataset
unique_values = df1[~df1['Accession'].isin(df2['Accession'])].reset_index(drop=True)
# Output the unique protein dataset to a new file
unique_values.to_excel('UniqueProteins_Output.xlsx', index=False)
# Repeat this process using the output dataset and the second mass spectrometry data
        set
```

3 Chapter 1 – Establishing our tools

3.1 Introduction

Cytonemes are typically distinct from filopodia in nomenclature as being specialised for communicating with neighbouring cells via signalling peptides and receptors (Mattes & Scholpp, 2018; Stanganello et al., 2015). Despite this, there is less knowledge on the characteristics of cytonemes that distinguish them from general filopodia other than the presence of a signalling peptide. Without labelling all possible signalling peptides, it is impossible to deduce whether cytonemes are unique from filopodia or redundant. Furthermore, which factors initiate the production, elongation, stability and retraction of cytonemes remain unclear. In addition, many studies explore filopodia in the general sense, leaving little to no research investigating cytonemes as a signalling structure. To date, the only investigations exploring Wnt-related cytoneme proteome exist from examining individual proteins (Stanganello et al., 2015). In order to elucidate the proteome specific to cytonemes that distinguish them from typical filopodia (and specifically explore Wnt-interacting peptides), I generated a novel assay using functionalised nanobodies to localise to Wnt on cytonemes.

As explained in the introduction, Nanobodies are fast-maturing, stable peptides with high affinity for their specific epitope (Aguilar, Vigano, et al., 2019). These characteristics ensure a rapid, high volume of nanobody expression, an extremely desirable aspect for enriching sample size. Specifically, I chose the secVHH, a secreted nanobody that binds to a GFP epitope. As opposed to generating a nanobody that binds to an individual Wnt epitope, a GFP binding nanobody allows robust assessment of as many GFP-fused peptides as desired. While nanobodies present themselves as an extremely useful for the unbiased identification of Wnt related cytoneme proteome, there remain many optimisation and development steps necessary before we can commit to the final assay.

In this chapter, I aim to evaluate all tools available for developing an assay to extract all cytoneme localised Wnt transport proteins. As explained previously, Wnt proteins are transported through a variety of mechanisms not limited to filopodia contact (Routledge & Scholpp, 2019). To eliminate alternative methods of Wnt transport and identify Wnt proteins transported exclusively via

cytonemes, I implement a functionalised nanobody toolset. An exogenously introduced nanobody would theoretically localise to Wnt only accessible when presented extracellularly, therefore only delivering its payload to Wnt proteins in transit. Here, I explore the various cell lines and Wnt proteins available for my project and compare each for their optimal ratio of Wnt expression to presentation on filopodia. I characterise the nanobody secVHHmCh expression, observe its localisation and binding efficiency to Wnt-GFP overexpressed cells, and investigate potential options for regulating cytoneme behaviour as a possible control in the final assay. Lastly, I coalesced these results to finalise the working assay development conditions and explore bioinformatically supported Wnt binding partners that are expected to be observed. These bioinformatic investigations identify the highest likely binding partner candidates to be used as a reference for the final nanobody-biotin ligase assay mass spectrometry dataset.

3.2 Results

3.2.1 Characterising our toolset and filopodia morphology

Before any toolset development or optimisation can take place, we must first characterise the tools at our disposal as well as the methods of analysis we wish to take to characterise filopodia development. The aim of this thesis is to develop and optimise an assay that accurately and unbiasedly extracts Wnt interacting partners involved in Wnt transport, handover, and uptake from cytonemes. To perform this, I chose to employ a cell culture-based assay. This is to allow easy manipulation of assay conditions, ensure repeatability of results, easily identify complications and or obstacles during optimisation and allow a setting for altering the assay in different applications. The following cell lines were selected for testing morphological expression of filopodia and their expression of Wnt and nanobody based constructs.

HeLa cells were chosen as a standard robust cancer cell line for its reliability of cell culture and deep literature history. HeLa cells are female human cervical cancer cells isolated in 1951 by Henrietta Lacks (Masters, 2002). The cell line is fast growing and strongly resistant to culture stresses such as passaging and transfection. This in turn generates a high transfection efficiency, making it an ideal candidate for the purposes of the nanobody-biotin ligase assay. The caveats of the Hela cell line propose significant problems for its implementation, most notably its enormous genetic variation, multi-karyo phenoptype with an unusual number of chromosomes and departure from standard human genome (Masters, 2002).

AGS cells are another cancer cell line selected for similar reasons proposed for the HeLa cell line. AGS cells are a gastric adenocarcinoma cancer cell line isolated in 1979 (*ECACC General Cell Collection: AGS*, n.d.). These cells are equally fast growing and robust to environmental stresses, enabling similarly high transfection levels to that of HeLa. AGS cells were chosen among HeLa cells, as the results would complement work undertaken by colleagues that investigate Wnt involvement in gastric cancer within our lab, making the results of these cells of particular interest to these studies, in parallel. However, the caveat of AGS cells is that, similarly to HeLa cells, do not reflect physiological phenotypes due to their cancerous origins. In this way, both HeLa and AGS

cells cannot be used to directly compare against physiological cytonemes, but can be inferred from.

MEF and PAC2 cells are non-cancerous mouse and zebrafish embryonic fibroblast cell lines. The human analogue available for use were the HEK-293 cell line, a human embryonic kidney cell line. HEK-293 cells were not investigated as they display poor filopodia phenotype (Leijnse et al., 2015). MEF and PAC2 cells have reduced doubling time compared to the HeLa and AGS cell lines, as expected from their non-cancerous background. Furthermore, MEF and PAC2 cells are more sensitive to culture conditions and transfection efficiency reflects this reduced robustness (not quantified). The MEF and PAC2 cells are superior to the HeLa and AGS cells as they possess physiological genome and reflect a physiological handling of Wnt relative to their organism of origin, making them ideal model cultures for direct comparison to *in vivo* analysis. In particular, PAC2 cells are superior to MEF cells in this regard, as the zebrafish embryo presents an ideal model organism for observing Wnt handover during development. Taken together, these four cell lines were investigated to observe the appropriateness of filopodia morphology, DNA transfection and Wnt accessibility for use in the nanobody-biotin ligase assay.

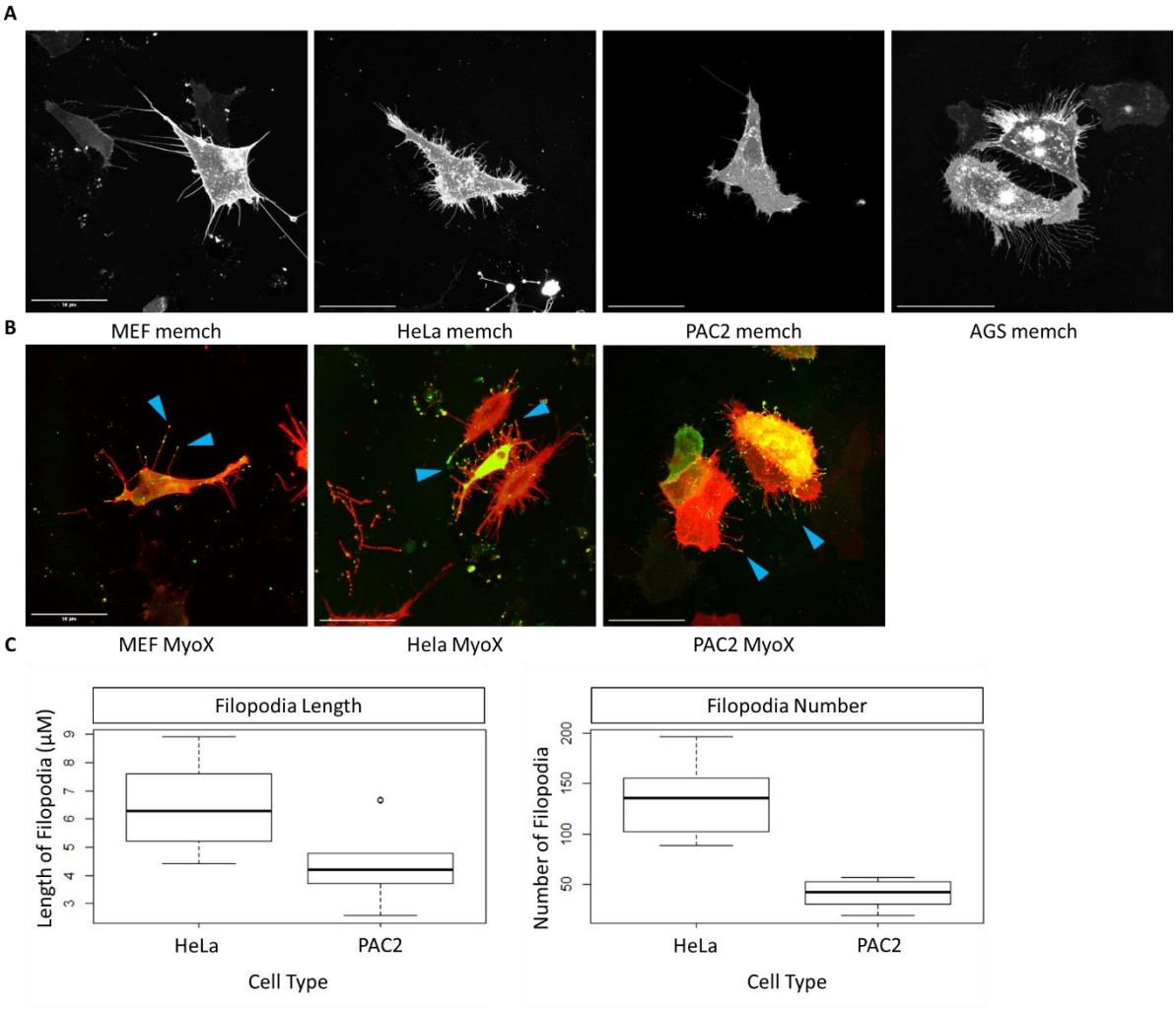

Figure 5. Characterising the four cell types. *(A) Membrane-mCh staining of MEF, HeLa, PAC2 and AGS cells respectively to highlight cell morphology. (B) MyoX-GFP (green) and membrane-mCh (red) co-transfection to highlight cell cytonemes, indicated by blue arrows. (C) Quantification of filopodia length and number, n=8 and 9 respectively. Scale = 50μM.*

HeLa cells displayed the highest number of filopodia with an average of 134 filopodia per cell, followed by PAC2 with an average of 40 filopodia per cell (Fig 5.C). Less variability is observed in the length of filopodia, with HeLa cells bearing an average of 6.4μM and PAC2 an average of 4.5μM (Fig 5.C). AGS and MEF cell filopodia number and length were not quantified. Cytonemes are distinct from filopodia as they are specialised for handing over or collecting signalling peptides between cells. Identifying these specialised structures from typical filopodia requires either observing signalling peptides in transit on these structures or another marker peptide to visualise them. MyoX is an

unconventional myosin motor protein that shuttles components that extend and stabilise the filopodia. MyoX has been shown to co-localise to Wnt8a on developing cytonemes and is implicated to be important in Wnt transport (Bohil et al., 2006). To highlight and observe these potential cytonemes, cells were transfected with membrane-mCh and MyoX-GFP. All cell lines showed suitable transfection and displayed a high efficiency of MyoX filopodia loading efficiency suggesting a high proportion of cytoneme phenotype (Fig 5.B). As observed with membrane-mCh overexpression alone, HeLa produce the highest number of MyoX filopodia, followed by PAC2, AGS and finally MEF. For the purposes of selecting cell lines that demonstrate the highest number of cytonemes, MEF cells were no longer investigated as PAC2 cells performed the same role as a physiologically relevant model but possess far more filopodia. Furthermore, PAC2 cells allow the development of tools, which can be used in zebrafish embryos *in vivo* for subsequent studies.

3.2.2 Wnt expression and phenotype.

Aside from identifying suitable cell lines that demonstrate large numbers of filopodia, it is essential that the cell line also express high percentage of Wnt positive filopodia. To investigate this, cells were co-transfected with both membrane-mCh and Wnt8a-GFP overexpression.

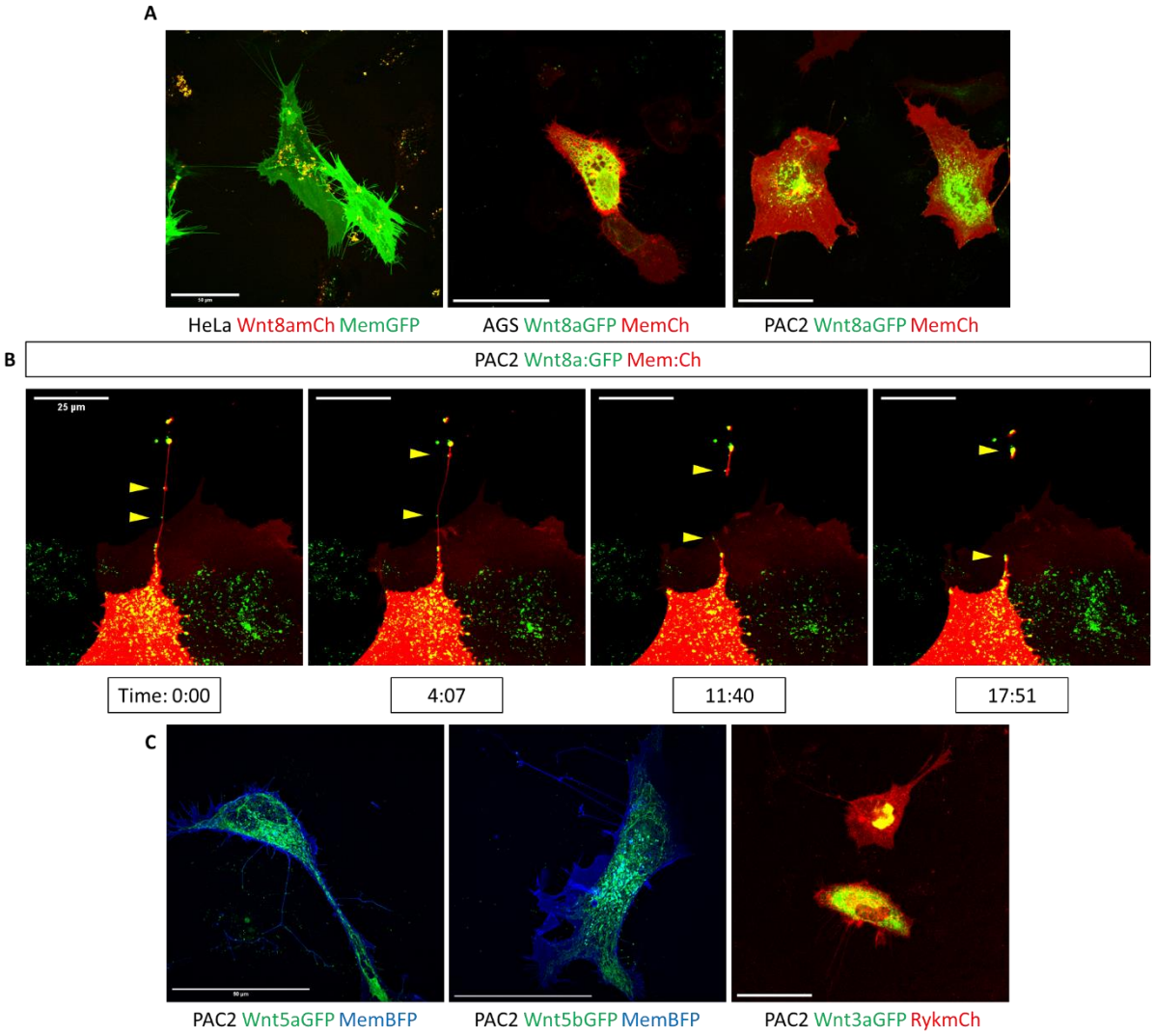

Figure 6. Wnt-GFP expression translocate to cytoneme tips. *(A) Wnt8aGFP overexpression in the three cell types HeLa, AGS and PAC2 cells. (B) Timelapse of PAC2 cells extending a Wnt8aGFP positive filopodia contacting neighbouring cell. (C) Alternate Wnt-GFP overexpression in PAC2 cells. Scale = 50µM.*

As shown in (Fig 6), all three cell types demonstrated Wnt bearing filopodia to various degrees of efficiency with PAC2 cells boasting the highest efficiency. Noticeably, the Wnt bearing cytoneme appears very limited. Coupled with the low transfection efficiency and the high proportion of Wnt-GFP existing in the cell body compared to the filopodia for all cell types suggests a very low degree of available Wnt targets on the cell surface. We investigated four different Wnts to examine their overexpression profile and decide on the Wnt-GFP that would produce the highest transfection efficiency and localisation to filopodia

protrusions. Wnt8aGFP and Wnt3aGFP are both canonical Wnt/b-catenin as opposed to Wnt5aGFP and Wnt5bGFP which primarily signal through the non-canonical Wnt/PCP/JNK pathway (Routledge & Scholpp, 2019). Wnt8aGFP appeared to show the most appealing phenotype out of all Wnt constructs with clearly defined puncta of Wnt scattered across both the cell body but also among filopodia. Wnt3a in contrast has less clearly defined puncta and a higher accumulation within the cell body. The non-canonical Wnts also show puncta but to a lesser degree to that of Wnt8a and appear to give way to a general cell body 'hazy' expression profile. Despite this, puncta of Wnt5a/b are observed on filopodia and in receiving cells. Importantly, the transfection efficiency of Wnt5a appears to trump all other Wnts studied (no quantification) which both consistently transfects multiple cells but is also observed in high quantity in receiving cells, suggesting a high degree of handover and therefore extracellularly presented targets. Whilst no functional studies were conducted to observe the functional capacity of these overexpressed Wnts, studies conducted by work colleagues using these constructs (Brunt et al., 2021; Mattes et al., 2018) prove their functionality. This is further corroborated by the appropriate expression profile expected for Wnt proteins. All in all, all four Wnt proteins present ideal candidates for the use as targets of the nanobody-biotin ligase assay. However, considering the proportion of available extracellular Wnt targets on the cell surface along with the low transfection efficiency it appears that quantity over quality may be more desired, leaving Wnt5aGFP the foremost candidate for the upcoming assay.

3.2.3 Nanobody expression and binding

The main goal of the assay is to generate an unbiased yet comprehensive extraction of all Wnt-interacting protein partners involved in intercellular handover of Wnt. To accomplish this goal, we aim to employ a biotin ligase approach which ligates an activated biotin molecule to any and all proteins within a very short distance to the ligase itself. Typically this approach is performed by fusing the biotin ligase directly to the protein of interest itself, however doing so to Wnt would violate the first goal of the assay which explicitly aims to elucidate binding partners at the very specific stage of extracellular mobilisation. Wnt undergoes many stages of modification, intracellular

translocation, recycling and handover (Routledge & Scholpp, 2019). Therefore, a Wnt-biotin ligase fusion product would extract protein binding partners at all these stages, producing protein hits without any distinction to the purpose they served Wnt at each stage of the Wnt proteins existence. This is where nanobodies provide an attractive yet elegant solution to this problem. secVHH, a GFP binding secreted nanobody can be produced from a non-Wnt-GFP producing cell to therefore localise only to accessible extracellularly presented Wnt-GFP which dramatically cuts down on the noise generated from binding partners in alternate stages of Wnt signalling. Furthermore, with the generalisability of a GFP-binding nanobody instead of a Wnt-specific binding nanobody, or a Wnt-biotin ligase fusion construct, we can employ this technique to any and all extracellularly secreted signalling proteins. Theoretically, the assay generated from employing these proteins provides not only a robust but easy to implement model allowing large throughput of screening of multiple different GFP-tagged Wnts. This could provide an invaluable resource for identifying all binding partners in a myriad of different signalling proteins for future investigations. To investigate the expression and binding capacity to Wnt-GFP we overexpressed secVHHmCh with various WntGFP constructs in co-transfected, co-culture and conditioned media.

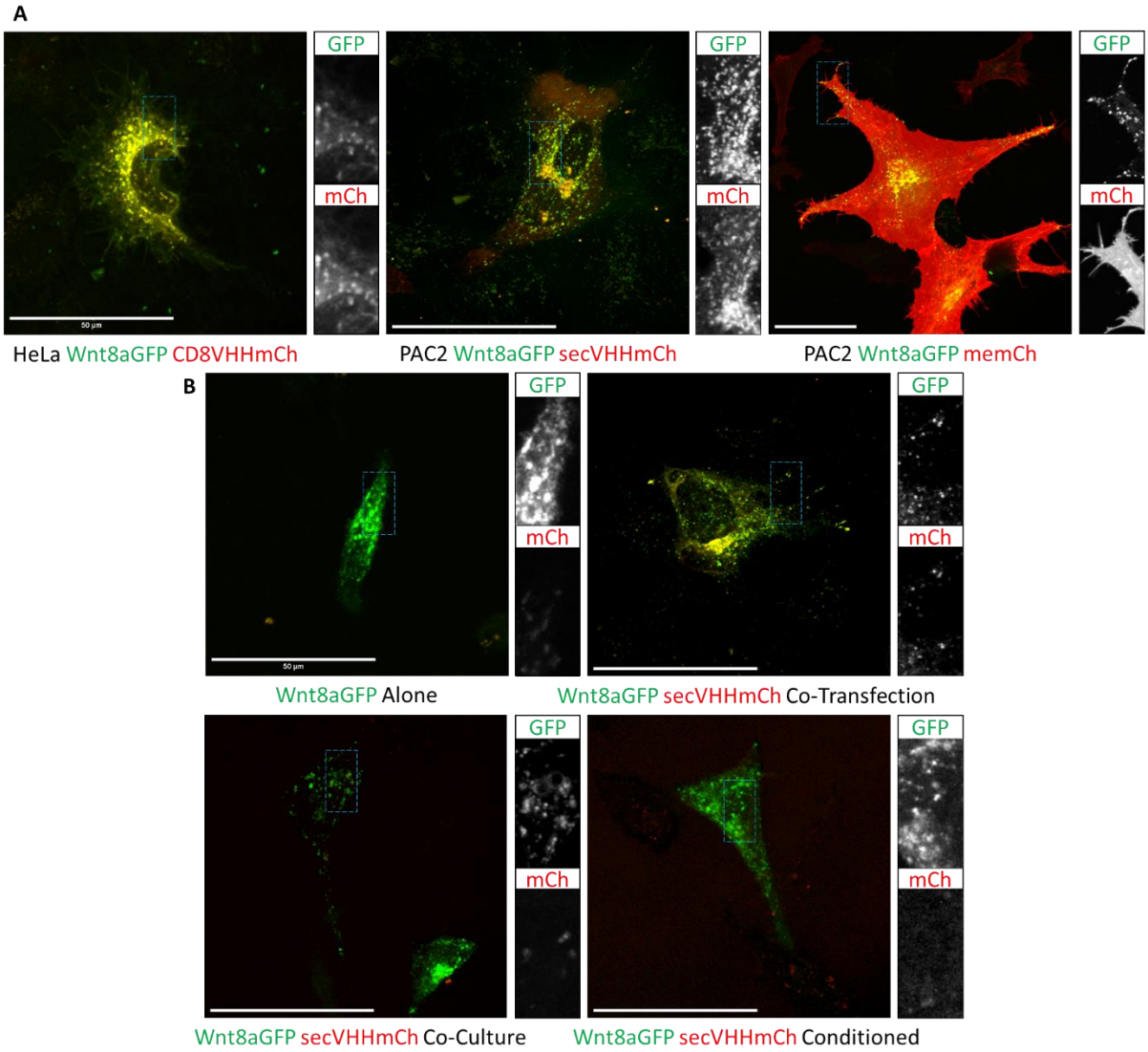

Figure 7. secVHH shows strong co-localisation to Wnt-GFP. *(A) VHH nanobody constructs co-expressed with Wnt8aGFP as either membrane bound CD8-VHH (morphotrap (Harmansa et al., 2015)), secreted VHH (secVHH) or negative control membrane-mCh. (B) PAC2 secVHHmCh co-localisation to Wnt8aGFP as either co-transfection, co-culture or conditioned media of transfected samples. Scale = 50μM.*

Morphotrap is a membrane bound CD8-VHH-mCh construct that binds to extracellular GFP on the surface of the expressing cell. As indicated by the name, morphotrap is often implemented as a system of retaining and binding GFP fused ligands to the surface of the membrane and prevent extracellular diffusion (Harmansa et al., 2015). Here, we used morphotrap to compare binding to GFP of that to secVHHmCh, a secreted variant of VHH nanobody. As

seen in figure 7, morphotrap appears to have near constant binding to GFP, essentially coating the cell in Wnt8aGFP. In contrast, secVHHmCh appears in lower quantity and tighter puncta but also co-localises to Wnt8aGFP. Of note, it can be observed puncta of secVHHmCh on Wnt8aGFP positive cells that do not appear to co-localise. Furthermore, a secVHHmCh producing cell will not present nearly as much co-localisation to that of morphotrap, though this is hardly surprising as the morphotrap is localised on the cell surface whereas secVHH must be secreted and therefore is far more diffuse in the media. Both constructs show significant co-localisation to Wnt8aGFP in comparison to membrane-mCh (Fig 7). As expected, co-transfected cultures demonstrate the highest level of co-localisation for mCh-GFP pixels compared to the co-culture and conditioned media samples. A concerning observation is the drop in co-localisation for GFP to mCh pixels for co-cultured and conditioned media samples (Fig 7). This may be due in part to multiple factors, the chief being the quantity of both free Wnt8aGFP and secVHHmCh in culture to be able to interact. As observed in figure 6, the proportion of Wnt on filopodia or cell surface membrane is vastly outweighed by the quantity found within the cell body. This further impedes the chance of interaction between secVHH and Wnt8aGFP when the modest levels of transfection efficiency are involved. Taken together, it appears that quantity of available binding for both Wnt and secVHH will be a significant challenge to overcome.

3.2.4 Cytoneme control and modulation

Whilst the nanobody based approach promises a reduction in Wnt interacting partners that aren't specifically involved in the Wnt handover it cannot achieve structural specificity. Wnt ligands are transported in a variety of different mechanisms, from juxtacrine cell-cell contact, to chaperone mediated diffusion via sFRPs or vesicles (Routledge & Scholpp, 2019). In the majority of methods, Wnt ligands are presented extracellularly and membrane-tethered which allows binding to secVHH. To distinguish results from only cytoneme-based handover of Wnt we must impose further controls. One such control can be the direct manipulation of filopodia through overexpression or chemical based inhibition. This would allow us to identify protein hits that do not survive in the cytoneme knock out control and therefore identify them as unique to such structures. To

approach this, we investigated two forms of inhibiting filopodia formation. Chemical inhibition presents a partially unspecific yet robust approach to force reduction in all filopodia across the culture. The two chemicals that we tested are ML141 and Latrunculin B. ML141 is a reversible non-competitive inhibitor of the small GTPases Cdc42 and Rac1 which are responsible for controlling cell morphology, migration, endocytosis and cell cycle progression, mainly through the modulation of the actin cytoskeleton (Surviladze et al., 2010). Latrunculin B is an actin polymerisation inhibitor, serving to reduce filopodia and lamellipodia outgrowth in a similar fashion to ML141 by directly inhibiting the actin cytoskeleton (Coué et al., 1987). I refer to these chemicals as partially unspecific as their functions are broad and not confined to a single function/phenotype. To achieve target specificity to only filopodia then the use of knock down of the inverted bar domain protein IRSp53 was also investigated. This was achieved using a mutant of IRSp53 in which four alanines are replaced by to lysines termed IRSp53^{4k} (Meyen et al., 2015). ISRp53 functions as a membrane inverse bar domain whose function is proposed to be either or both generating cell membrane defamations for actin cytoskeleton outgrowth and as a stabilising structural protein for filopodia (Yamagishi et al., 2004).

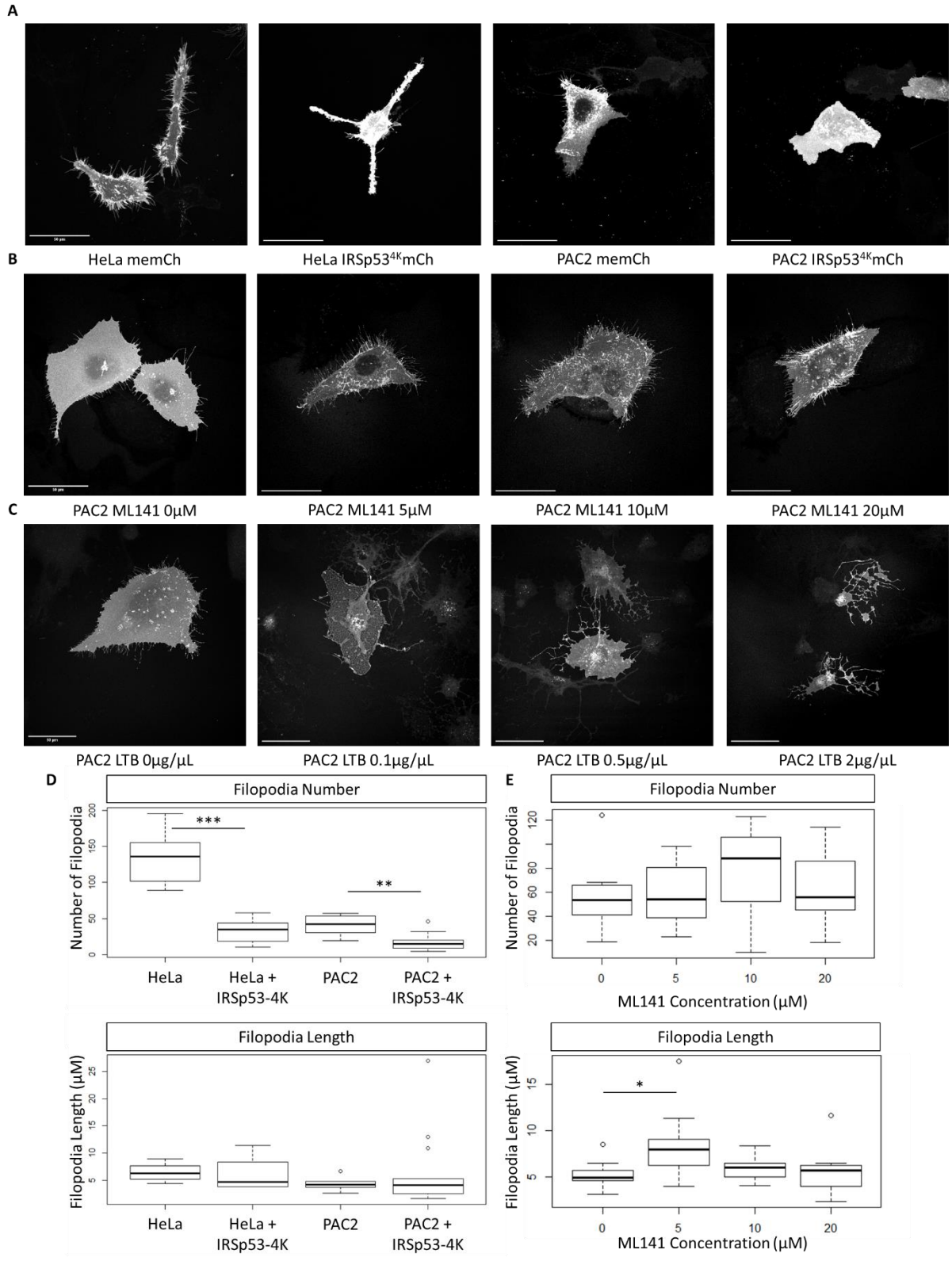

Figure 8. Cytoneme modulation by mutant overexpression and chemical inhibition. *(A) HeLa and PAC2 cells overexpressing membrane-mCh or IRSp53^{4k}mCh mutant. (B+C) Chemical inhibition of HeLa cells using various concentrations of (B) ML141 or (C) LatrunculinB small molecule inhibitors. (D) Quantification of filopodia length and number with or without IRSp53^{4k}mCh*

mutant. t10.41= 7.11, P < 0.0001 for HeLa and t14.99= 4.19, P < 0.001 for PAC2. (E) Quantification of PAC2 filopodia length and number with or without ML141. Scale = 50μM.

Two mutants of IRSp53^{4k} were generated fused to either mCh or GFP (Meyen et al., 2015). Interestingly, the GFP tagged IRSp53^{4k} had no noticeable effect on filopodia whereas the IRSp53^{4k}mCh mutant significantly reduced filopodia number for both HeLa and PAC2 cells but not a complete ablation (HeLa Mean ±SE = 134 ±12.69, HeLa-IRSp53-4K Mean ±SE = 32.29 ±0.55, PAC2 Mean ±SE = 40.44 ±4.71, PAC2-IRSp53-4K Mean ±SE = 16.61 ±0.46). The mutant had no effect on filopodia length on the other hand. An interesting phenotype observed for IRSp53^{4k}mCh was an increase in cellular bulging as seen in (Fig 8.A), a phenomena more pronounced in HeLa cells than PAC2 cells. The small molecule inhibitors were far less impressive with ML141 not demonstrating any decrease in filopodia number or length and LatrunculinB producing an incredibly severe phenotype (Fig 8.C). Interestingly, an increase in filopodia length was observed using only 5μM of ML141. Although further optimisation could have been conducted using these small molecule inhibitors, it was decided that any modulation of cytonemes would be done so using IRSp53^{4k}mCh.

3.2.5 Bioinformatics analysis and likely candidates.

This project relies heavily on the development, optimisation and success of the nanobody-biotin ligase assay to achieve the primary aims of the project. Success or failure of the final assay would be the deciding factor in discovering tangible binding partners' specific to cytoneme mediated Wnt signalling. An early step to defining a successful outcome for the assay would be to explore known biological mechanisms through bioinformatics analysis of the Wnt signalling pathway. Comparing the results of the final assay to the expected results generated from such a bioinformatics analysis would yield interesting results in both positive and negative protein hits. For example, we would expect results to vary depending on the Wnt ligand used but also for the different cell type or organisms used. Furthermore, in the event that we could not accomplish a functioning assay within project timelines, or should we discover that the aims

set out to achieve by such an assay were ultimately impossible, then a candidate protein chosen through this analysis would provide a useful contingency option.

A

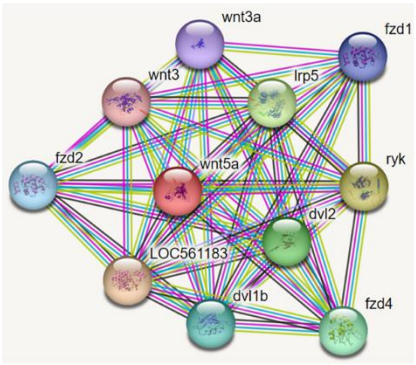

node1	node2	score
wnt5a	ryk	0.977
wnt5a	LOC561183	0.977
wnt5a	lrp5	0.976
wnt5a	dvl2	0.974
wnt5a	fzd4	0.972
wnt5a	dvl1b	0.965
wnt5a	fzd2	0.963
wnt5a	fzd1	0.963
wnt5a	wnt3a	0.959
wnt5a	wnt3	0.951

B

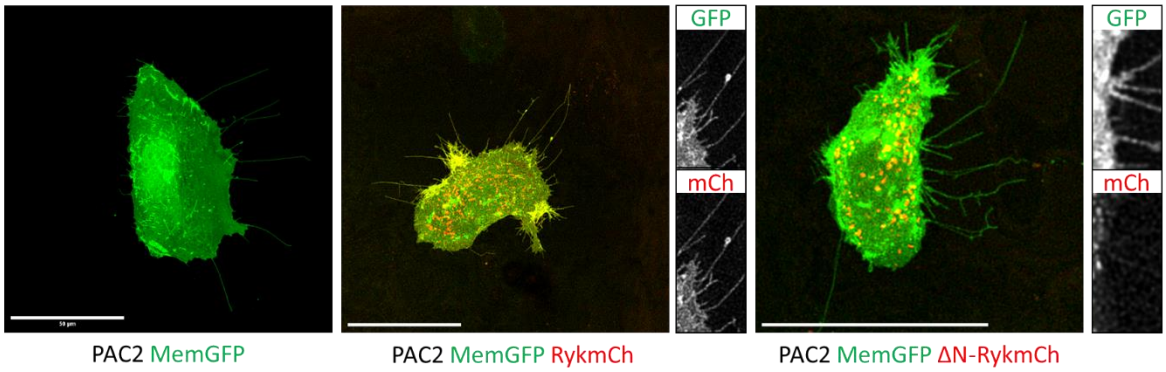

C

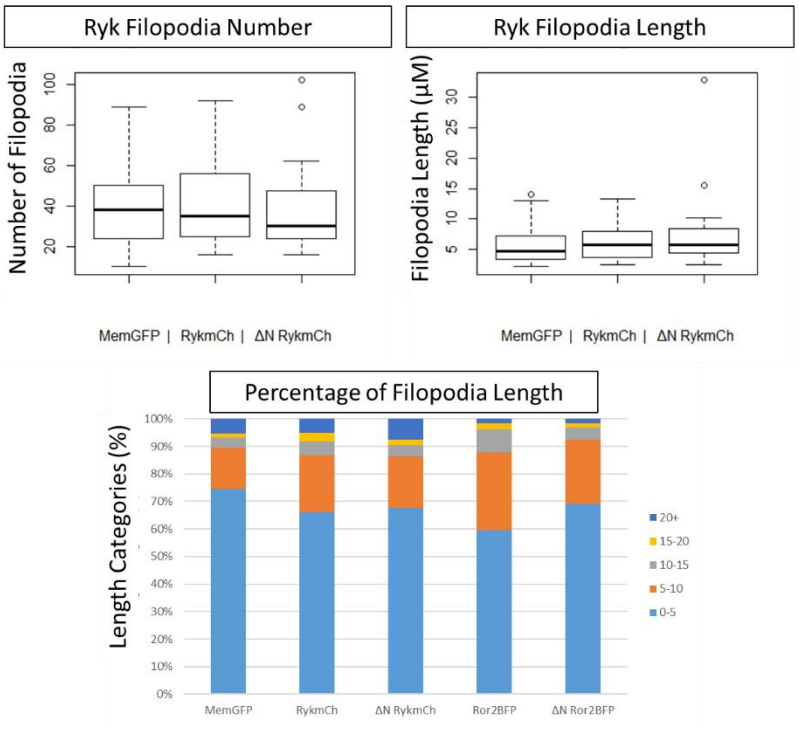

Figure 9. Bioinformatic exploration of potential Wnt5a interacting partners. *(A) Stringdb analysis of Wnt5a in the zebrafish. (B) Table of Wnt5a*

binding partners ranked on interaction score determined through Stringdb algorithm identifying frequency of target correlating within the genome, cellular co-expression, experimental data and associations within curated databases and publications. (C) Phenotype of Ryk and DnRyk overexpression in PAC2 cells, scale = 50μM. (D) Quantification of filopodia length, number and filopodia length distribution between Ryk and DnRyk overexpression.

Stringdb was used to explore the curated interactome of Wnt5a across the zebrafish database. Stringdb is a database of known and predicted protein-protein interactors whose purpose is identify direct and indirect associations between proteins for predicting system level function. The highest scored interacting partners to Wnt5a is the Ryk and Ror2 (LOC561183) protein (score=0.977), followed by Lrp5 (score=0.976), dvl2 (score=0.974) and fzd4 (score=0.972). Of note, these proteins Ryk, Ror2, LRP5 and Fzds all constitute cell surface membrane bound receptors for Wnt ligands. This make these candidates of the highest likelihood to be detected within the assay. As a contingency option, Ryk was selected out of this list for preliminary analysis. The decision to start investigating Ryk comes as twofold. Firstly, as Ryk presents itself (among Ror2) as the highest likely interactor with Wnt5a, it would save on both time and resources to investigate and optimise Ryk studies in parallel to the nanobody-biotin ligase assay. Secondly, should the results of this assay fail to meet expectations, then investigations into Ryk interaction with Wnt5a on cytoneme mediated signalling would provide tangible results. In this vein, PAC2 cells were overexpressed with both a functional and kinase-dead non-functional mutant of Ryk termed RykmCh and DnRykmCh respectively (Fig 9.B). The most notable aspect of RykmCh expression is a simultaneous membrane marker expression but also several small intracellular puncta (Fig 9.B). In contrast, the membrane localisation of DnRykmCh seems limited to the cell body with very little visible on filopodia, suggesting that the intracellular kinase plays an important role in its localisation. Sequence analysis and functional assays indicate that this kinase region is functionally dead; therefore, this observation could shed insight into its unknown function (Green et al., 2014). Interestingly, there appears to be no significant difference in the number and length of filopodia expressed by the cell with Ryk or DnRyk overexpression,

suggesting that the receptor does not influence cytoneme behaviour, at least in the absence of an overexpressed Wnt in co-transfection (Fig 9.C).

3.3 Discussion

In order to develop a biotin ligase based assay to unbiasedly extract and identify Wnt interacting proteins in the Wnt handover event we must satisfy various crucial stages. The first stage is to generate an assay that maximises the signal to noise ratio. This can achieved by maximising the quantity of our protein of interest and our nanobody-biotin ligase in culture. The ideal method of achieving this would be to generate a stably expressing cell line utilising a robust promoter. Further improvements to increasing signal to noise ratio would be to increase the number of available targets for our nanobody-biotin ligase construct. As seen in (Fig 5), overexpression in Wnt-GFP constructs mainly accumulate within the cell body while puncta of Wnt-GFP are observed on few of the total filopodia. While there is not a clear option to enhance the loading of Wnt-GFP on filopodia, this leaves us with relying on bolstering the quantity of the ligand itself to maximise availability to the nanobody-biotin ligase. On the flip side, maximising the quantity of nanobody is of equal importance, as observed in (Fig 6) the quantity of secVHHmCh pixels existing within Wnt8aGFP expressing cells is strikingly low. As localisation of the nanobody to Wnt-GFP is highly specific (Fig 6), non-specific binding should not pose a problem in the assay.

3.3.1 Intracellular accumulation of secVHHmCh/Wnt-GFP

An interesting property observed of co-localised secVHHmCh to WntGFP is the high quantity of intracellular accumulation (Fig 7.B). The secVHHmCh pixels show high abundance within perinuclear regions of the cell, perhaps an accumulation within recycling and or lysosomal degradative organelles (Pu et al., 2016). Regardless of the specific location of these accumulations, this phenotype raises a significant concern on the specificity of biotinylated proteins generated from the assay. In theory, an extracellularly introduced nanobody-biotin ligase would bind to an extracellularly presented Wnt-GFP peptide and subsequently biotinylate all Wnt related/critical proteins within proximity. An accumulation of intracellular secVHH would therefore suggest that we not only raise the risk of biotinylating Wnt interacting proteins that aren’t specific to this handover event, but that we also reduce the signal to noise ratio of desired

peptide extracted to the undesired intracellular peptide fraction. This therefore raises the need for carefully curating the controls to prevent this over-accumulation of intracellular secVHH involved in the final assay to minimise this hazard, however achieving a meaningful enhancement of desired signal over noise proteins may present itself a fruitless endeavour, and instead must be embraced as a significant caveat of the nanobody-biotin ligase assay as a whole.

3.3.2 Considerations to modulating cytonemes

Engineering a robust method for selecting specific subcellular regions of Wnt handover goes further than the aforementioned problem of intracellular accumulation of nanobody-biotin ligase. As mentioned previously, the nanobody-biotin ligase would bind unspecifically to all Wnt-GFP provided it is presented extracellularly. The assay by itself would therefore extract Wnt interacting proteins existing on extracellular vesicles, in extracellular chaperone proteins/extracellular matrix protein reserves, unspecific and or generic cell surface membrane and finally on cytoneme tips and or along length. Using controls to knockdown cytonemes provides an attractive option to filter out protein hits that cannot interact with Wnt as a result of this phenotype. As shown in figure 8, this is a feasible option and results in a satisfying significant reduction in number of filopodia, however it doesn't completely ablate all filopodia development. Should this result in a significant reduction in cytoneme specific Wnt related proteins then the application of this control would be warranted, however we must also inspect further complications associated with introducing more experimental parameters to our assay culture. Firstly, this requires a double or triple transfection for Wnt-GFP and IRSp534KmCh with or co-cultured nanobody-biotin ligase. As single transfection imposes significant culture stresses on the cells which result in modest to low transfection efficiencies, introducing more constructs for transfections would require significant optimisations and or volume of cells for culture. Should the work required to achieve this extra control warrant the effort and possible restrictions in culture viability then it should be pursued.

3.3.3 The tools at our disposal

Overall, the tools selected propose a strong potential for delivering the outlined goals of the assay. The nanobody secVHH demonstrates strong affinity for the Wnt-GFP protein of interest and is capable of localising to Wnt-GFP in co-transfection and co-culture assays. A long road of optimisations and development are to be expected to be necessary to overcome the limitations apparent at even this stage of the method development. Regardless of the challenges presented, it appears that the assay should deliver to at least a proof of concept for future usage and hopefully build a framework for future application for multiple different Wnt proteins and even different ligands/receptors on the cytoneme.

4 Chapter 2 – The Development and Optimisation

4.1 Introduction

Wnt-GFP transfections in chapter 1 demonstrated strong expression with consistent localisation to the cell surface membrane and filopodia tips. Furthermore, secVHH-mCh demonstrated equally strong expression profile. Both constructs co-localise to one another with high efficiency, demonstrating a strong foundation for the nanobody-biotin ligase assay framework. However, many questions were raised from these preliminary results, namely the high intracellular accumulation of Wnt-GFP/secVHH-mCh and the relatively low transfection efficiency. Both aspects raising a troubling prospect of high biotinylation signal noise. These aspects therefore require substantial optimisations to strike the right conditions of high protein expression with specific nanobody-biotin ligase localisation for strong signal-to-noise ratio.

The secreted nanobody secVHH-mCh alone cannot perform the biotinylation required for protein isolation and identification. Before full optimisations can take place, a suitable biotin ligase must be selected and ligated to secVHH-mCh. Indeed, this will introduce further optimisations required to identify ideal conditions for maximum biotinylation in minimal time. With the final nanobody-biotin ligase construct determined, only then can full optimisations be performed.

In this chapter, I aim to develop and optimise the nanobody-biotin ligase assay to co-localise to Wnt-GFP for proximity based biotinylation and subsequent extraction. I aim to develop a host of secVHH-biotin ligase constructs to compare expression and localisation to un-modified secVHH-mCh. Following on from this, I seek to maximise assay transfection efficiency and protein expression to maximise biotinylation from the nanobody-biotin ligase to Wnt-GFP. Finally, I observe the extent of protein biotinylation through western blot and streptavidin pulldown.

4.2 Results

4.2.1 Generating secVHH-biotin ligase

To generate the nanobody-biotin ligase construct I proposed cloning three possible biotin ligases. These included BioiD2, Apex2 and MiniTurboID. Each performs the same task with unique differences. BioID is the first promiscuous biotin ligase developed for biotin labelling. As such, several studies have demonstrated its robust utility in the literature (Samavarchi-Tehrani et al., 2020). BioID is slow to biotinylate, requiring a minimum of 3 hours of incubation to produce significant biotinylated proteins for use in Western blot or pulldowns (Samavarchi-Tehrani et al., 2020). BioID2, on the other hand, is a marked improvement on its predecessor, improving both biotinylation rate and robustness. Despite these improvements, BioID2 still requires overnight incubation for any appreciable rate of biotinylation (Samavarchi-Tehrani et al., 2020). Apex2 is a biotin ligase dependent on the presence of hydrogen peroxide for function. Apex2, unlike BioID2, is extraordinarily fast in biotinylating large volumes of protein in as little as one minute of incubation. This comes at the cost of requiring hydrogen peroxide, which is highly toxic to cell culture, however, if performed fast enough, it should not be of concern. Overall, Apex2 acts similarly to taking a photograph – generating a ‘snapshot’ of biotinylated proteins of a single instance in time as opposed to the long incubation period of BioID2, a desirable trait to biotinylate proteins found on the highly transient cytonemes. Finally, MiniTurboID is a relatively new biotin ligase generated through the directed evolution of yeast to generate one of two biotin ligases that specialise in rapid biotinylation without hydrogen peroxide. This directed evolution produced both the MiniTurboID and TurboID biotin ligases, both acting as superior versions of the BioID2 biotin ligase. As the name suggests, the MiniTurboID is the smaller of the two biotin ligases, being 28KDa in size, as opposed to TurboID, which is 35KDa. As size is a significant variable when designing a nanobody-biotin ligase, the MiniTurboID biotin ligase selected over the TurboID.

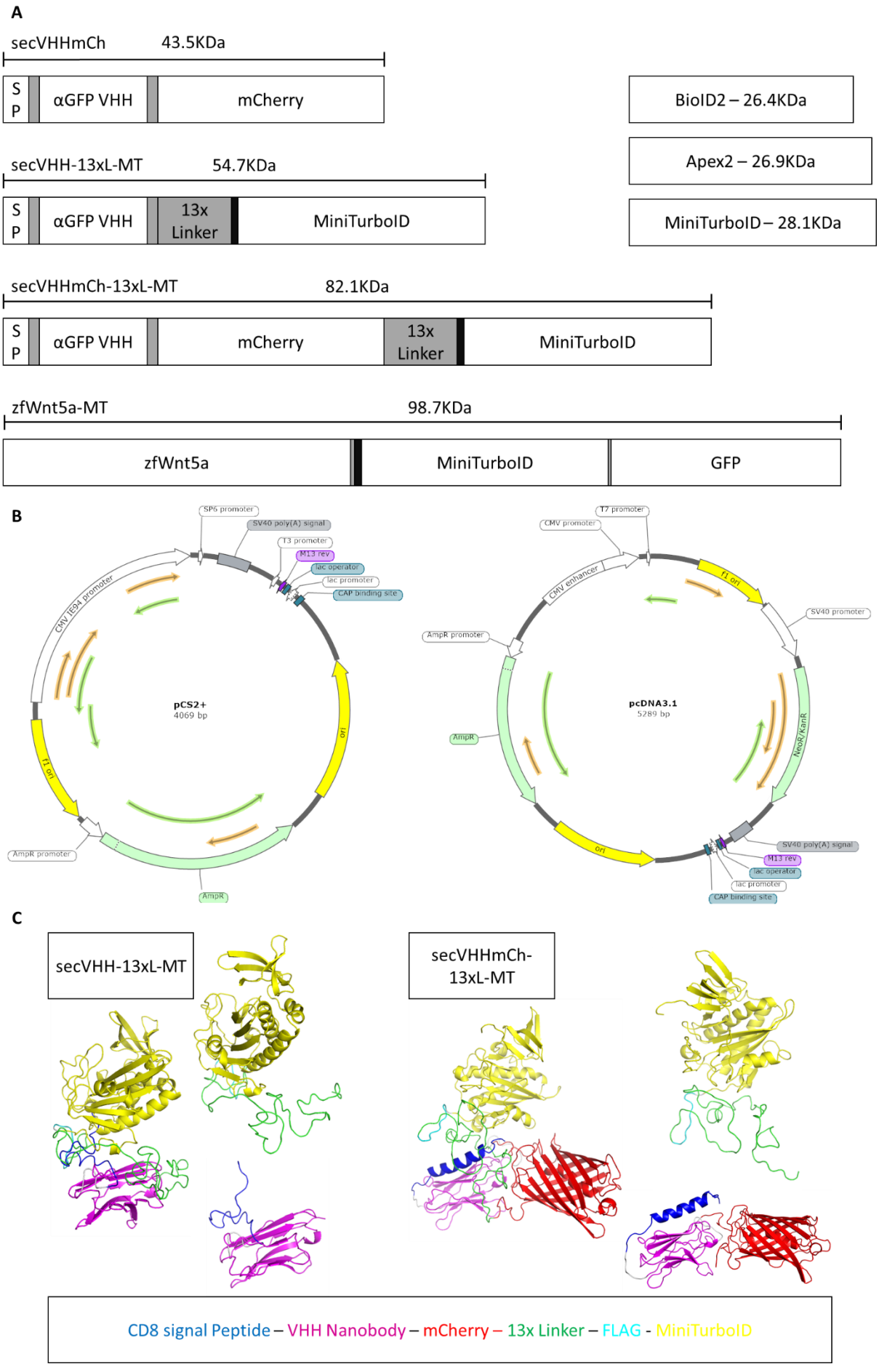
A
secVHHmCh
43.5KDa
S P
αGFP VHH
mCherry
BioID2 – 26.4KDa
secVHH-13xL-MT
54.7KDa
S P
αGFP VHH
13x Linker
MiniTurboID
Apex2 – 26.9KDa
MiniTurboID – 28.1KDa
secVHHmCh-13xL-MT
82.1KDa
S P
αGFP VHH
mCherry
13x Linker
MiniTurboID
zfWnt5a-MT
98.7KDa
zfWnt5a
MiniTurboID
GFP
B
pCS2+
4069 bp
SP6 promoter
SV40 poly(A) signal
T3 promoter
M13 rev
lac operator
lac promoter
CAP binding site
CMV IEPA promoter
ori
f1 ori
AmpR promoter
AmpR
pcDNA3.1
5289 bp
T7 promoter
CMV promoter
CMV enhancer
f1 ori
SV40 promoter
AmpR promoter
AmpR
ori
NeoR/KanR
SV40 poly(A) signal
M13 rev
lac operator
lac promoter
CAP binding site
C
secVHH-13xL-MT
secVHHmCh-13xL-MT
CD8 signal Peptide – VHH Nanobody – mCherry – 13x Linker – FLAG - MiniTurboID

Figure 10. Cloning of secVHH and biotin ligase. *(A) All biotin ligase plasmid constructs using either secVHH or Wnt. Black boxes represent FLAG tag. SP represent CD8 Signal Peptide. Figure sizes are proportional. (B) Plasmid vectors and all promoter sequences used for secVHH/Wnt expression. pcDNA3.1 plasmid contains the G418 resistance gene required for generating stable cell lines that the pCS2 plasmid lacks. (C) Predicted protein structures of secVHH/mCh – MiniTurboID using Phyre2 online software (Kelley et al., 2015).*

Before merging secVHH to a biotin ligase, I added an additional linker region to the nanobody-biotin ligase construct (Fig 10.A). I cloned out the FLAG tag/13xL linker region present on the BioID2 plasmid using ClaI and AscI overhangs for standard T4 cloning. In the first iteration of cloning products, I decided to omit the mCh region in order to minimise the size of the final construct, thereby increasing the protein maturation speed and penetrance in culture. As I later discovered, this would cause significant problems when generating stable cell lines. Therefore, the mCh was re-inserted using Gibson cloning into the secVHH-MiniTurboID (secVHH-MT) construct.

In order to maximise success, these three biotin ligases were selected and cloned simultaneously. The secVHH-Apex2 construct could not be cloned within the period allowed for this stage, however, the secVHH-BioID2 and secVHH-MT were successfully generated. A Wnt-biotin ligase construct was also attempted, initially designed as a comparison and contingency option. Although this construct contradicts the aim of using nanobodies for extracellular localisation to Wnts, it was sensible to ensure a biotin ligase system with a higher chance of success should the nanobody option fail.

secVHHmCh was received in the form of a *Drosophila* specific plasmid vector (pUAS) and so was subcloned into a pCS2+ plasmid for mammalian transfection. This plasmid was selected as it was routinely used for our cell culture with reliable transfection efficiency and intensity. Furthermore, this plasmid is excellent for generating mRNA for zebrafish embryo injections, opening up another avenue for experimentation. The pCS2+, however, does not contain any selectable markers for generating stable cell colonies, necessitating the need for the pcDNA3.1 plasmids. pcDNA3.1 plasmids are significantly larger

than the pCS2+ plasmid (1,200+ bp, Fig 10.B). The increased plasmid size caused concern for changes to transfection efficiencies, so all constructs were cloned in pCS2+ where possible and pcDNA3.1 for stable cells. Another aspect of these vectors was using a CMV promoter for transfection. CMV (Cytomegalovirus) is a robust standard promoter for typical transfection; however, it is viral in origin. As discussed later in the chapter, a viral promoter would not be suitable for long-term stable expression as many cell types can identify and silence it. Several attempts were made at replacing the CMV promoter with a zebrafish-Ubiquitin B promoter; however, these attempts took too long to achieve and were eventually stopped. Cloning of the promoter was likely hindered by its large sequence size (3,400+ kb) which would make both Gibson and T4 cloning challenging. Ultimately, the CMV promoter was retained, and stable cells were eventually achieved in the AGS cell line.

I also attempted cloning Wnt8/5a – MiniTurboID as a contingency option to the nanobody – biotin-ligase constructs and as a reference control. Despite multiple attempts at both T4 and Gibson cloning, this construct proved challenging to generate. I attempted to generate Wnt8a-MT first, following the same philosophy of the secVHH-MT construct by omitting the GFP. Similarly, to secVHH-MT, the lack of a fluorescent probe resulted in further steps required for visualisation by fixation and staining. Cloning for this construct appeared to be successful in both PCR and digest analysis; however, the construct could not be sequenced after multiple attempts. The Wnt5a-MT-GFP construct was attempted at the same time as the secVHHmCh-MT constructs. Unlike the Wnt8a-MT construct, the Wnt5a-MT-GFP construct was faster to clone. However, an error in the cloning design caused a frame shift in the construct was introduced at the beginning of the GFP, resulting in correct Wnt-MiniTurboID peptide sequence followed by a long sequence of incorrect peptide. Due to these cloning limitations, these two constructs were not used for the rest of the thesis.

4.2.2 SecVHH-MT effectively biotinylates *in vitro*

With the secVHH-MT constructs prepared, I aimed to observe its localisation and activity constructs in various cell types. Specifically, I wanted to observe the

differences in expression and sub-cellular localisation between secVHH and secVHH-MT in both intensity and transfection efficiency. As the secVHH-MT construct lacks the mCh fluorophore, fixations and staining with αFLAG was necessary.

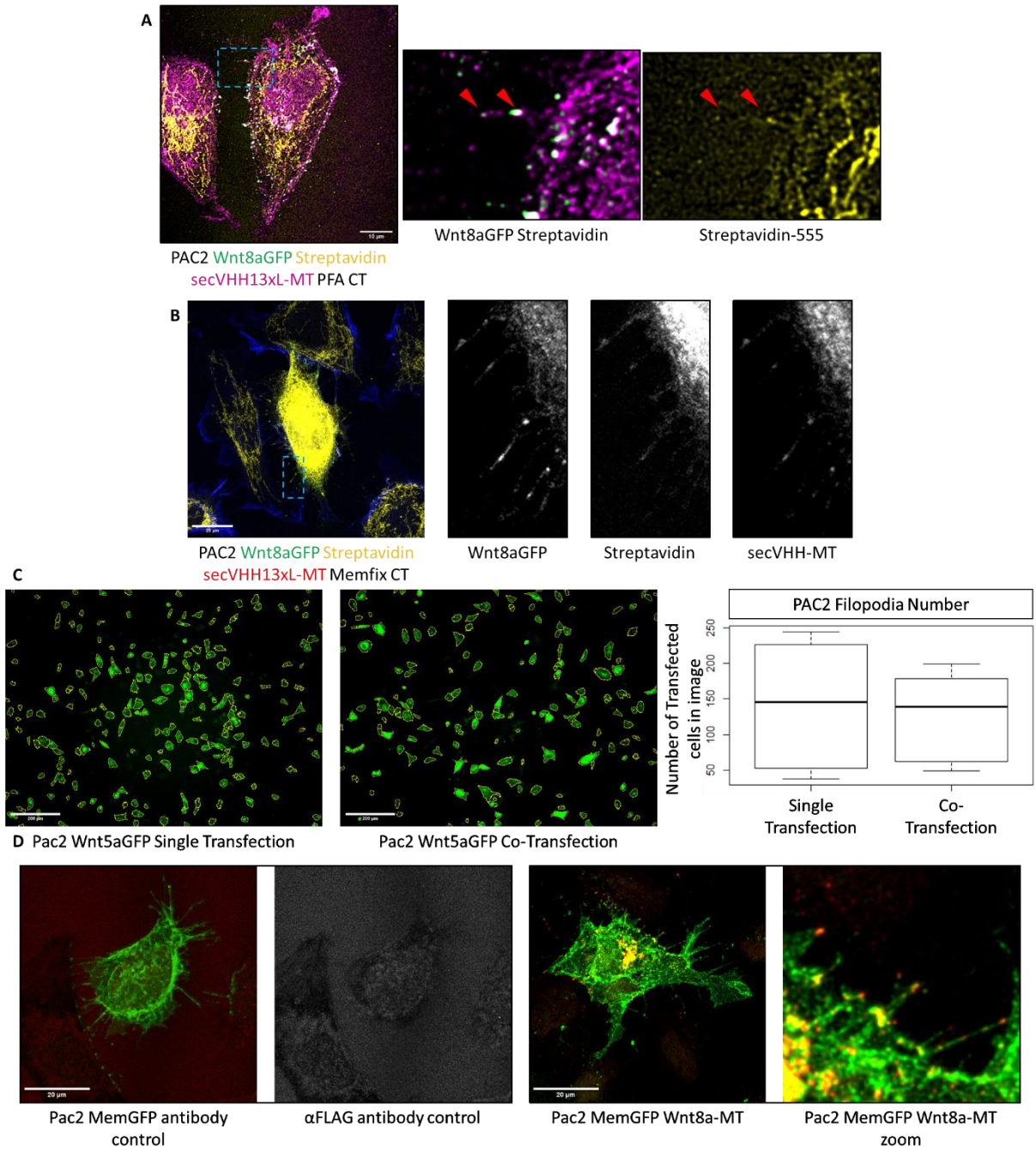

Figure 11. secVHH-MT biotinylates effectively in transfected cells. *(A) Wnt8aGFP expressing PAC2 cells fixed in PFA stained with streptavidin and αFlag (secVHH-MT). Red arrows highlight biotinylated filopodia. Scale bar = 10μM. (B) Wnt8aGFP expressing PAC2 cells fixed in Memfix stained with*

streptavidin and αFlag (secVHH-MT). Scale bar = 20μM. (C) Comparisons of transfection efficiency when using single or co-transfection. Scale bar = 200μM. Boxplot shows mean and standard deviation. N=12. (D) Mem-GFP and Wnt8a-MT transfected PAC2 cells fixed in PFA and stained with αFlag (Wnt8a-MT) compared to no-primary antibody and MemGFP only controls. Scale bar = 20μM.

The secVHH-MT appears to localise and behave identically to the secVHH by localising to Wnt-GFP (Fig 11). When stained with streptavidin-555, we see a generic mitochondrial staining, evidences by the several 'strings/matrix' of streptavidin staining, as expected of the high endogenous biotin accumulation in these structures (Fig 11.A). In Fig 11.B, streptavidin staining can be seen on the filopodia tagged with both Wnt8aGFP and secVHHMT, suggesting that the biotin ligase is active and biotinylates proteins within proximity. It should be noted the low ratio between possible secVHH-MT biotinylation highlighted by streptavidin staining between filopodia and cell body. This is extremely evident in Fig 11.B where the streptavidin channel is increased to show staining on the filopodia.

4.2.3 Optimising transfection efficiency

As observed in chapter one and secVHH-MT transfections images (Fig 6+7), standard transfection demonstrated low transfection efficiency in the cell population. As shown in Fig 11.A+B, the biotinylation from endogenous and secVHH-MT sources generated a small signal to noise ratio. It is therefore of importance that the maximum number of transfected cells are made in order to increase the already small proportion of filopodia biotinylated proteins.

As routine for our lab group, all cell culture transfections were conducted using Fugene, a non-liposomal transfection reagent combined with a serum-free media called Optimem (Nagy & Watzele, 2006). Exploring alternative transfection options was a logical step in identifying the most optimal transfection process. I used Lipofectamine-3000 and electroporation and compared the general transfection efficiency in PAC2 cells using Wnt8aGFP.

Lipofectamine generates plasmid-containing liposomes to inject the plasmid directly into the cell as the liposomes merge with the outer cellular membrane, thereby releasing its contents within the cell (Chong et al., 2021). Electroporation, on the other hand, uses short electrical pulses to disturb the cellular membrane, allowing permeabilization to plasmids (Shi et al., 2018). Both methods have demonstrated good success in a variety of cell types (Chong et al., 2021).

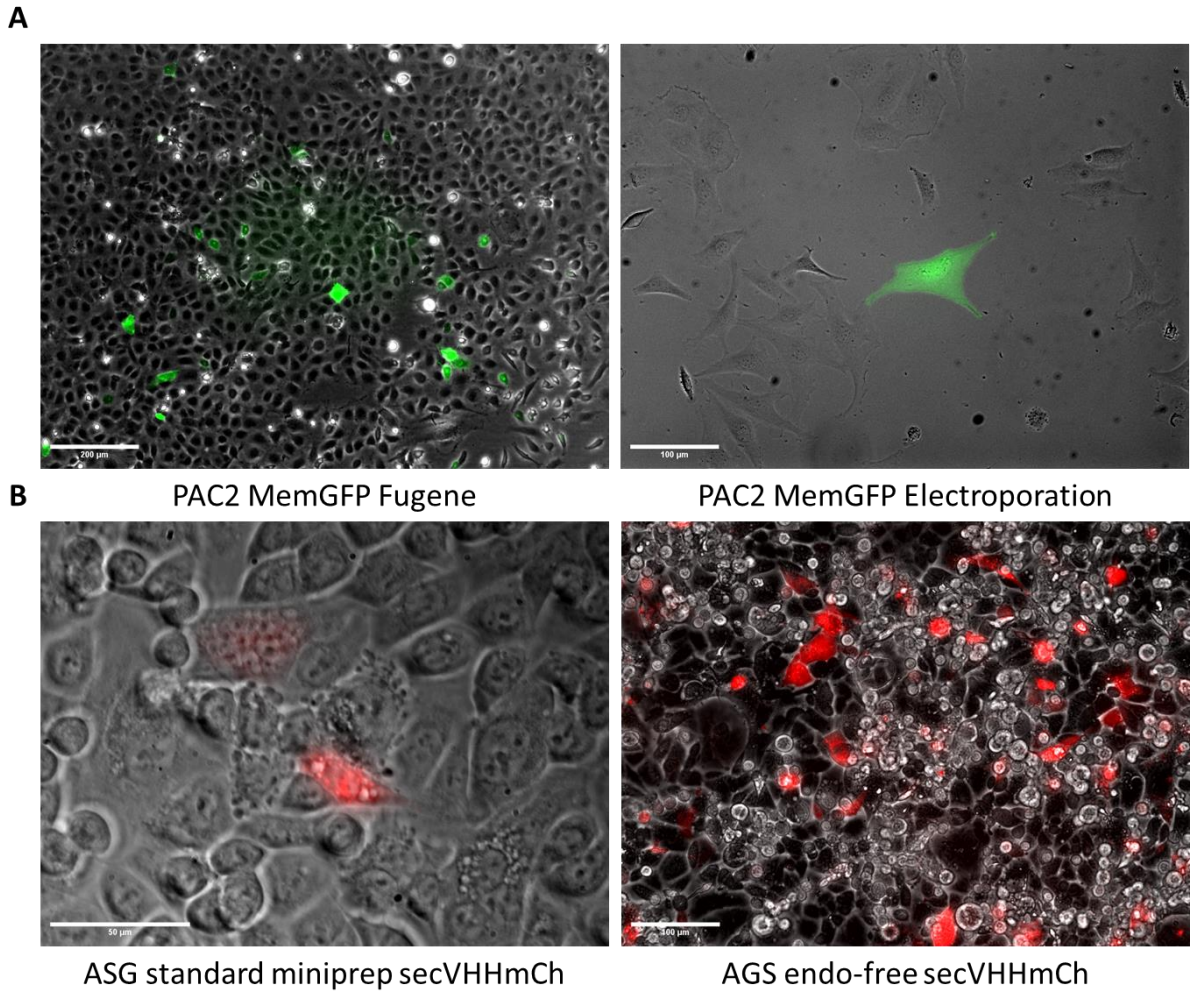

Figure 12. Endo-free prepped Fugene demonstrates the best transfection vehicle. *(A) Transfection efficiency comparison between Fugene and electroporation techniques. (B) Transfection efficiency between standard and endo-free maxi-preparation of the plasmid construct secVHHmChMT.*

All attempts using Lipofectamine ended in failure to transfect any cells and, at worst, resulted in severely high toxicity to the cell culture. While this phenotype was shocking, it is unlikely to be attributed to a fault in the Lipofectamine kit due to its prevalent use in literature, but rather, improper use of the kit and/or experience. Despite multiple attempts, Lipofectamine transfection was excluded. Electroporation, on the other hand, had substantial success with several colleagues in the lab group. The successful transfection attempts were seen in both AGS and PAC2 cells, however, for unknown reasons, this success was not transferable to my culture conditions. It is possible that while the electroporation conditions were set correctly for the cell type in question, the plasmid constructs used were not suitable. As observed in published works (Chong et al., 2021), the size of the plasmid can have dramatic effects on transfection efficiency. Regardless of speculation, electroporation was equally ineffective, if not worse, than Fugene transfection as Lipofectamine had demonstrated.

While alternate transfection strategies had proven fruitless, an alternative method of preparing DNA plasmid constructs had remarkable benefits. A typical plasmid preparation technique involves transforming E. coli bacteria to generate a large plasmid DNA concentration. The bacteria are then dissolved in strong detergents and filtered to yield pure plasmid DNA in water (Kachkin et al., 2020). The standard mini-prep removes bacterial proteins and precipitates only DNA using isopropanol. This process, however, does not extract only plasmid DNA as trace amounts of endotoxin are present in the final eluent. Endo-free mini-prep takes this process and incorporates extra steps to remove this contaminant, thereby reducing cellular toxicity and improving transfection efficiency. Using an endotoxin-free preparation produced vastly improved transfection efficiency as seen in Fig 12.B. The result of this made all subsequent plasmid transfection switch over to an endo-toxin free preparation.

4.2.4 PAC2 Stable cell line generation

Despite the benefits of using endotoxin-free plasmids, the final assay would benefit greatly from maximising transfection efficiency to as close as 100% as possible. The final option for increasing the proportion of transfected cells was

to generate a stable cell line for each plasmid construct. As such, I generated stable cell lines to express Wnt8aGFP and secVHH-MT in PAC2 cells. As seen in chapter 1 Fig 6, PAC2 cells demonstrated the most attractive Wnt loaded phenotype of all cell types investigated. PAC2 cells also presented the highest proportion of Wnt loaded cytonemes compared to unloaded cytonemes. Finally, PAC2 cells are non-cancerous, primary zebrafish embryo fibroblasts, allowing all results generated from this cell line to be directly translatable for use in zebrafish embryo experiments. In conjunction with Wnt8aGFP and secVHH-MT cell lines, I generated Wnt8aGFP/IRSp534K and MiniTurboID cell lines for a cytoneme and cell body negative controls, respectively.

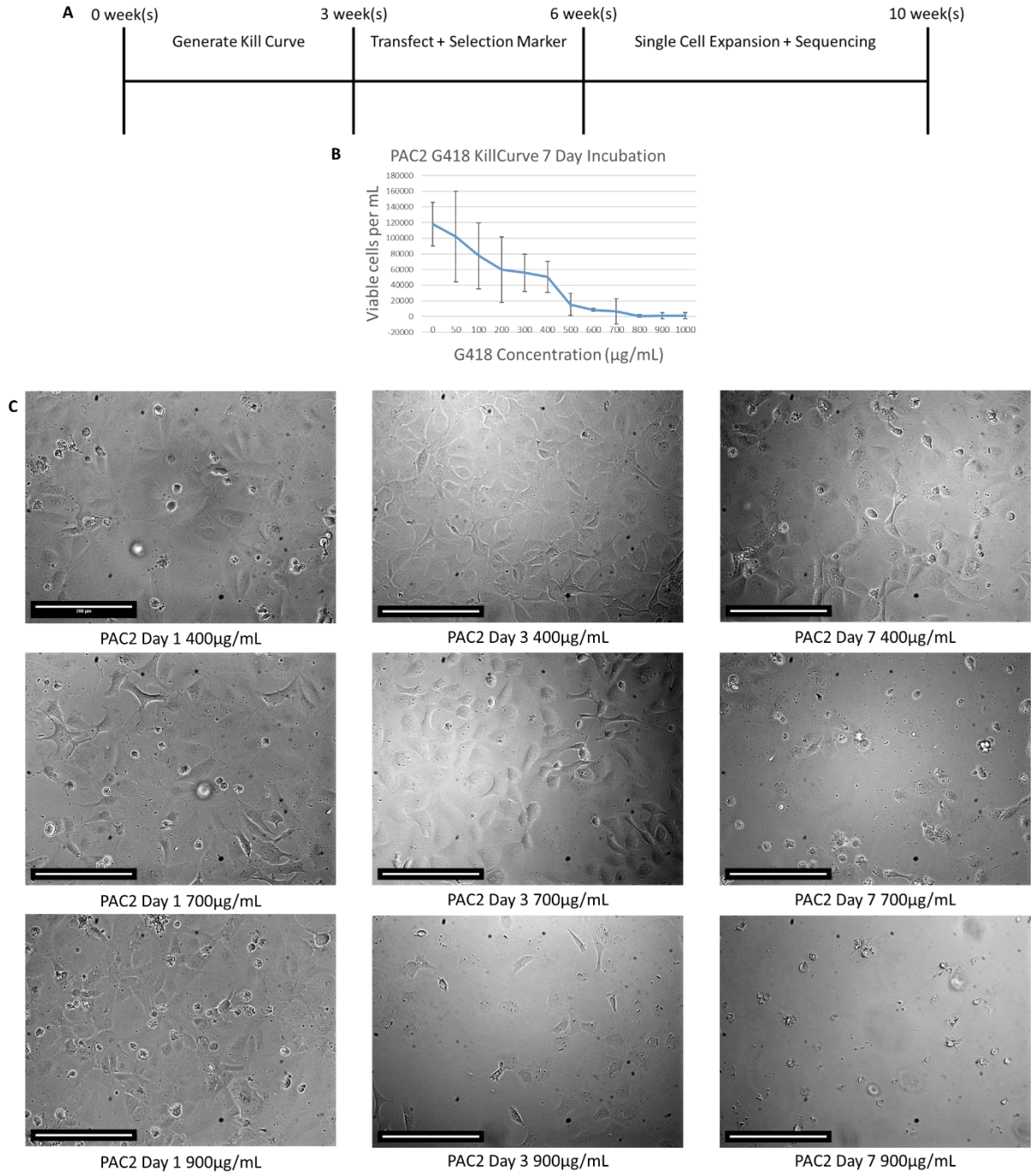

Figure 13. Stable PAC2 Cell Kill Curve Generation. *(A) Timeline of the stable cell line generation process. (B) PAC2 kill curve in response to G418. (C) PAC2 cell culture response to varying concentrations of G418 over the seven-day incubation period. 400/700/900 µg/mL represent the low, optimal and high doses of G418 selected for generating the stable cell lines.*

Before transfecting the cells, I sought to determine the concentration of Genetecin (G418) required to select for cells that contain the pcDNA3.1 plasmid. To do this, I developed a kill curve of concentrations ranging from 0 –

1000µg/mL of G418 over the course of seven days and measured the culture viability by passaging and counting the cells in the same manner as typical passage. As we see in Fig 13.B, the cell culture begins to react to as little as 50µg/mL up until a maximum of 800µg/mL which caused extensive cell death. This resulted in generating three different concentrations of G418 to apply to the polyclonal culture of transfected cells. The low concentration being 400µg/mL, optimal concentration 700µg/mL and high concentration being 900µg/mL. Cells were transfected with pcDNA3.1 plasmids and left to grow for 2 days to allow insertion into the genome. Following the incubation period, the cells that were transfected were subjected to varying concentrations of G418 and incubated for a duration of 7 days. Cells were then transferred as single cells into 96 well plates and left to grow as a colony.

During the course of my PhD, I had attempted to generate stable cells twice. The first attempt was using PAC2 cells. I intended to generate a Wnt8aGFP, Wnt8aGFP+IRSp53^{4K}, secVHH-MT and FLAG-MiniTurboID cell lines. The Wnt8aGFP and secVHH-MT cell lines were chosen to be co-cultivated for the final mass spectrometry analysis. The Wnt8aGFP+IRSp53^{4K} was chosen to generate a cytoneme negative control to identify proteins specifically localised to the cytonemes and the FLAG-MiniTurboID was chosen to identify intracellular biotinylated proteins that were not specific to Wnt8a-GFP interaction.

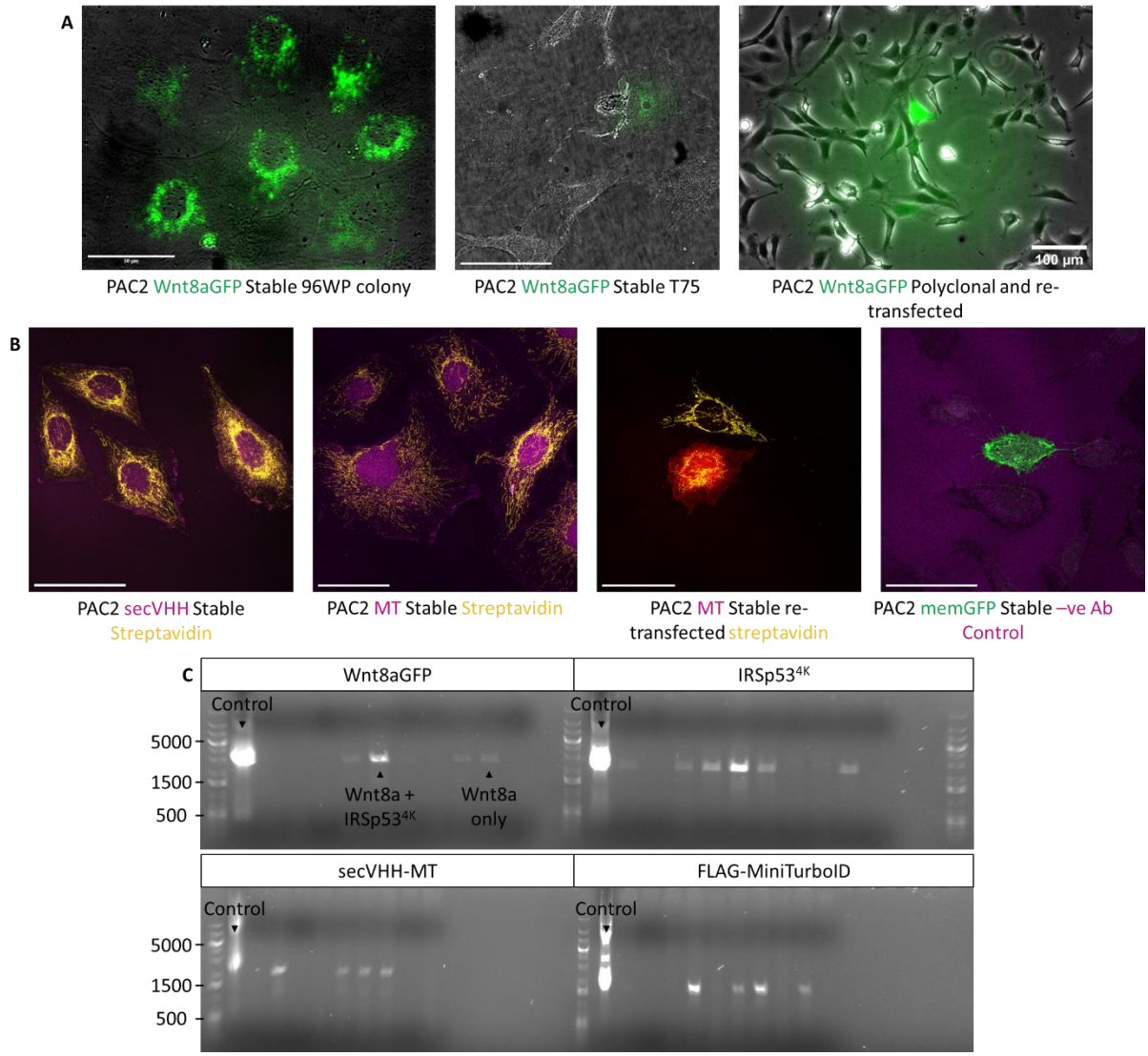

Figure 14. PAC2 stable cell lines failed to mature. *(A) PAC2 cell colony expressing Wnt8aGFP in the 96 well plate vs the same colony left to grow to confluence in a T75 plate. In comparison, polyclonal Wnt8aGFP cells used for the first mass spec (see chapter 3). (B) Stable PAC2 cell colonies grown to T75 plate confluence fixed in PFA and stained with anti-FLAG and streptavidin. Re-transfection of PAC2 MT stable colony highlights the lack of MiniTurbo in the stable cells and the subsequent absence of cell body wide biotinylation produced from the MiniTurbo. Negative control stained with secondary but no primary antibody. (C) PCR of stable cell lines using primers labelled for each gel. The control band shows original plasmid. Wnt8aGFP and IRSp53^{4K} PCR gels depict identical cell colonies. Wnt8aGFP or IRSp534K exclusive cell lines are indicated. secVHH-MT and FLAG-MiniTurboID cell lines are not from identical cell colonies.*

Unfortunately, there were several mistakes during my first attempt at generating these lines. The first oversight was the time to generate a stable cell line. As PAC2 cells are primary, non-cancerous cells, their lifetime is limited. As the final cultures developed, the cells slowed their doubling time, with the Wnt8aGFP+IRSp53^{4K} cell line senescing almost entirely. The second oversight was the removal of mCh in the secVHH-MT/FLAG-MiniTurboID plasmids. While intended to enhance protein production by reducing size and, therefore increasing effectiveness, this error massively increased the time and effort required to generate the line. Instead of using fluorescent cells as an indicator of stable expression, each cell colony from the 96wp across both lines were grown to maturity to then be sequenced via PCR. Positive PCR tests were not sufficient to prove expression in the line and so fixation of the cells or western blotting with anti-FLAG tag stains were required to prove presence of mature protein. Finally, the third oversight was the use of the CMV promoter to drive expression of the construct. The CMV promoter is standard in plasmids for its robust and powerful expression; however, in many cell types, this viral promoter is detected by the host and silenced (Mehta et al., 2009). This aspect was not addressed during the cloning of these constructs as generating stable cell lines using CMV in AGS cells were demonstrated by lab colleagues with great success. In the event of PAC2 cells, it appears that this was not the case and in Fig 14.A we see significant reduction in GFP expression and in Fig 14.B near negligible staining.

4.2.5 Transfected secVHH-MT Activity and Western Blot Optimisations

Despite the various problems faced trying to optimise transfection efficiency, it was important to investigate and optimize the activity of transfected secVHH-MT. I decided to examine the culture conditions when introducing biotin to the media and observe the ideal incubation period and concentrations for effective biotinylation. As described previously, cytonemes are highly transient and dynamic, with Wnt traversing along the length of and on the tip of these structures (Stanganello & Scholpp, 2016). Therefore, I decided to limit the biotin incubation time to capture Wnt present on these structures and avoid prolonged biotinylation of Wnt that escaped the cytonemes. MiniTurboID has demonstrated robust biotinylation in 10 mins of incubation, equivalent to 18

hours of BioID2 in the same concentration of biotin (Branon et al., 2018). To determine the ideal biotin incubation period, I compared the biotinylation levels of cells exposed to biotin for up to an hour. Similarly, I investigated the minimum concentration of biotin required to generate the most optimal biotinylation. Ideally, I sought to add enough biotin until I received diminishing returns on biotinylation to avoid adding excessive biotin, which could impede pulldowns during protein extraction due to competition between biotinylated proteins and free biotin molecules for streptavidin.

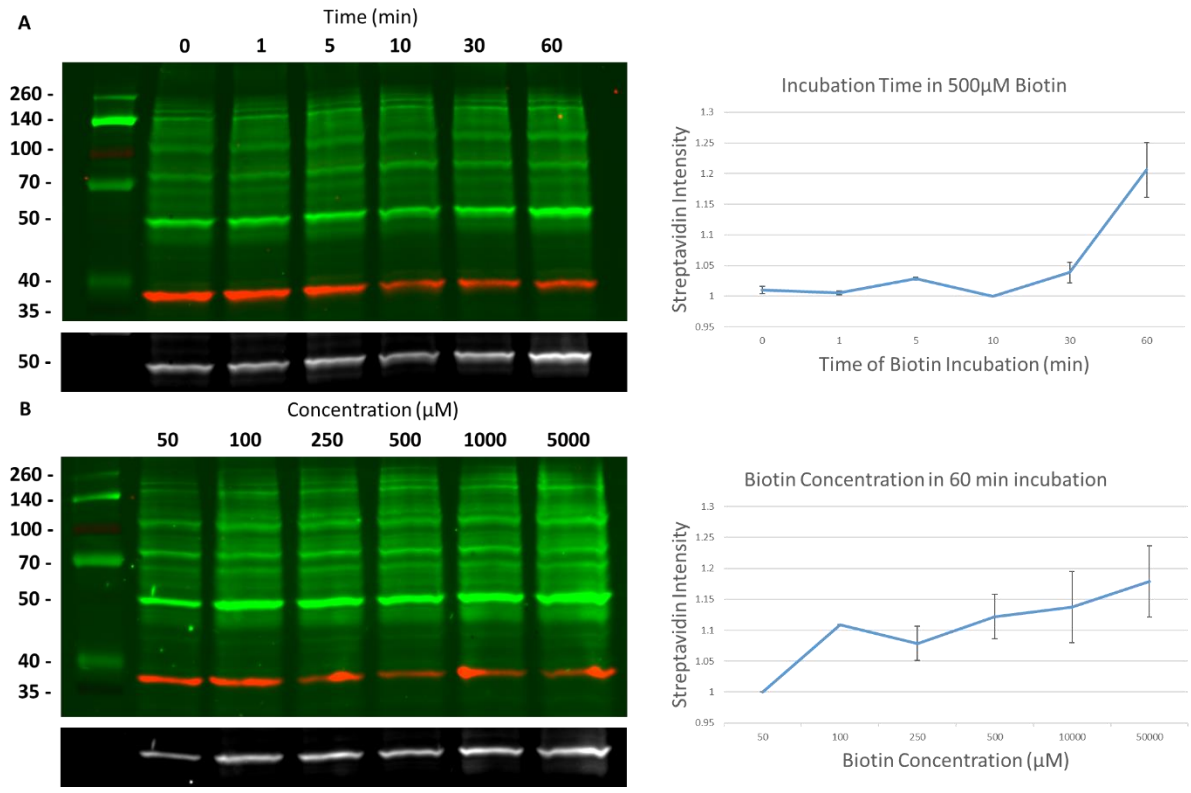

Figure 15. MiniTurboID Culture Response to Biotin Concentration and Incubation Time. *(A) Western blot of transfected secVHH-MT AGS cells incubated in increasing lengths of time in 500µM of biotin. Quantification of this western blot measuring the intensity of streptavidin band representing secVHH-MT (highlighted by bright streptavidin band at 55KDa). (B) Western blot of transfected secVHH-MT AGS cells incubated in increasing concentrations of biotin for a total of 60 mins. Quantification of this western blot in the same manner as (A). (A)(B) Western blots stained with GAPDH (red + grey bands below colour blot) to measure protein concentration and streptavidin (green) to measure biotinylated proteins. All samples were transfected identically and*

simultaneously. Both graphs have N=2. Streptavidin intensity normalised over GAPDH staining. Error bars show standard deviation between data.

As expected, the level of biotinylation rises as the incubation time increases (Fig 15.A). It was surprising to see that the levels of biotinylation show little difference up until the 30-minute mark, increasing by only 0.03-pixel intensity, then rapidly increasing at 1 hour five-fold by 0.17-pixel intensity. Initially, I expected levels of bitoinylation to increase rapidly after even a short exposure to biotin as demonstrated in the literature (Branon et al., 2018). As this was not the case, I decided to use 60 mins as the standard incubation time as a compromise between maximising biotinylation while reducing the possibility of non-cytoneme specific biotinylation that may occur when the bound WntGFP – secVHH-MT complex escapes the cell surface membrane/cytoneme.

It is worth noting the unique streptavidin patterning on these blots, termed a ‘biotin barcode’ (Fig. 15). This biotin barcode is a result of proteins of various molecular weights being biotinylated and therefore stained in western blot. However, without the wild type comparison, it is impossible to identify unique biotinylated bands distinct from endogenous biotinylation.

A similar trend to the incubation time was observed for the biotin concentration assay, although this time with a more proportionate increase (Fig 15.B). The levels of biotinylation raise rapidly by 0.1-pixel intensity from 50µM to 100µM, then a further 0.02 from 100µM to 500µM where it slowly raises another 0.05 from 500µM to 5mM. Although there is high variance as the concentration increases, it was decided that a concentration of 500µM would be made standard. This was decided from two decisions; the first decision as this concentration was reported by previous experiments using a similar nanobody-based biotin proteomic study (Xiong et al., 2021). The second being that while gains in biotinylation are only 1/5th of that made from 100µM, a concentration of 500µM would ensure an excess of biotin present for maximal biotinylation without causing too much hindrance to streptavidin-based extraction later.

4.2.6 Transfected secVHH-MT Biotinylation

With biotin incubation conditions established, the last step before running the final assay would be to characterise the activity of secVHH-MT in culture with Wnt-GFP. To investigate this, I cultured AGS cells transfected with secVHH-MT and Wnt-GFP to extract their lysate for western blot analysis. In contradiction to the data gathered thus far, I opted to use AGS cells for western blot as the cell count far exceeded that produced by PAC2 cells. The reduction in cells of PAC2 made generating enough lysate for western blot a significant challenge in of itself, an obstacle later tackled through increasing culture volume from 6wp to T25/T75 culture plates. In addition, I opted to extract the cell lysis without the use of Trypsin. This avoids damage to cell surface membrane proteins, which should constitute most extracted proteins post-biotinylation. Thus, unless stated otherwise, all protein lysates will be extracted without Trypsin for this reason.

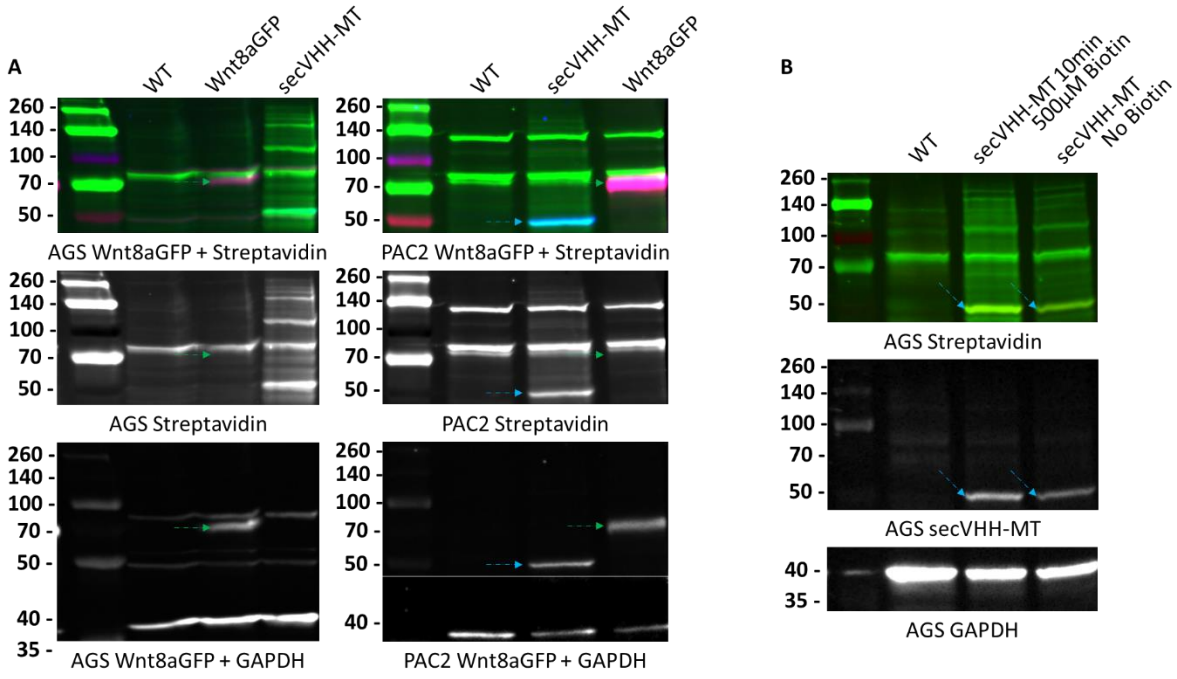

Figure 16. secVHH-MT and Wnt8a-GFP protein quantity post-transfection. *(A) Comparison western blots of AGS and PAC2 cells transfected with either Wnt8aGFP or secVHH-MT. Western blots stained with αGFP (Wnt8aGFP – Red), αFLAG (secVHH-MT – Blue) and streptavidin (biotinylated proteins – green). (B) Western blot comparing secVHH-MT transfected AGS cells collected with or without 10 min incubation in 500µM biotin. Western blot stained with αFLAG (Blue) and streptavidin (green). (A+B) Green arrows*

indicate Wnt8aGFP and blue arrows secVHH-MT. Both Western blots stained with GAPDH using the same secondary as Wnt8aGFP (red).

All samples collected and analysed by western blot were loaded with equal quantities of protein as demonstrated by GAPDH staining (Fig 16.A+B). secVHH-MT develops a biotin barcode unique from the wild type samples in both PAC2 and AGS cells (Fig 16.A). Endogenous biotinylation can be observed in PAC2 cells at 75 and 130 KDa (R. Ahmed et al., 2014; Housley et al., 2014) and in AGS cells at 75 KDa (Grant et al., 2019), both sources originating from the mitochondria as biotin dependant carboxylases. Excluding endogenous biotinylation, we see a unique and distinct biotin barcode from secVHH-MT with unique bands in AGS cells at ≈100 and 140 KDa. PAC2 secVHH-MT transfected cells have a broader range of biotinylation, with no bands standing out more than the rest. Furthermore, the secVHH-MT band at 55 KDa is also intensely stained with streptavidin. This is expected as secVHH-MT should biotinylate itself the most, suggesting that the biotin ligase is active and functional. The αFLAG for the AGS western blot is not shown as the signal was poor.

Interestingly, when compared to the GAPDH staining, PAC2 cells appear to express higher levels of Wnt8aGFP than AGS cells. This may have been due to confounding factors such as the greater culture volume required for PAC2 cell lysate collection or the differences in GAPDH staining between the two species resulting in less GAPDH staining.

As expected, we see an increase in streptavidin staining in as little 10 minutes of 500µM biotin added to transfected secVHH-MT (Fig 16.B).

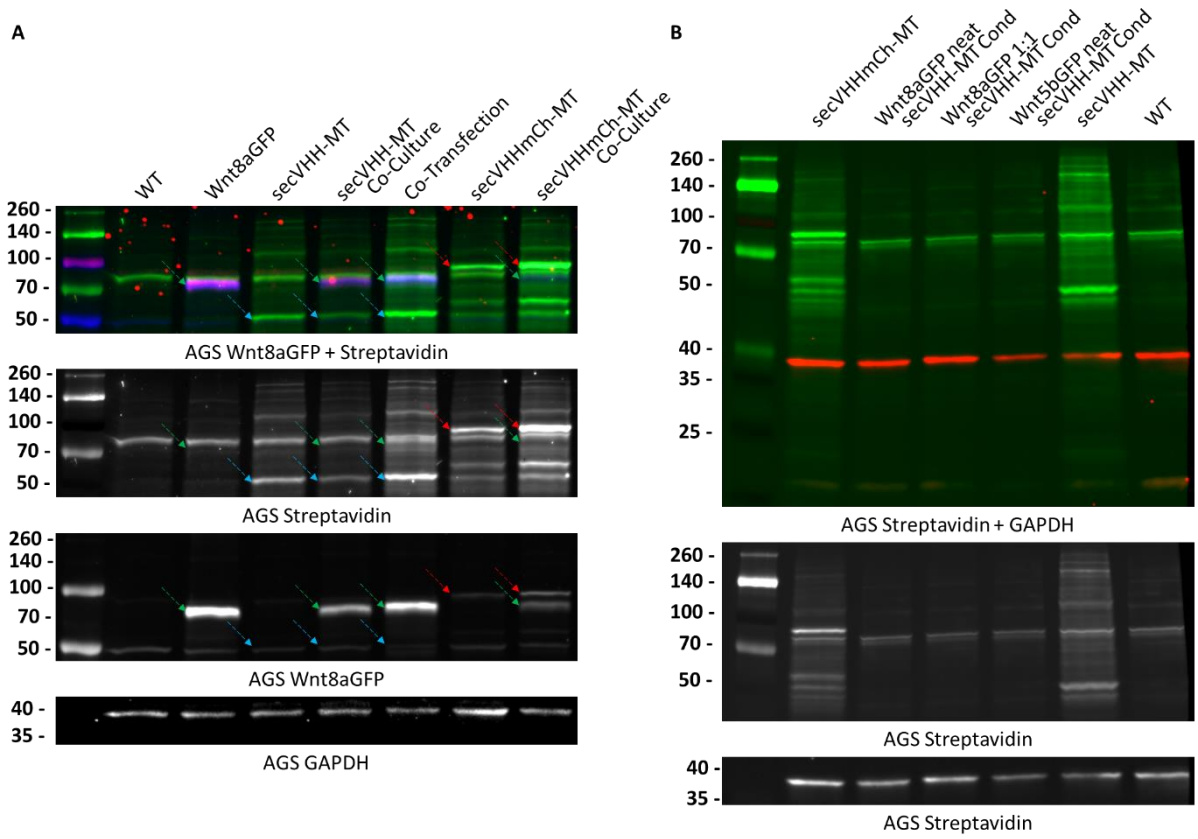

Figure 17. Co-Transfection, Co-Culture and Conditioned Media of secVHH-MT with Wnt-GFP. *(A) Western blot of AGS cells transfected with Wnt8aGFP and/or secVHH-MT in a co-culture or co-transfection. Western blot stained with streptavidin (green), αGFP (blue) and GAPDH. Green arrows indicate Wnt8aGFP, blue arrows secVHH-MT and red arrows secVHHmCh-MT. (B) Western blot of AGS cells transfected with Wnt8a/5aGFP and treated to conditioned media of secVHH-MT. Western blot stained with streptavidin (green) and GAPDH (red).*

secVHHmCh-MT produces its own streptavidin barcode like secVHH-MT, however, secVHHmCh-MT produces a unique barcode different from the secVHH-MT barcode, suggesting a difference in localisation as a result of the additional mCh (Fig 17). secVHHmCh-MT also heavily biotinylates itself as shown by streptavidin staining, all together demonstrating it is active and functional (Fig 17.A).

Wnt8aGFP shows similar levels of expression from the single transfection and co-transfection. Half of the signal intensity is observed from the co-culture, which is to be expected as half of the pool of transfected cells is mixed with

another half of non-Wnt8aGFP transfected cells. Streptavidin staining shows endogenous staining at 75 KDa, making observations for biotinylated Wnt8aGFP difficult as the Wnt8aGFP is 69 KDa. Despite this overlap, it appears there is a lack of a definitive streptavidin band at the Wnt8aGFP. This may, however, not be indicative of no biotinylation from the reasons described above, and the signal may not be detectable. The αGFP antibody appears to be promiscuous in binding as it stains secVHHmCh-MT. As the antibody is polyclonal, it is likely that the antibody has a small affinity to GFP-like proteins like mCh.

Unfortunately, all attempts at conditioned media have no effect on Wnt-GFP transfected cells regardless of using neat conditioned media or conditioned media diluted in fresh media. This is likely a limitation resulting from the low transfection efficiency resulting in too few secVHH-MT in the conditioned media to be detectable in the western blot.

This point marks the first attempt at generating the cell lysate of Wnt8aGFP PAC2 cells either co-transfected or co-cultured with secVHH-MT for the first mass spectrometry analysis. As the stable PAC2 cells failed to develop, the decision was made to use polyclonal cells generated after 7 days of G418 incubation. These polyclonal cells were then re-transfected to increase transfection efficiency further (Fig 14.a). To see the results of this first round, see chapter 3 section 5.2.1.

4.2.7 AGS Stable Cell Line Generation

Learning from the mistakes of the PAC2 stable cells, I re-attempted to generate stable cells in the AGS cell line. Unlike PAC2 cells, AGS cells do not have a time limit on cellular senescence, addressing the first oversight. Furthermore, as mentioned previously, AGS cells have demonstrated strong and persistent expression under a CMV promoter from colleague's works (data not shown). Finally, all plasmid constructs used contained a fluorescent marker to reduce workload and time of generating the stable lines.

At this stage of development, a decision was made to change the principle Wnt investigated from Wnt8a-GFP to Wnt5a-GFP. Wnt5a is a non-canonical Wnt with preferential binding to non-canonical Wnt co-receptors such as Vangl2, Ror2, Ryk and Fzd2 as opposed to Wnt8a preference for canonical Wnt co-receptors LRP5/6. Despite this, both Wnts have been observed to transport in identical methods. I chose to switch to Wnt5a for two reasons, the first being that much of the latest published data from our lab have used Wnt5a-GFP. The second reason being the high Wnt5a-GFP transfection efficiency (demonstrated in Fig 11.C) which would help overcome the limitation of low signal-to-noise biotinylation.

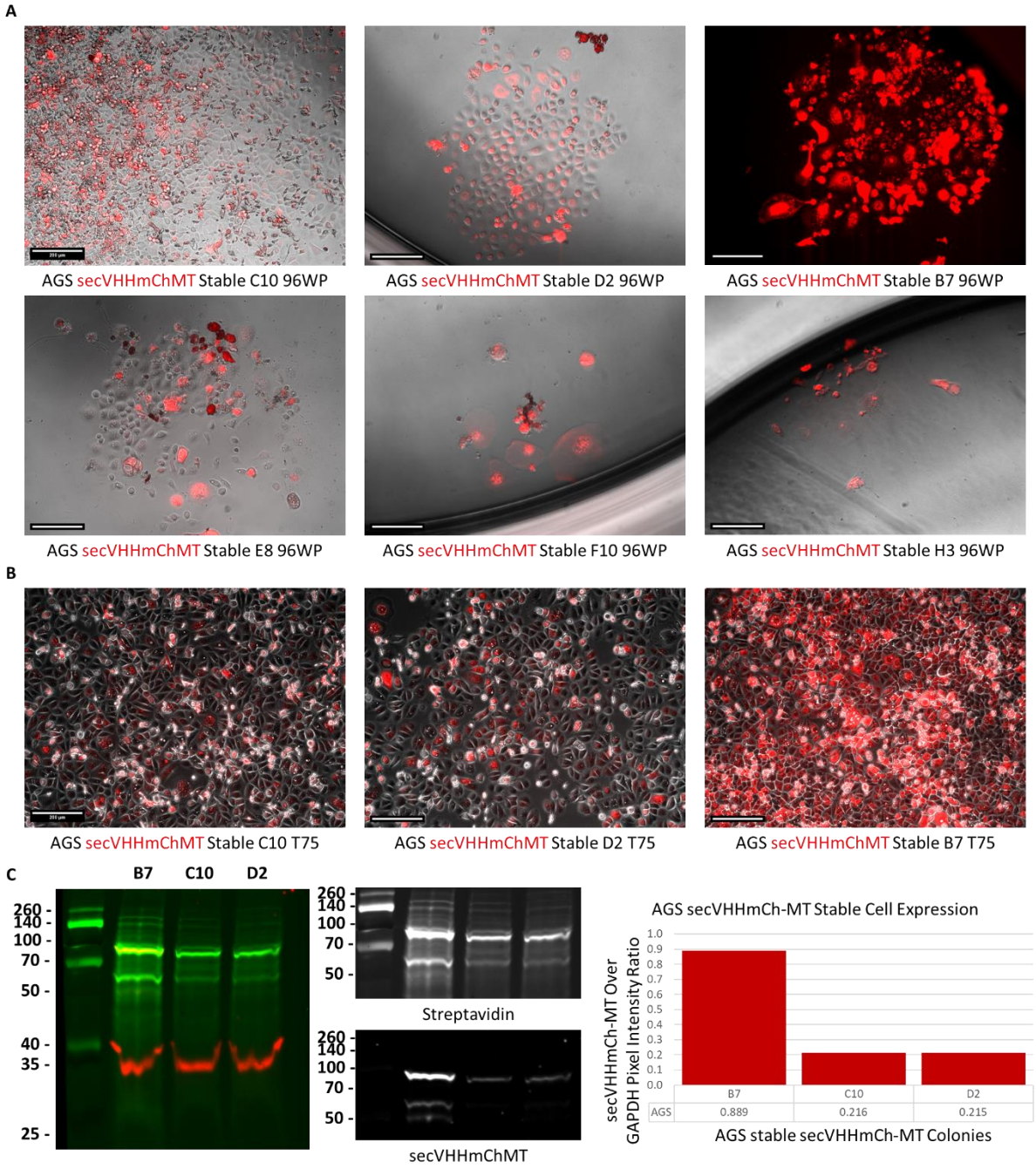

Figure 18. AGS stable cell lines exceeded expectations. *(A) Brightfield and mCh fluorescence images of AGS stable cell colonies expressing secVHHmCh-MT in 96 well plate. B7 brightfield data was oversaturated and so removed. Scale bars = 200µM. (B) Brightfield and mCh fluorescence images of AGS secVHHmCh-MT stable cells in T75. (C) Western blot of AGS secVHHmCh-MT stable cells to compare levels of secVHHmCh-MT and intensity of biotinylation. Samples were not incubated in biotin prior to collection. Cell lysates collected using Trypsin. Western blot stained with streptavidin (green) and GAPDH (red) to measure biotinylated proteins and total protein mass of sample respectively.*

Quantification of αFLAG (secVHHmCh-MT) pixel intensity divided by the GAPDH pixel intensity to compare protein load. N=1.

For an unknown reason, the Wnt5aGFP transfected AGS cells did not survive the G418 incubation period, and so could not be generated. Despite this, the secVHHmCh-MT lines were immensely successful, producing three lines of strong and consistent secVHHmCh-MT expression (Fig 18.A). These lines lasted for several passages each but displayed reduced fluorescence intensity after an excess of 15 passages and a unique culture morphology (data not shown) of excessive clumping. Cell lines that reached this point were terminated.

Interestingly, each colony brought to T75 confluence exhibited unique physiology compared to standard AGS cells and between colonies. Colony C10 was the first colony to grow to confluence, demonstrating rapid doubling time. Colony D2 grew faster than B7 but slower to C10, making it the second colony to reach confluence. Colony B7 by contrast grew very slowly, reaching confluence weeks after colony C10 and D2. For this reason, colony C10 was used initially for co-culture experiments. This changed once B7 reached confluence as it demonstrated the strongest and most persistent expression of mCh out of all colonies (Fig 18.B). Indeed, B7 outperformed both C10 and D2 4-fold when comparing secVHHmCh-MT and GAPDH pixel density ratio (0.889 vs 0.216 and 0.215 respectively). This is also apparent by the increased streptavidin intensity from B7 in comparison to C10 and D2 despite no additional biotin added prior to collection.

4.2.8 AGS Sourced secVHHmCh-MT phenotype

The advent of a stable and robustly expressing secVHHmCh-MT cell line provided an invaluable resource for the Wnt-cytoneme proteomic assay. These stable cells heralded a turning point in assay optimisation as it promised to solve the leading issue obstructing the success of the assay; maximising secVHHmCh-MT protein load. Up until this stage, generating enough nanobody to localise to Wnt-GFP constructs seemed only feasible with co-transfected

cells. Now that the AGS secVHHmCh-MT B7 line producing significantly increased quantities of secVHHmCh-MT I decided to investigate possibilities in co-culture and conditioned media treatments of Wnt-GFP transfected cells. This raised an interesting conundrum however, as the stable cells are human cancer AGS, do I switch the principal cell line to AGS, or would it be possible to co-culture AGS cells with PAC2 cells in PAC2 cell culture conditions? I first investigated this through live imaging of AGS secVHHmCh-MT cells in co-culture to AGS and PAC2 cells.

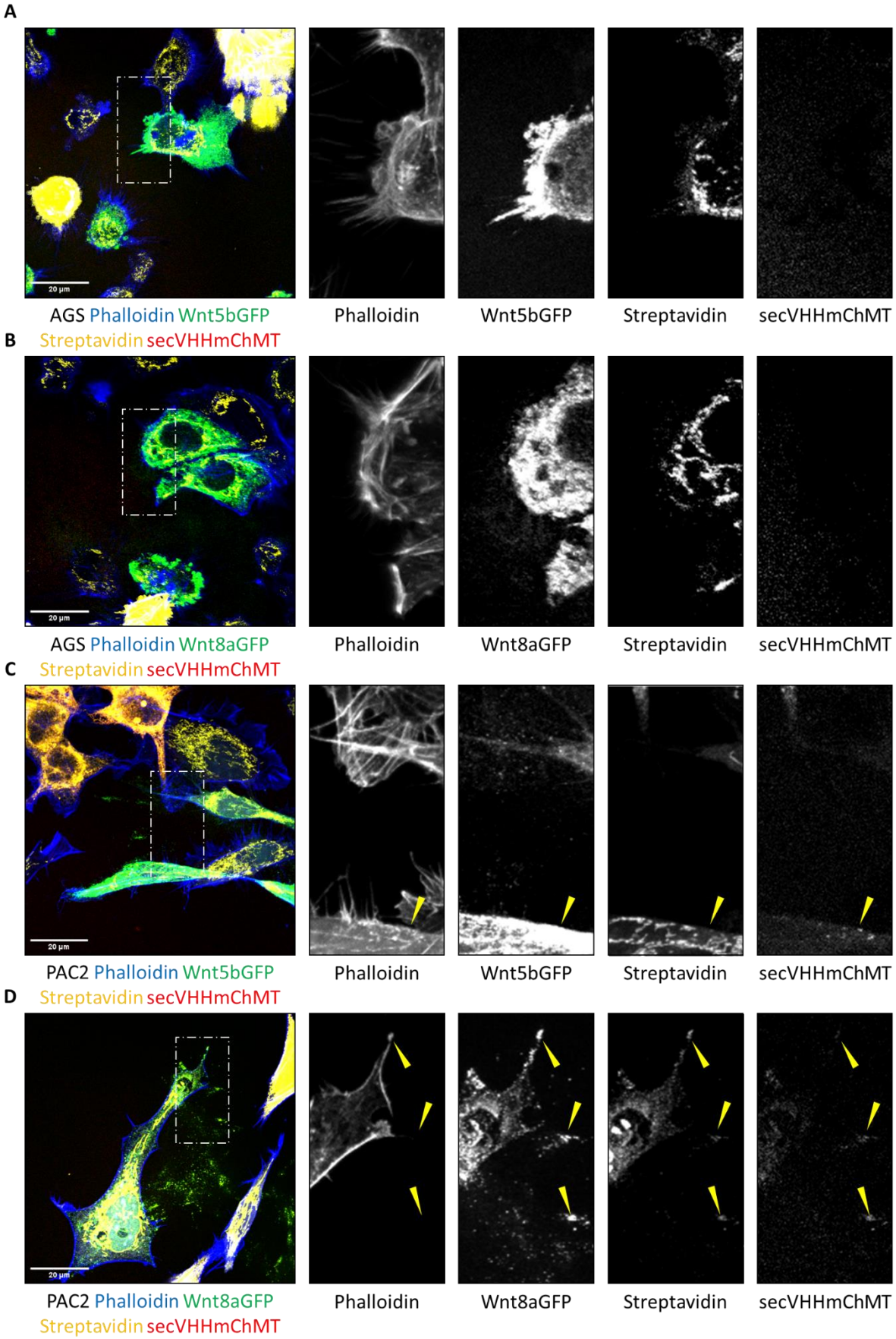

Figure 19. Wnt-GFP Co-Culture with AGS secVHHmCh-MT Stable Line C10. *(A-D) PFA fixed cells transfected with Wnt-GFP co-cultured with AGS*

secVHHmCh-MT stable cell line C10. Cells are permeabilised and stained with phalloidin (blue) and streptavidin (orange). Yellow arrows indicate secVHHmCh-MT localisation. Scale bars = 20µM. (A) AGS cells transfected with Wnt5bGFP. (B) AGS cells transfected with Wnt8aGFP. (C) PAC2 cells transfected with Wnt5bGFP. (D) PAC2 cells transfected with Wnt8aGFP.

Prior to co-culture of AGS and PAC2 cells, I attempted various methods for changing the culture conditions of the AGS cells to be identical to PAC2 cell culture conditions. AGS cells are cultured in DMEM media supplemented with 10% FBS at 37°C and 5% CO_2. PAC2 cells, conversely are cultured in Leibovitz L-15 media supplemented with 10% FBS at 28°C and normal atmosphere. Given the several differences, I experimented with gradual changes of media over time, which typically resulted in severe cell death of the AGS cells. Surprisingly, however, simply changing the media completely and placing the AGS cells in the 28°C incubator was immensely successful. The AGS cells were left to adapt for one week and then passaged as per normal. The AGS cells themselves only demonstrated slightly slower growth and otherwise no detriment to culture viability. Indeed, several passages of AGS were possible in these conditions, however, the cells did inevitably stop growth in a manner like senescence. To avoid this, I split AGS cells into two cultures and incubated one in 28°C for experiment, splitting the original stock of AGS for the next future experiments.

As seen prior with Wnt-GFP transfected cells, there were few GFP positive filopodia and equally less secVHHmChMT being either co-localised to GFP or within the cell body. This is also shown in the streptavidin staining of Wnt-GFP positive AGS cells as their pattern remains unchanged to that of the mitochondrial matrix. Conversely, the Wnt-GFP PAC2 cells show a more impressive GFP distribution along cytonemes (Fig 19). As opposed to the AGS cells, the PAC2 cells show an intracellular accumulation of secVHHmCh-MT within the cell body and along GFP positive cytonemes (Fig 19.D). An interesting aspect of fixation seems to largely reduce secVHHmCh-MT signal intensity. As shown in (Fig 20), there is proportionally far more secVHHmCh-MT signal than shown in fixations (Fig 19). Another observation to be made is the enormous volume of biotinylation occurring within the AGS secVHHmCh-MT

stable cells. So much biotinylation occurs within these cells that to observe physiological levels of biotinylation in non-stable cells (from the mitochondrial matrix) I had to oversaturate the streptavidin channel.

The PAC2 cells demonstrate biotinylation in structures other than mitochondria. As seen in Fig 19.D we see overlap between Wnt8aGFP, secVHHmCh-MT and streptavidin along the filopodia and intracellularly. Indeed this phenomenon was not limited to the rare individual cell, but was observable across multiple incidents (quantification not shown as errors from oversaturation in streptavidin channel and poor mCh signal made autonomous quantification impossible, therefore this is strictly an observation). Overall, the co-culture of Wnt-GFP transfected PAC2 cells with secVHHmCh-MT stable cells works better than expected and makes co-culture a viable and improved strategy for the main assay.

The fixation of cells significantly impacted the mCh signal of the secVHHmCh-MT protein. Therefore, to properly observe the full range of co-localisation I imaged live Wnt-GFP transfected cells co-cultured with the stable AGS secVHHmCh-MT B7 line.

A

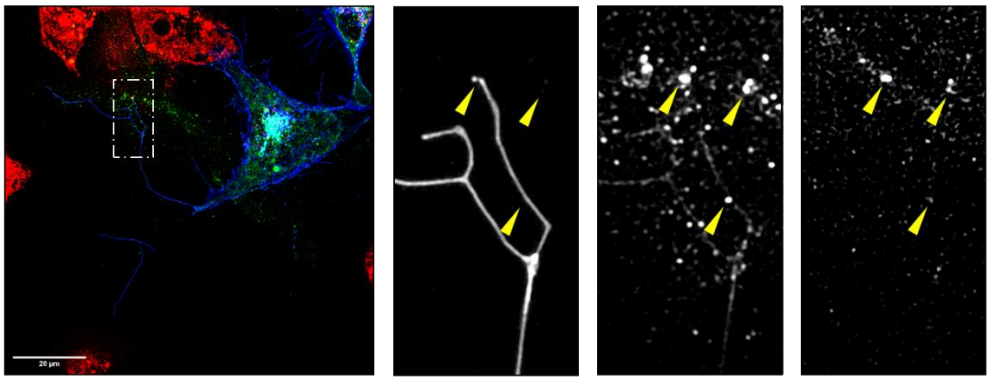

PAC2 Live memBFP Wnt8aGFP secVHHmChMT | memBFP | Wnt8aGFP | secVHHmChMT

B

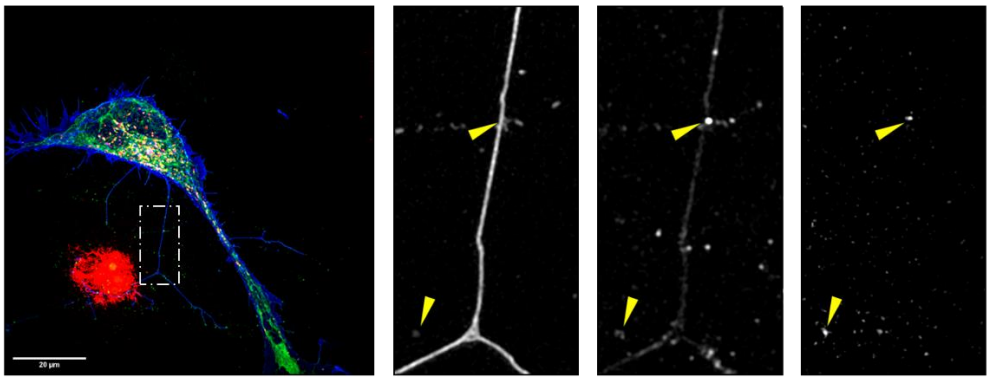

PAC2 Live memBFP Wnt5aGFP secVHHmChMT | memBFP | Wnt5aGFP | secVHHmChMT

C

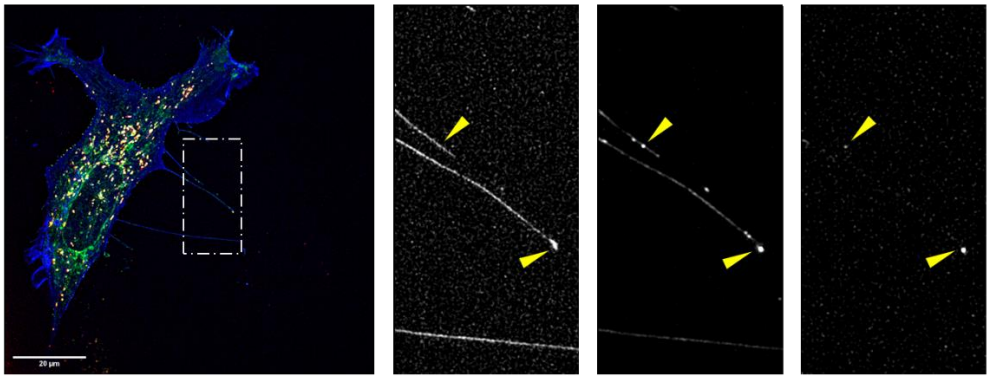

PAC2 Live memBFP Wnt5bGFP secVHHmChMT | memBFP | Wnt5bGFP | secVHHmChMT

D

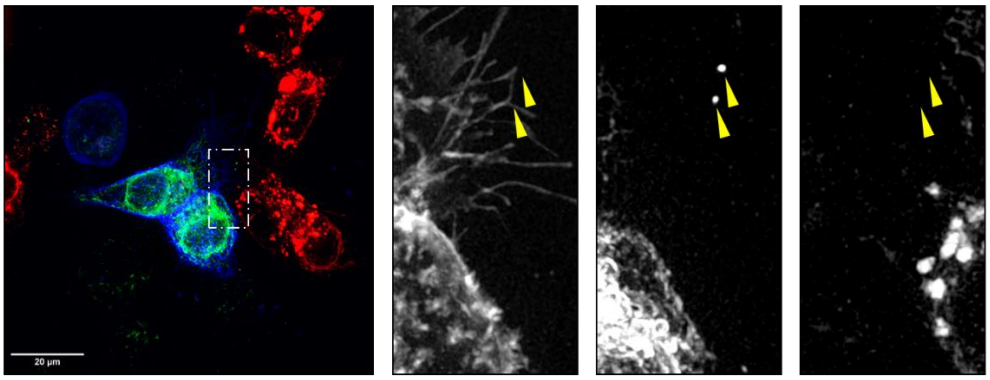

AGS Live memBFP Wnt5aGFP secVHHmChMT | memBFP | Wnt5aGFP | secVHHmChMT

Figure 20. Live Co-Culture of Wnt-GFP Cells and AGS secVHHmCh-MT B7. *(A-D) Live Wnt-GFP and membrane-BFP co-transfected cells co-cultured with AGS secVHHmCh-MT stable cell line B7. Yellow arrows indicate (D) GFP only or (A-C) GFP and mCh correlated pixels. Scale bar = 20μM. (A-C) PAC2 cells expressing (A) Wnt8aGFP, (B) Wnt5aGFP and (C) Wnt5bGFP. (D) AGS cells expressing Wnt5aGFP.*

Live imaging showed high levels of co-localisation of secVHHmCh-MT to Wnt-GFP, far more than fixations (Fig 20). Live imaging highlighted a large proportion of intracellular accumulation of secVHHmCh-MT, along with binding occurring on the filopodia and cell surface membrane. All three Wnts tested (Wnt8a/5a/5b-GFP) co-localise to secVHHmCh-MT. Wnt transfected AGS cells showed poorer intracellular accumulation of secVHHmCh-MT, and no incidence of Wnt-GFP and secVHHmCh-MT imaged on filopodia. Co-localisation of Wnt-GFP and secVHHmCh-MT was also observed extracellularly (Fig 20.B), potentially in some form of vesicle. Overall, Wnt-GFP transfected PAC2 cells demonstrate an incredible Wnt loaded cytoneme phenotype that co-localise with secVHHmCh-MT reliably.

4.2.9 Stable AGS Co-Culture Activity and Biotinylated Protein Extraction

Attempting to compare streptavidin staining with Wnt-GFP overlap was not sufficient to confirm biotinylation let alone observe any difference. As the final assay will focus on extracting biotinylated proteins for mass spectrometry, even a small population of biotinylated proteins should be detectable. Western blots, however, do not possess such sensitivity, and so an extra step is required to remove the noise from the signal. Streptavidin is an exceptionally sensitive biotin binding peptide that is routinely used for identifying and/or extracting biotin labelled peptides (Samavarchi-Tehrani et al., 2020). Using streptavidin coated beads, we can incubate the cell lysates post biotin incubation to bind and immobilise biotinylated proteins. In conjunction with a series of harsh washes developed by the Ting lab (Branon et al., 2018), we can remove secondary binding partners and non-specific peptides that aren't themselves biotinylated. This process leaves only peptides that came within proximity of

secVHH-MT at the time of biotin incubation, which should therefore make them a Wnt-interacting partner by association. First, I sought to identify the ideal pulldown conditions before extracting cell lysate through a streptavidin bead titration.

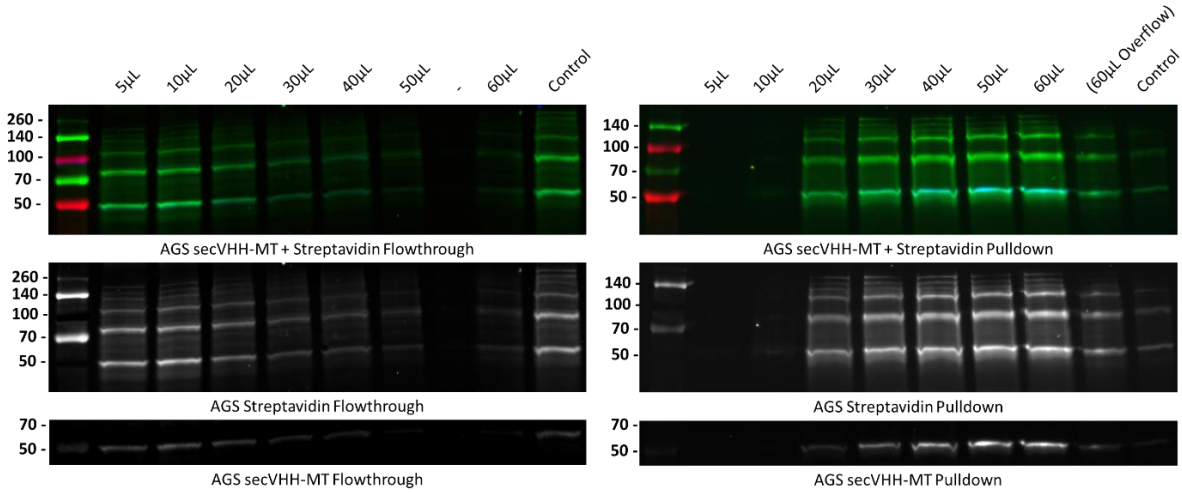

Figure 21. Streptavidin pulldown titration. *Pulldown of secVHH-MT transfected AGS cells in varying volumes of streptavidin beads. Flowthrough of beads (non-bound) are on the left and the pulldown on the right. Western blots stained with streptavidin (green) and αFLAG (blue). Poor comb alignment meant skipping a well in the flow through and overflow of 60µL well in the pulldown into the well to its right (denoted by '60µL Overflow').*

The pulldown successfully extracts biotinylated proteins with an effectiveness proportional to the volume of streptavidin beads used (Fig 21). A minimum of 20µL streptavidin is required to see effective pulldown of biotinylated proteins. Interestingly, streptavidin staining is seen in all volumes of streptavidin beads flowthrough, suggesting that all biotinylated proteins cannot be fully extracted regardless of bead volume. As increasing the volume of beads would increase the surface area for non-biotinylated proteins to attach to, 30µL was used for all subsequent pulldowns. 20µL volume was not selected as this volume was the first observed to pulldown effectively, and so a slight margin of error was accounted for in 30µL.

When comparing pulldown results with colleagues, I noticed certain discrepancies between my pulldowns and theirs. Most notably, with help from the Costello lab, I decided to compare the pulldown measurements of two competing brands of streptavidin beads. I had been using the 'Dynabeads™ MyOne™' beads for the pulldown optimisation and initial cell culture pulldowns, but I noted a degree of non-biotinylated protein in the final pulldown (Fig 22). I decided to compare the pulldown efficiency of these beads and the 'Pierce™' beads using a typical co-culture between Wnt8a-GFP and the stable secVHHmCh-MT expressing AGS cell line B7.

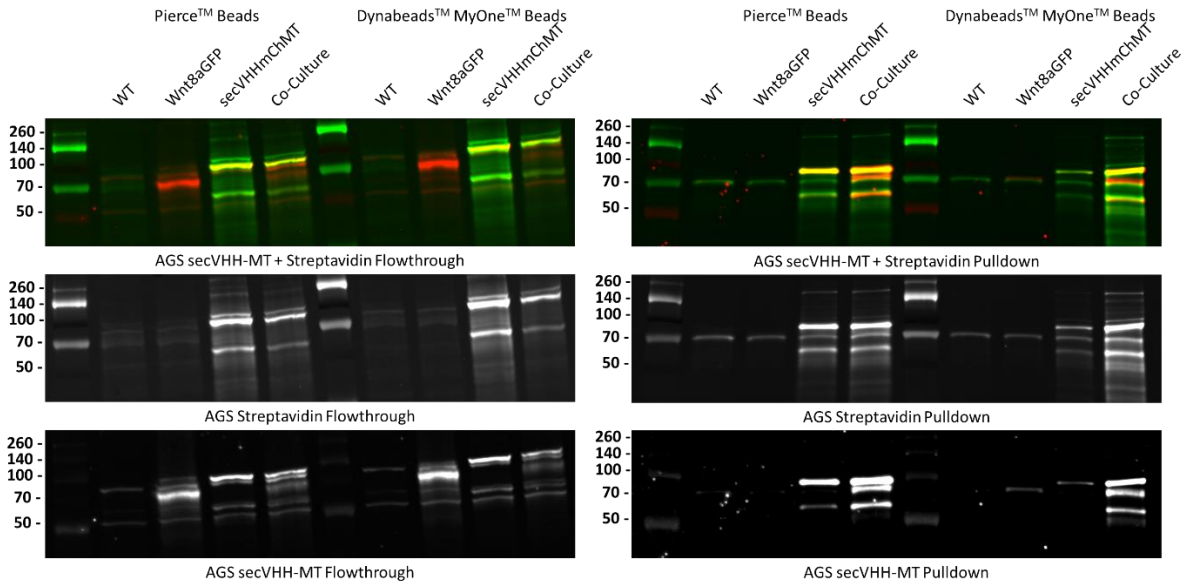

Figure 22. Streptavidin Bead Comparisons of Wnt8aGFP Pulldown.
Pulldown of Wnt8a-GFP transfected AGS cells co-cultured with stable secVHHmCh-MT AGS B7 incubated in 500µM biotin for one hour before collection in RIPA. Left blot shows flowthrough sample and right pulldown. The same lysate is used for two different streptavidin beads 'Pierce™' and 'Dynabeads™ MyOne™' indicated by left and right of the centre ladder respectively. Blots stained with streptavidin (green) and polyclonal αGFP (red). Green arrows indicate Wnt8aGFP, red arrows secVHHmCh-MT.

Both beads successfully pull down biotinylated proteins including secVHHmCh-MT and its streptavidin barcode (Fig 22). As seen with the streptavidin bead titration (Fig 21), the streptavidin barcode is seen in both the pulldown and

flowthrough for both beads, highlighting further that not all biotinylated proteins are pulled down completely. The most exciting aspect of this pulldown is the presence of Wnt8a-GFP in the pulldown for both beads. Wnt8aGFP is present for both the pulldown and flowthrough, suggesting that Wnt8aGFP must be biotinylated in the presence of secVHHmCh-MT. However, Wnt8aGFP is detected in the secVHHmCh-MT negative channel for the 'Dynabeads™ MyOne™' but not in the 'Pierce™' channel. This suggests that the specificity of the 'Pierce™' is greater than the 'Dynabeads™ MyOne™', therefore, all subsequent pulldowns and the final assay pulldown will be performed using the 'Pierce™' beads. Further repeats of the pulldown are required to deduce whether Wnt8aGFP is significantly enriched in the co-cultures.

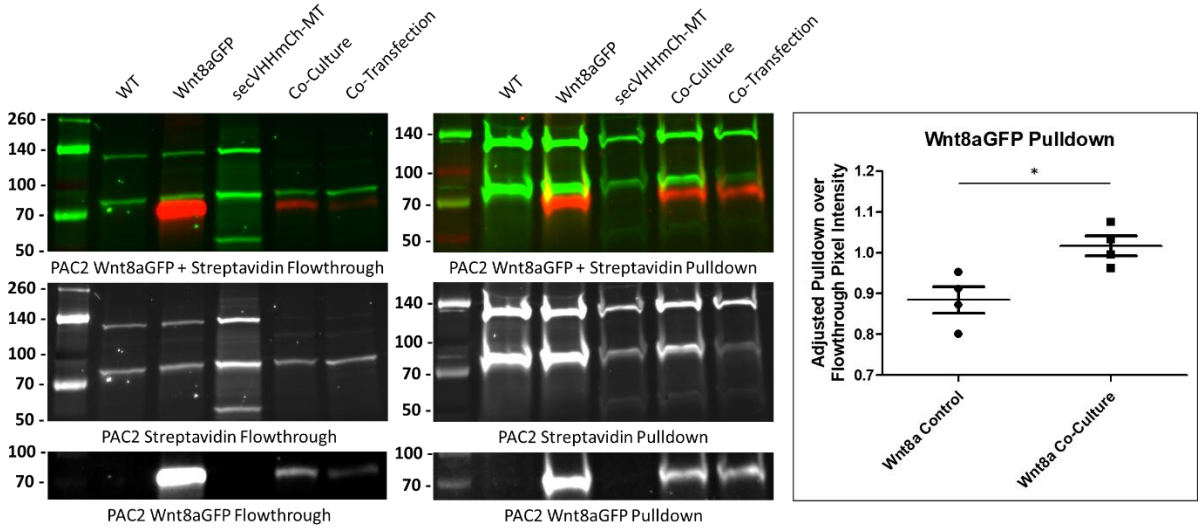

Figure 23. Pulldown of Wnt8aGFP with or without co-culture of secVHHmCh-MT. *Pulldown of Wnt8a-GFP transfected PAC2 cells co-cultured with stable secVHHmCh-MT AGS B7 incubated in 500μM biotin for one hour before collection in RIPA. Left blot shows flowthrough sample and right pulldown. A co-transfection of Wnt8aGFP and secVHHmCh-MT was also performed for comparison. Blots stained with streptavidin (green) and polyclonal αGFP (red). Graph on right quantifies the difference between pixel intensity for Wnt8aGFP band in co-culture between pulldown and flowthrough. N=4, p=0.0306.*

Indeed, after four repeats, pixel intensity for Wnt8aGFP significantly increases (0.13 pixel intensity $p = 0.03$) in the pulldown compared to the flowthrough only when co-cultured with secVHHmCh-MT (Fig 23). No quantification was done for co-transfection. I quantified this data comparing the co-culture Wnt8aGFP band with itself in the pulldown verses the flowthrough instead of comparing it to the Wnt8aGFP alone control for two reasons. The first reason is that comparisons are more reliable when comparing the effects of the pulldown to the same single lysate as opposed to two different lysates. The second reason was the extremely high signal intensity found on both flowthrough and pulldown. It is highly unlikely that Wnt8aGFP is biotinylated endogenously without the presence of secVHHmCh-MT; therefore, the beads are unlikely to have pulled it down specifically. The most likely reason for its presence is its extremely high expression compared to the general population of endogenous peptides. This vast over-representation of the single peptide likely comprises the major proportion of non-specific peptides that make it through the pulldown process, and so are therefore stained with such high intensity in the pulldown.

After biotin incubation, the cell cultures are washed repeatedly in cold PBS to remove biotin in the media and deplete biotin in cell lysate. Although reasonably unlikely, it was worth investigating the possibility that MiniTurboID is still actively biotinylating the lysate post collection. To assess this, I co-cultured Wnt5aGFP with secVHHmCh-MT to identify biotinylation of Wnt5a specific receptor Ror2. PAC2 cells transfected with either Ror2-mCh alone or co-transfected with Wnt5aGFP was co-cultured with AGS secVHHmChMT B7 and pulled down.

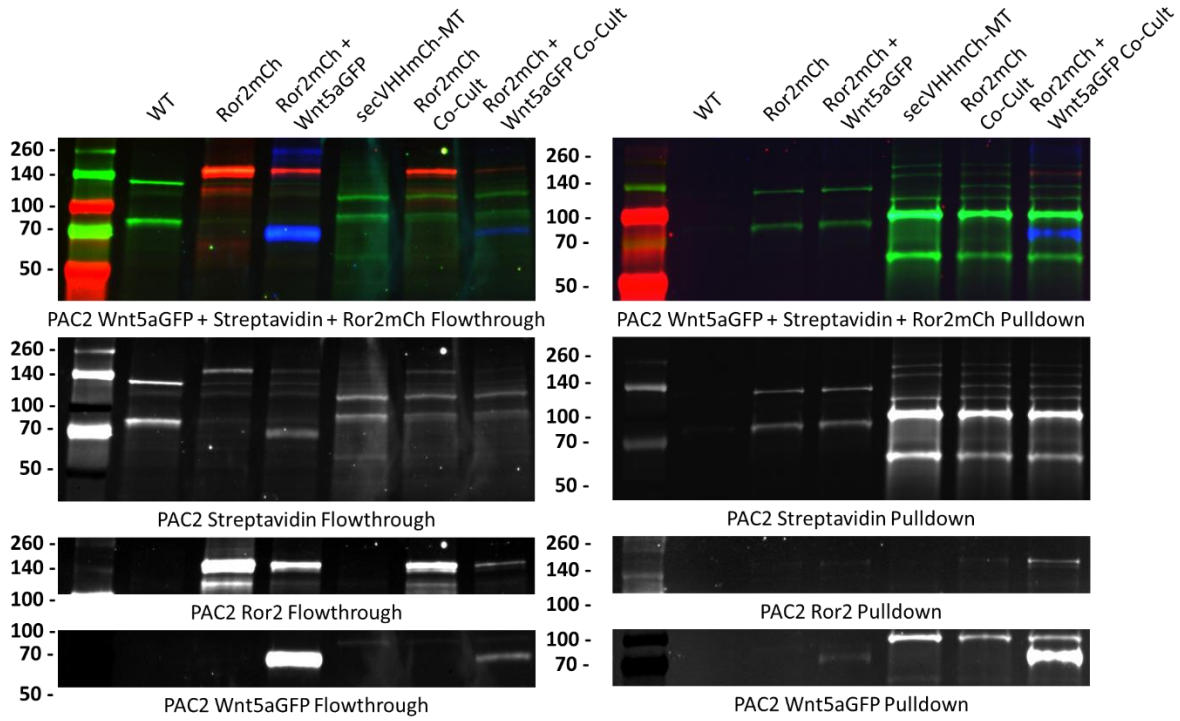

Figure 24. Ror2 was pulled down only in the presence of both Wnt5aGFP and secVHHmCh-MT. *Pulldown of Wnt5a-GFP and/or Ror2-mCh transfected PAC2 cells co-cultured with stable secVHHmCh-MT AGS B7 incubated in 500μM biotin for one hour before collection in RIPA. Left blot shows flowthrough sample and right pulldown. Blots stained with streptavidin (green), monoclonal αGFP (blue) and αRor2 (red). N=1.*

Multiple attempts were made to generate repeat experiments; however, errors arose when staining for αRor2. As Ror2 is 135KDa, optimisations were made to transfer higher molecular weight peptides, but these changes came at the cost of lower molecular weight peptides such as Wnt5aGFP. Furthermore, several αRor2 antibodies were experimented with and only one (D3B6F) showed staining in pulldown. Additional problems arose from PAC2 cell co-transfection of Wnt5a-GFP and Ror2-mCh and their co-culture with AGS secVHHmCh-MT B7 causing low transfection efficiency and/or low cell count. As this experiment lacks repeats, we can only infer minimally. Regardless, when performing a pulldown on Wnt5aGFP with or without secVHHmCh-MT, we still observe an enrichment of Wnt5aGFP in the pulldown only in the presence of secVHHmCh-MT (Fig 24). Ror2-mCh stains well for all Ror2-mCh samples, with the highest intensity in the Ror2-mCh single transfection flowthrough lane as expected. In

the pulldown the Ror2-mCh staining drops almost completely in all channels other than the channel that contains all three proteins. Consistent with enrichment of Wnt5aGFP in the presence of secVHHmCh-MT, Ror2-mCh appears only enriched in the presence of both Wnt5aGFP and secVHHmCh-MT and not when one protein is absent. This result suggests that Ror2-mCh is only biotinylated by secVHHmCh-MT because of Wnt5aGFP localising to its cognate receptor.

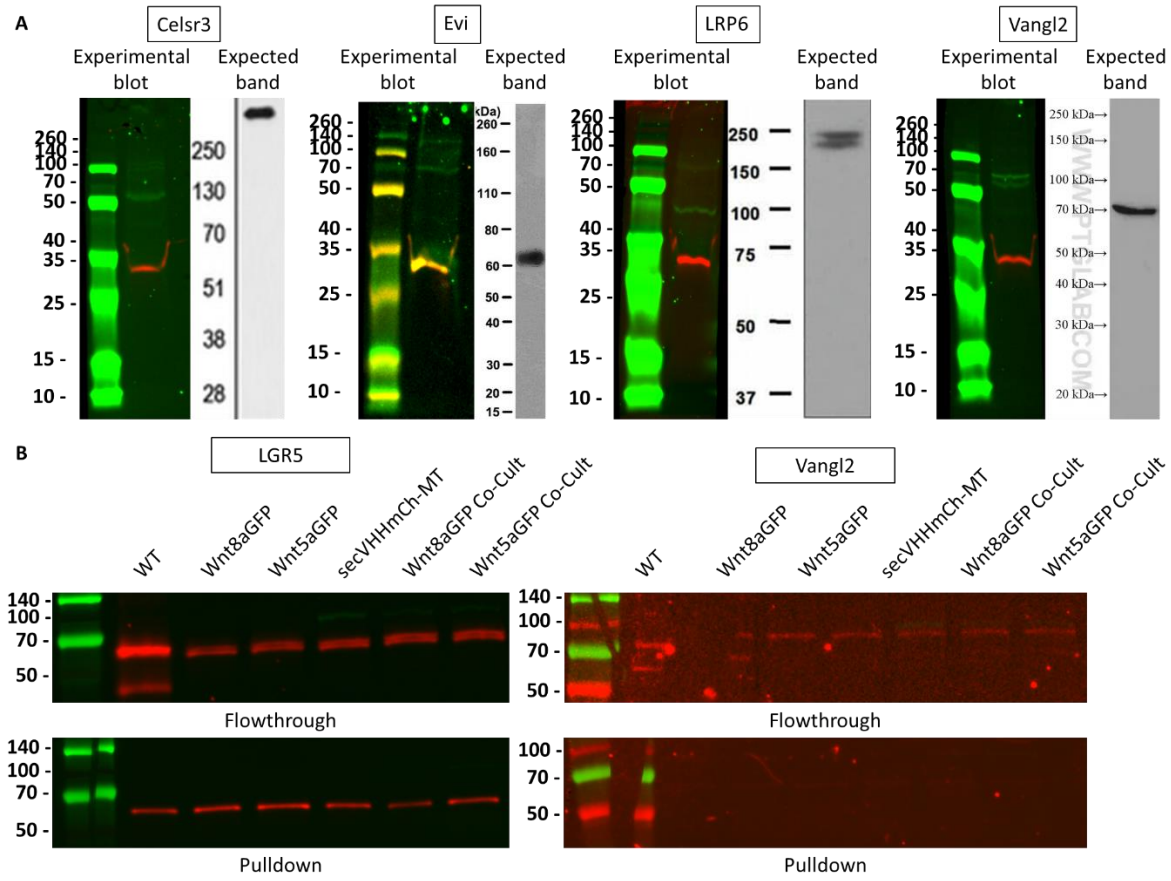

Figure 25. Endogenous proteins could not be detected in streptavidin pulldown. *(A) Crude western blot of PAC2 cell wild type lysates stained with GAPDH (red) and Wnt interacting peptides (green). Left blot shows PAC2 WT lysate and right blot shows antibody manufacturer blot. (B) Streptavidin flowthrough and pulldown western blots of PAC2 cell culture stained with LGR5 (left) and Vangl2 (right).*

Following the apparent success of the Ror2-mCh biotinylation, I sought to elucidate endogenous biotinylation from Wnt-GFP/secVHHmCh-MT localisation.

I tested a range of Wnt interacting protein antibodies that I expect to be biotinylated in the presence of both Wnt-GFP and secVHHmCh-MT as Ror2 did in Fig 25. Only two antibodies showed staining to PAC2 cell lysates. PAC2 cells were transfected with either Wnt8a-GFP or Wnt5a-GFP and co-cultured in AGS secVHHmCh-MT B7 cells. However, no differences were observed between any channels for flowthrough or pulldown samples of the Wnt receptors LGR5 or Vangl2 (Fig 25).

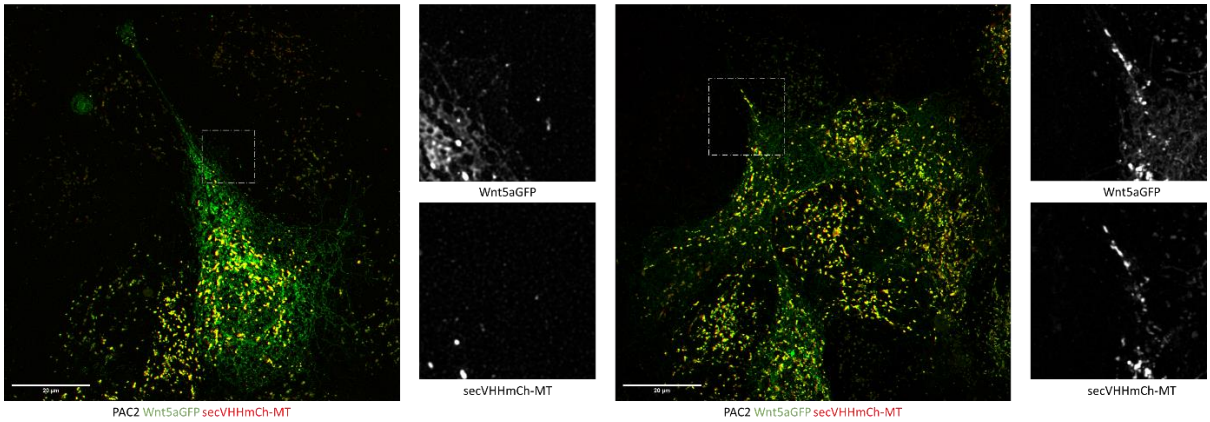

Figure 26. Wnt5aGFP PAC2 cells cultured in conditioned secVHHmCh-MT media. *Live PAC2 cells transfected with Wnt5a-GFP incubated in secVHHmCh-MT conditioned media for 24 hours. Conditioned media generated by AGS secVHHmCh-MT stable B7 cells cultured in Leibovitz media for 24 hours. Scale bar = 20μM.*

As stable AGS cells demonstrated strong co-localisation of secVHHmCh-MT to co-cultured PAC2 cells, both in imaging and western blot analysis, I decided to investigate its effectiveness in conditioned media. Utilising conditioned media would remove a source of non-specific biotinylation produced by secVHHmCh-MT producing AGS cells, thereby increasing signal to noise ratio. As shown previously (Fig 26), transfected secVHHmCh-MT cells couldn't produce enough protein to show binding in conditioned media sample. Despite this, the stable AGS secVHHmCh-MT cells B7 exceeded expectations and displayed very high levels of co-localisation in live imaging (Fig 26). This phenomenon was demonstrated through multiple repeats of conditioned media (n=3, quantifications not shown). Indeed, secVHHmCh-MT co-localisation to

Wnt5aGFP was not limited to intracellular accumulations, but also observed along filopodia projections (Fig 26).

4.3 Discussion

The overall aim of this chapter was to develop the nanobody-biotin ligase assay for use in proximity dependent biotinylation and extraction of Wnt related proteins for identification. To this end, I generated a nanobody-biotin ligase fusion construct that demonstrates high levels of protein expression and biotinylation activity. Furthermore, I demonstrated co-localisation of this nanobody-biotin ligase to Wnt-GFP that resulted in localised biotinylation during imaging and successful pulldown of biotinylated proteins such as Wnt-GFP. Overall, this chapter had successfully developed the tools necessary for the next stage in assay development – application of the assay. Indeed, the tests performed in this chapter provide a strong degree of confidence in the assay design for success. This is complimented, however, with its fair share of limitations in the form of low signal-to-noise ratio and protein expression. The various stages of this development revealed various obstacles that were necessary to overcome before advancing further.

4.3.1 Nanobody-biotin ligase cloning considerations

The first main hurdle was the development of the nanobody-biotin ligase fusion construct. As shown in figure 10, many biotin ligases were proposed to be compared against for the ideal candidate. Apex2, the pea derived peroxidase, could not be cloned within the time allocated and so was not included. As MiniTurboID and BioiD2 comparisons have been documented robustly in the field (Branon et al., 2018), the MiniTurboID construct was selected without contest. What was not mentioned in the results was the deliberation of the linker region used to ligate secVHH to MiniTurboID/BioID2. Size plays a significant factor in intracellular activity of protein binders (Samavarchi-Tehrani et al., 2020) as demonstrated by full size antibodies. While antibodies are significantly limited by their post-translational modifications and disulphide bridges affecting intracellular stability, their enormous size of 150Kd generates significant steric hindrance. Furthermore, the biotinylation radius of promiscuous biotin ligases are proposed to have an average of 10nm (Samavarchi-Tehrani et al., 2020). An overly large nanobody-biotin ligase construct would therefore suffer both culture penetrance and limited biotinylation activity. This was the reason for

omitting the mCh fluorophore in the first round of cloning. As discussed in the results, this omission was swiftly reverted. The linker region was a crucial element of design, requiring length and flexibility. Indeed, it needed to be long enough to enhance the biotinylation radius and overcome overall construct size without becoming too long that we lose the tight and specific biotinylation radius that captures Wnt interacting proteins only. The linker region chosen consisted of 13 repeats of one serine followed by four glycine amino acids, termed '13xL'. These amino acids allow for extreme disordered regions and high flexibility. The linker region was cloned from the BioID2 source plasmid; therefore, its length was assumed long enough fit for purpose. Given more time for development, more constructs would have been generated that explore this linker region in more depth, for example, observing biotinylation with shorter or longer lengths. Despite this, clearly the linker region was of sufficient length as we observe biotinylation of Wnt-GFP in pulldown western blots (Fig 23). As the biotin ligase resides at the C-terminal whereas the nanobody is N-terminal, this would suggest that the linker region allows for full 360° biotinylation, therefore hindrance is not an issue.

4.3.2 Expression optimisations

A significant portion of this chapter is dedicated to the improvement of transfection efficiencies of Wnt-GFP and secVHH-MT. This aspect of the nanobody-biotin ligase assay would be the single greatest obstacle to overcome and the most prevalent bottleneck in development. Indeed, many attempts were made at exploring various options for improving transfection. These include enhancing the quality of the plasmids used and trialling different methods of delivery (Fig 12). The only success was found in the plasmid quality and not in the delivery. The failure to use lipofectamine or electroporation delivery was very interesting. Indeed, lipofectamine transfections were not observed by just myself, but for many of my colleagues too. A possibility for this is the small tricks that other labs employ to find success with lipofectamine transfection that are not otherwise stated in the product's protocol. These include pre-treatment of cells a day prior to lipofectamine transfection, which enhances cell culture viability, or the removal and replacement of fresh media one hour post transfection. Indeed, with more time allocated to this, these tricks could have

been attempted with potential success. As for electroporation, our lab routinely uses this technique for both AGS and PAC2 cells to great success. I believe the lack of Wnt-GFP or secVHHmCh transfection using this technique lies in the plasmids themselves as other colleagues attempted transfections on my behalf but failed to do so. In retrospect, these attempts at increasing transfection efficiency would not warrant the effort required, as generating stable cell lines were vastly superior. However, as the stable cell lines took considerable time and effort, plus the many failed attempts at PAC2 stable cells, investigating different transfection techniques was still beneficial. Indeed, the nanobody-biotin ligase assay was developed with generalised applicability in mind, where the assay can be easily performed on multiple different GFP constructs. To this end, generating a stable cell line for every GFP construct would not be considered as easily accessible as a high transfection efficiency based approach. Regardless, standard transfection with Fugene and a stably expressing secVHH cell line would be sufficient for Wnt-GFP biotinylation and extraction (Fig 23).

4.3.3 secVHH-MT expression and activity

The cloning of secVHH-MT and secVHHmCh-MT developed a construct that expressed as highly as its predecessor secVHHmCh (Fig 11). Indeed, no further improvements to the cloned construct were necessary, as its activity in transfected cells was evident in both imaging and western blot analysis (Fig 19+23). That being said, its activity was exclusively linked to its concentration in culture. Indeed, stable cell production of secVHHmCh-MT clearly demonstrated greater accumulation to Wnt-GFP intracellularly (Fig 20) and its subsequent biotinylation (Fig 19). However, given more time for cloning, it would have been very interesting to compare it to a non-nanobody biotin ligase system. A Wnt ligated MiniTurboID would have done just this. While a Wnt-MT construct would theoretically demonstrate large non-specific biotinylation, as outline in my introduction aims, there exists a commercially available biotin substrate that is cell surface membrane impermeable (Karhemo et al., 2012). Comparisons of the biotinylation in imaging, western blots and later mass spectrometry analysis between Wnt-MT and secVHHmCh-MT would provide invaluable data and

further test the robustness and utility of the secVHHmCh-MT assay. Given more time for cloning this should be pursued.

Biotinylation from secVHH-MT and secVHHmCh-MT in western blot suggest discrepancies between them. This is highlighted by the unique biotin barcode being different between the two. In figure 17.B, we can see a unique biotinylation band of 100 and 140KDa for secVHH-MT but unique biotinylation bands of two bands at 50KDa for secVHHmCh-MT. With the only difference being the mCh, this could be because of either some affinity of the mCh towards an unknown endogenous protein or that the larger size results in altered protein localisation. Indeed, investing time to determine secVHHmCh-MT localisation would be desirable to characterise its expression behaviour. While not necessary for conditioned media, these investigations would be useful for co-cultures or co-transfections as we can identify biotinylation bias to subcellular regions and/or proteins. However, the best possible method to determine this would be using mass spectrometry, which would require considerable effort.

Overall, this chapter achieved its aims set out to generate a nanobody-biotin ligase fusion construct, develop and optimise assay conditions and provide convincing evidence of Wnt-GFP/secVHH-MT co-localisation and biotinylation. Given these results, we can expect a good possibility for successful protein extraction and subsequent mass spectrometry analysis to identify the proteome surrounding cytoneme mediated Wnt handover in cultured cells.

5 Chapter 3 – Mass Spectrometry Analysis of Biotinylated Proteins

5.1 Introduction

The nanobody-biotin ligase assay secVHH-MT and secVHHmCh-MT demonstrated all the desirable qualities outlined in the aims of this thesis. Strong co-localisation to Wnt-GFP and evidence of active biotinylation of the Wnt-GFP/secVHH(mCh)-MT in both imaging and western blot analysis points towards a successful streptavidin based pulldown and sample identification by mass spectrometry. Although further optimisations could be performed as stated in the discussion of chapter 2, the nanobody-biotin ligase assay is in a state ready for full application. In this chapter, I extract biotinylated proteins from PAC2 cell culture lysate for mass spectrometry analysis. However, many steps are still required for full optimisations, and so several mass spectrometry analyses were performed. Each mass spectrometry test generating new information for the next stages of improvement making this an iterative process of development. Therefore, I aim to further improve the nanobody-biotin ligase assay using mass spectrometry in the pursuit of generating a dataset with enriched biotinylated protein hits.

5.2 Results

5.2.1 First mass spectrometry attempt

The first attempt at running mass spectrometry on the secVHH-MT assay was performed using polyclonal PAC2 cells re-transfected 24 hours before collection to ensure maximum transfection efficiency. At this stage, I had demonstrated expression and localisation of secVHH-MT to Wnt-GFP proteins in live and fixed samples (Chapter 2, Fig 11+20). Furthermore, I observed active biotinylation of secVHH-MT in fixed samples and western blots (Chapter 2, Fig 19+23). In fixed samples, PAC2 cells demonstrated biotinylated cytonemes only in the presence of both Wnt8a-GFP and secVHH-MT. In western blots, secVHH-MT biotinylates itself and generates a unique 'biotin barcode' demonstrating an active biotin ligase. Taken together, it appeared that the experimental conditions were suitable and ready for protein extraction and pulldown for identification by mass spectrometry. As mass spectrometry is a highly sensitive technique, I reasoned that despite low transfection efficiencies and low signal to noise ratio, mass spectrometry should be capable to identify significantly increased fractions of biotinylated proteins because of secVHH-MT localisation to Wnt8a-GFP.

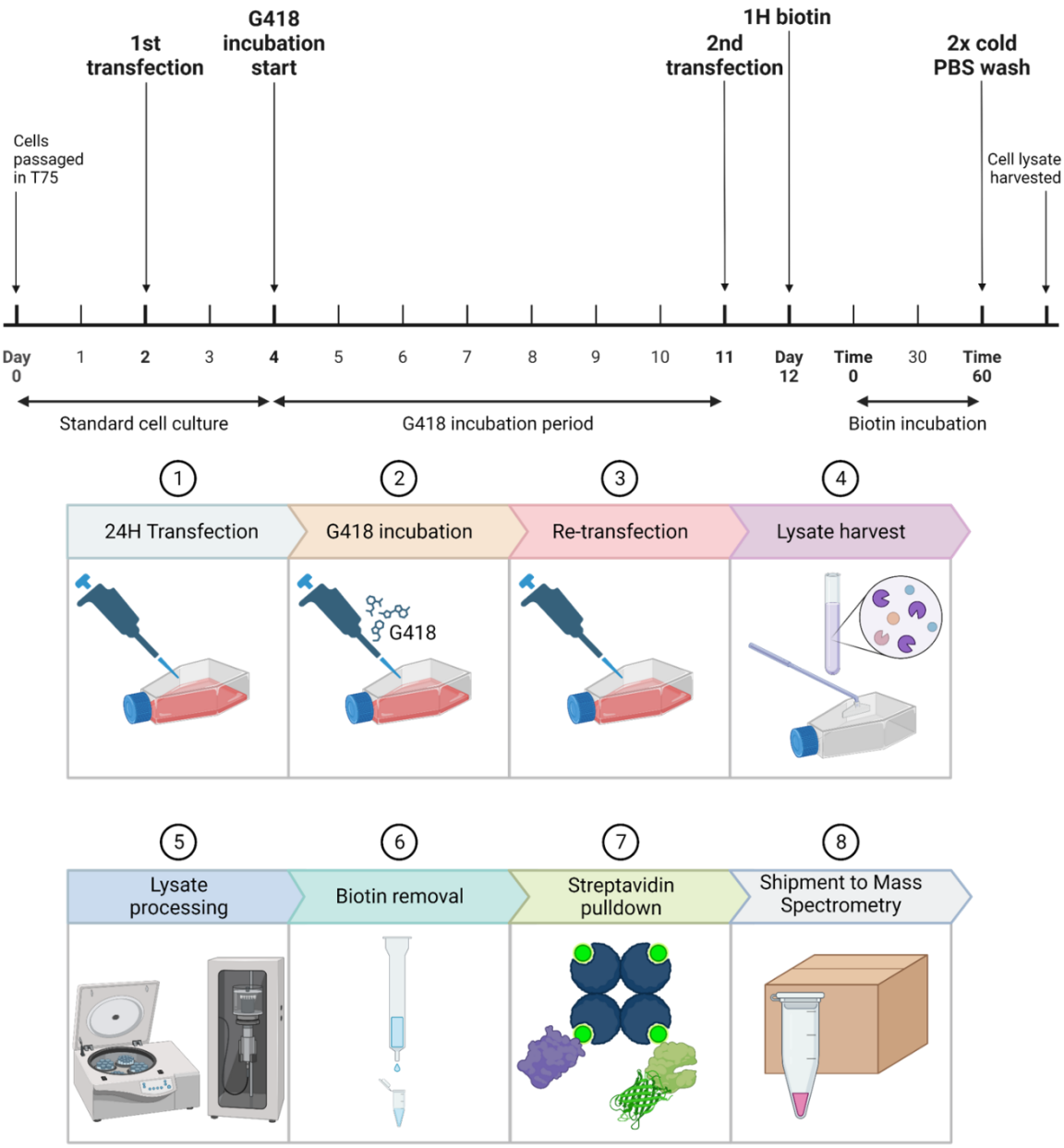

Figure 27. 1st Mass spectrometry protocol. *(A) Timeline of PAC2 polyclonal cell generation and protein lysate extraction. (B) General protocol of producing PAC2 polyclonal cells, lysate extraction, processing, pulldown and shipment to University of Bristol for mass spectrometry. Created with BioRender.com.*

As PAC2 stable cells lost expression and ended in senescence (Chapter 2, Fig 14), polyclonal PAC2 cells were generated in their place. G418 incubation removed all PAC2 cells that did not uptake the G418 resistance marker in pcDNA3.1, thereby significantly increasing the proportion of transfected cells in culture. However, this did not guarantee that the protein construct was expressing along with the G418 resistance gene. To improve upon this, I re-

transfected the culture and harvested the cells 24 hours later (Fig 27.A). Across the different experimental conditions, this was successful in raising the ratio of transfected cells, however the total cell population suffered from the extensive treatment. To address this, several T75 culture flasks were generated for each repeat. As we are interested in cytoneme specific proteins, cell lysates were harvested using RIPA lysis buffer and a cell scraper (Fig 27.B4) without the use of trypsin. Omitting trypsin ensures peptides were not digested prior to streptavidin pulldown and sonication sheared any DNA and cell membrane micelles (Fig 27.B5).

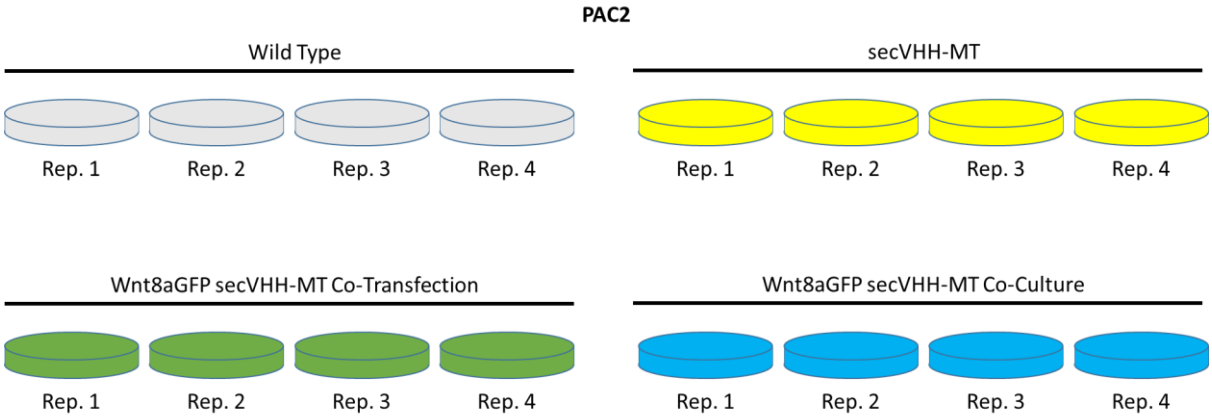

Figure 28. 1st Mass spectrometry experimental conditions. *PAC2 cell culture conditions prior to lysate extraction. Wild type cells are standard passage of PAC2 cells. All other conditions are polyclonal cells treated in the protocol outlined in Fig 27.A.*

The mass spectrometry conditions were outlined in Fig 28. Four repeats of four conditions were selected; Wild type, secVHH-MT alone, Wnt8aGFP co-transfected or co-cultured with secVHH-MT. The wild type and secVHH-MT conditions are control groups designed to identify proteins significantly enriched only in the presence of Wnt8a-GFP. This is necessary despite the streptavidin pulldown as it removes endogenous biotinylated proteins (carboxylases) and secVHH-MT 'biotin barcode' biotinylated proteins. Ideally, a co-culture of Wnt8a-GFP and secVHH-MT alone would be sufficient for the experimental conditions. This ensure that the secVHH-MT is exogenously introduced to Wnt8a-GFP, therefore removing the possibility of intracellular biotinylation from

pre-mature Wnt8a-GFP binding to secVHH-MT. Live and fixed co-culture staining in development of the assay showed a significantly reduced co-localisation between secVHHmCh and Wnt8a-GFP (typically because of low transfection efficiency) (Chapter 1 Fig 7). Because of this, a co-transfection condition was added, as a contingency option to the co-culture, should the experimental condition fail.

An extra step was incorporated in protein lysate processing to enhance the streptavidin pulldown. This was a desalting step to remove small molecules such as excess biotin to prevent unbound biotin blocking biotinylated proteins on the streptavidin beads. There came two caveats to the desalting step; the first being a significant dilution of the lysate. Desalting requires adding more RIPA solution to the sample to ensure all protein passes through the column; this in turn dilutes the sample several fold (the effect exacerbated with smaller sample volumes). Dilution of the lysate for our purposes poses little threat, as the streptavidin bead step should pulldown efficiently despite the increased lysate volume. The second caveat is a small but non-uniform loss of protein mass post desalting, which undermines protein concentration balancing for mass spectrometry analysis. To determine the effect of this the concentration of protein prior to and post desalting was measured to determine the protein recovery efficiency (Fig 29).

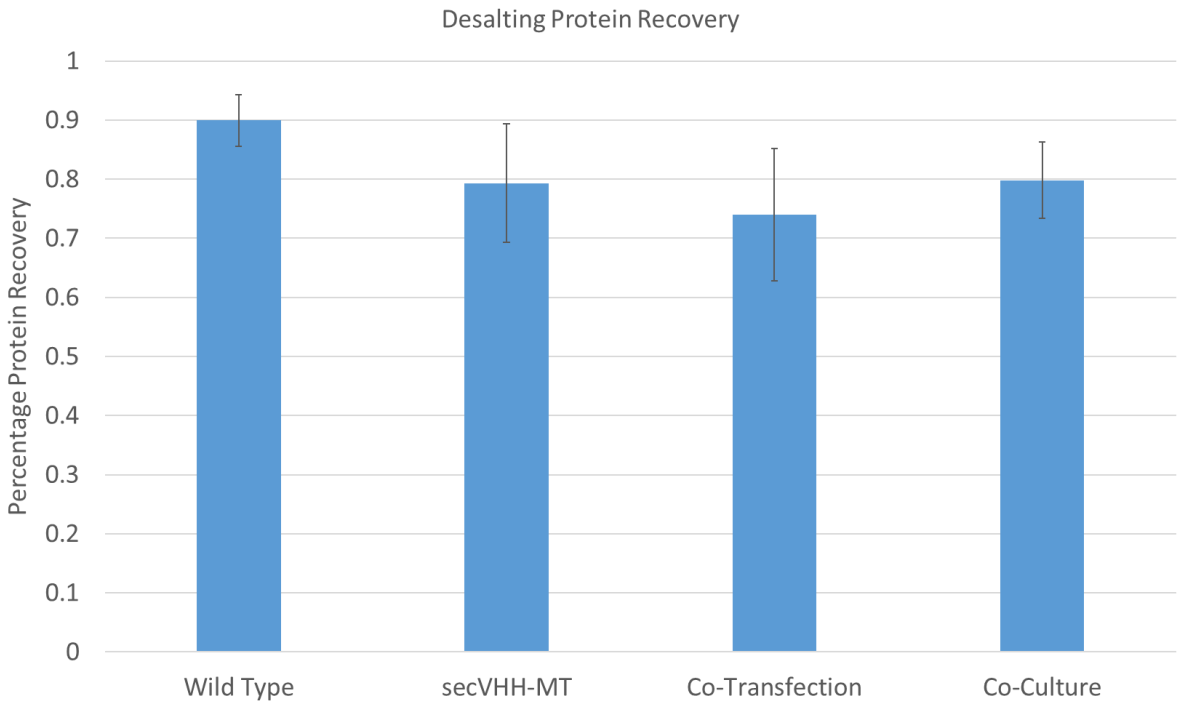

Figure 29. Cell lysate desalting protein recovery efficiency. *Ratio of protein measured post over pre desalting of PAC2 cell culture lysate for each experimental condition. N=4. One way ANOVA performed on each treatment. P-value = 0.1112, F = 2.477, R^2 = 0.3825. Error bars represent standard deviation.*

Desalting of PAC2 cell lysates yielded an average 80.75% protein recovery (Fig 29). Individual groups of experimental conditions were not significant to each other by one-way ANOVA analysis (assuming normal variance and parametric data). Despite a non-significant difference, co-transfection samples averaged 74% protein recovery whereas wild type samples averaged 89.9% protein recovery, generating 15.9% difference. All samples were loaded into streptavidin beads using 360µg of protein equally.

Streptavidin beads were washed according to the Ting protocol (Branon et al., 2018) and shipped to the University of Bristol for mass spectrometry analysis. Tandem mass tag (TMT) mass spectrometry was performed on the shipped samples, incorporating all 16 conditions simultaneously through 15 fractionations.

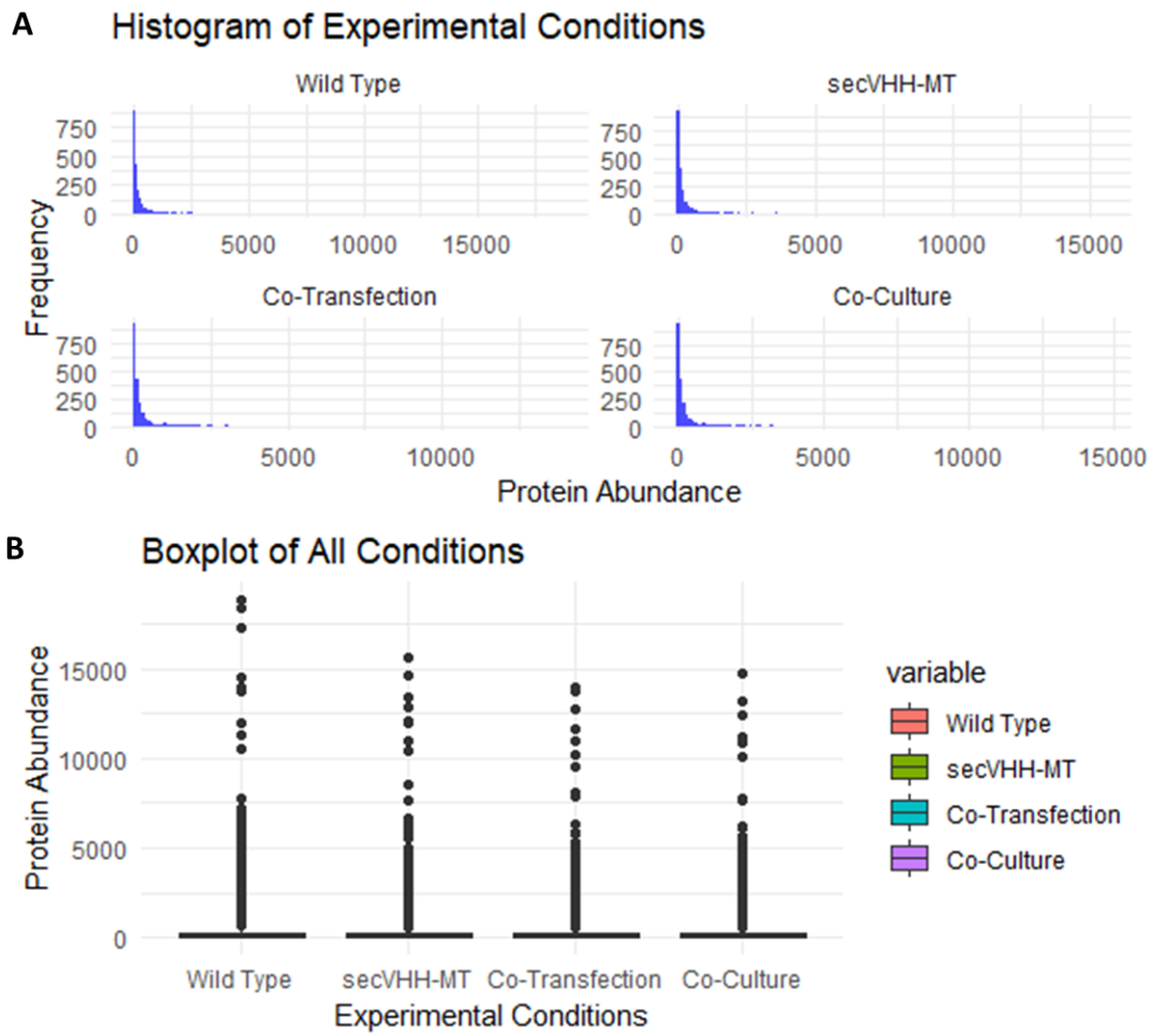

Figure 30. 1st Mass spectrometry data distribution and normality. *(A) Histogram of average frequency of peptides for a given abundance. (B) Distribution of protein abundance between the four experimental conditions. One way ANOVA Kruskal-Wallis's test was performed for the four conditions. chi-squared = 5.2053, df = 3, p-value = 0.1574.*

As expected, the protein abundance is non-normally distributed and is skewed towards zero (Fig 30.A). To measure the distribution of protein abundance, a Kruskal-Wallis one-way ANOVA was used to determine conditions with significantly different levels of protein abundance. No conditions presented significantly different levels of protein abundance; however, it is interesting to note a similar distribution observed in the desalting protein recovery (Fig 29).

The mass spectrometry worked as intended, however a significant problem was immediately apparent. No peptides of Wnt8a-GFP were detected in any

conditions, and between all 16 samples, only a single peptide of secVHH-MT was detected. This immediate issue renders the entire mass spectrometry data set null. We should expect secVHH-MT to be the highest abundant peptide in the data set as it should biotinylate itself first. Logically, if we assume that secVHH-MT localises to Wnt8a-GFP effectively, we should therefore assume Wnt8a-GFP to be equally highly abundant in the dataset. For these reasons, we should use significant increases of secVHH-MT and Wnt-GFP as an indicator for a successful assay, let alone their existence within the dataset to begin with. Despite the lack of these two essential peptides, I investigated the dataset further to illuminate reasons for its apparent failure.

Score Sequest Rank	Protein Name	Molecular Weight (KDa)
1	Propanoyl-CoA:carbon dioxide ligase subunit alpha	78
2	Pyruvate carboxylase	130
10	Propionyl-CoA carboxylase subunit beta	61
11	Pyruvate carboxylase	130
33	Acetyl-CoA carboxylase	273

Figure 31. Endogenous protein hits from 1st mass spectrometry. *Table of biotin binding proteins from mass spectrometry analysis. Proteins are ranked by their score Sequest.*

I first checked the identity of the top scoring protein abundances from all experimental conditions. Taking an average of the abundance of each sample, I ranked the highest abundant protein peptides and identified all carboxylases from the list. Carboxylases constitute the vast majority of endogenous biotinylated proteins, and so should occupy the top protein hits of background proteins. Indeed, carboxylases were identified from the top protein hits, occupying both the first and second highest abundant proteins from the mass spectrometry (Fig 31). In the interest in comparing these results to the western blots performed in chapter 2 Fig 17, I highlight the relative molecular weights (Fig 31). Consistent with endogenous biotinylation observed in western blots, the two top protein hits propanoyl-CoA and pyruvate carboxylase have molecular weight of 78 and 130KDa respectively.

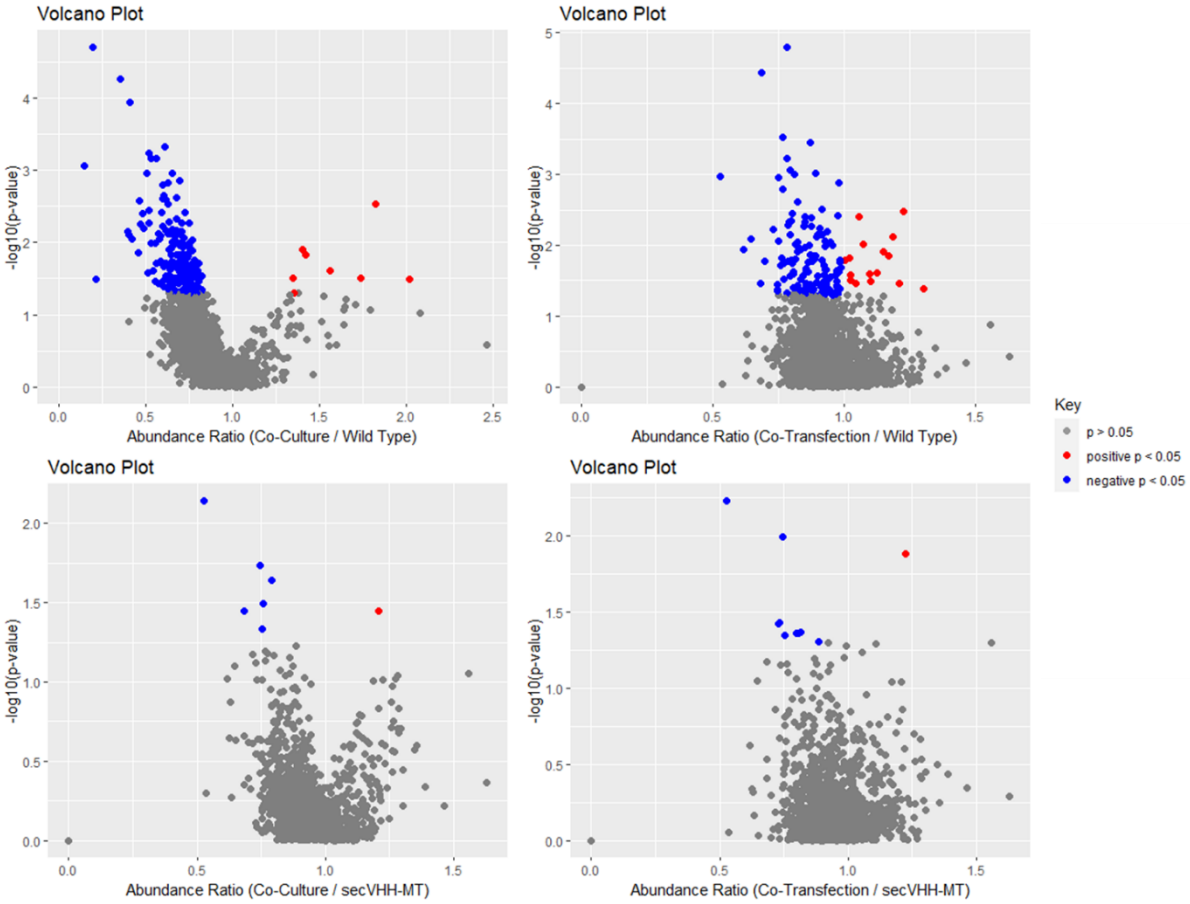

Figure 32. Volcano plot of Co-Culture and Co-Transfection abundance ratio over controls. *Volcano plots of abundance ratio of experimental over control condition. T-test performed on each individual protein between experimental and control conditions to plot the p value on y axis. Grey pixels indicate non-significant proteins, blue indicate significantly downregulated proteins and red indicate significantly upregulated proteins to a p value of >0.05.*

To explore the data I compared the abundance ratios of the experimental conditions to the two controls 'Wild Type' and 'secVHH-MT' and ran a T-test for every protein (Fig 32). A list of the significant protein hits is listed in Fig 33. 'Co-Culture' showed the best separation of abundance ratio when compared to either 'Wild Type' or 'secVHH-MT' whereas the 'Co-Transfection' sample demonstrates poor separation, indicating strong and poor abundance identity respectively. Several proteins are significantly enriched for both 'Co-Culture' and 'Co-Transfection' samples when compared to 'Wild Type' (Fig 33). These proteins include myo5aa, sumo2, adprs, sumo3b and stoml2. No significant

gene ontology hits could be generated from any data set in figure 33. Despite this, the common proteins enriched from 'Wild Type' control appear to fall under three separate compartments of cytoskeleton, mitochondrial matrix and nucleus. The lack of coherence to the localisation and gene ontology enrichment supports the notion of false positive error. Furthermore, there are no consistent protein hits for 'secVHH-MT' control sets, of which both comparisons yield only one significant enrichment.

Co-Culture vs Wild Type

Accession	Protein Name	Gene Name	Abundance	p value
Q1LXI2	Myosin VAa	myo5aa	2.014	0.0324
Q6DHL4	Small ubiquitin-related modifier 2	sumo2	1.82	0.003
Q5RHR0	Poly [ADP-ribose] polymerase	parp1	1.734	0.0316
B2GP19	Zgc:92867	adprs	1.558	0.0244
Q6DGI3	Nucleolar protein 16	nop16	1.421	0.0149
F1QRX2	Small ubiquitin-related modifier	sumo3b	1.4	0.0126
Q7SY50	Zgc:63505	stoml2	1.355	0.0495
Q7ZUX9	Ribosome biogenesis protein NSA2	nsa2	1.346	0.0309

Co-Culture vs secVHH-MT

Accession	Protein Name	Gene Name	Abundance	p value
E9QHD9	Ornithine carbamoyltransferase, mitochondrial	otc	1.208	0.0357

Co-Transfection vs Wild Type

Accession	Protein Name	Gene Name	Abundance	p value
B8JL82	Signal sequence receptor subunit gamma	ssr3	1.303	0.0414
B2GP19	Zgc:92867	adprs	1.226	0.0033
B8JL34	Zgc:123010	zgc:123010	1.212	0.0341
Q6DHL4	Small ubiquitin-related modifier 2	sumo2	1.187	0.0075
Q1LXI2	Myosin VAa	myo5aa	1.171	0.0139
Q7SZR5	Small ubiquitin-related modifier 1	sumo1	1.151	0.0123
Q6DHQ0	Cyclin-dependent kinase 2-associated protein	cdk2ap2	1.128	0.0243
Q6ZM19	Eukaryotic translation initiation factor 6	eif6	1.103	0.0318
Q7SXX4	Hippocalcin-like 1	hpcal1	1.099	0.0254
B3DJR2	Myo5a protein	myo5aa	1.072	0.0098
F1QRX2	Small ubiquitin-related modifier	sumo3b	1.057	0.0039
Q6DRI5	Nucleolar GTP-binding protein 1	gtpbp4	1.045	0.0347
Q7SXW6	Actin-related protein 2-A	actr2a	1.027	0.031
Q6DG11	Spliceosome-associated factor 1	sart1	1.026	0.0259
Q7SY50	Zgc:63505	stoml2	1.021	0.0149
A2RUY2	Ribosomal protein S6 kinase	rps6ka3b	1.005	0.0163

Co-Transfection vs secVHH-MT

Accession	Protein Name	Gene Name	Abundance	p value
B2GP19	Zgc:92867	adprs	1.226	0.0132

Figure 33. Table of 1st mass spectrometry significantly increased protein abundance. *Table of significantly increased protein abundances of experimental conditions over controls. T-test p value and protein abundance indicated for each protein name and accession number. Each protein is represented as red points in figure 32.*

In summary, we observe a lack of any detectable control peptides Wnt8a-GFP and secVHH-MT, poor protein abundance separation, non-specific enriched protein hits and an inability to generate gene ontology analysis. In light of this, I conclude failure for the first mass spectrometry analysis. The greatest weakness of the assay appears to be poor transfected protein abundance.

5.2.2 The second mass spectrometry attempt

As generating stable PAC2 cells resulted in failure, a polyclonal approach was made in contingency. This, in retrospect, still fell short of success, and so a re-design of protein expression is necessary. To address this, stable cell lines were re-attempted using AGS cells instead, resulting in the extremely successful AGS secVHHmCh-MT 'B7' stable cell line (chapter 2 Fig 18). Stable cell line generation of Wnt-GFP were unfortunately unsuccessful, however, as the assay developed, improvements to transfection protocol alongside a switch from Wnt8a-GFP to Wnt5a-GFP yielded observed increase in transfection efficiency (data not shown). A second mass spectrometry attempt was conducted using AGS B7 secVHHmCh-MT stable cells and Wnt5aGFP transfected PAC2 cells in conditions similar to the first mass spectrometry. Learning from the first mass spectrometry attempt, the desalting step was omitted to prevent loss of protein (Fig 34).

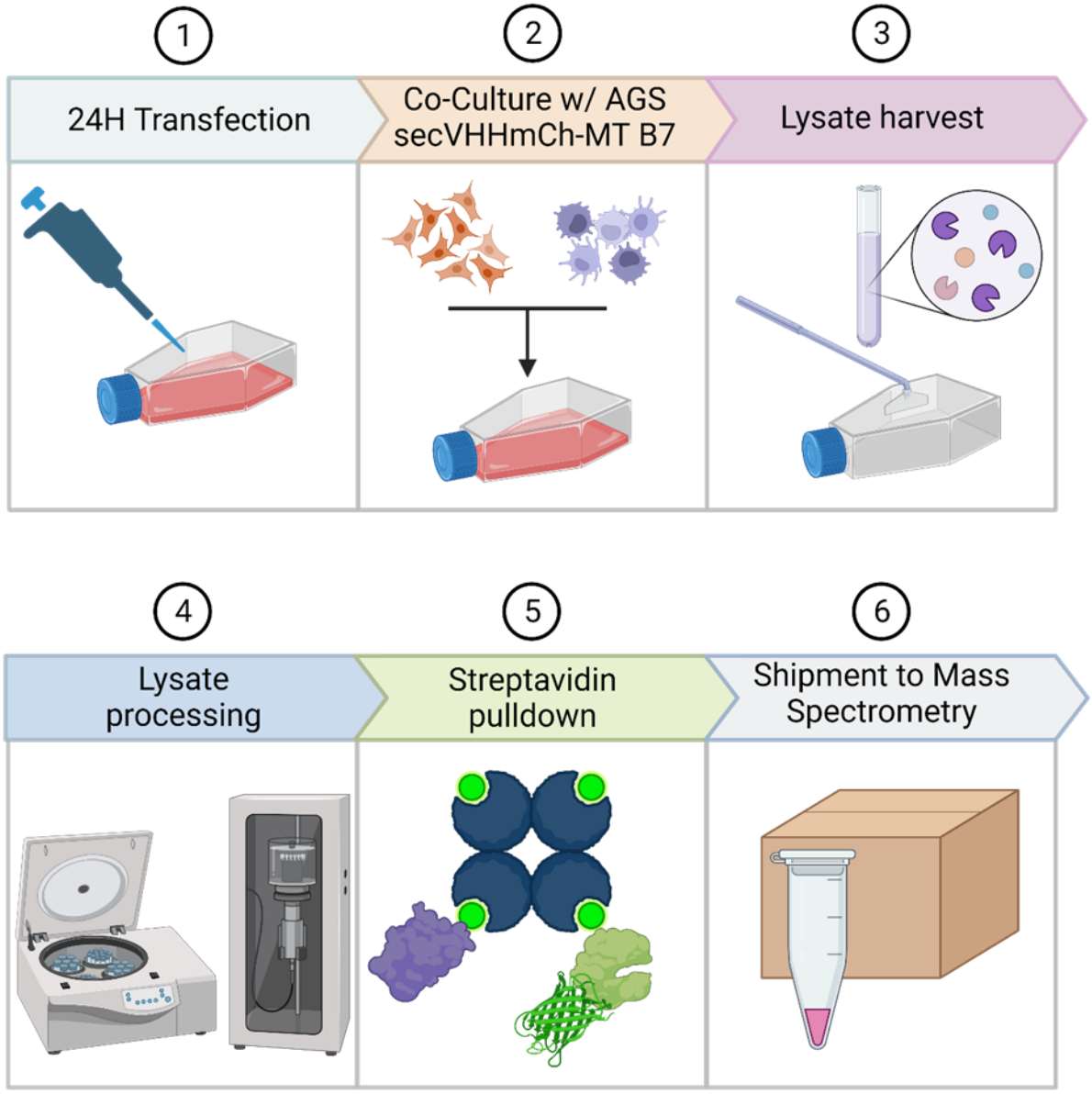

Figure 34. 2nd Mass spectrometry protocol. *General protocol of producing PAC2 AGS co-culture assay, lysate extraction, processing, pulldown and shipment to University of Bristol for mass spectrometry. Created with BioRender.com.*

The experimental setup was originally set to contain three conditions; 'Wild Type', AGS 'secVHHmCh-MT' B7 and 'Co-Culture' of Wnt5aGFP transfected PAC2 and AGS secVHHmCh-MT B7 cells. The decision to expand on the experimental parameters was made shortly before submitting the samples to add a 'Co-Transfection' and 'Conditioned' media conditions. As typical TMT mass spectrometry allows up to 16 samples to run simultaneously, three repeats of these five conditions was used for a 15plex TMT analysis. Shortly

before shipment of samples, I decided to investigate the full potential of the AGS B7 line by observing conditioned media of PAC2 Wnt5aGFP (chapter 2 Fig 26). The conditioned media exceeded expectations, and so were included in the final assay. Furthermore, to gauge the sensitivity of the mass spectrometry, I submitted an extra 'Test' sample of 'Co-Culture'. This 'Test' sample aimed to determine the amount of fractionations needed for the final assay. The 'Test' sample returned a plethora of Wnt-related proteins (explained further in section 5.2.3) and so no changes to TMT conditions were altered.

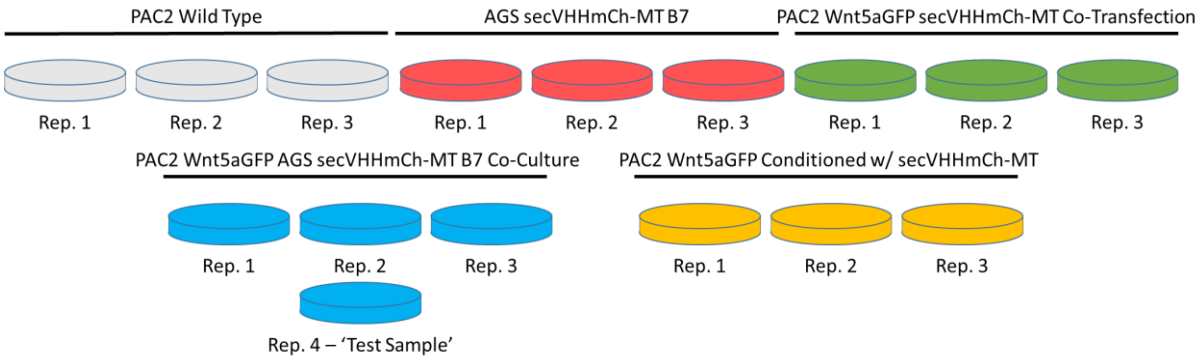

Figure 35. 2nd Mass spectrometry experimental conditions. *PAC2 cell culture conditions prior to lysate extraction. Wild type cells are standard passage of PAC2 cells. Cultures incubated in 500μM biotin for 1 hour prior to RIPA lysis. An extra 'Co-Culture' sample was generated for fractionation testing.*

Transfection efficiency of PAC2 cells expressing Wnt5a-GFP shows clear improvement over that seen in the first mass spectrometry assays expressing Wnt8a-GFP (Fig 11). Both culture population and ratio of transfected cells to non-transfected cells address the first problem faced in the first mass spectrometry – transfected protein abundance.

Similarly to the first mass spectrometry, when analysing the results dataset, the first step was to explore data distribution and identify any groups with significant bias.

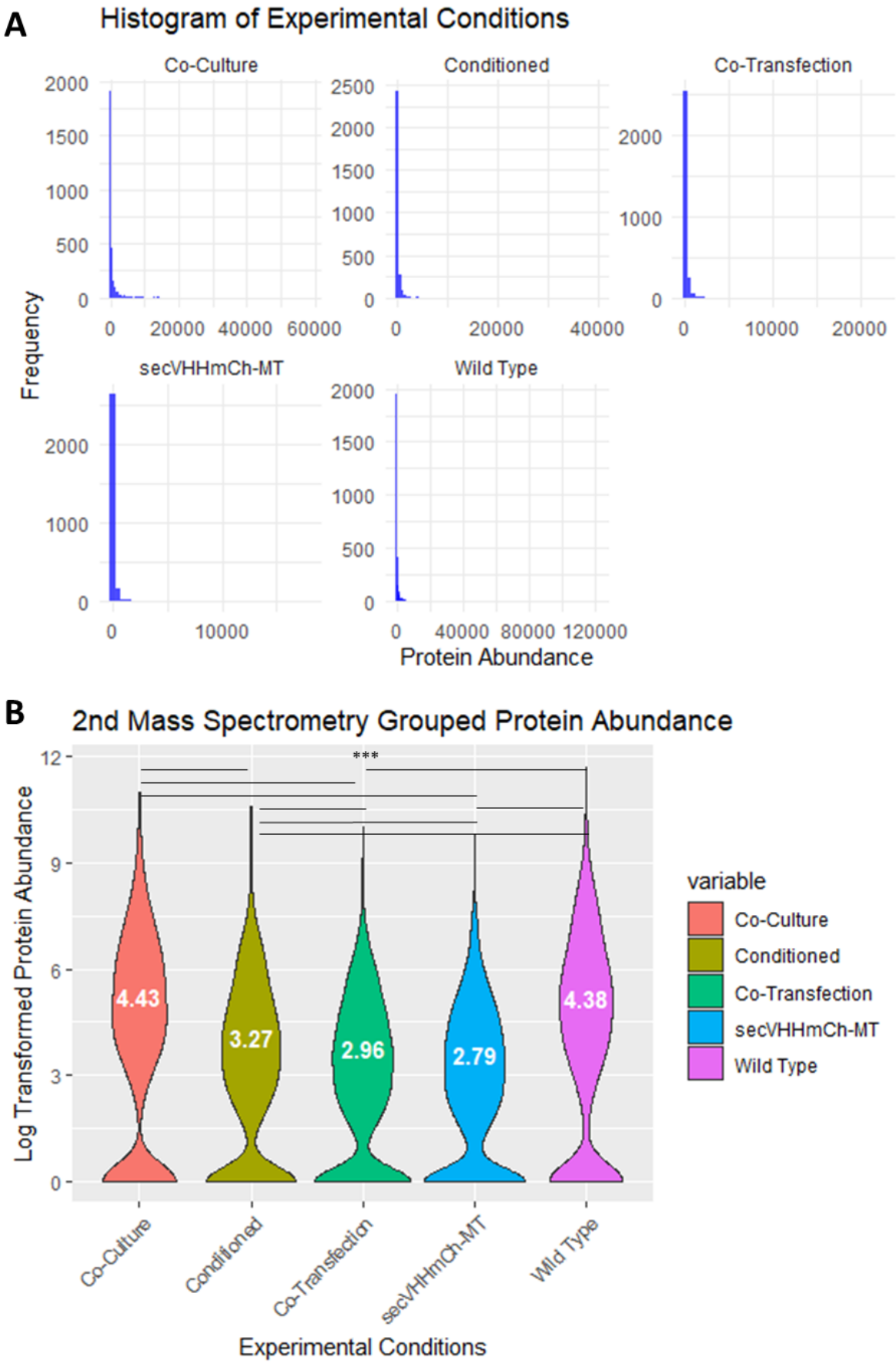

Figure 36. Second mass spectrometry data distribution and normality. *(A) Histogram of average frequency of peptides for a given abundance. (B) Violin*

plot of protein abundance between the five experimental conditions. Protein abundance data transformed by log to display values on plot. Log of median highlighted for each condition. One way ANOVA Kruskal-Wallis test was performed for the four conditions. chi-squared = 725.34, df = 4, p-value = $2.2_{x10^{-16}}$. All groups with significant difference have p<0.0001.

Similarly to the first mass spectrometry data, the data for the second are non-normally distributed with a heavy skewness towards zero. Because of this, a one-way Kruskal-Wallis ANOVA is required to fit the data. Unlike the first mass spectrometry, the grouped protein abundance was significant for Kruskal-Wallis ANOVA, suggesting significant differences in protein abundance between experimental conditions. I used a Dunn's post hoc test to compare pairs of groups to determine which pairs are significantly different. Strikingly, the only two pairs that were not significantly different were 'co-transfection' – 'secVHHmCh-MT' and 'co-culture' – 'wild type'. Considering how eight pairs of groups out of the ten total pairs are significantly different, it is highly likely that protein quantities detected by the mass spectrometry machine are not balanced. Indeed, we expect the majority of pairs to be non-significant from one another if all protein abundances were loaded in equal quantities. This could be from either improper protein balancing during the streptavidin pulldown step, improper balancing of streptavidin quantity (highly unlikely) or poor labelling of protein peptides with isobaric tag for TMT mass spectrometry identification. This difference in grouped general protein abundance is a severe problem for identifying significantly enriched peptides as it cannot be discerned whether the peptide is being biased by the over or under-weighting of the experimental condition.

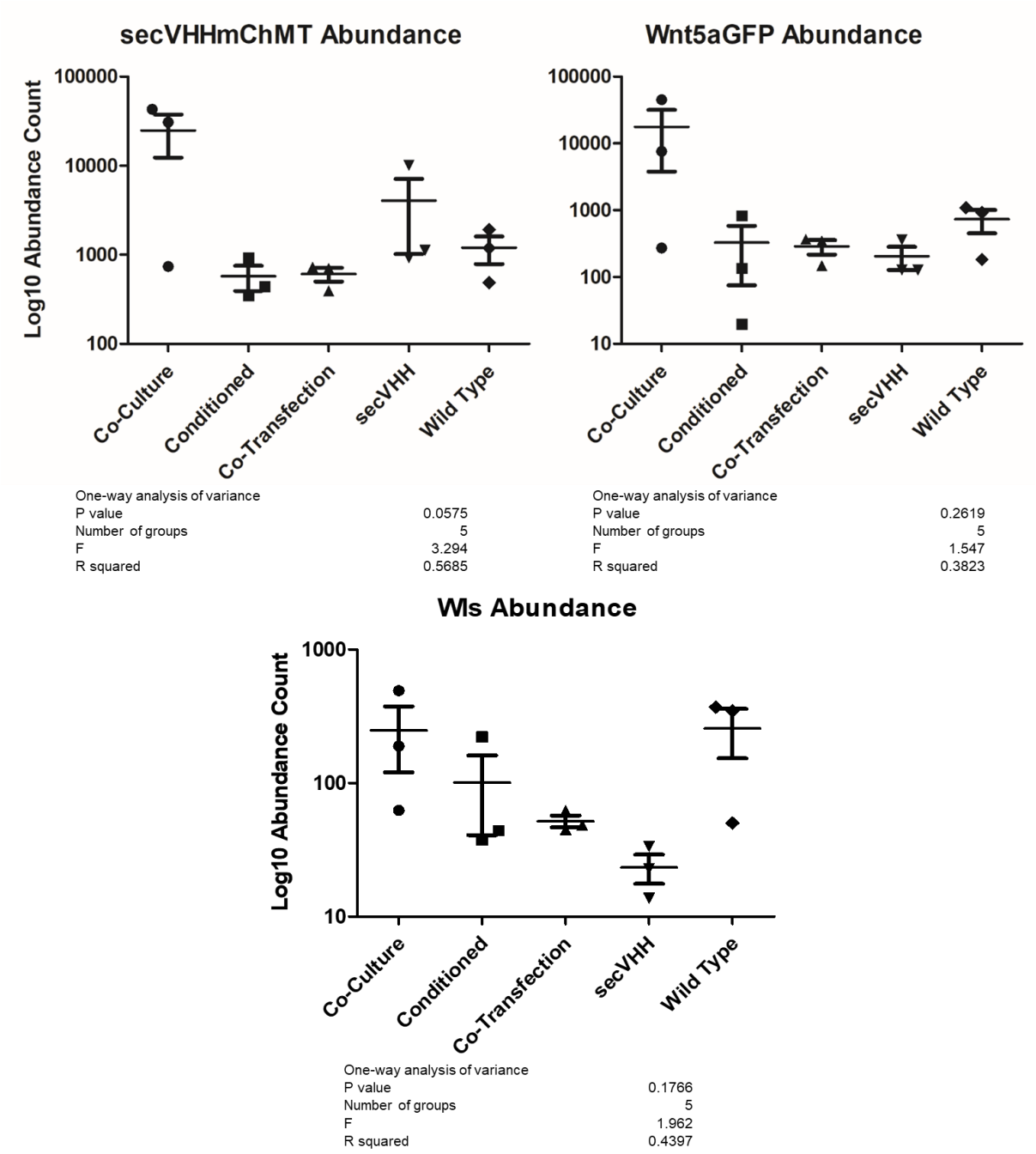

Figure 37. Comparisons of secVHHmCh-MT, Wnt5a-GFP and Wnt transport protein Wls. *Protein abundance comparisons between the five experimental conditions for transfected proteins secVHHmCh-MT and Wnt5aGFP and Wnt interacting protein Wls. Protein abundance transformed by Log10. One-way ANOVA analysis results highlighted for each protein.*

Transfected proteins Wnt5a-GFP and secVHHmCh-MT were detectable in high quantities with secVHHmCh-MT ranked 11th and Wnt5a-GFP ranked 31st in score Sequest. The high score Sequest ranking demonstrates high protein

abundance, which can be attributed to either or both high abundance in crude lysate or high biotinylation. This confirms the successful increase in transfection efficiency of the cell culture, solving the issue surrounding low transfected protein abundance. Considering the issue of significantly different grouped protein abundance in Fig 36, individual protein trends should be consistent with those for the experimental condition. Despite this, neither Wnt5a-GFP nor secVHHmCh-MT showed any significant differences between any groups in a one-way ANOVA analysis ($p = 0.26$, $F = 1.55$, $R^2 = 0.38$ and $p = 0.058$, $F = 3.29$, $R^2 = 0.57$ for Wnt5a-GFP and secVHHmCh-MT respectively) (Fig 37). For secVHHmCh-MT, the ANOVA regression fitting explains a little over half of the variability and the large F statistic of 3.29 suggests a significant difference between group means. This is highlighted by the high median seen in the 'Co-Culture' and 'secVHHmCh-MT' conditions (Fig 37). The p value falls just shy of the significance cut off, therefore we observe a trend that secVHHmCh-MT abundance is increased for these two conditions, but cannot reject the null hypothesis. As for Wnt5a-GFP, the model explains less variance in data. Furthermore, less variability in data between conditions and even less significant difference in mean is observed. Whereas the data for secVHHmCh-MT could suggest a trend despite non-significance, Wnt5a-GFP shows none.

Wls is an evolutionarily conserved trans-membrane protein responsible for binding to and transporting acetylated and glycosylated Wnt peptides for secretion (Bänziger et al., 2006). When reviewing the list of protein hits, Wls was the only directly Wnt related protein identified and so was chosen to assess any difference in abundance between groups. Unfortunately, Wls too showed no significant difference between experimental conditions ($p = 0.18$, $F = 1.96$, $R^2 = 0.44$). Common observations between the three peptides is that the 'co-culture' condition has consistently higher protein abundances to the remaining conditions. This condition also shows two high protein abundances and a single significantly smaller abundance. Indeed, this trend of similar protein abundance between repeats of a single condition appears consistent, suggesting a high disparity between repeats. This high disparity contributes to the high variance within each condition that impedes the power of the ANOVA analysis.

A

Top 7 Mass Spectrometry Hits of Second Mass Spectrometry Attempt

Accession	Description	Gene Name	Marked as	# Peptides	Score Sequest HT
A0A0R4IFJ4	Pyruvate carboxylase	pcxa	Zebrafish	61	2061.42
A0A1B0GVI3	Keratin, type I cytoskeletal 10	KRT10	Human	39	1706.03
Q6DGE2	Propanoyl-CoA:carbon dioxide ligase subunit alpha	pcca	Zebrafish	45	1457.46
P15924	Desmoplakin	DSP	Human	164	1314.19
B3DGZ9	Pyruvate carboxylase	pcxb	Zebrafish	29	1053.19
F1QH12	Acetyl-CoA carboxylase	acaca	Zebrafish	93	848.17
secVHHmCh-MT	secVHHmCh-MiniTurboID	secVHHmCh-MT	Zebrafish	23	834.63

B

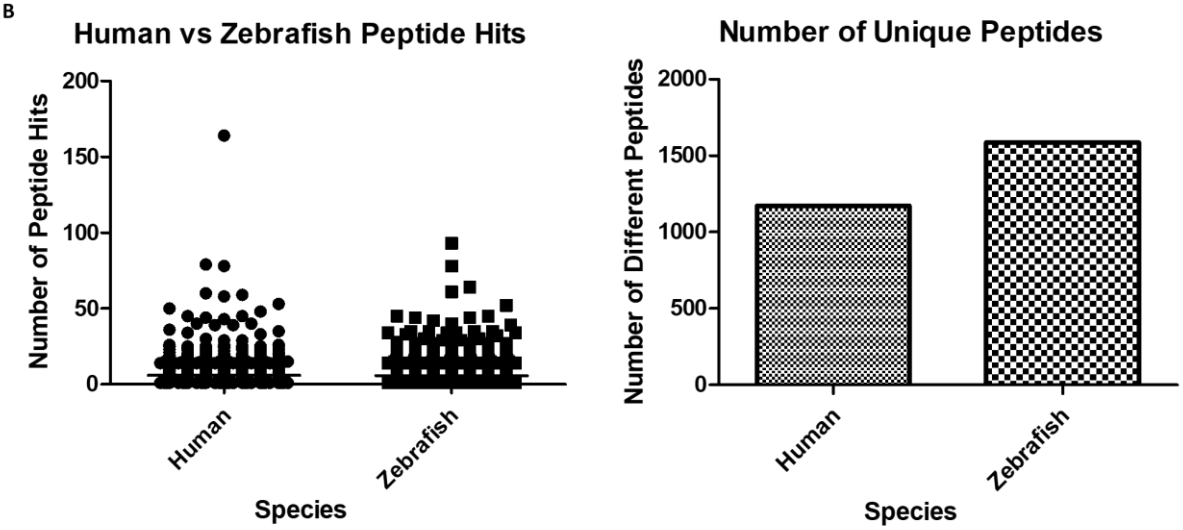

Figure 38. Top mass spectrometry hits and differences between species of second mass spectrometry attempt. *(A) Top seven protein hits ranked by score Sequest. (B) Scatter-plot comparing number of human to zebrafish protein peptides. Boxplot highlighting the number of unique peptides identified.*

The first mass spectrometry analysis returned two carboxylases in the first seven protein hits ranked by score Sequest (Fig 31). The second mass spectrometry analysis returned four carboxylases in the top seven protein hits, including secVHHmCh-MT as the 7th ranked protein hit. The only difference in lysate processing was the omission of a desalting step for the second mass spectrometry. It is unlikely that the desalting step would negatively interfere with the streptavidin pulldown, resulting in fewer endogenous protein hits. Regardless, the higher frequency of carboxylases with high Score Sequest reflects either a higher streptavidin pulldown efficiency or lack of biotinylated proteins from secVHHmCh-MT. Interestingly, there were 1172 human specific proteins compared to the 1587 zebrafish specific proteins, a difference of 415 unique proteins. As AGS cells grow faster than PAC2 and occupy a higher population per surface area of culture plate, this should increase bias of human

proteins over zebrafish proteins. The likely culprit is the influence of experimental conditions that do not have AGS cells. As it is impossible to separate the ‘co-culture’/’secVHHmCh-MT’ samples from experimental conditions that do not contain any AGS cells, we cannot understand the balance of human peptide variety and number over zebrafish peptides from the combined TMT analysis alone.

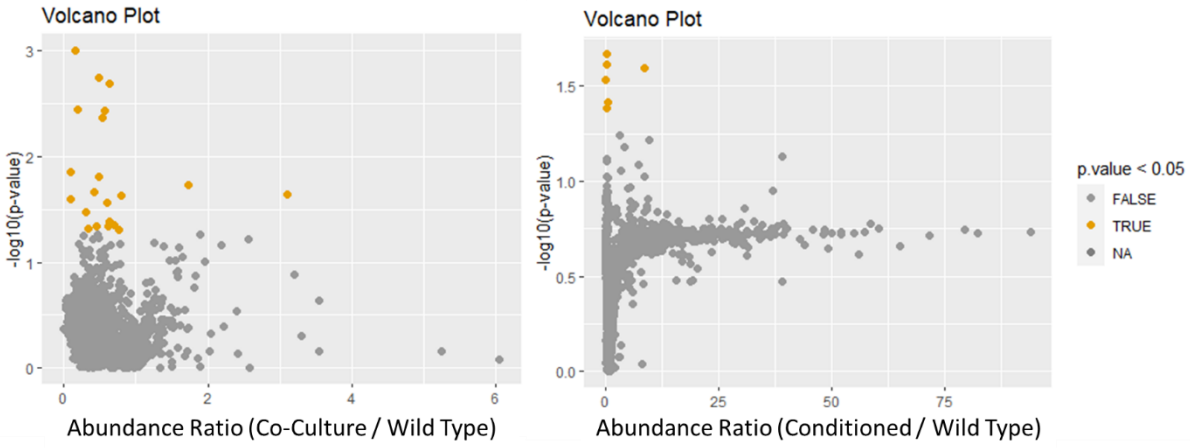

Gene Name	Abundance Ratio: (Cond) / (WT)	p.value
COL1A2	3.097	0.02271475
CD2AP	1.73	0.01861621
abhd10b	0.797	0.02334602
cnpy3	0.772	0.04959929
frem2a	0.704	0.04498106

Gene Name	Abundance Ratio: (CC) / (WT)	p.value
zranb2	8.768	0.025371
prpf4bb	0.607	0.038241
zgc:63882	0.392	0.024171
serbp1a	0.352	0.021377
rbm39a	0.232	0.041158
MYH11	0.141	0.029157

Figure 39. Volcano plot of Co-Culture and Conditioned media samples over Wild Type. *Volcano plots of abundance ratio of experimental over ‘Wild Type’ condition. T-test performed on each individual protein between experimental and ‘Wild Type’ conditions to plot the p value on y-axis. Grey pixels indicate non-significant proteins and yellow pixels indicate p value of >0.05. Significant proteins listed with abundance ratio and p value listed.*

Generating a volcano plot comparing the abundance ratio between ‘Co-Culture’ and ‘Conditioned’ conditions over ‘Wild Type’ yielded similar plots to those observed in the first mass spectrometry. Similarly, to the first attempt, more proteins are significantly decreased than enriched in experimental conditions over ‘Wild Type’ control. The only enriched proteins are COL1A2 and CD2AP for Co-Culture and zranb2 for Conditioned media samples. COL1A2 is a gene encoding for collagen and CD2AP encodes for a scaffold protein binding to CD2, localised within the cytoplasm on actin cytoskeleton and on membrane

ruffles, lipid rafts, and the leading edges of cells (Kirsch et al., 1999; Lehtonen et al., 2002). Both proteins hold potential for interacting with secVHHmCh-MT at any stages of culture. Conversely, zranb2 is a zinc finger enabling RNA binding activity localised exclusively to the nucleus (Loughlin et al., 2009). Given the evidence generated for the data produced in the second mass spectrometry, this dataset failed and must be ignored.

5.2.3 The ‘Test’ mass spectrometry

The second mass spectrometry analysis demonstrated significant improvement over the first iteration in terms of transfected protein abundance and culture conditions. However, it also introduced a host of new problems concerning significant differences in protein abundance between experimental groups and high variance between repeats that prevented significant comparisons. The greatest problem thus far that has not shown improvement is the presence of any Wnt-specific and or related proteins other than Wls in the data set. Upon discovering both Wnt5a-GFP and secVHHmCh-MT presence in the data set, it would stand to reason we should equally observe biotinylated proteins associated with them. Therefore, a lack of any related proteins would simply suggest a failure of the assay working on a level strong enough for applicable use. The ‘Test’ mass spectrometry analysis would prove otherwise.

The ‘Test’ mass spectrometry dataset consisted of a single sample of ‘Wnt5a-GFP secVHHmCh-MT co-culture’ with no control samples to filter the data set (Fig 35). Because of this, it is impossible to run statistical analysis on the data to samples enriched from the ‘Co-Culture’ condition. As a crude subtraction of non-specific background noise of the data set, any protein accession numbers that existed within the ‘Test’ data set and either the first or second mass spectrometry data set were excluded. The remaining data set was submitted to String.db for protein-protein interactome mapping based on a variety of factors such as co-expression across organisms, experimental and biochemical co-occurrence in the databases and associations in curated databases.

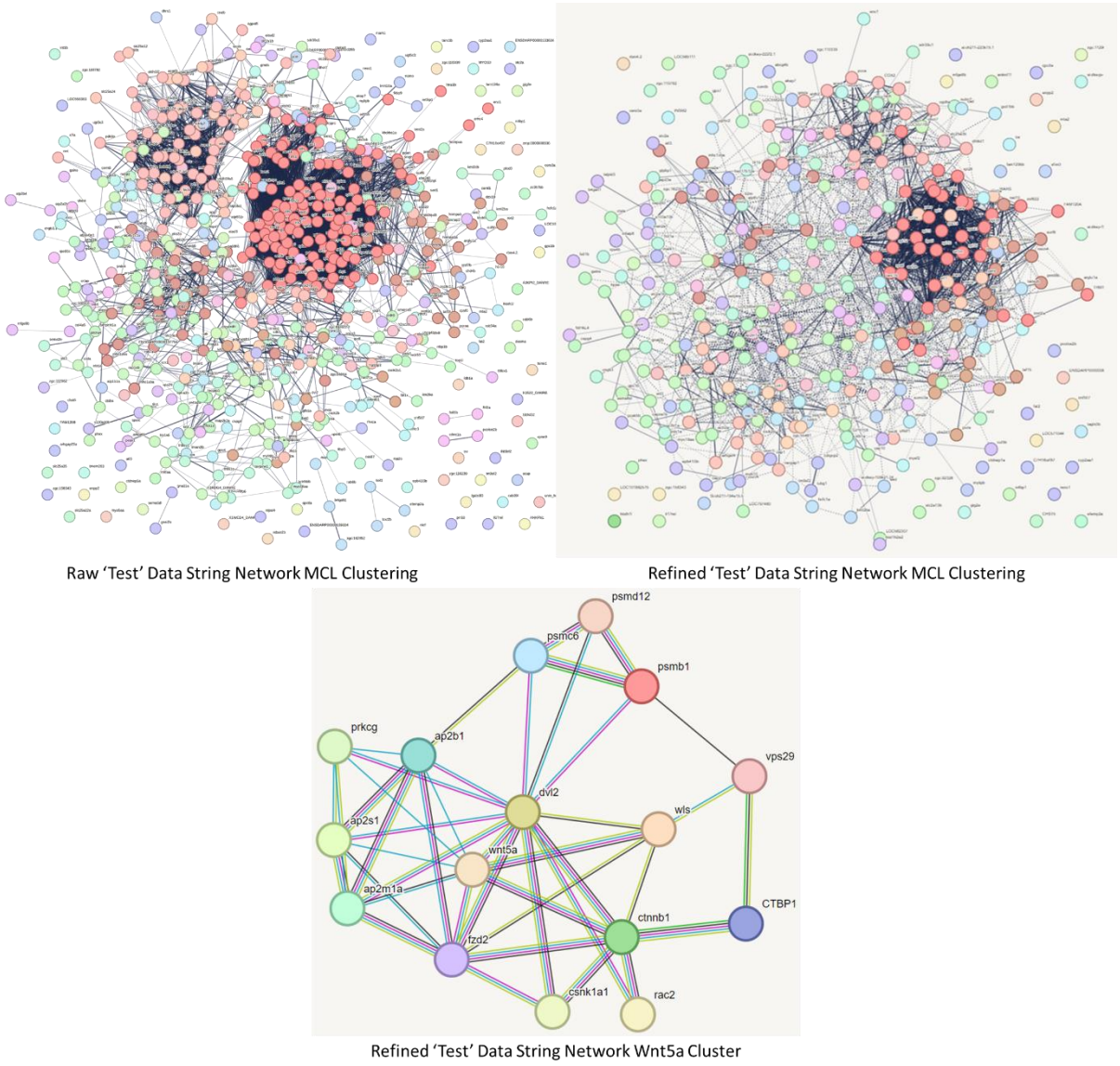

Figure 40. Zebrafish 'Test' mass spectrometry data represented by String.db. *String network of whole mass spectrometry data from 'Test' data (left) and unique proteins not found in first or second mass spectrometry database (right). (Bottom) Wnt5a cluster generated from refined 'Test' data. Created with Stringdb.com.*

408 zebrafish proteins of 732 and 1110 human proteins of 1467 were unique to the 'Test' data set. The second mass spectrometry analysis reported an equal number of human to zebrafish peptides (Fig 38) however; nearly twice as many human proteins are detected over zebrafish proteins. Of the remaining unique proteins, the largest cluster (22 proteins) constitute ribosomal or related subunits (Fig 40). The second largest cluster (14 proteins) constitute alpha-catenin or Frizzled binding. Indeed, looking at the entire unique protein string,

the top returning reactome pathway constitutes ‘Wnt5a-dependant internalisation of FZD4’. Astonishingly, several Wnt related proteins were identified such as fzd2, Wnt7b, β-catenin, dvl2, flot1 and wls (Fig 40). Wls was observed in both mass spectrometry results thus far, however human Wls was not. The detection of human Wls unique to the ‘Test’ dataset suggests the possibility of Wls – Wnt5a-GFP interaction in receiving cells.

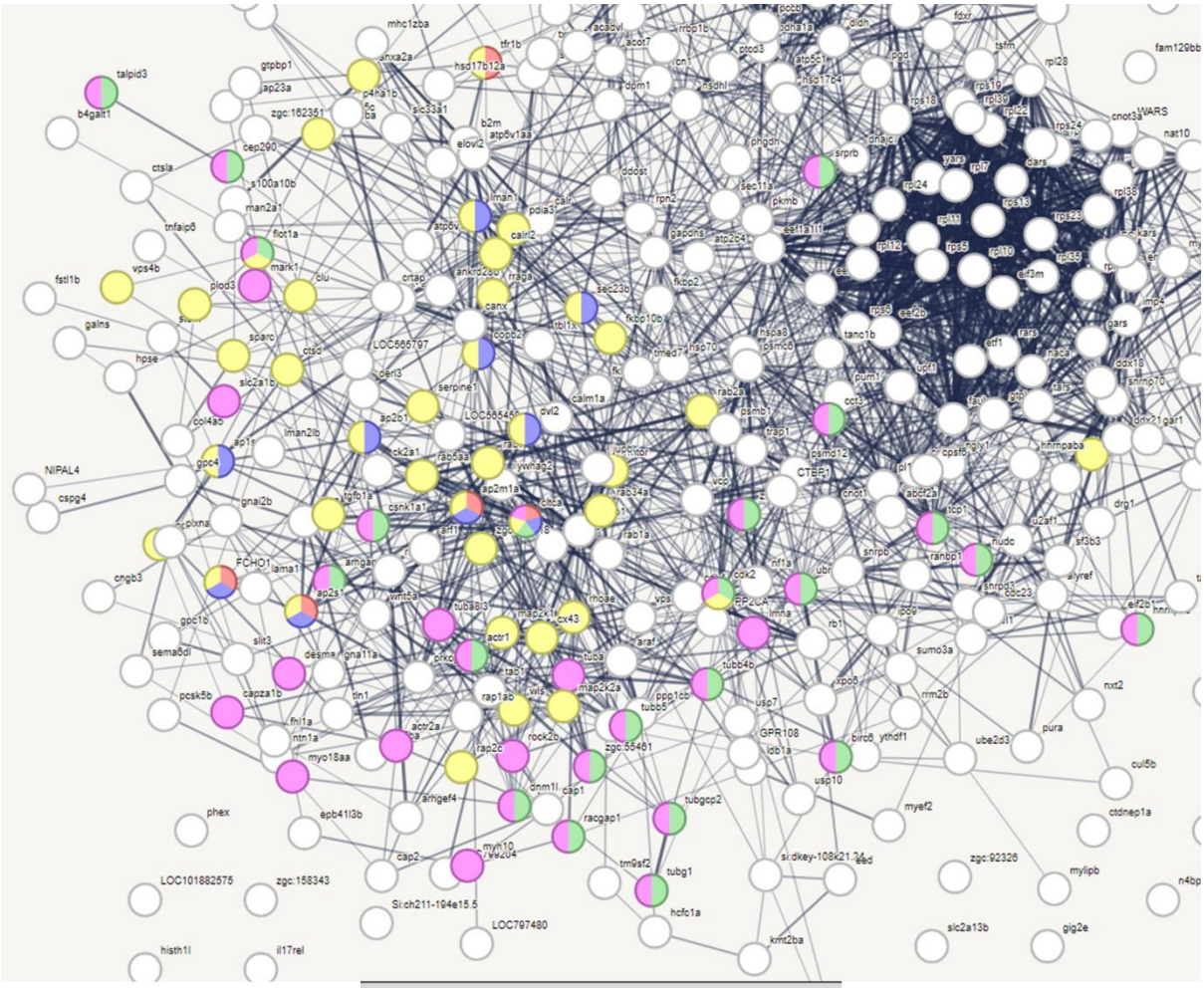

Key	
Red	Clathrin Coated Pit
Blue	Coated Vesicle
Green	Microtubule Cytoskeleton
Yellow	Vesicle
Pink	Cytoskeleton

Figure 41. Cytoskeleton hits for ‘Test’ mass spectrometry analysis. *String network of unique proteins not found in first or second mass spectrometry database. Proteins relating to cytoskeleton are highlighted with the colour respective the specific aspect of the cytoskeleton. Created with Stringdb.com.*

A large proportion of the unique proteins constitute various elements of the actin cytoskeleton (Fig 41). Vesicular proteins constitute the majority of these cytoskeletal elements, followed by general cytoskeleton. Proteins such as Clathrin Heavy Chain A (cltca), Flottilin 1 (Flot1), various Rab proteins (Rab1b/a, 2, 5a/b/c, 6a, 7a, 8b, 34) and several tubulin proteins (TUBB2c, 4a, 5 and several beta chains) were detected. The high proportion of cytoskeletal and endocytosis elements suggest the possibility of enrichment of these pathways possibly as secVHHmCh-MT is internalised once bound to Wnt-GFP.

5.2.4 The third and final mass spectrometry

The evidence generated from the 'Test' mass spectrometry data provided new clues as to the failings of the previous two mass spectrometry attempts. Alone, the co-culture sample yielded various Wnt-related proteins and a variety of endocytosis and actin cytoskeletal protein such as Flotillin, Clathrin, tubulin and myosin motor proteins. When combined with multiple control and experimental samples in the same TMT analysis, these protein hits were lost. It stands to reason that the greatest flaw of the analysis is the minute signal to noise ratio. This has been a prevalent problem during all stages of the nanobody-biotin ligase assay design and it appears the TMT analysis lacks the sensitivity for combining several conditions simultaneously. To address this, the third mass spectrometry analysis refined the experimental conditions to two; four repeats of 'Wild Type' control and 'Conditioned Media' experimental. There was much debate whether to choose a co-culture or a conditioned media sample as the experimental condition. While proof for co-culture success was demonstrated in the 'Test' mass spectrometry, it was also shown that human proteins outweigh zebrafish 2:1. Strong evidence for the efficacy of 'Conditioned Media' samples was demonstrated in chapter 2 Fig 26, therefore, replacing 'Co-Culture' samples with 'Conditioned Media' can remove all human protein interference to enhance the sensitivity of zebrafish proteins. The experimental protocol was not changed from the second mass spectrometry (Fig 34). I want to declare that a large majority of the work presented from here were contributions made by our collaboration partners Kristína Gömöryová from the Vítězslav Vita Bryja lab.

Any figures and data analysis produced from Kristína will be highlighted in the figure legend.

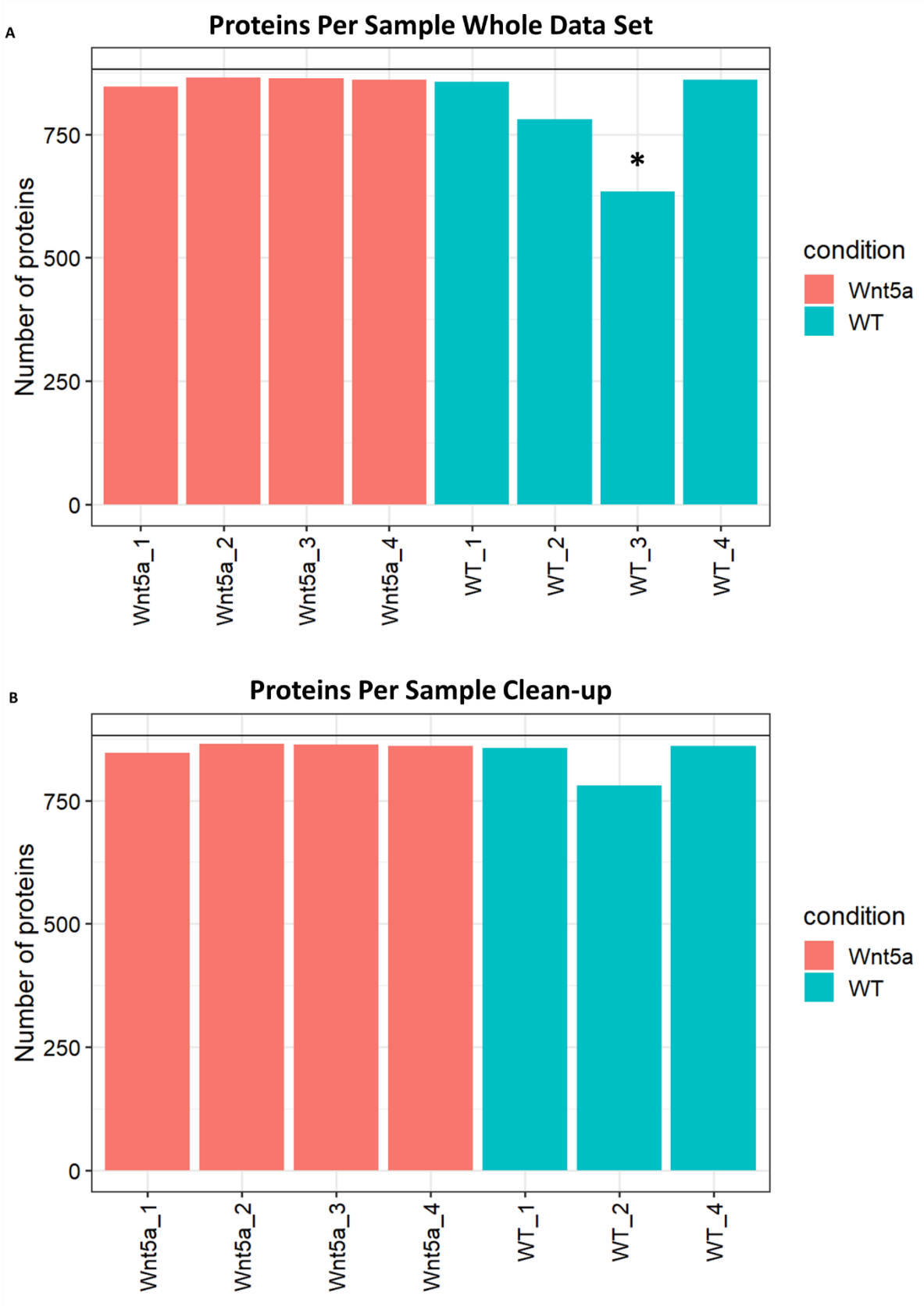

Figure 42. 3rd Mass spectrometry protein distribution and cleanup. *(A) Whole mass spectrometry dataset of protein abundance per experimental sample. Asterix indicate 'Wild Type' repeat three demonstrating reduced protein*

abundance. (B) Mass spectrometry data set excluding 'Wild Type' repeat three. Figure and analysis performed by Kristína Gömöryová.

Five of the eight experimental conditions demonstrate proportionally similar protein abundances. Slight drops from the global mean are observed for conditioned media sample 'Wnt5a_1' and Wild Type control 'WT_2'. Wild Type control 'WT_3' however demonstrated a large drop from the mean. Normalisation of the data sets to equilibrate protein abundance would be a potential fix for the large drop in 'WT_3'; however, it could introduce more issues. As there are four repeats for each condition, 'WT_3' was dropped entirely, avoiding any issues arising from over biased data sets pulling the entire 'WT' control mean down (Fig 42.B).

Next, the distribution for each individual protein mean was addressed with the variance normalised by a variance stabilising transformation. Once the data distribution was stabilised, the data was normalised to ensure conditions such as 'Wnt5a_1' and 'WT_2' are within acceptable ranges.

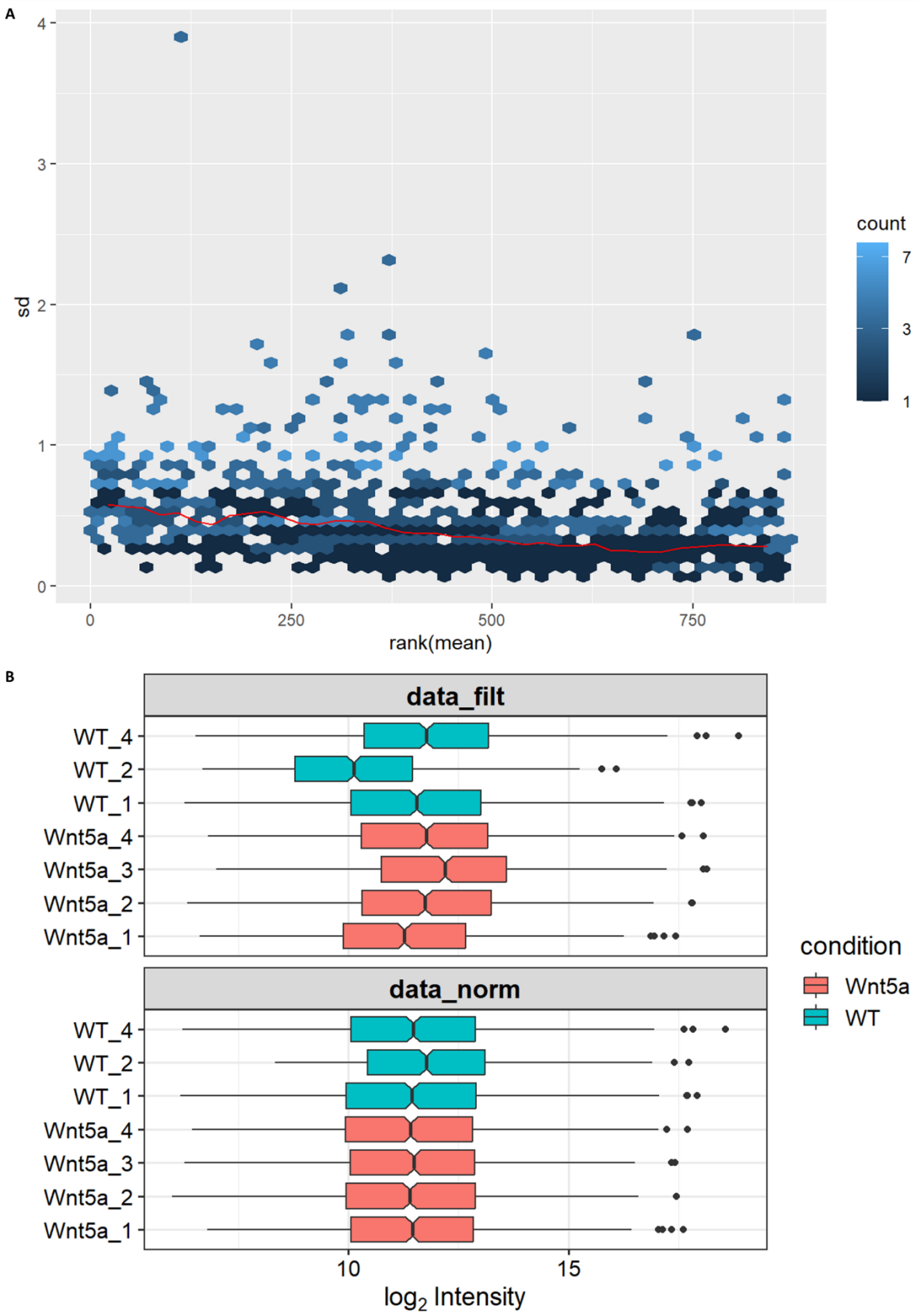

Figure 43. Mass spectrometry data transformation and normalisation. *(A) Mass Spectrometry data adjusted using variance stabilising transformation and plotted standard deviation for every rank of mean. Colour intensity represent*

frequency of proteins for each rank of mean and standard deviation. Red line indicates average standard deviation for each rank of mean. (B) Box and Whisker plot of Log2 transformed protein abundance for every sample before and after data normalisation. Figure and analysis performed by Kristína Gömöryová.

The standard deviation distribution post variance stabilising transformation shows an even distribution of standard deviation across every rank of mean (Fig 43.A). There are a few points of extreme standard deviation, however these are rare. The standard deviation trend line has a slight negative correlation slope but is acceptable. Protein abundance normalisation also appears acceptable post normalisation, with little extremes from the average. 'WT_2' still appears to be off from the normal, but is far closer to the average then prior to normalisation. Interestingly, 'WT_2' has been shifted above the average post normalisation, whereas it was below the average prior.

Once the data was transformed, it was time to investigate the individual values themselves. The first aspect of the data to explore was the proportion of protein abundance values that were zero and/or missing for each sample. To do this, a heat map plotting each sample against one another comparing values present or missing was produced to identify the extent of missing values and if any single sample requires extra processing.

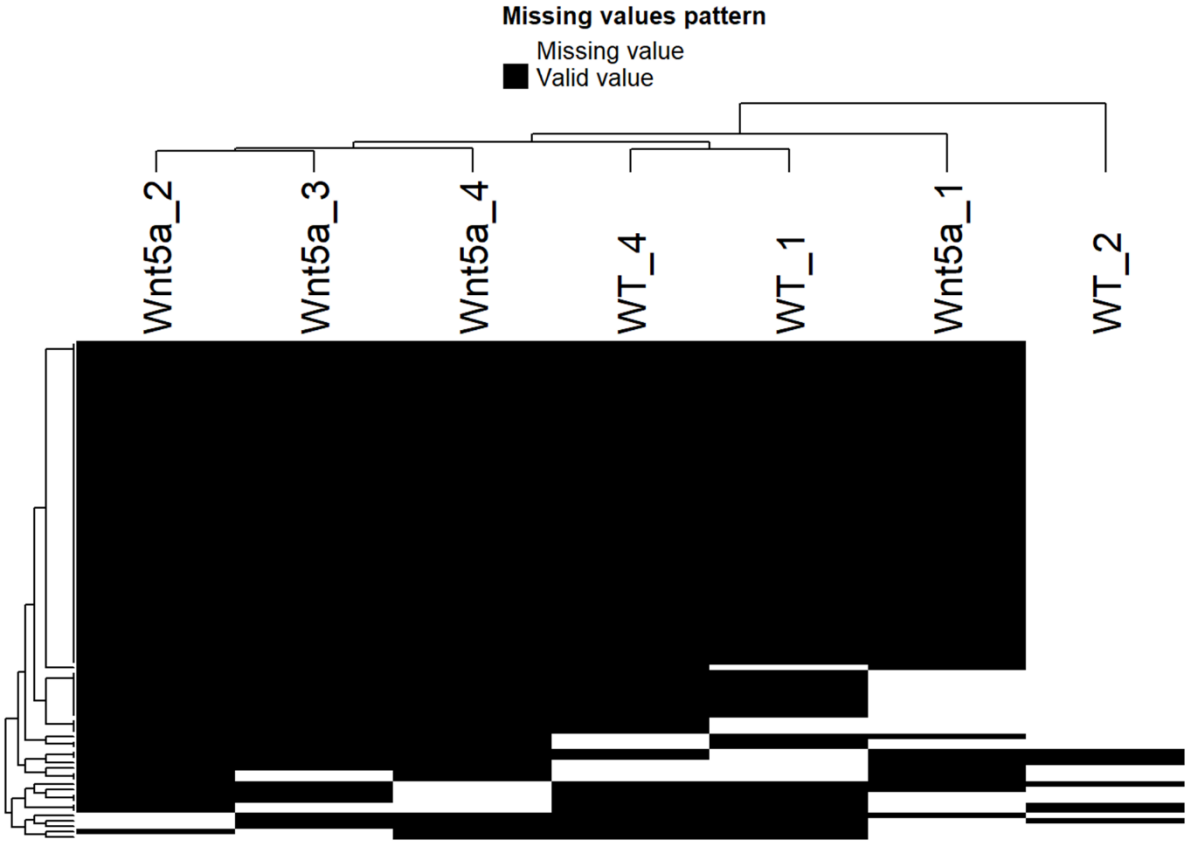

Figure 44. Mass spectrometry data post normalisation missing values heat map. *Heat map of Mass Spectrometry data three post normalisation. Heat map compares each sample for whether they contain missing or valid values. Figure and analysis performed by Kristína Gömöryová.*

The majority of data sets between all samples except ‘WT_2’ show proportionally high rates of valid values, a positive sign for comparing protein abundance between samples for statistical analysis. ‘WT_2’ sample has proportionally the highest number of missing values of any sample by a very large margin. ‘Wnt5a_1’ also has a high proportion of missing values compared to the remaining data sets, however it proportionally contains more than half of the missing values compared to those missing in ‘WT_2’.

The heavy bias of missing values exhibited by ‘WT_2’ causes concern for the analysis of protein peptides with low abundance scores. Indeed, such peptides with low abundance scores would be the peptides we expect to be biotinylated by secVHHmCh-MT due to the low signal to noise ratio. To avoid biases in statistical analysis of these peptides due to the missing values of ‘WT_2’, a differential enrichment analysis based on linear models and empirical Bayes

statistics (limma) was imputed. Firstly, missing not at random (MNAR) proteins were identified using intensity values of proteins in all replicates of at least one condition. Missing proteins not identified as MNAR are missing at random (MAR) and so are handled differently. Missing values for MNAR are imputed from the normal data using a mixed model, whereas MAR values are imputed using k-nearest neighbours. The mixed imputation data set was then tested for significant differences to the wild type control, with significant differences under 'log fold change > 1' and 'adjusted p-value < 0.05'. The frequency of p-value values were plotted on a histogram to identify any significant protein changes.

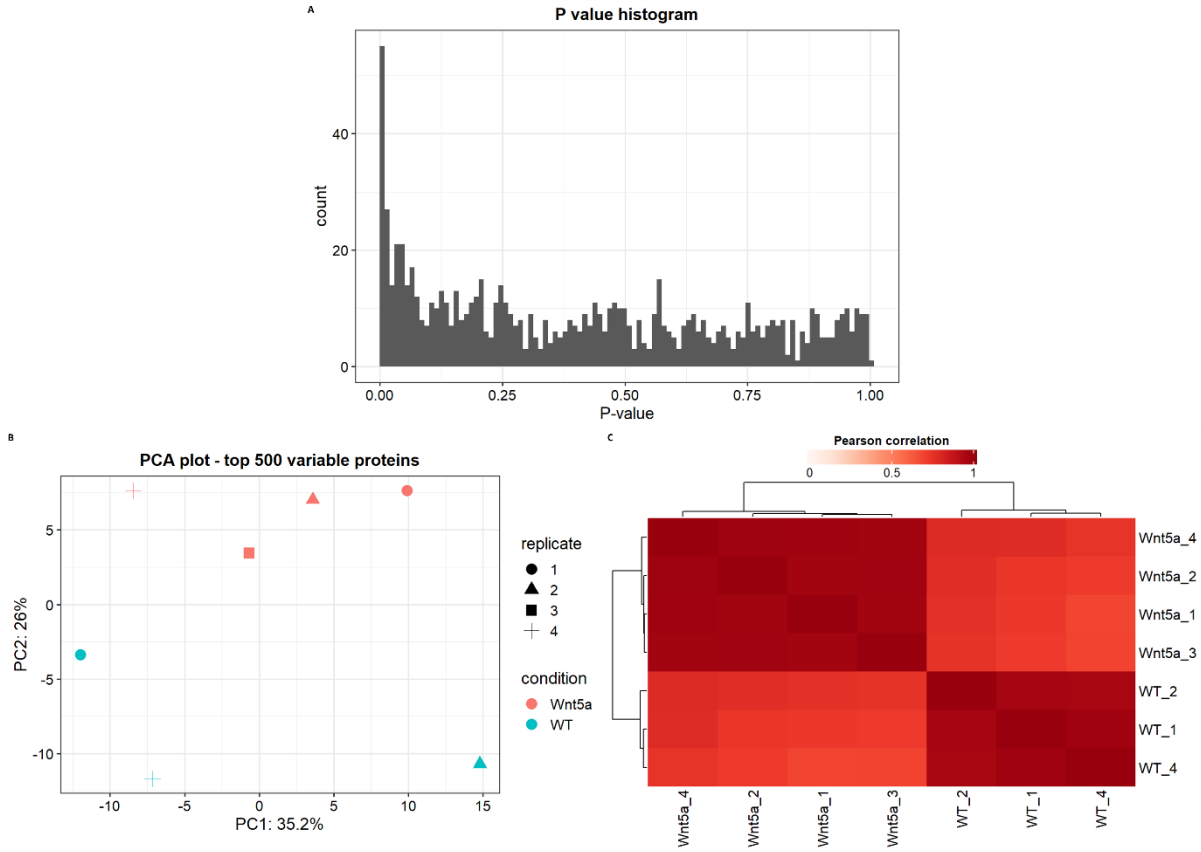

Figure 45. Imputation of missing values and associations between samples. *(A) Histogram of whole mass spectrometry data comparing Wnt5a to Wild Type using missing imputed data plotting frequency of P-value values. (B) Principle component analysis plotting the imputed data against principle component 1 vs principle component 2. (C) Heat map of Pearson's correlation mapping the relationship/correlation between samples. Statistically significant correlations between pairs of samples are represented by increasing intensity of red. Figure and analysis performed by Kristína Gömöryová.*

As expected of a p-value histogram, we see a sharp peak towards zero, denoting a significant fraction of the proteins are significantly different (Fig 45.A). Proteins beyond this peak follow a general trend, with only a few peaks representing a small population of changed proteins because of the mixed imputation. This small volume of changed proteins is acceptable and in general the p-value histogram highlights a healthy spread of data. A principle component analysis (PCA) was also performed to gauge the relationship or variance between samples based on the first two principal components (PC1 and PC2) (Fig 45.B). The patterns of Wnt5a and WT plots appear consistent of repeats of a given experimental condition, with the exception of the sample 'WT_2'. This is demonstrated by the tight clustering of Wnt5a points that is distinct from the clustering of WT points. The greatest difference is shown by the PC2 axis as the WT samples occupy only negative PC2 and the Wnt5a only occupy positive PC2. 'WT_2', however, does not associate itself closer to the Wnt5a condition than the WT condition, which makes its relationship between the two conditions acceptable. The Wnt5a repeats are all spaced within close proximity of one another, indicating strong consistency in protein abundance. In total, the PCA captures 61.2% of the total data set's variance.

While the PCA demonstrates good similarity between repeats, a Pearson's correlation heat map was generated to gauge the correlation between repeats and between experimental conditions (Fig 45.C). All repeats for a given condition follow very high correlation when compared to one another. Repeats of a condition compared to repeats of the opposite condition show half the correlation observed when comparing between themselves. This again shows good consistency and correlation between repeats, which demonstrates suitability of statistical comparisons between the two experimental conditions.

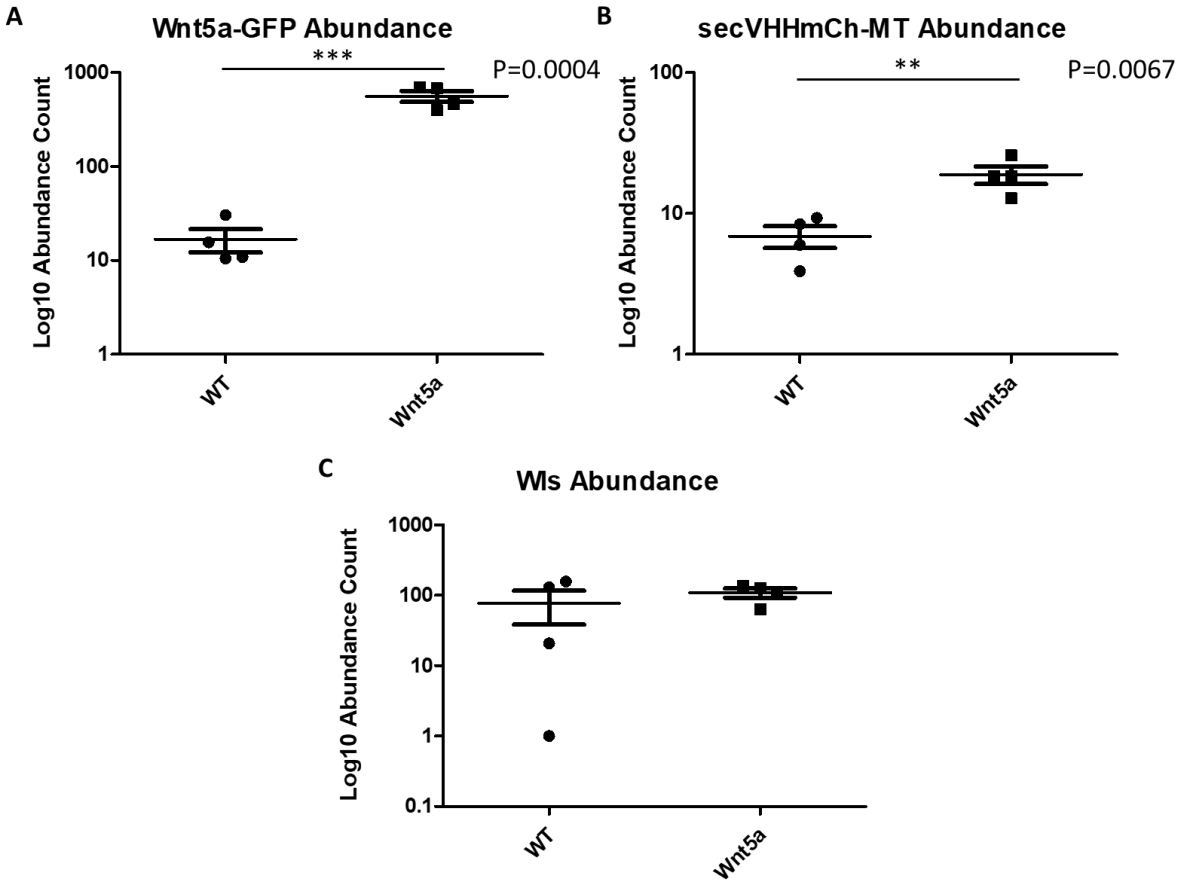

Figure 46. Comparisons of secVHHmCh-MT, Wnt5a-GFP and Wnt Transport Protein Wls for Final Mass Spectrometry. *Plots comparing log10 transformed protein abundance for (A) Wnt5a-GFP, (B) secVHHmCh-MT and (C) Wls between 'Wild Type' and 'Wnt5a' using non-mixed imputed mass spectrometry data. Plots indicate data mean (large horizontal line) with standard deviation error bars. T-test performed for each protein. ** denotes P value < 0.005, *** denotes P value < 0.001.*

When comparing the standard, non-mixed imputation mass spectrometry data set, we see significant differences in our control peptides Wnt5a-GFP and secVHHmCh-MT. Using a T-test between 'Wild Type' and 'Wnt5a-GFP' conditions, Wnt5a-GFP protein abundance is significantly increased by an abundance of 544 ±75.71 in the 'Wnt5a-GFP' group ($P = 0.004$, $F = 262.6$, $R^2 = 0.8959$). The excessively large F statistic suggests that the variance is not equal between the two groups, however, when using a Welch's T-test, we still see a significant increase ($P = 0.0056$, $F = 262.6$, $R^2 = 0.9451$). The secVHHmCh-MT is also significantly increased in the 'Wnt5a-GFP' sample over the 'Wild Type'

by an abundance of 11.98 ±2.951 (P = 0.0067, F = 4.866, R^2 = 0.7329). Unfortunately, Wls has no significant differences between the two groups despite the success with Wnt5a-GFP and secVHHmCh-MT (P = 0.4839, F = 5.827, R^2 = 0.8488).

As the control peptides are finally significantly enriched over the control group, all conditions are set to analyse the whole data set for significant protein hits. Using the mixed imputation mass spectrometry data set, a volcano plot is generated to identify proteins significantly enriched in the Wnt5a-GFP sample.

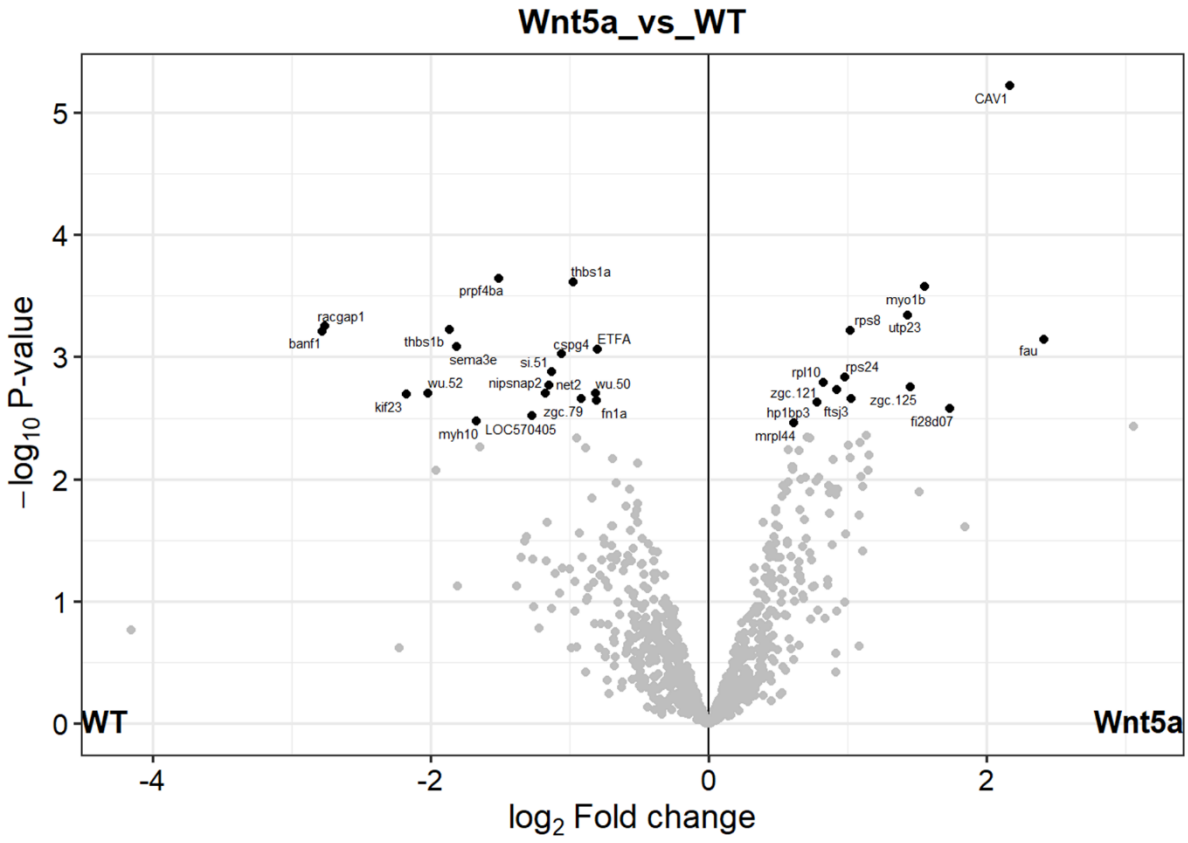

Figure 47. Mass spectrometry 3 volcano plot of mixed imputation proteins. *(A) Volcano plot of protein abundance measuring statistical significance over log fold change ratio of mixed imputation mass spectrometry three data set. Proteins with p-value greater than 0.05 are greyed out. Proteins with p-value less than 0.05 are black, labelled and listed in (B) a table with respective p-value and ratio listed. Figure and analysis performed by Kristína Gömöryová.*

Normalisation of the data set significantly enhances the distribution of peptides across the volcano plot (Fig 47), generating a clear distinction between ‘WT’ and ‘Wnt5a’ enrichment. In the first mass spectrometry analysis (Fig 32), we observed a maximum of 16 significantly enriched ‘co-transfection’ proteins. For the third mass spectrometry analysis, we see 12 proteins up-regulated for the ‘Wnt5a’ condition and 18 proteins downregulated for the ‘WT’ condition (Fig 47). The low quantity of statistically significant proteins is suggestive of poor mass spectrometry resolving of real biotinylated protein hits, as it follows a similar trend observed in the previous two mass spectrometry analysis. Indeed, gene ontology analysis of the upregulated protein data set showed no significant hits for biological processes or molecular function. Only a single significantly enriched ontology hit for the cellular component ‘small ribosomal subunit’ (false discovery rate = 0.027, $P = 4.93_{x10^{-5}}$) was identified by 2 of the 12 proteins. Equally, no gene ontology analysis could be performed on the down regulated protein list. Looking more closely at the list of ‘Wnt5a’ enriched proteins, protein CAV1 appears distinct from the typical proteins observed in the final volcano plot analysis thus far. In previous mass spectrometry analysis, significant protein hits constitute a range of non-specific ribosomal, cytoplasmic and nuclear or the occasional myosin proteins. Caveolin 1 (Cav1) is a membrane protein responsible for endocytosis and cell signalling among other aspects (Nwosu et al., 2016). Cav1 has the highest potential of any protein hit observed thus far to interact with Wnt, likely during endocytosis. Unfortunately, we cannot single out CAV1 from the list based purely on its role, while excluding other equally significantly enriched proteins. Therefore, a more stringent correction of p-values may elucidate more information on the protein enrichment list.

A

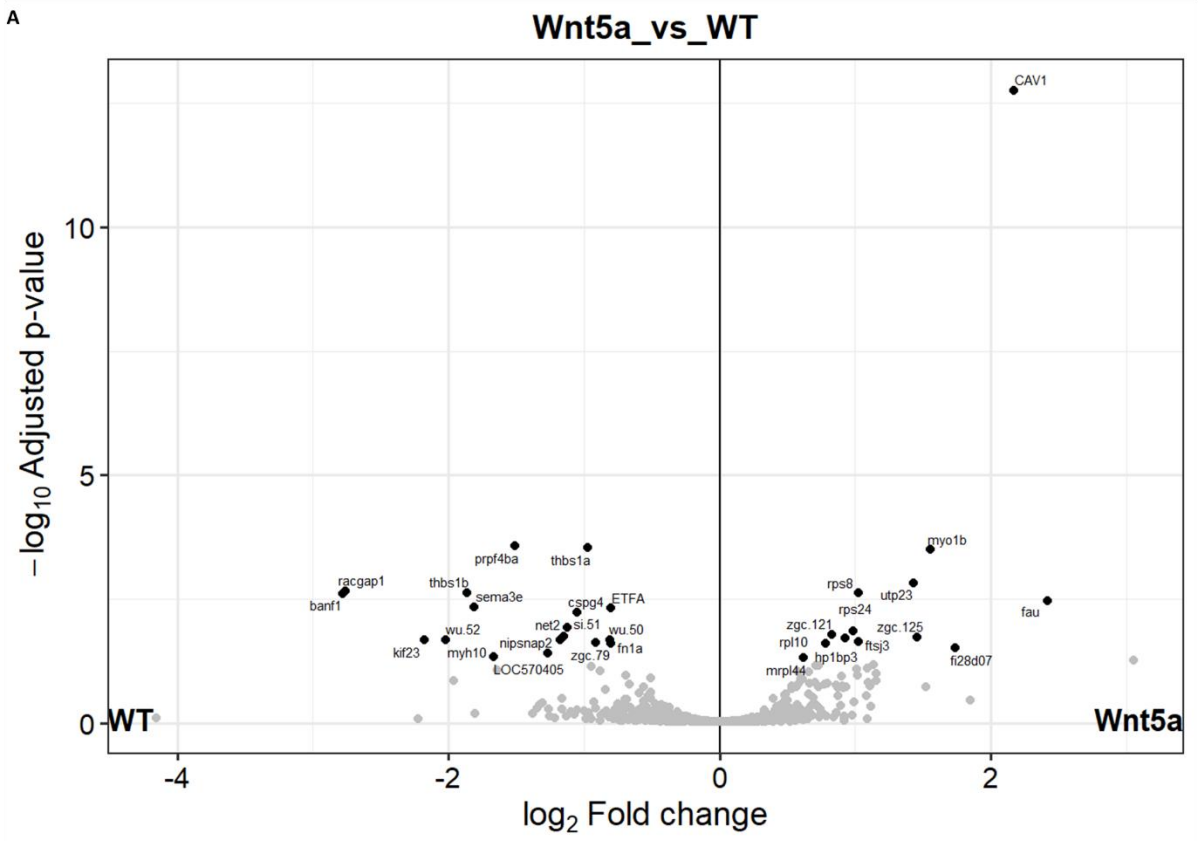

B

Up-regulated proteins			
name	ID	Wnt5a vs WT p.adj	Wnt5a vs WT ratio
1fau	Q6PC01	3.43E-03	2.41
2CAV1	Q6YLH9	1.79E-13	2.17
3fi28d07	Q7ZVR0	3.06E-02	1.74
4myo1b	A0A8M2BG11	3.18E-04	1.55
5zgc.125	Q6PFQ5	1.81E-02	1.46
6utp23	A0A0R4IA74	1.48E-03	1.43
7ftsj3	A0A8M1P1T0	2.30E-02	1.03
8rps8	P62247	2.39E-03	1.02
Down-regulated proteins			
name	ID	Wnt5a vs WT p.adj	Wnt5a vs WT ratio
1cspg4	E7FCN9	5.75E-03	-1.05
2si.51	A3KPI6	1.16E-02	-1.12
3net2	O42140	1.73E-02	-1.15
4nipsnap2	Q9PU58	2.05E-02	-1.17
5LOC570405	A0A8M6Z1M4	3.90E-02	-1.27
6prpf4ba	B0V1K6	2.69E-04	-1.51
7myh10	A0A8M3BA62	4.58E-02	-1.67
8sema3e	Q1LYS1	4.52E-03	-1.81
9thbs1b	F1QL35	2.35E-03	-1.86
10wu.52	Q6TLH6	2.09E-02	-2.02
11kif23	A0A8M9PLX5	2.12E-02	-2.18
12racgap1	Q6P3H8	2.17E-03	-2.76
13banf1	Q6P026	2.45E-03	-2.78

Figure 48. Volcano plot and significantly enriched proteins post FDR-Tool adjustment. *(A) FDRtools correction (Rstudio) for multiple testing volcano plot of protein abundance. Statistical significance over log fold change ratio of mixed imputation mass spectrometry 3 data between 'Wnt5a' and 'WT' groups. Proteins with p-value less than 0.05 are black, labelled and listed in (B) a table*

with respective p-value and ratio listed. Figure and analysis performed by Kristína Gömöryová.

Two correction algorithms were employed to further process the p-value generated for each protein. The first, Fdrtools correction for multiple testing, is a package in Rstudio that is used for the correction of multiple testing issues. The package estimates and controls the false discovery rate of each protein based on its p-value to provide an adjusted p-value based on the number of proteins analysed in total. This package addresses the type 1 error likely to be generated from a large number of individual p-values. A lower FDR-adjusted p-value means that the test result is more trustworthy. FDRtools correction significantly separates CAV1 p-value from the list of significantly enriched 'Wnt5a' proteins ($1.79_{x10^{-13}}$ vs $3.18_{x10^{-4}}$ for Cav1 and Myo1b respectively) (Fig 48). This reduced the list of total significantly upregulated proteins to 8, and downregulated proteins to 13.

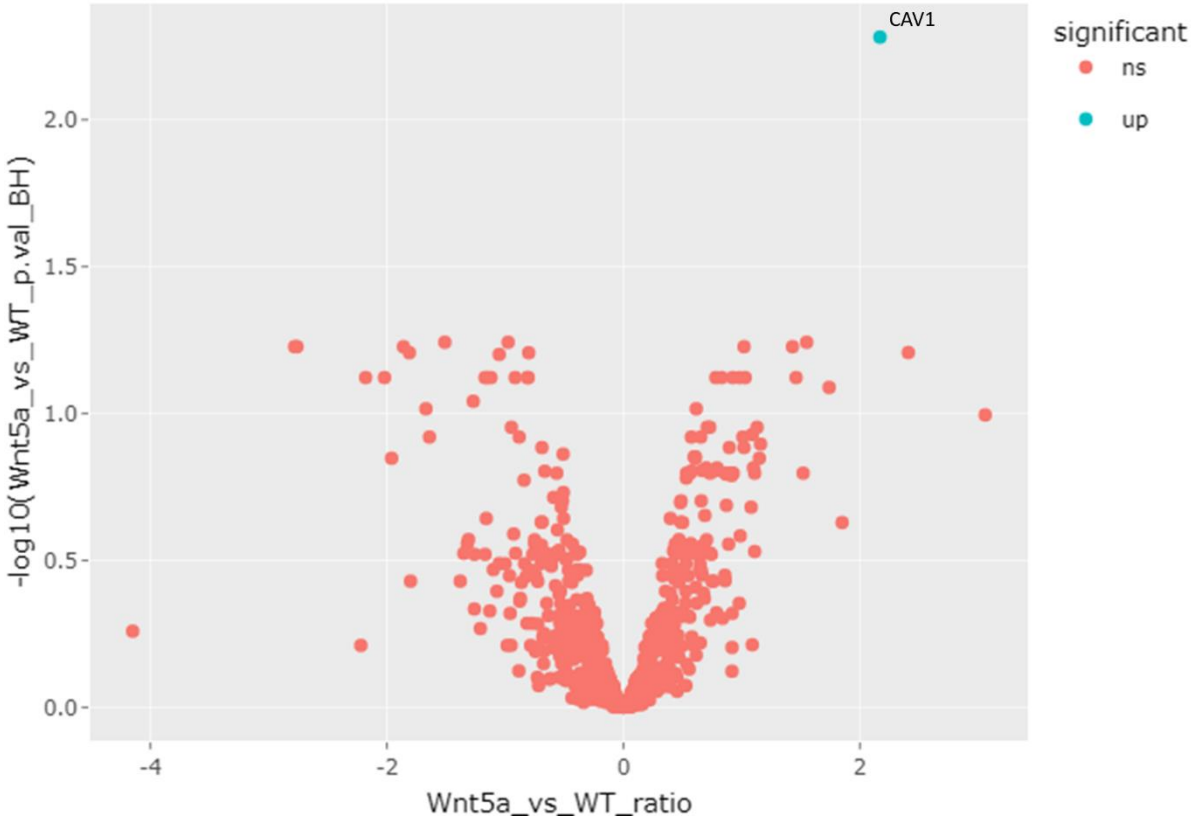

Figure 49. Volcano plot of proteins post Benjamini-Hochberg correction.
Benjamini-Hochberg correction volcano plot of protein abundance, p>0.05 are red and p<0.05 are blue. Figure and analysis performed by Kristína Gömöryová.

The second correction test, Benjamini-Hochberg correction, approaches the same problem in a simpler, more direct approach by determining whether the p-value is less than or equal to its p-value rank (ranked smallest to largest) divided by total number of tests, multiplied by the desired false discovery rate (0.05). The only significantly enriched protein surviving Benjamini-Hochberg correction is CAV1 (Fig 49), suggesting convincing evidence that CAV1 is a real protein hit as a result of biotinylation from secVHHmCh-MT.

5.3 Discussion

In this chapter, I aimed to employ the nanobody-biotin ligase assay to identify the Wnt related biotinylated proteins through mass spectrometry. The nanobody-biotin ligase secVHHmCh-MT went through two iterations of development because of multiple rounds of mass spectrometry analyses, each analysis identifying further improvements that were necessary to overcome. Indeed, it was only in the third and final mass spectrometry analysis that we were able to identify a significant protein hit because of secVHHmCh-MT biotinylation. Further improvements to the nanobody-biotin ligase assay are still possible which could identify more biotinylated proteins and eventually solve the question of the cytoneme mediated Wnt proteome. As it stands, this assay is still young in its development; however, only small adjustments are needed for full maturity of the protocol. Despite this, the assay can already provide real hits that require another round of investigations to confirm localisation to Wnt-GFP.

5.3.1 Development of the mass spectrometry technique

Each mass spectrometry analysis gave new insights into assay design, which were capitalised on and rewarded with the successor mass spectrometry analysis. Indeed, this chapter has been an example of iterative assay design, with every step demonstrating greater success than the former. The first iteration of mass spectrometry involved TMT 16plex analysis of four repeats of four conditions. The samples used were polyclonal transfections of PAC2 cells. Given what we observed in the results, it is clear in retrospect that these conditions severely lacked the protein abundance and sensitivity of mass spectrometry needed. However, given the success of co-localisation of Wnt8a-GFP to secVHH-MT in both imaged cells and western blot analysis, it was not unreasonable to assume that mass spectrometry would possess the sensitivity necessary. Indeed, TMT mass spectrometry demonstrates both higher sensitivity to low abundance proteins and smaller coefficients of variation than non-labelling mass spectrometry techniques (Pappireddi et al., 2019; Sonnett et al., 2018). The greatest weakness was simply the level of protein expression, as these polyclonal cells appear inferior to both stable cell lines and transfected cells. The latter being surprising, as we would expect a higher proportion of

expressing cells in polyclonal lines. However, in this instance, it appears likely that the increased culture toxicity from G418 incubation, paired with the repeat transfection prior to collection might have resulted in far fewer cells than standard transfection. This would ultimately result in reduced Wnt-GFP or secVHH-MT protein concentration.

The second mass spectrometry was performed taking advantage of the AGS stable cell line secVHHmCh-MT B7. Combined with transient transfections of Wnt5a-GFP, we overcame a significant hurdle by detecting high abundance of both Wnt5a-GFP and secVHHmCh-MT in the mass spectrometry dataset. Indeed, this mass spectrometry was a significant improvement, however, it left little clue as to the next avenue of optimisations by itself. The second mass spectrometry failed to produce both significantly enriched Wnt-related proteins and an increase in transfected proteins over the wild type control. Without any reason for the lack of enriched biotinylated protein hits, all that could be gained from the second attempt was that either the secVHHmCh-MT assay was itself incapable of biotinylating enough material for functional application or that the mass spectrometry technique lacked sensitivity. Both options would require substantial effort to elucidate the underlying cause, involving re-attempts at generating a Wnt-GFP stable cell line, further optimisations in the secVHHmCh-MT design all with the attempt at exploring different mass spectrometry techniques. It was the fortunate revelation of the ‘Test’ mass spectrometry data that the next step in optimisations was illuminated. This led to the refinement of the samples’ selection and third mass spectrometry that resulted in significant differences in Wnt5a-GFP and secVHHmCh-MT protein abundance. Overall, the third mass spectrometry analysis can be concluded as a success, however, a true success would be the enrichment of far more Wnt-related proteins and a list of the cytoneme mediated Wnt proteome.

5.3.2 The Isobaric Labelling Issue

In light of the success of the third mass spectrometry, much was still to be desired from the assay. Indeed, only a single protein hit was demonstrated, whereas a standard mass spectrometry analysis would yield multiple protein hits (Xiong et al., 2021). If this assay aims to identify the cytoneme-mediated

Wnt handover proteome, the assay must produce either more biotinylated protein abundance or increased detection sensitivity. A significant drawback to the enriched protein sensitivity was the considerable protein abundance variation experienced in all three mass spectrometry analyses. This variance could be due to labelling efficiency. Our bioinformatics collaboration partner explored the raw mass spectrometry data and could identify a significant, undiscovered flaw in the protein TMT labelling efficiency prior to mass spectrometry. Labelling efficiencies were unexpectedly operating at ≈50% whereas the acceptable limit is no less than 95%. When addressing this issue with the mass spectrometry team at University of Bristol, it was discovered that this under-labelling was prevalent for all three mass spectrometry attempts. This poor labelling efficiency could be responsible for the significant variance between datasets, which, before submission, were carefully balanced. Considering this revelation, given more time, this mass spectrometry analysis would need to be repeated.

5.3.3 Future Mass Spectrometry Considerations

Further mass spectrometry design elements were identified from the third mass spectrometry. Protein abundance of transfected proteins can be improved further by generating stable Wnt-GFP cell lines. Although previous attempts at PAC2 stable cell lines failed, there is still tremendous merit in investing more time in producing them. The largest hurdle in this aspect was developing plasmids expressing zebrafish Ubiquitin B promoter due to its large size. Exploring different promoter sequences, including those such as Elongation Factor-1a (EF-1a) or the simian virus 40 (SV40) could work. Using a stable cell line for each GFP-POI would limit generalisability of the assay, but if necessary for success would be worthwhile. Indeed, further resources in PAC2 stable cell lines would be preferable than generating AGS Wnt-GFP lines as demonstrated in chapter 2 Fig 20, where limited secVHHmCh-MT localisation to Wnt-GFP was observed.

Alternatively, it may be necessary to explore non-labelling methods of mass spectrometry. As demonstrated by the ‘Test’ dataset, a plethora of Wnt-related proteins was observed. Excluding the labelling efficiency problem, it could be

likely that a TMT based analysis may enrich higher abundance proteins at the expense of the lower abundance biotinylated proteins. This could be tackled by analysing each sample separately, and employing unique strategies to determine false discovery rate of protein hits and significant enrichments between samples (Lai et al., 2013).

Applying these few optimisations steps would likely greatly increase the nanobody-biotin ligase assay effectiveness to a level of proteomic study. Indeed, utilising stable cell lines for maximising protein construct abundance would still be applicable to the wide range of POI-GFP constructs available. Given the time to ensure a selectable marker is present within the plasmid and for stable cell generation, this assay could be applied to any Wnt ligand of interest and beyond. Furthermore, mass spectrometry analysis with standard labelling efficiencies of 95% or higher or individual non-labelling mass spectrometry technique would have a very high likelihood of successful detection and enrichment of biotinylated proteins. Overall, there remains only a few steps left for complete success of the assay at this stage of development.

5.3.4 Unique and Enriched Protein Hits

The ‘Test’ mass spectrometry data set is both a valuable resource for potential protein hits with an equally dubious reliability. Without any controls for comparison, all unique protein peptides from this dataset cannot be verified. Indeed, a simply enormous range of possible protein hits were detected in this data set, from direct Wnt interacting proteins fzd2, Wnt7b, β-catenin, dvl2 and wls, to cytoneme and endosomal related proteins cltca, Flot1, Rab5/7 and tubulin proteins. The only method of testing these protein hits lies in direct analysis of each protein individually. This can take the form of co-immunoprecipitations, co-localisation analysis and interaction-based studies such as FLIM/FRET or BirA/AviTag biotinylation/Yeast2 hybrid. Many proteins detected from the ‘Test’ dataset are confirmed interactors to Wnt5a, such as Fzd2. However, we cannot prove that these protein hits are detected at random or due to real biotinylation from secVHHmCh-MT. Despite this, further investigation into these and other protein hits from the dataset warrant co-localisation analysis to provide further evidence of real biotinylation.

Caveolin 1, on the other hand, is the only protein that we can suggest with a high degree of confidence to be a real biotinylated protein hit. The possibility that Cav1 is enriched by chance and not because of biotinylation stands at 1/10,000,000,000,000, accounting for the FDRtools adjusted p-value (Fig 48). Indeed Cav1 is linked to Wnt5a signalling in the literature, with its expression working antagonistically to Fzd2 and exosome uptake which hinders the Ha-RasV12 -Wnt5a-Stat3 pathway (Lin et al., 2018). Furthermore, Caveolin is necessary for the development of lipid rafts on the cell surface membrane required for various Wnt receptor localisation and endocytosis such as LRP5/6. Wnt3a triggers the interaction of LRP6 to Caveolin which causes the dissociation of Axin from β-catenin, with the endocytosis of Wnt3-LRP6 being dependant on Caveolin (Sakane et al., 2010; Yamamoto et al., 2006). However, direct Wnt5a internalisation has only been demonstrated via Clathrin-dependant internalisation, with Caveolin only demonstrating internalisation of Fzd2 in a Wnt5a context (Lin et al., 2018; Sato et al., 2010). Overall, several papers suggest a strong relationship between Caveolin and Wnt5a, therefore, further investigations to show co-localisation in cell culture would be the next step to confirm its biotinylation from the Wnt5a-GFP/secVHHmCh-MT complex.

6 Chapter 4 – Investigating Mass Spectrometry Hits

6.1 Introduction

The third mass spectrometry analysis yielded one conclusive protein hit, Caveolin1. As discussed in chapter 3, there is a range of factors that may have influenced the sensitivity of the mass spectrometry analysis to limit the outcome to a single protein hit. Further investigation on the mass spectrometry analysis would have simply been limited to this single protein had we not seen the success from the 'Test' mass spectrometry analysis. The 'Test' analysis boasted a wide range of direct Wnt-interacting proteins among similar but unrelated protein hits. As the 'Test' analysis was performed on a single sample, it is impossible to determine significantly enriched protein targets from the non-specific proteins. Despite this, a large repository of potential protein hits were uncovered that can be determined to interact with Wnt5a through further analysis.

In this chapter, I aim to develop the necessary protein constructs based off the protein hits from both the 'Test' and third mass spectrometry datasets. Using these constructs, I will conduct preliminary analyses to determine co-localisation to Wnt5a as a gauge for the likelihood of real biotinylation due to the Wnt5a-GFP/secVHHmCh-MT complex. For Caveolin1, I hypothesise a strong degree of co-localisation due to the extremely small false discovery rate in the third mass spectrometry. As for the 'Test' mass spectrometry data sets, co-localisation to Wnt5a will elucidate whether they are likely to be real biotinylated hits or not.

6.2 Results

6.2.1 Mass Spectrometry Protein Candidates

Many protein hits generated from the mass spectrometry had to be sourced for further analysis. The proteins available prior to this were Flot2, Wls/Evi, Rab5 and Rab7. The website Addgene was used to source commercially available plasmid constructs, however, these were not delivered within the project timeline. To account for missing protein candidates, cloning using cDNA was attempted for Wnt7b, Dvl2, Fzd2, Copb2, Fcho1, Flot1 and Cav1. Of the cloned products, only Cav1 and Flot1 showed positive cloning result by PCR, digest and sequencing. This left us with a total of 6 protein candidates to analyse for co-localisation/interaction to Wnt5a (Fig 50).

A

Proteins Investigated		
Origin of Protein Hit	Protein Name	Gene Name
Human 'Test'	Wntless	Wls
Zebrafish 'Test'	Flotillin 1	Flot1
Related to Flot1	Flotillin 2	Flot2
Zebrafish 'Test	Ras-related protein 5	Rab 5
Zebrafish 'Test	Ras-related protein 7	Rab 7
3rd Mass Spectrometry	Caveolin 1	Cav1

B

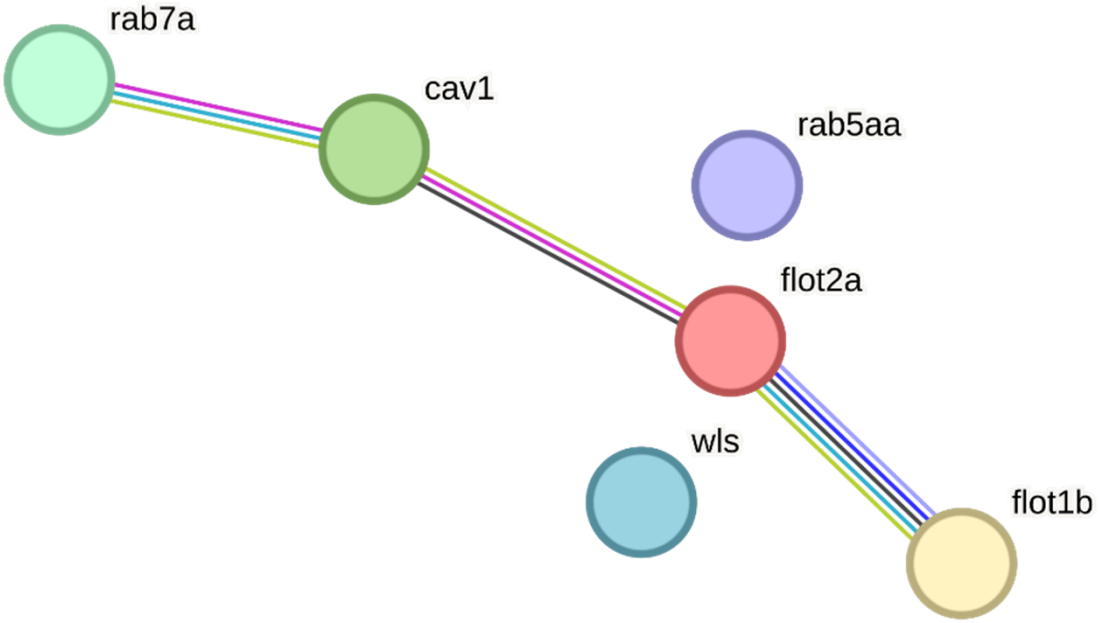

C

Alternative Candidates		
Origin of Protein Hit	Protein Name	Gene Name
Zebrafish 'Test'	Fetal Growth Factor 8	FGF8
Zebrafish 'Test'	Wnt-7b	Wnt7b
Zebrafish 'Test'	Dishevelled 2	Dvl2
Zebrafish 'Test'	Frizzled 2	Fzd2
Zebrafish 'Test'	Lipoprotein receptor-related protein 1	LRP1
Zebrafish 'Test'	F-BAR domain only protein 1	Fcho1
Zebrafish 'Test'	Coatomer subunit beta	Copb2
Zebrafish 'Test'	Ras-related protein 34	Rab34a

Figure 50. Protein Hits from Mass Spectrometry Analysis. P*rotein candidates generated from the 'Test' and third mass spectrometry analysis. (A) List of protein candidates selected for further analysis to determine success of biotin ligase assay. (B) String analysis from String.db showing links between genes determined by String.db algorithm that identifies genetic, experimental and database connections between proteins. (C) Remaining protein candidates that were not investigated further.*

As only a single protein was detected in the third mass spectrometry, all proteins other than Cav1 were detected in the 'Test' mass spectrometry analysis (Fig 50). Flot2 is the only exception and was chosen for two reasons. The first reason is our lab already possesses a Flot2-GFP construct. The second reason is Flot2 has been demonstrated by our lab to directly modulate Wnt localisation to cytonemes and cytoneme behaviour (Routledge et al., 2022). As we expected to observe Flot2 in the mass spectrometry but instead observed Flot1, it was sensible to observe both proteins to compare them.

Wls is an unusual protein choice to investigate co-localisation to Wnt5a as it has been proven essential in transporting Wnt for secretion (Nygaard et al., 2021). However, while zebrafish Wls was observed in every mass spectrometry performed, human Wls was unique to the 'Test' mass spectrometry analysis. While unknown whether human Wls would appear in the mass spectrometry for non-specific reasons similar to the zebrafish Wls observed, it raises an extremely interesting question whether it plays a role in Wnt-receiving cells. As the human Wls is not known to be transported between cells, it would only have contact to the zebrafish originated Wnt5a-GFP intracellularly. I therefore decided to investigate the possibility of Wnt5a-GFP co-localisation to Wls-mCh in co-culture to explore this possibility.

Using String.db, I mapped out all interactions between the proteins chosen for further analysis (Fig 50). All proteins with the exception of Rab5 and Wls shared a link associated to protein localisation (5 proteins, FDR = 0.0413) and protein localisation to the membrane (3 proteins, FDR = 0.0413). All proteins examined constitute components of endosomes (FDR = $7.87_{x10^{-7}}$). Indeed, all proteins are involved in endocytosis from the cell surface membrane.

6.2.2 Ras Associated Protein Co-localisation to Wnt5a

I investigated the possible co-localisation of Wnt5a and Rab5/7 using both a co-transfection and co-culture of PAC2 cells. As Rab5 was only available plasmid tagged with a GFP, Wnt5a-mCh (long form) was necessary for co-localisation study. Interestingly, there are slight differences in expression between the Wnt5a-GFP and mCh constructs that should be noted. Specifically, it appears that the Wnt5a-GFP construct has a more diffuse expression within source cells, whereas the Wnt5a-mCh has more punctate expression. Wnt5b-GFP acts similarly to the Wnt5a-GFP expression pattern, however puncta of Wnt5a/b is present on top of the diffuse pattern. Of note, all Wnt constructs tested are biologically active as proven by previous published lab work, demonstrating activation of downstream Wnt target pathways upon transfection (Brunt et al., 2021; Routledge et al., 2022; Stanganello et al., 2015). The Wnt5a-mCh expression resembles a pattern more akin to Wnt8a-GFP by its clearly defined puncta.

A

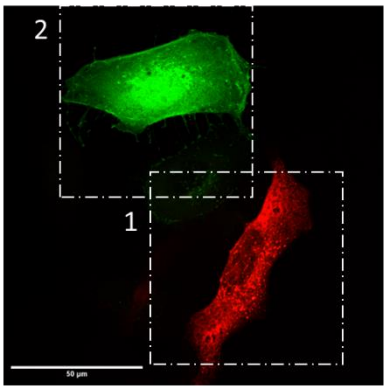

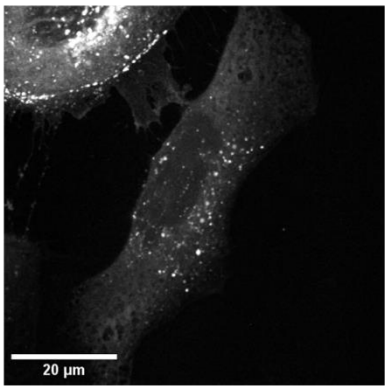

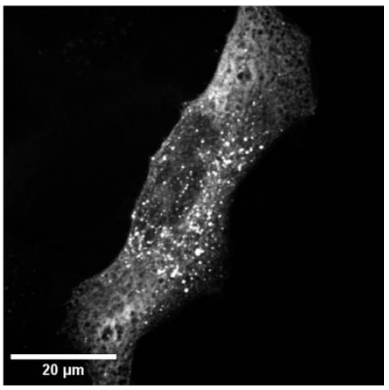

PAC2 Mem-Fixed Co-Cult
Wnt5amCh Rab5GFP

1 Rab5GFP

1 Wnt5amCh

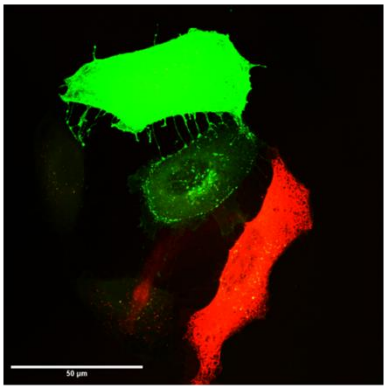

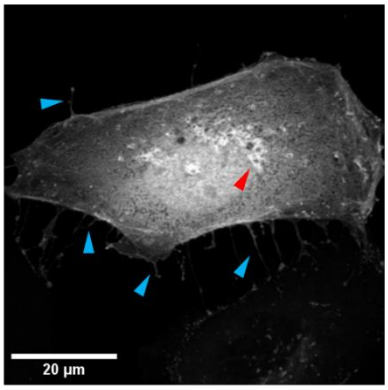

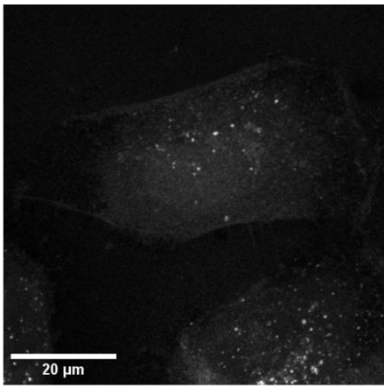

PAC2 Mem-Fixed Co-Cult
Wnt5amCh Rab5GFP Oversaturated

2 Rab5GFP

2 Wnt5amCh

B

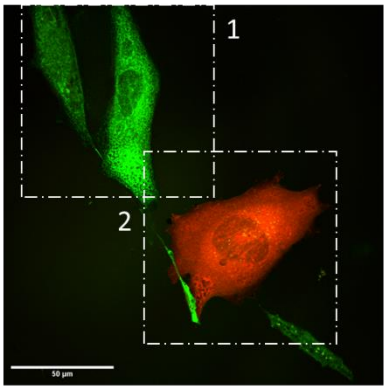

PAC2 Mem-Fixed Co-Cult
Wnt5aGFP Rab7RFP

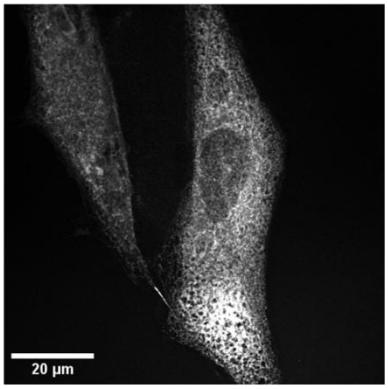

1 Wnt5aGFP

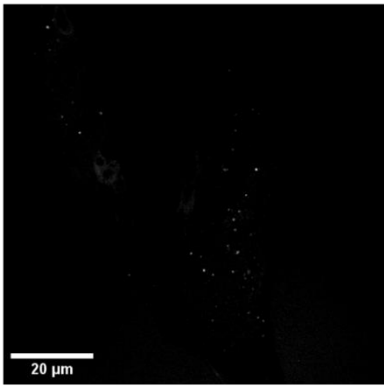

1 Rab7RFP

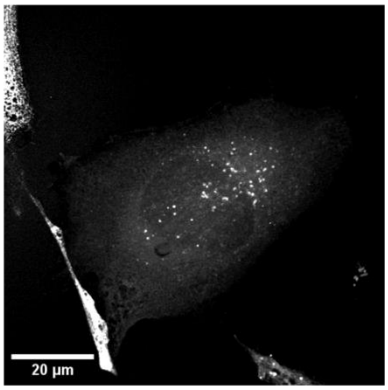

2 Wnt5aGFP

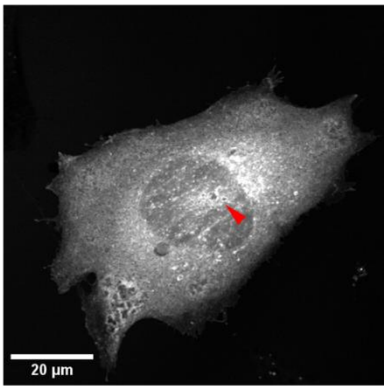

2 Rab7RFP

Figure 51. Wnt5a Shows Limited Co-localisation to Rab5 or Rab7 in Co-culture. *(A) PAC2 cells transfected with either Wnt5a-mCh or Rab5-GFP, co-cultured for 24 hours and fixed in Mem-Fix. A repeat of the whole image is shown with oversaturated pixels to highlight low intensity values. (B) PAC2 cells transfected with either Wnt5a-GFP or Rab7-RFP, co-cultured for 24 hours and fixed in Mem-Fix. Scale bar = 20μM. Images are labelled 1 or 2 representing Wnt-expressing or Rab-expressing cells. Red arrows indicate 'rings' of Rab protein, blue arrows indicate Rab positive filopodia.*

As shown in figure 51, Rab5-GFP and Rab7-RFP express with good intensity and transfection efficiency. Equally, both Wnt5a-GFP and mCh have good expression and show uptake into neighbouring, non-transfected cells (Fig 51). The expression of Rab5-GFP and Rab7-RFP show a diffuse cytoplasmic phenotype with notable 'rings' of intensity, indicative of endosomal localisation (Fig 51.A+B). In Fig 51.B, these 'rings' of intensity are overshadowed by the large general diffuse signal. Wnt5a-GFP and mCh is observed in these Rab-producing cells; however, their overlap on Rab signal appears limited. Indeed, attempting co-localisation analysis yields statistically insignificant results because of the thresholding being above the mean signal intensity due to low average number of pixels. This is a limitation of co-localisation analysis within co-cultured samples, as the signal intensity differences between the two channels is too large to quantify any co-localisation or the lack thereof. Any observations made must therefore be limited to speculation when using co-cultured co-localisation, with further investigations required proving localisation such as a co-immunoprecipitation. Overall, it appears that any Wnt signal shows little co-localisation to any Rab5- or Rab7-positive endosomal vesicles on receiving cells, if not to exist within gaps of the 'rings' of Rab signal. If true, then this can suggest that Wnt5a is endocytosed within Rab5/7 positive vesicles, but that Wnt5a does not directly interact.

A uniquely interesting phenotype observed by the Rab5-GFP is its existence outside of Rab5-GFP transfected cells. Rab5 shows strong filopodia localisation (Fig 51.A) that can be seen making contact with a neighbouring cell. Because this is a co-culture, we can assume that the Wnt5a-mCh positive cell should not be transfected with Rab5a-GFP too. However, Rab5-GFP signal is indeed

detected in low intensity within Wnt5a-mCh positive cell (Fig 51.A). The levels of Rab5-GFP signal intensity is comparable to the levels of Wnt5a-mCh intensity within the Rab5-GFP positive cell. Furthermore, Rab5-GFP pixels show high co-localisation to Wnt5a-mCh pixels within the Wnt5a-mCh transfected cell. As mentioned earlier, co-localisation analysis cannot be conducted on these images. Instead, observations of these co-cultured cells suggest that endocytosed Wnt5a-mCh cells in Rab5-GFP transfected cells do not co-localise, whereas Rab5a-GFP in Wnt5a-mCh cells co-localise extremely well. In contrast, the Rab7-RFP shows no signal intensity in Wnt5a-GFP transfected cells. Technical artefacts could result in the GFP channel autoflourescing in the mCh channel and not in reverse. However, this is unlikely as typically mCh signals are excited by GFP as the excitation frequency of mCh (585nm) is close to the emission frequency of GFP (510nm), and very distant in reverse(Tsien, 1998). Furthermore, as these are fixed samples, the images were taken stack sequential to remove possible cross excitation between channels.

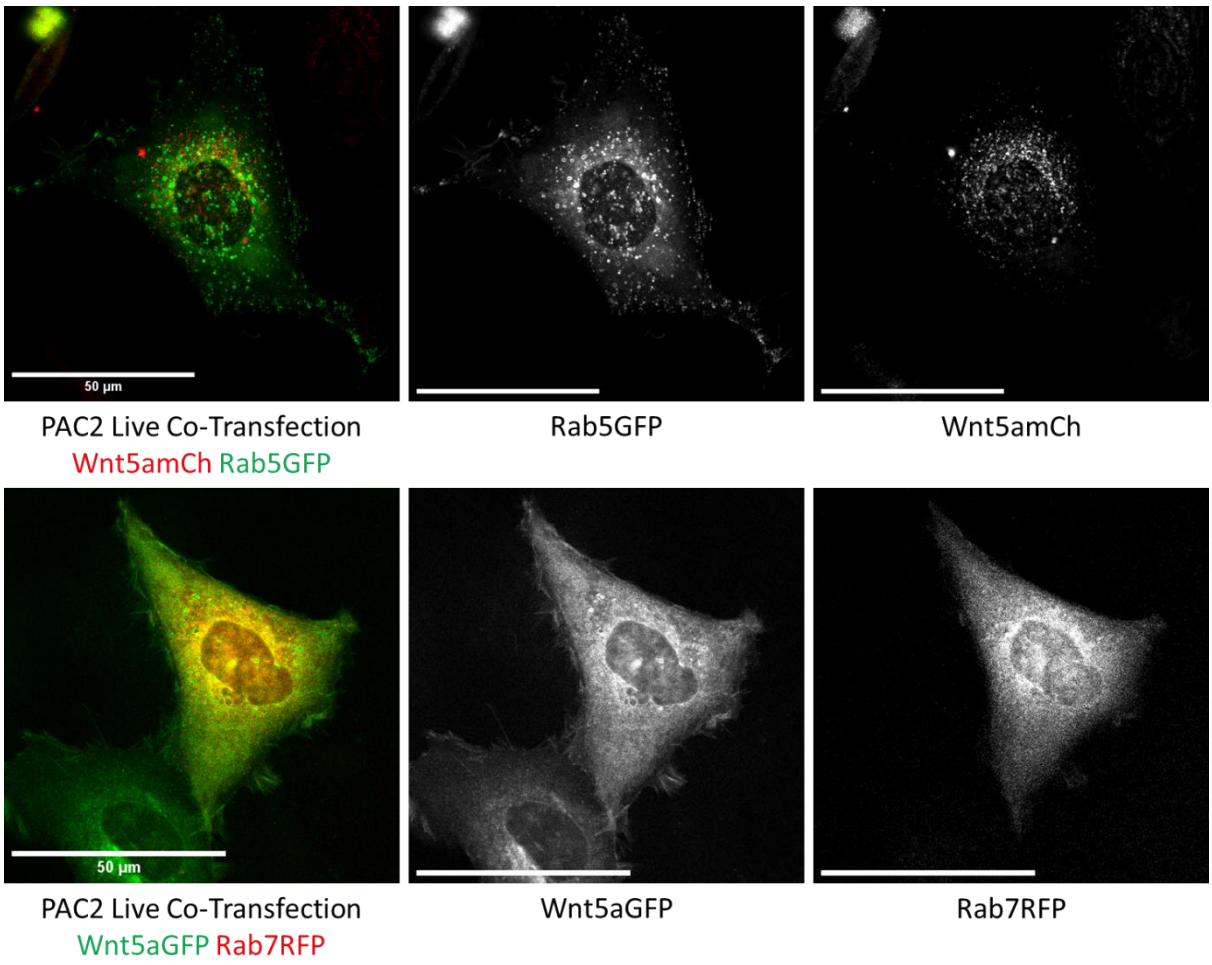

Figure 52. Wnt5a Co-localises to Rab7 but not Rab5 in Co-transfection.
Live PAC2 cells co-transfected with either Wnt5a-GFP and Rab7-RFP or Wnt5a-mCh and Rab5-GFP. Scale = 50µM.

Co-transfections of Wnt5a and Rab5 or Rab7 show little co-localisation between the two. Indeed, Rab5-GFP shows nearly zero co-localisation to Wnt5a-mCh. Wnt5a-GFP however, has a far more diffuse expression profile than the puncta profile seen in Wnt5a-mCh. This diffuse profile appears very similar to the expression of Rab7-RFP. When comparing Wnt5a-GFP and Rab7-RFP, it appears a high degree of co-localisation. This co-localisation appears more prevalent in perinuclear regions which is consistent to Rab7 role in late endosomes and lysosomal generation (Guerra & Bucci, 2016).

Taken together, these results suggest evidence for Wnt5a-GFP endocytosis within Rab5 and Rab7 positive vesicles as expected, albeit without direct interaction or co-localisation. Further investigations are required to investigate

Rab5 internalisation within Wnt5a-mCh positive cells to confirm this phenomenon, along with the possible function for this phenotype.

6.2.3 Flotillin Co-Localisation to Wnt

Flotillin1a (Flot1a) was detected as a unique protein in the test data. Our lab has extensively investigated the role of Flot2 which shares a lot of similarity to Flot1 (Routledge et al., 2022). Routledge *et al* demonstrated how Flot2 directly modulates cytoneme length and number to alter Wnt3 signalling *in vitro* and Wnt8a *in vivo*. While Flot2 was not detected in the 'Test' mass spectrometry data set, it was interesting to see if Flot1 interacts with Wnt5a in a similar way. Our lab did not possess a Flot1 construct, and so a new Flot1a-GFP construct was generated using zebrafish cDNA.

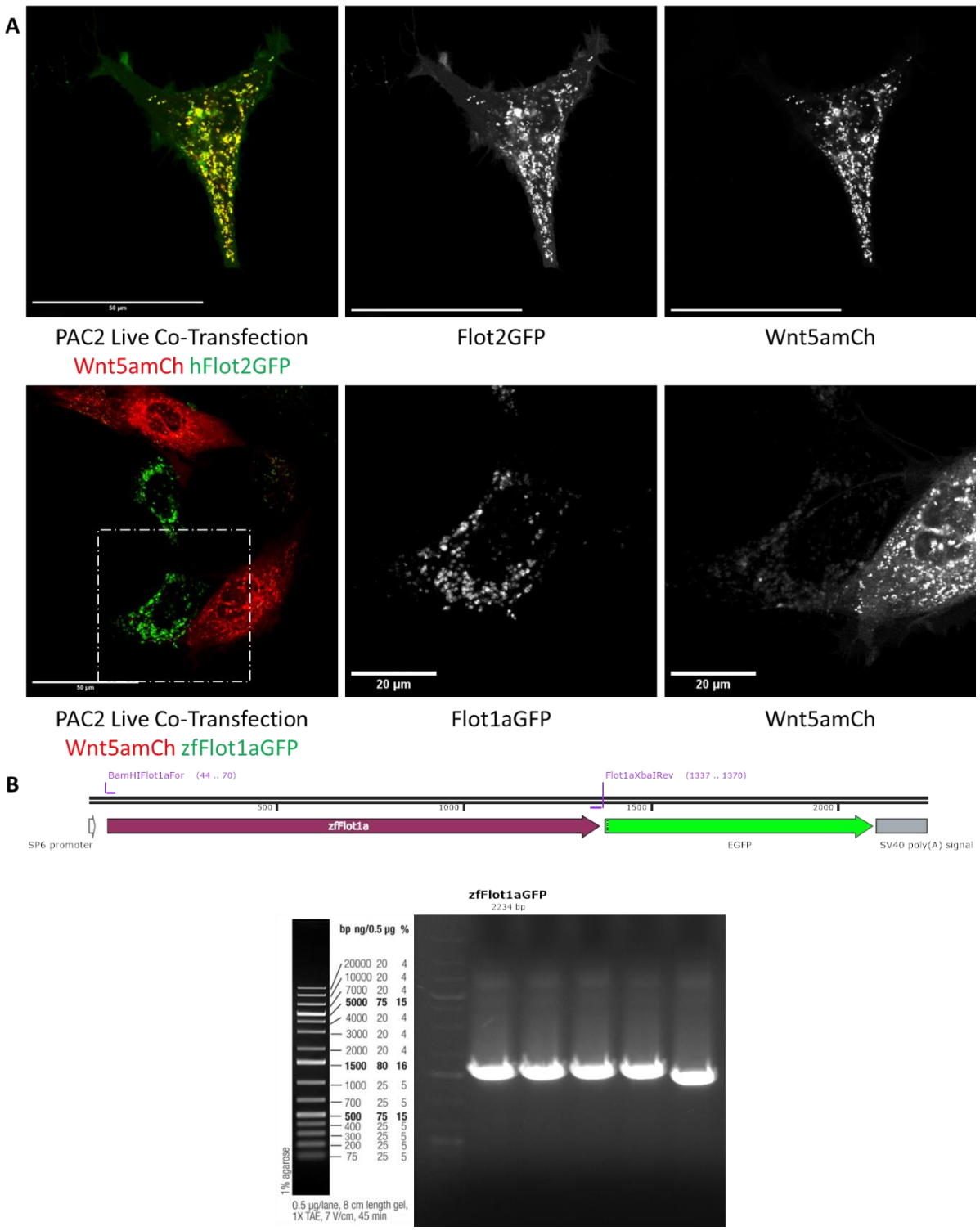

Figure 53. Flotillin 1 and 2 Co-localise Highly to Wnt5a. *(A) Live PAC2 cells co-transfected with Wnt5a-mCh and either Flot2-GFP or Flot1a-GFP. Scale = 50µM and 20µM. (B) cloned zebrafish Flot1a-GFP construct and PCR gel of five individual miniprep colonies.*

The Flot2-GFP construct is of rat origin, however despite differences in species, shows extremely high co-localisation to Wnt5a-mCh as expected (Fig 53.A).

Flot2-GFP demonstrated strong and consistent transfection efficiency, however the Flot1a-GFP construct was poor in contrast. Indeed, the Flot1a-GFP construct was confirmed by PCR, digest and sequencing to be correct (Fig 4.B). However, Flot1a-GFP was poor to transfect in cells. Flot1a-GFP was also maxi-prepped to remove endotoxin. Further improvement to the construct is needed to improve upon its transfection efficiency, however with the little expression generated, it showed similarly good co-localisation to Wnt5a-mCh. Unlike with Flot2-GFP, it is hard to rule out the increased risk of imaging artefacts observed with Flot1a-GFP due to its low signal intensity. However, as mentioned with Rab5-GFP co-culture, imaging artefacts of cross-fluorescence is typically a problem for mCh activation from GFP fluorescence, and not the other way around. Furthermore, Flot1a-GFP is not observed ubiquitously for all cells, suggesting that this signal is not a result of autofluorescence. Given these circumstances, it is more likely that the Flot1a-GFP signal and co-localisation to Wnt5a-mCh is not an artefact (Fig 53.A). Further analysis is required for definitive confirmation of Flot1a co-localisation to Wnt5a, however these results suggest that it is likely and that this is a real protein hit generated from the ‘Test’ mass spectrometry analysis.

6.2.4 Caveolin 1 Co-localisation to Wnt5a

Caveolin 1 (Cav1) was the only protein hit generated from the third mass spectrometry analysis. After careful analysis of the mass spectrometry data, Cav1 was found to be conclusively enriched only in the presence of Wnt5a. It stands to reason that Cav1 would demonstrate a strong degree of co-localisation to Wnt5a in transfected PAC2 cells. However, as we did not possess a Cav1 construct, a new construct was generated using zebrafish cDNA.

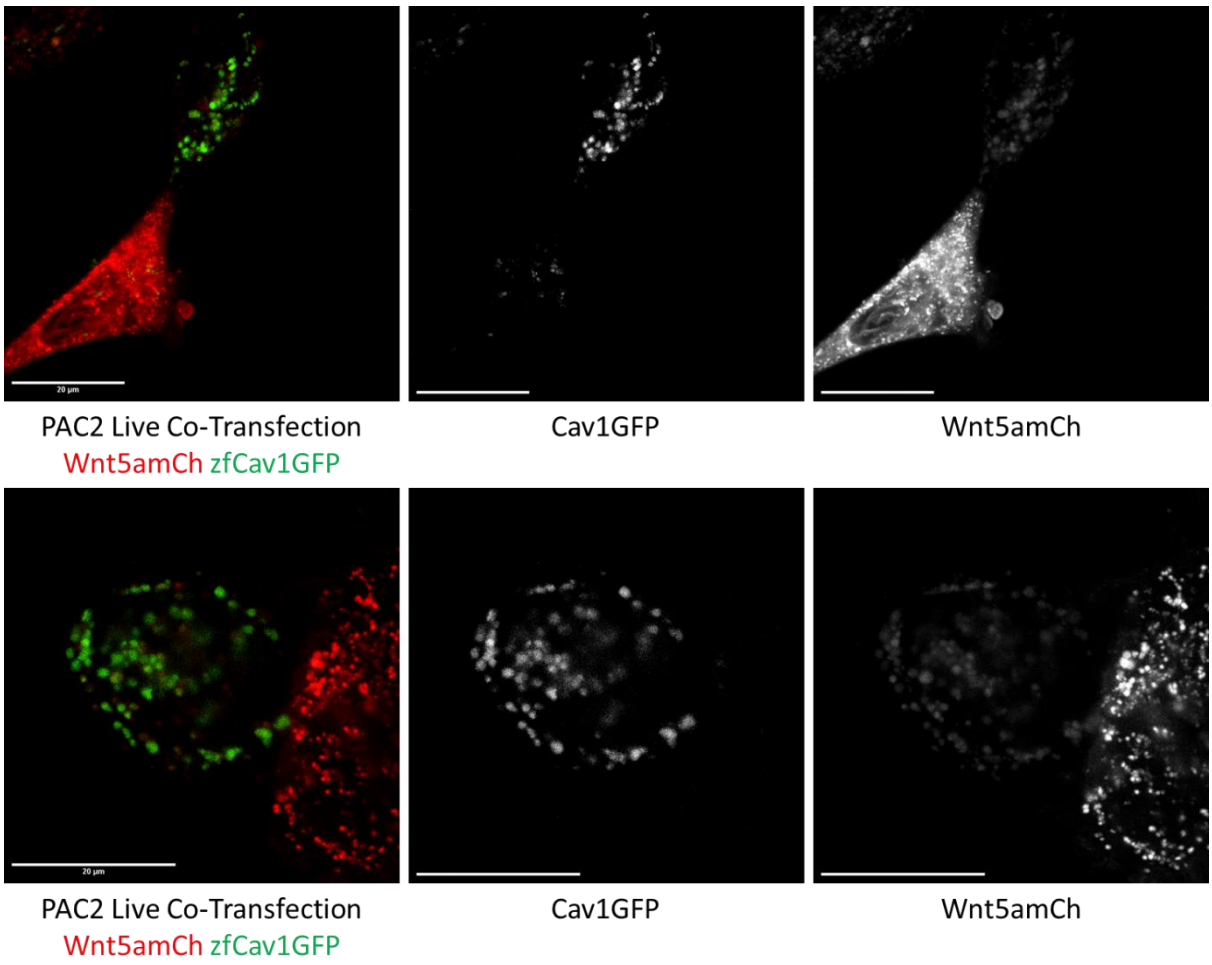

Figure 54. Caveolin 1 Co-localise Highly to Wnt5a. *Live PAC2 cells co-transfected with Wnt5a-mCh and Cav1-GFP. Scale = 20μM.*

Similarly, to the Flot1a-GFP construct, Cav1-GFP suffered from low signal intensity and poor transfection. Indeed, all constructs generated to examine co-localisation to Wnt5a could not be cloned successfully or produced low transfection efficiency. Despite this, for reasons stated in Flot1a-GFP expression, it appears that the Cav1-GFP signal is unlikely to be generated due to imaging artefacts. Furthermore, Cav1-GFP appears to co-localise highly to Wnt5a-mCh. It is interesting to note the differences in Wnt5a-mCh signal in Cav1-GFP positive cells. As Cav1-GFP expression is presented as large vesicular bodies, Wnt5a-mCh appears to change from small tight puncta to match the same large vesicular body phenotype on Cav1-GFP expressing cells. The reason for this difference may be a result of imaging artefacts caused by cellular autofluorescence. Alternatively, this could be a result of Cav1 overexpression changing the phenotype of Wnt5a-mCh expression.

6.2.5 Wls and Wnt5a Co-localisation in receiving cells

The final protein to test for co-localisation to Wnt5a is Wls. Wnt Ligand Secretion mediator (Wls), otherwise known as Evenness Interrupted (Evi) for its drosophila paralogue (Nygaard et al., 2021), is a transport protein responsible for transporting and secreting mature Wnt to the cell surface membrane. Wls is a known Wnt interactor protein, demonstrating direct binding to Wnt through numerous publications (Nygaard et al., 2021; J. Yu et al., 2014). Given the well-documented interactions of Wls and Wnt5a, I did not investigate this in our system. The real question from the 'Test' mass spectrometry was rather their interaction in Wnt receiving cells. From the 'Test' mass spectrometry data set, human Wls was detected as a unique protein. The human Wls hit would have originated in the human AGS B7 secVHHmCh-MT stable cell line which cannot produce Wnt5a-GFP. This leaves three potential reasons for its appearance in the 'Test' dataset. The first reason is that human Wls was detected as its levels in the lysate were high enough to survive streptavidin pulldown and so exist in the mass spectrometry analysis similarly to zebrafish Wls. It is possible that human Wls levels are lower in AGS cells than zebrafish Wls is in PAC2 cells, and so its presence is not detectable in TMT analysis of B7 and PAC2 Wnt5a-GFP co-culture. The second reason may be the possibility of human Wls being transported from AGS cells to PAC2 cells during co-culture. Wls has been previously suggested to be loaded onto exovesicles with Wnt3a in HeLa cells, albeit at very low levels (10 ±6%) (Gross et al., 2012). The third possible reason is that Wnt5a interacts with Wls in a Wnt receiving cell after endocytosis. To investigate the potential of Wnt and Wls interaction in Wnt receiveing cells, I generated co-culture of PAC2 cells expressing either Wnt5a-GFP or Wls-mCh and imaged their localisation within Wls-GFP expressing cells.

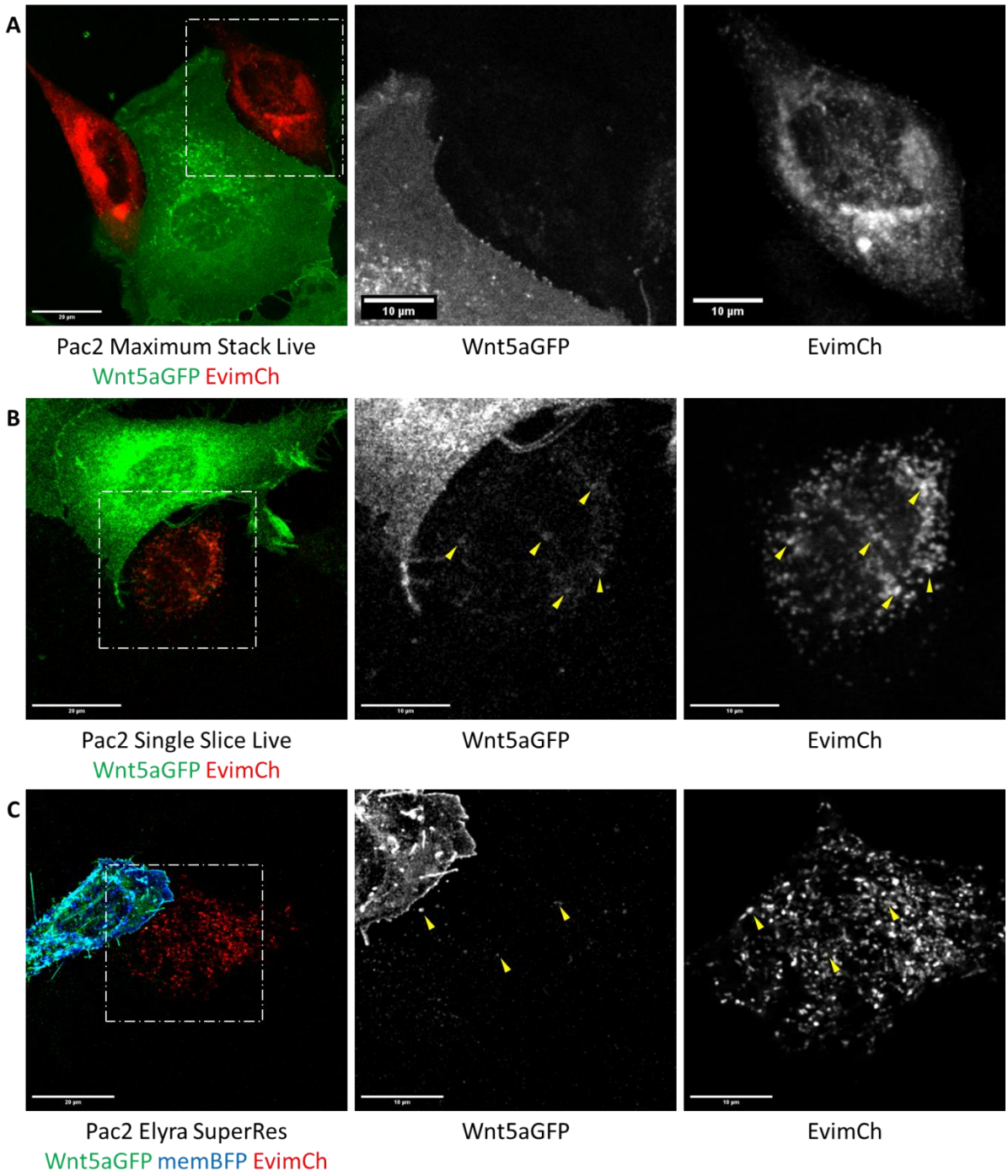

Figure 55. Co-culture of Wnt5a-mCh and Evi-GFP in Wnt Receiving Cells. *(A,B,C) PAC2 cells transfected with either Wnt5a-GFP or Evi-mCh and co-cultured for 24H before imaging. Yellow arrows indicate co-localised pixels. (A) Confocal image of Wnt5a-GFP and Evi(Wls)-mCh co-culture maximum intensity stack of slices. (B) Confocal image of Wnt5a-GFP and Evi-mCh co-culture single image slice. (C) Elyra Sim2 super-resolution image of Wnt5a-GFP and Evi-mCh co-culture maximum intensity stack. Membrane-BFP co-transfected with Wnt5a-GFP but not in Evi-mCh cells. Scale bars = 20µM (left images), 10µM (middle and right images).*

Co-culture of PAC2 cells expressing Wnt5a-GFP and Evi-mCh demonstrated strong and consistent expression with high transfection efficiency. Consistent with this, many pairs of differently expressing cells were captured and imaged. However, a significant problem arose when imaging Wnt5a-GFP in Wnt receiving/Evi-mCh expressing cells; Wnt5a-GFP signal intensity sharply diminished in Evi-mCh expressing cells. While Wnt5a-GFP signal was present and its intensity substantial enough for imaging, it required specific confocal optimisations to properly capture the low signal. When observing the low Wnt5a-GFP signal intensity in combination with the several magnitudes higher Evi-mCh signal, a balance between imaging conditions and speed was required. This phenomena of low Wnt5a-GFP signal intensity in Evi-mCh expressing cells is most notable in figure 55.A. Standard confocal imaging for live cells must take into consideration the imaging time for increased image quality against the speed of live cellular movements. Standard live confocal imaging in figure 55.A would not be sufficient to capture the low Wnt5a-GFP signal. Instead, compromises in imaging time were necessary. These compromises involved increasing the number of line accumulations, laser intensity, frame sequential imaging and reduced laser speed to enhance the low Wnt5a-GFP signal. These comprises came at the cost of overall imaging speed, which can result in changes of fluorophore locations between imaging the two different channels.

An obvious strategy to solve longer imaging times would be to use fixed samples. However, fixation techniques introduce new complications such as autofluorescence of the sample due to the crosslinking of peptides from PFA or aldehyde species from mem-fix. Indeed, fixations were attempted and imaged but autofluorescence prevented imaging of the low Wnt5a-GFP sample in Evi-mCh expressing cells. Further optimisations would be necessary to eliminate this autofluorescence, along with the use of α-GFP antibodies to boost Wnt5a-GFP signal. Due to project timeline limitations, this was not done.

Despite the problems outlined above concerning live imaging, single slice images of Wnt5a-GFP and Evi-mCh yielded very low but detectable Wnt5a-GFP fluorescence in Evi-mCh expressing cells (Fig 55.B). Indeed, in cells with particularly high intracellular Wnt5a-GFP signal and using optimised imaging settings, there are a few instances where Wnt5a-GFP signal is co-localised to

Evi-mCh signal. Of note, due to the very low Wnt5a-GFP signal in Evi-mCh producing cells, we must remain vigilant to the risk of low-signal imaging artefacts. As mentioned previously, it is unlikely that GFP channel is excited from a mCh signal. Autofluorescence within the sample is a possibility; however, the likelihood of autofluorescence co-localising mCh pixels as opposed to random is unlikely.

A third technique that combines high imaging speed with good signal detection is with the use of lattice structured illumination microscopy (SIM) imaging from the Elyra 7 microscope. Lattice SIM imaging utilises a wide field laser through a lattice pattern to identify signal generated from the pattern or from the sample (Zheng et al., 2022). Wide field imaging is faster than conventional confocal microscopy, and when combined with the lattice SIM, allows for super-resolution down to 60nM. When imaging Wnt5a-GFP co-cultured with Evi-mCh, we also observe instances of Wnt5a-GFP signal co-localising with Evi-mCh in Evi-mCh expressing cells (Fig 55.C). Artefacts produced from lattice SIM imaging differ from confocal analysis; however, they can occur with very low signal intensity similarly to confocal. This is mitigated by thresholding the raw SIM data or by imaging samples with grey pixels over a minimum of 1000. For the images analysed, both of these considerations were taken and images were produced after proper thresholding.

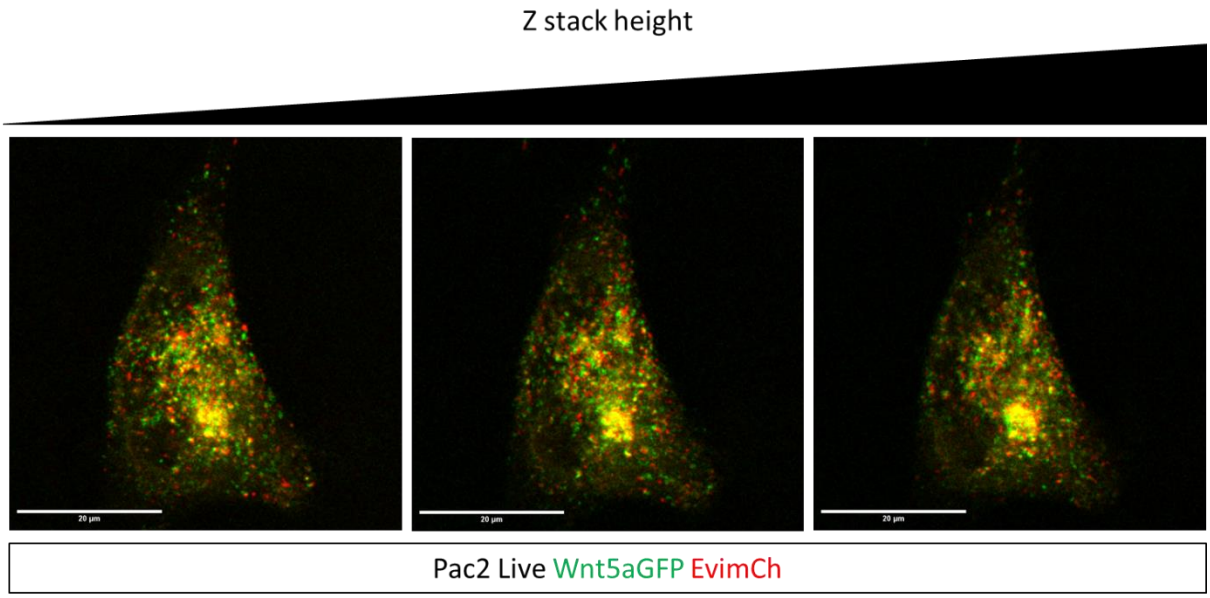

Figure 56. Live Wnt5a-GFP and Evi-mCh Co-culture through Image Stack. *PAC2 cells transfected with either Wnt5a-GFP or Evi-mCh and co-cultured for 24H before imaging. Confocal imaging optimised for long exposure of Wnt5a-GFP signal. Image slice taken from bottom to top of cell going left to right. Scale = 20μM.*

When performing full optimisations for maximum Wnt5a-GFP signal intensity on live cells, the time to image between the two channels becomes great enough that cellular movement impacts pixel localisation. Indeed, maximising Wnt5a-GFP signal detection in Evi-mCh producing cells appears to generate slices of Wnt5a-GFP puncta existing side-by-side to Evi-mCh puncta (Fig 56). When applying a maximum intensity stack, these puncta converge to form a blurred image, rendering the maximum image projection obsolete. However, when observing each slice of the stack individually, we observe many co-localised pixels among several pixels existing side-by-side. The side-by-side pixels are most notable in the top portion of the cell in figure 56, presumably, as this region has a high degree of intracellular mobility. Notably, a large proportion of co-localised pixels exist in perinuclear regions of the cell. These co-localisation results further suggest a possibility of Wnt5a interacting with Wls in receiving cells, a phenomenon never explored in the literature that could improve our understanding of Wls role in the Wnt signalling pathway.

6.3 Discussion

The primary aim of this chapter was to investigate protein hits generated from the mass spectrometry analysis in chapter 3 for their interactions to Wnt5a. To do this, I used confocal microscopy to generate preliminary observations for protein co-localisation to Wnt5a-GFP/mCh. Although a comprehensive analysis was not possible, these preliminary results provide an interesting insight into potential future investigations. The principle reason owing to the short project time length post mass spectrometry, complimented with long cloning period of novel protein constructs. Ideally, there would be a plethora of experiments to conduct on these novel protein hits, which would further elucidate their interactions, if any, to Wnt5a. As it stands, these results simply provide a glimpse to possibilities rather than conclusive evidence. Regardless, a large insight into these protein hits is uncovered which, in many cases, pose highly interesting questions that I believe warrant further investigation.

6.3.1 Rab5/7 Interactions to Wnt5a

The first protein investigated were the RAB proteins Rab5 and Rab7. Rab proteins are responsible for regulating intracellular membrane trafficking (Homma et al., 2021). There are approximately 60 known mammalian RAB genes, each specialising in a unique facet of intracellular trafficking. From secretion to endocytosis, many RAB proteins regulate one or multiple intracellular trafficking roles, generating a high degree of redundancy. Rab5 and Rab 7 are highly documented RAB genes, responsible primarily for early endosome/plasma membrane/phagosome and late endosome/phagosome/lysosome respectively. These two proteins were detected in the ‘Test’ mass spectrometry and were selected for these investigations for their involvement in endocytosis and end-stage lysosomal processing. I hypothesised that these two protein hits may have been generated because of internalisation of Wnt5a-GFP/secVHHmCh-MT complex and subsequent biotinylation. Indeed, Rab5 is known to co-localise to Wnt co-receptor LGR5 in Rab5 positive early endosomes after LGR5 internalisation (de Lau et al., 2011; Glinka et al., 2011; Yuan & Song, 2020). However, co-culture and co-transfections of PAC2 cells expressing Wnt5a-GFP/mCh and Rab5-GFP

or Rab7-RFP demonstrated limited co-localisation (Fig 51+52). For co-transfections, Rab5-GFP appeared to demonstrate almost zero co-localisation to Wnt5a-mCh (Fig 52). However, Rab7-RFP showed an apparent co-localisation to Wnt5a-GFP, especially in perinuclear regions. These results are not surprising considering the roles these specific RAB proteins have. Rab5 would canonically localise to endocytosed material whereas the Wnt5a is marked for secretion. Similarly, an excess of Wnt5a-GFP (an expected hallmark of fluorescent protein overexpression) would mark a significant fraction for autophagasomes and lysosomal destruction in Rab7 positive lysosomes. Interestingly, when observing co-cultures, we do not observe an increase in co-localisation between Wnt5a and Rab5/7 in Rab5/7 positive cells. Instead, we observe a diffuse Rab5/7 expression profile populated with puncta or ‘rings’ of Rab5/7 as expected of standard vesicle protein morphology. It should be noted that while Wnt5a-mCh does not appear to co-localise with Rab5-GFP in Rab5-GFP positive cells, there are a few instances where Wnt5a-mCh signal is detected within the centre of these Rab5-GFP ‘Rings’. This could indicate the possibility of Wnt5a-mCh being internalised within Rab5-GFP positive early endosomes, perhaps in complex with a receptor or transport protein that generates steric distance between the two fluorophores to produce this effect.

Rab5 is not known to be secreted but instead retained within the cell for endocytic pathways (Yuan & Song, 2020) which makes this result quite puzzling. One potential clue is the very strong localisation of Rab5-GFP to the filopodia. In figure 51.A, this is highlighted by a neighbouring cell contacting many Rab5-GFP positive filopodia and exhibiting a high degree of Rab5-GFP signal. There remains the possibility that this neighbouring cell is indeed transfected, albeit at levels low enough to prevent over-expression. However, the more interesting aspect is Rab5-GFP signal in the Wnt5a-mCh expressing cell which cannot be as a result of Rab5-GFP transfection. I suggest two possibilities for this observation, the first reason being a consistent technical obstacle for many of the images discussed in this chapter. The first reason is likely an imaging artefact brought about from low signal intensity imaging. These artefacts can arise from one of two problems; autofluorescence of the cell or cross excitation from neighbouring fluorophores. The second reason would suggest that the Rab5-GFP signal is indicative of Rab5-GFP

translocation from producing to receiving cell. Imaging artefacts have been discussed in the results but must always be considered, especially concerning the nature of these preliminary studies post mass spectrometry. Despite the risk of these imaging artefacts, it is possible that these are genuine signals. This would have highly interesting implications for Rab5 and for the wider RAB family for the possibility of paracrine handover between cells. The most interesting aspect of this Rab5-GFP handover is its very strong co-localisation to Wnt5a-mCh. Indeed most puncta of Rab5-GFP in Wnt5a-mCh expressing cells are co-localised to Wnt5a-mCh, suggesting that any endocytosed Rab5-GFP is either in complex to Wnt5a-mCh, or sorted in same endosomes responsible for transporting Wnt5a-mCh. The reasons for this complex would be unknown if true, however as this phenotype is beyond expectations for Rab5-GFP to be secreted, further investigations are required before we can speculate on its function in this circumstance. These experiments would consist of endogenous immunofluorescence, fixed cell overexpression with immunofluorescence enhancement and co-immunoprecipitations. Overall, when concerning both Rab5 or Rab7 proteins, there appears to be limited co-localisation to Wnt5a with the exception of co-transfection of Rab7 and Wnt5. These results suggest a low likelihood that these protein hits from the ‘Test’ dataset are because of real biotinylation from the Wnt5a-GFP/secVHHmCh-MT complex.

6.3.2 Flotillin1/2 Interactions to Wnt5a

The next group of proteins investigated was the family of flotillins (Flot1 and 2). Flotillins are highly conserved, membrane-bound scaffolding proteins that form lipid rafts in either vesicles or cell surface membrane to facilitate clustering of various protein receptors (Stuermer et al., 2001). Our lab has demonstrated the importance of such Flot2 in its role in facilitating Wnt3 secretion in AGS gastric cancer cells and its role in modulating filopodia for this purpose (Routledge et al., 2022). Discovering a hit for Flot1 in the ‘test’ mass spectrometry dataset peaked our interest for this reason. This is why I chose to investigate both Flot1 and 2 to compare and contrast Flot1 co-localisation to Wnt5a to a known Wnt interactor and homologue Flot2. A simple co-transfection of Flot2-GFP and Wnt5a-mCh yielded expected results as the two demonstrated extremely high co-localisation (Fig 53.A). Flot1-GFP expression was less clear and definitive

however. The problem mainly stemmed from the low signal intensity of Flot1-GFP despite proper attempts at generating the construct. Indeed, tests of the cloned product concluded correct sequence analysis, paired with maxi-prepping of the plasmid should yield an expression intensity akin to the Flot2-GFP. Further optimisations in the Flot1-GFP construct are needed for future experiments, perhaps with a subclone of the construct in a different vector or sequencing of the whole vector to detect any anomalies that would cause sub-optimal expression. Despite the setbacks, Flot1-GFP expression was possible and the signal demonstrated high co-localisation to Wnt5a-mCh (Fig 53.A). The expression of both Flot1-GFP and Flot2-GFP share many similarities, with a diffuse membrane localisation paired with puncta of signal that co-localise to Wnt5a-mCh. These results could suggest that Flot1 performs a role similarly to or in conjunction with Flot2 in the Wnt secretory pathway. Understanding the exact nature of this role would require repeat experiments performed for Flot1 as was done for Flot2 (Routledge et al., 2022). However, the data presented here would provide a preliminary rational for these investigations. This would involve observing cytoneme number and length when treated to Flot1 overexpression or knock down, Jnk/TCF reporter assays in co-culture and co-transfections to determine changes in Wnt activity and protein lysate pulldowns to confirm Flot1-Wnt5a complex interaction. Overall, despite drawbacks concerning Flot1-GFP signal intensity, I believe these co-transfections reveal strong evidence for the Wnt5a-GFP/secVHHmCh-MT complex interacting with Flot1 in the ‘Test’ mass spectrometry dataset. An unanswered question remains as to why Flot2 was not detected. Perhaps further repeats of the ‘Test’ mass spectrometry analysis would yield Flot2 results in conjunction to Flot1.

6.3.3 Caveolin 1 Interactions to Wnt5a

As Caveolin 1 was the only confidently enriched protein hit from the third mass spectrometry test, I hypothesised that Cav1-GFP and Wnt5a-mCh would have the highest likelihood of all proteins tested to show co-localisation. Indeed, given the co-localisation data presented in figure 54, Cav1 does co-localise with Wnt5a. This conclusion is not however without its fair share of limitations. Similarly, to Flot1a-GFP expression, Cav1-GFP struggled to produce reasonable signal intensity and suffered low transfection efficiency. When

comparing the two constructs, Cav1-GFP demonstrated the least expression. Cav1-GFP was confirmed by PCR, digest and sequence analysis and was prepared using endotoxin-free maxi-prep. As mentioned for Flot1-GFP, perhaps a full vector sequencing and possible subcloning of the construct into a different vector is required. The signal intensity generated from Cav1-GFP is so low that imaging artefacts are a severe risk. Therefore, repeat confocal images are necessary before any conclusions are drawn from such experiments. Regardless, assuming this is real signal demonstrating co-localisation to Wnt5a-mCh, we can assume that Cav1 positive caveosomes (Cav1 coated vesicles) play a role in transporting Wnt5a. Caveolin and cavin proteins form the structural core of the cholesterol rich caveolae pits that subsequently internalise to form caveosomes for endocytosis (Cheng & Nichols, 2016; Lamaze et al., 2017). These caveosomes later form lysosomes or multivesicular bodies. Conversely, Cav1 is also responsible for secretory pathways. Being synthesised at the endoplasmic reticulum, matured at the Golgi apparatus and then transported to the cell surface membrane as large complexes associated with cholesterol rich membrane lipid rafts, similarly to Flot2 (Choudhury et al., 2006; Hayer et al., 2010). It is for both endocytosis or secretion that Cav1 might have the opportunity to interact with Wnt5a. Indeed, Cav1 shares similarities to Flot2 in regards to assembling lipid rafts which are known to shuttle Wnt-binding receptor cargo such as LRP5/6, Ror2 and Fzds (Riitano et al., 2020; Sammar et al., 2009). Furthermore, Cav1 is known to aid sequestering of β-catenin to the plasma membrane, regulating β-catenin/Tcf-Lef-dependent signalling in the process (Galbiati et al., 2000; Torres et al., 2006, 2007). Lastly, a link between Wnt5a and Cav1 was demonstrated by Hsiu-Kuan Lin *et al* (Lin et al., 2018) to show an antagonistic relationship between Cav1 expression reducing Wnt5a/Fzd2 signalling. Taken together with the data shown in this chapter, with consideration to repeat experiments required, suggest strong evidence for Cav1 interaction with Wnt5a-GFP/secVHHmCh-MT complex in the third mass spectrometry analysis.

6.3.4 Evi Interaction to Received Wnt5a

The last protein was unique among the proteins investigated in this chapter as I decided to explore a known Wnt binding protein in an unexplored circumstance.

Wls is a Wnt chaperone protein for all Wnt proteins known to date and is responsible for transporting Wnt to the cell surface membrane for secretion (J. Yu et al., 2014). As Wls is so vital to the Wnt signalling pathway, it was routinely examined between the three mass spectrometry analyses performed to date for its enrichment in Wnt-GFP expressing cells. To my surprise, in all three mass spectrometry data sets, Wls was detected but never significantly enriched (Ch3 Fig 37+46). As discussed in chapter 3, this is likely because of the zebrafish Wls protein abundance being high enough to survive pulldown enrichment despite not being biotinylated. The likely reason for the lack of biotinylation is the inability for secVHHmCh-MT to access Wnt5a-GFP during its first stages of development and subsequent transport to the cell surface membrane. Human Wls was never detected despite the co-cultures involving human AGS cells, but was detected as a unique protein hit in the 'Test' mass spectrometry data set. This suggested to me the possibility of human Wls interacting with the Wnt5a-GFP/secVHHmCh-MT complex due to endocytosis. Wnt/Wls re-endocytosis and recycling is a known and common phenomenon involving the trafficking of both proteins to and from the endoplasmic reticulum and cell surface membrane, with instances of the pair moving multiple times in time-lapse imaging (Pfeiffer et al., 2002). Similarly, Wnt/Wls has been demonstrated to move from apical to basal cell surface in a planar transcytosis manner (Yamazaki et al., 2016). However, this Wls/Wnt recycling within the source cell could not explain the fact that the unique Wls detected was human. Should this result be a true biotinylated protein hit, would suggest an entirely new and unexplored role of Wls in the Wnt signalling pathway; Wls recycling of an exogenously sourced Wnt5a. To explore this possibility, I investigated Wnt5a-GFP co-localisation in Wls-mCh producing cells. Unfortunately, the recurring theme of low signal intensity was ever present when imaging Wnt5a-GFP in receiving cells. Despite this limitation, many instances of co-localised signal was observed between Wnt5a-GFP and Wls-mCh (Fig 55.B,C and Fig 56). This was demonstrated best in Fig 56 where Wnt5a-GFP pixels show either complete co-localisation to Wls-mCh or existing as a 'side-by-side' pair due to the long imaging time between channels. Of course, many of the images presented in this chapter are subject to the scrutiny of imaging artefacts. However, I believe that these results are worthy of further investigations as they elude to a completely new level of Wls behaviour. Indeed, should Wls interact with

endocytosed Wnt5a this could suggest a role for re-cycling of the Wnt5a protein for re-secretion. Canonically, once Wls releases its Wnt cargo on the cell surface membrane, it is recycled back for either reutilisation for more Wnt shuttling or destined for lysosomal degradation (Belenkaya et al., 2008; Port et al., 2008; Silhankova et al., 2010; Yang et al., 2008). This retrograde trafficking of Wls is characterised by Clathrin and Rab5 positive early endosomes (Port et al., 2008; Rojas et al., 2008; Silhankova et al., 2010). If Wls were to come in contact to an endocytosed Wnt5a, it would be likely to occur at this stage of Wls retrograde transport. This would be either to dissociate Wnt from its cognate receptor and prime it for re-secretion or to localise within the lysosome for degradation. The concept of re-secreting or planar transcytosis of Wnt ligands has further implications to Wnt morphogen gradients as a whole. A contested model of Wnt morphogen gradients are characterised by a 'source and sink' model where a population of source cells secrete a morphogen whose concentration is diffused as the radius from the source cells increase (Crick, 1970). However, many researchers dispute that a source-sink model simplifies a morphogen gradient, where instead of a linear decrease in concentration, we see an exponential decrease resulting from a morphogen 'sink' throughout the tissue (Gregor et al., 2007; Kicheva et al., 2007; Yu et al., 2009). To date, Wnt 'sinks' are terminal for the ligand as it is endocytosed and subsequently degraded. Should Wnt be recycled by Wls instead, then this phenomena may play a pivotal role in the gradient patterns we observe. Indeed, Wnt morphogen gradients in certain tissues remain contested, such as the Wnt gradient in the liver acinus. Canonical Wnt signalling in the acinus is vital for perivenous gene expression (Benhamouche et al., 2006; Gebhardt & Matz-Soja, 2014). However, how the Wnt morphogen gradient is generated against the flow of blood is less understood and not investigated. Methods of Wnt transport such as chaperone-assisted diffusion or cytoneme mediated transport must operate against a negative pressure environment. Evidence for planar transcytosis of Wnt would be an interesting and viable candidate for generating a proportion of the Wnt morphogen gradient in such instances. Of course, there remains a more simple explanation for endocytosed Wnt5a co-localisation to Wls in the accumulation of lysosomes for degradation. As live cell confocal analysis relies on over-expression of a protein construct, a large proportion of the fluorescent proteins will be degraded. It is entirely possible that endocytosed Wnt5a-GFP is

simply degraded once it has transduced its effector signalling alongside the large quantity of over-expressed Wls-mCh. Overall, Wls co-localisation to Wnt5a produced the most interesting result of the mass spectrometry protein hits, which certainly warrants further investigation. Further experiments in determining co-localisation could be performed using the biotin ligase system. A Wls-MiniTurboID can be co-cultured with Wnt5a-GFP cells and a pulldown performed to detect Wnt5a-GFP enrichment. Should we see continued co-localisation in further repeats, then we can conclude that human Wls was a real protein hit from the ‘Test’ mass spectrometry data set.

7 General Discussion and Concluding Remarks

In this thesis, I have demonstrated the functional applicability of the secreted GFP-binding nanobody/biotin ligase secVHHmCh-MT for the use of a specific proximity based biotinylation and isolation of POI-related proteins for mass spectrometry analysis. I identified the ideal cell culture system, which consistently produces Wnt laden cytonemes that co-localise to exogenous secVHHmCh-MT both *in vivo* and in western blot analysis. Using these tools, I was able to detect biotinylated proteins enriched over control samples that demonstrate a high likelihood for real co-localisation to Wnt5a in living systems. Furthermore, this assay has been demonstrated on multiple different Wnt-GFP constructs, showing generalisability for the assay to many different morphogen contexts.

The nanobody-biotin ligase assay required several stages of development and optimisations to reach the level of functionality demonstrated in this thesis. These stages included characterisation of materials, the design of the biotin-ligase construct, development of stable cell lines, optimisations to culture conditions and finally the three rounds of mass spectrometry improvements. While the assay provided strong evidence for the Wnt5a-GFP/secVHHmCh-MT complex biotinylation of Cav1, there remains further optimisations necessary for full protocol maturation. Indeed, in this thesis, I demonstrate that the assay is capable of completing the task set out in the aims of identifying the proteome surrounding the cytoneme mediated Wnt handover. However, further optimisations are required to achieve the full potential of the assay. As discussed in chapter 3; labelling efficiencies, stable cell line generation of POI-GFP and appropriate mass spectrometry techniques are all that is left to realise this potential. Unlike a standard biotin-ligase based assay that fuses the biotin ligase directly to the POI, the nanobody-biotin ligase assay is limited by the volume of biotinylated proteins produced. Therefore, improving the signal-to-noise ratio of this assay is paramount for future assay improvements.

The protein hits generated by the nanobody-biotin ligase assay demonstrated mixed results when observing the co-localisation to Wnt5a. The Rab proteins demonstrated reduced co-localisation to Wnt5a compared to Flot1a, Cav1 and Wls proteins. However, with the exception of Cav1, these preliminary studies were not expected to show co-localisation for all proteins as they originated

from the ‘Test’ mass spectrometry analysis. Indeed, all these protein co-localisations are preliminary investigations that require further testing for conclusive results. That being said, out of all the protein hits investigated, the Wnt-Wls interactions in Wnt receiving cells were the most interesting result. Indeed, Wls co-localisation to Wnt in receiving cells is not well understood in the field, and its existence poses further questions about the role of Wls behaviour and function. Overall, while the assay requires further development, it was nonetheless able to demonstrate novel Wnt5a localisation to Flot1a, Caveolin 1 and Wls in receiving cells.

8 References

Ackers, I., & Malgor, R. (2018). Interrelationship of canonical and non-canonical Wnt signalling pathways in chronic metabolic diseases. *Diabetes and Vascular Disease Research*, *15*(1), 3–13. https://doi.org/10.1177/1479164117738442

Aguilar, G., Matsuda, S., Vigano, M. A., & Affolter, M. (2019). Using Nanobodies to Study Protein Function in Developing Organisms. *Antibodies*, *8*(1), 16. https://doi.org/10.3390/antib8010016

Aguilar, G., Vigano, M. A., Affolter, M., & Matsuda, S. (2019). Reflections on the use of protein binders to study protein function in developmental biology. *WIREs Developmental Biology*, *8*(6). https://doi.org/10.1002/wdev.356

Ahmed, K. A., & Xiang, J. (2011). Mechanisms of cellular communication through intercellular protein transfer. *Journal of Cellular and Molecular Medicine*, *15*(7), 1458–1473. https://doi.org/10.1111/j.1582-4934.2010.01008.x

Ahmed, R., Spikings, E., Zhou, S., Thompsett, A., & Zhang, T. (2014). Pre-hybridisation: An efficient way of suppressing endogenous biotin-binding activity inherent to biotin–streptavidin detection system. *Journal of Immunological Methods*, *406*, 143–147. https://doi.org/10.1016/j.jim.2014.03.010

Almuedo-Castillo, M., Bläßle, A., Mörsdorf, D., Marcon, L., Soh, G. H., Rogers, K. W., Schier, A. F., & Müller, P. (2018). Scale-invariant patterning by size-dependent inhibition of Nodal signalling. *Nature Cell Biology*, *20*(9), 1032–1042. https://doi.org/10.1038/s41556-018-0155-7

Attanasio, F., Caldieri, G., Giacchetti, G., van Horssen, R., Wieringa, B., & Buccione, R. (2011). Novel invadopodia components revealed by differential proteomic analysis. *European Journal of Cell Biology*, *90*(2–3), 115–127. https://doi.org/10.1016/j.ejcb.2010.05.004

Ayers, K. L., Gallet, A., Staccini-Lavenant, L., & Thérond, P. P. (2010). The Long-Range Activity of Hedgehog Is Regulated in the Apical Extracellular Space by the Glypican Dally and the Hydrolase Notum. *Developmental Cell*, *18*(4), 605–620. https://doi.org/10.1016/j.devcel.2010.02.015

Baeg, G.-H., Lin, X., & Perrimon, N. (2001). Heparan Sulfate Proteoglycans are critical for the organization of the extracellular distribution of Wingless. *Biochemical Society Transactions*, *29*(1), A10–A10. https://doi.org/10.1042/bst029a010c

Bänziger, C., Soldini, D., Schütt, C., Zipperlen, P., Hausmann, G., & Basler, K. (2006). Wntless, a Conserved Membrane Protein Dedicated to the Secretion of Wnt Proteins from Signaling Cells. *Cell*, *125*(3), 509–522. https://doi.org/10.1016/j.cell.2006.02.049

Beckett, D., Kovaleva, E., & Schatz, P. J. (1999). A minimal peptide substrate in biotin holoenzyme synthetase-catalyzed biotinylation. *Protein Science*, *8*(4), 921–929. https://doi.org/10.1110/ps.8.4.921

Beckett, K., Monier, S., Palmer, L., Alexandre, C., Green, H., Bonneil, E., Raposo, G., Thibault, P., Borgne, R. Le, & Vincent, J.-P. (2013). Drosophila S2 Cells Secrete Wingless on Exosome-Like Vesicles but the Wingless Gradient Forms Independently of Exosomes. *Traffic*, *14*(1), 82–96. https://doi.org/10.1111/tra.12016

Belenkaya, T. Y., Wu, Y., Tang, X., Zhou, B., Cheng, L., Sharma, Y. V., Yan, D., Selva, E. M., & Lin, X. (2008). The Retromer Complex Influences Wnt Secretion by Recycling Wntless from Endosomes to the Trans-Golgi Network. *Developmental Cell*, *14*(1), 120–131. https://doi.org/10.1016/j.devcel.2007.12.003

Benhamouche, S., Decaens, T., Godard, C., Chambrey, R., Rickman, D. S., Moinard, C., Vasseur-Cognet, M., Kuo, C. J., Kahn, A., Perret, C., & Colnot, S. (2006). Apc Tumor Suppressor Gene Is the “Zonation-Keeper” of Mouse Liver. *Developmental Cell*, *10*(6), 759–770. https://doi.org/10.1016/j.devcel.2006.03.015

Berg, J. S., & Cheney, R. E. (2002). Myosin-X is an unconventional myosin that undergoes intrafilopodial motility. *Nature Cell Biology*, *4*(3), 246–250. https://doi.org/10.1038/ncb762

Bilić, J., Huang, Y.-L., Davidson, G., Zimmermann, T., Cruciat, C.-M., Bienz, M., & Niehrs, C. (2007). Wnt Induces LRP6 Signalosomes and Promotes

Dishevelled-Dependent LRP6 Phosphorylation. *Science*, *316*(5831), 1619–1622. https://doi.org/10.1126/science.1137065

Bobrow, M. N., Litt, G. J., Shaughnessy, K. J., Mayer, P. C., & Conlon, J. (1992). The use of catalyzed reporter deposition as a means of signal amplification in a variety of formats. *Journal of Immunological Methods*, *150*(1–2), 145–149. https://doi.org/10.1016/0022-1759(92)90073-3

Bohil, A. B., Robertson, B. W., & Cheney, R. E. (2006). Myosin-X is a molecular motor that functions in filopodia formation. *Proceedings of the National Academy of Sciences*, *103*(33), 12411–12416. https://doi.org/10.1073/pnas.0602443103

Branon, T. C., Bosch, J. A., Sanchez, A. D., Udeshi, N. D., Svinkina, T., Carr, S. A., Feldman, J. L., Perrimon, N., & Ting, A. Y. (2018). Efficient proximity labeling in living cells and organisms with TurboID. *Nature Biotechnology*, *36*(9), 880–887. https://doi.org/10.1038/nbt.4201

Brunt, L., Greicius, G., Rogers, S., Evans, B. D., Virshup, D. M., Wedgwood, K. C. A., & Scholpp, S. (2021). Vangl2 promotes the formation of long cytonemes to enable distant Wnt/β-catenin signaling. *Nature Communications*, *12*(1), 2058. https://doi.org/10.1038/s41467-021-22393-9

Buechling, T., Chaudhary, V., Spirohn, K., Weiss, M., & Boutros, M. (2011). p24 proteins are required for secretion of Wnt ligands. *EMBO Reports*, *12*(12), 1265–1272. https://doi.org/10.1038/embor.2011.212

Casas-Tintó, & Portela. (2019). Cytonemes, Their Formation, Regulation, and Roles in Signaling and Communication in Tumorigenesis. *International Journal of Molecular Sciences*, *20*(22), 5641. https://doi.org/10.3390/ijms20225641

Caussinus, E., & Affolter, M. (2016). *deGradFP: A System to Knockdown GFP-Tagged Proteins* (pp. 177–187). https://doi.org/10.1007/978-1-4939-6371-3_9

Cervero, P., Himmel, M., Krüger, M., & Linder, S. (2012). Proteomic analysis of podosome fractions from macrophages reveals similarities to spreading initiation centres. *European Journal of Cell Biology*, *91*(11–12), 908–922. https://doi.org/10.1016/j.ejcb.2012.05.005

Chapman-Smith, A., & Cronan Jr, J. E. (1999). Molecular Biology of Biotin Attachment to Proteins. *The Journal of Nutrition*, *129*(2), 477S-484S. https://doi.org/10.1093/jn/129.2.477S

Chapman-Smith, A., Mulhern, T. D., Whelan, F., Cronan, J. E., & Wallace, J. C. (2001). The C-terminal domain of biotin protein ligase from E. coli is required for catalytic activity. *Protein Science*, *10*(12), 2608–2617. https://doi.org/10.1110/ps.22401

Chelius, D., & Bondarenko, P. V. (2002). Quantitative Profiling of Proteins in Complex Mixtures Using Liquid Chromatography and Mass Spectrometry. *Journal of Proteome Research*, *1*(4), 317–323. https://doi.org/10.1021/pr025517j

Cheng, J. P. X., & Nichols, B. J. (2016). Caveolae: One Function or Many? *Trends in Cell Biology*, *26*(3), 177–189. https://doi.org/10.1016/j.tcb.2015.10.010

Chiurillo, M. A. (2015). Role of the Wnt/β-catenin pathway in gastric cancer: An in-depth literature review. *World Journal of Experimental Medicine*, *5*(2), 84. https://doi.org/10.5493/wjem.v5.i2.84

Choi-Rhee, E., Schulman, H., & Cronan, J. E. (2004). Promiscuous protein biotinylation by Escherichia coli biotin protein ligase. *Protein Science*, *13*(11), 3043–3050. https://doi.org/10.1110/ps.04911804

Chong, Z. X., Yeap, S. K., & Ho, W. Y. (2021). Transfection types, methods and strategies: a technical review. *PeerJ*, *9*, e11165. https://doi.org/10.7717/peerj.11165

Chothia, C., Novotný, J., Bruccoleri, R., & Karplus, M. (1985). Domain association in immunoglobulin molecules. *Journal of Molecular Biology*, *186*(3), 651–663. https://doi.org/10.1016/0022-2836(85)90137-8

Choudhury, A., Marks, D. L., Proctor, K. M., Gould, G. W., & Pagano, R. E. (2006). Regulation of caveolar endocytosis by syntaxin 6-dependent delivery of membrane components to the cell surface. *Nature Cell Biology*, *8*(4), 317–328. https://doi.org/10.1038/ncb1380

Clevers, H., & Nusse, R. (2012). Wnt/β-Catenin Signaling and Disease. *Cell*, *149*(6), 1192–1205. https://doi.org/10.1016/j.cell.2012.05.012

Coué, M., Brenner, S. L., Spector, I., & Korn, E. D. (1987). Inhibition of actin polymerization by latrunculin A. *FEBS Letters*, *213*(2), 316–318. https://doi.org/10.1016/0014-5793(87)81513-2

Cox, J., Hein, M. Y., Luber, C. A., Paron, I., Nagaraj, N., & Mann, M. (2014). Accurate Proteome-wide Label-free Quantification by Delayed Normalization and Maximal Peptide Ratio Extraction, Termed MaxLFQ. *Molecular & Cellular Proteomics*, *13*(9), 2513–2526. https://doi.org/10.1074/mcp.M113.031591

Crick, F. (1970). Central Dogma of Molecular Biology. *Nature*, *227*(5258), 561–563. https://doi.org/10.1038/227561a0

Dayon, L., Hainard, A., Licker, V., Turck, N., Kuhn, K., Hochstrasser, D. F., Burkhard, P. R., & Sanchez, J.-C. (2008). Relative Quantification of Proteins in Human Cerebrospinal Fluids by MS/MS Using 6-Plex Isobaric Tags. *Analytical Chemistry*, *80*(8), 2921–2931. https://doi.org/10.1021/ac702422x

De, A. (2011). Wnt/Ca²⁺ signaling pathway: a brief overview. *Acta Biochimica et Biophysica Sinica*, *43*(10), 745–756. https://doi.org/10.1093/abbs/gmr079

de Lau, W., Barker, N., Low, T. Y., Koo, B.-K., Li, V. S. W., Teunissen, H., Kujala, P., Haegebarth, A., Peters, P. J., van de Wetering, M., Stange, D. E., van Es, J., Guardavaccaro, D., Schasfoort, R. B. M., Mohri, Y., Nishimori, K., Mohammed, S., Heck, A. J. R., & Clevers, H. (2011). Lgr5 homologues associate with Wnt receptors and mediate R-spondin signalling. *Nature*, *476*(7360), 293–297. https://doi.org/10.1038/nature10337

Duncan, R. N., Panahi, S., Piotrowski, T., & Dorsky, R. I. (2015). Identification of Wnt Genes Expressed in Neural Progenitor Zones during Zebrafish Brain Development. *PLOS ONE*, *10*(12), e0145810. https://doi.org/10.1371/journal.pone.0145810

Duquet, A., Melotti, A., Mishra, S., Malerba, M., Seth, C., Conod, A., & Ruiz i Altaba, A. (2014). A novel genome-wide *in vivo* screen for metastatic suppressors in human colon cancer identifies the positive WNT - TCF pathway modulators TMED 3 and SOX 12. *EMBO Molecular Medicine*, *6*(7), 882–901. https://doi.org/10.15252/emmm.201303799

ECACC General Cell Collection: AGS. (n.d.). ECACC. Retrieved October 21, 2023, from https://www.culturecollections.org.uk/products/celllines/generalcell/detail.jsp?refId=89090402&collection=ecacc_gc

Edman, P., Högfeldt, E., Sillén, L. G., & Kinell, P.-O. (1950). Method for Determination of the Amino Acid Sequence in Peptides. *Acta Chemica Scandinavica*, *4*, 283–293. https://doi.org/10.3891/acta.chem.scand.04-0283

Ezzoukhry, Z., Henriet, E., Cordelières, F. P., Dupuy, J.-W., Maître, M., Gay, N., Di-Tommaso, S., Mercier, L., Goetz, J. G., Peter, M., Bard, F., Moreau, V., Raymond, A.-A., & Saltel, F. (2018). Combining laser capture microdissection and proteomics reveals an active translation machinery controlling invadosome formation. *Nature Communications*, *9*(1), 2031. https://doi.org/10.1038/s41467-018-04461-9

Farin, H. F., Jordens, I., Mosa, M. H., Basak, O., Korving, J., Tauriello, D. V. F., de Punder, K., Angers, S., Peters, P. J., Maurice, M. M., & Clevers, H. (2016). Visualization of a short-range Wnt gradient in the intestinal stem-cell niche. *Nature*, *530*(7590), 340–343. https://doi.org/10.1038/nature16937

Fenn, J. B., Mann, M., Meng, C. K., Wong, S. F., & Whitehouse, C. M. (1989). Electrospray Ionization for Mass Spectrometry of Large Biomolecules. *Science*, *246*(4926), 64–71. https://doi.org/10.1126/science.2675315

Fernández-Suárez, M., Chen, T. S., & Ting, A. Y. (2008). Protein−Protein Interaction Detection in Vitro and in Cells by Proximity Biotinylation. *Journal of the American Chemical Society*, *130*(29), 9251–9253. https://doi.org/10.1021/ja801445p

Flanagan, D. J., Barker, N., Nowell, C., Clevers, H., Ernst, M., Phesse, T. J., & Vincan, E. (2017). Loss of the Wnt receptor Frizzled7 in the gastric epithelium is deleterious and triggers rapid repopulation in vivo. *Disease Models & Mechanisms*. https://doi.org/10.1242/dmm.029876

Furutani, Y., & Yoshihara, Y. (2018). Proteomic analysis of dendritic filopodia-rich fraction isolated by telencephalin and vitronectin interaction. *Frontiers in Synaptic Neuroscience*, *10*(AUG). https://doi.org/10.3389/fnsyn.2018.00027

Galbiati, F., Volonte', D., Brown, A. M. C., Weinstein, D. E., Ben-Ze'ev, A., Pestell, R. G., & Lisanti, M. P. (2000). Caveolin-1 Expression Inhibits Wnt/β-Catenin/Lef-1 Signaling by Recruiting β-Catenin to Caveolae Membrane Domains. *Journal of Biological Chemistry*, *275*(30), 23368–23377. https://doi.org/10.1074/jbc.M002020200

Galli, L. M., Barnes, T. L., Secrest, S. S., Kadowaki, T., & Burrus, L. W. (2007). Porcupine-mediated lipid-modification regulates the activity and distribution of Wnt proteins in the chick neural tube. *Development*, *134*(18), 3339–3348. https://doi.org/10.1242/dev.02881

Gammons, M. V., Renko, M., Johnson, C. M., Rutherford, T. J., & Bienz, M. (2016). Wnt Signalosome Assembly by DEP Domain Swapping of Dishevelled. *Molecular Cell*, *64*(1), 92–104. https://doi.org/10.1016/j.molcel.2016.08.026

Gasnereau, I., Herr, P., Chia, P. Z. C., Basler, K., & Gleeson, P. A. (2011). Identification of an Endocytosis Motif in an Intracellular Loop of Wntless Protein, Essential for Its Recycling and the Control of Wnt Protein Signaling. *Journal of Biological Chemistry*, *286*(50), 43324–43333. https://doi.org/10.1074/jbc.M111.307231

Gebhardt, R., & Matz-Soja, M. (2014). Liver zonation: Novel aspects of its regulation and its impact on homeostasis. *World Journal of Gastroenterology*, *20*(26), 8491–8504. https://doi.org/10.3748/wjg.v20.i26.8491

Glinka, A., Dolde, C., Kirsch, N., Huang, Y., Kazanskaya, O., Ingelfinger, D., Boutros, M., Cruciat, C., & Niehrs, C. (2011). LGR4 and LGR5 are R-

spondin receptors mediating Wnt/β-catenin and Wnt/PCP signalling. *EMBO Reports*, *12*(10), 1055–1061. https://doi.org/10.1038/embor.2011.175

Grant, M. K. O., Shapiro, S. L., Ashe, K. H., Liu, P., & Zahs, K. R. (2019). A Cautionary Tale: Endogenous Biotinylated Proteins and Exogenously-Introduced Protein A Cause Antibody-Independent Artefacts in Western Blot Studies of Brain-Derived Proteins. *Biological Procedures Online*, *21*(1), 6. https://doi.org/10.1186/s12575-019-0095-z

Green, J., Nusse, R., & van Amerongen, R. (2014). The Role of Ryk and Ror Receptor Tyrosine Kinases in Wnt Signal Transduction. Cold Spring Harbor Perspectives in Biology, 6(2), a009175–a009175. https://doi.org/10.1101/cshperspect.a009175

Gregor, T., Tank, D. W., Wieschaus, E. F., & Bialek, W. (2007). Probing the Limits to Positional Information. *Cell*, *130*(1), 153–164. https://doi.org/10.1016/j.cell.2007.05.025

Groft, C. M., Uljon, S. N., Wang, R., & Werner, M. H. (1998). Structural homology between the Rap30 DNA-binding domain and linker histone H5: Implications for preinitiation complex assembly. *Proceedings of the National Academy of Sciences*, *95*(16), 9117–9122. https://doi.org/10.1073/pnas.95.16.9117

Gross, G. G., Junge, J. A., Mora, R. J., Kwon, H.-B., Olson, C. A., Takahashi, T. T., Liman, E. R., Ellis-Davies, G. C. R., McGee, A. W., Sabatini, B. L., Roberts, R. W., & Arnold, D. B. (2013). Recombinant Probes for Visualizing Endogenous Synaptic Proteins in Living Neurons. *Neuron*, *78*(6), 971–985. https://doi.org/10.1016/j.neuron.2013.04.017

Guerra, F., & Bucci, C. (2016). Multiple Roles of the Small GTPase Rab7. *Cells*, *5*(3), 34. https://doi.org/10.3390/cells5030034

Hall, E., & Ogden, S. (2018). Preserve Cultured Cell Cytonemes through a Modified Electron Microscopy Fixation. *BIO-PROTOCOL*, *8*(13). https://doi.org/10.21769/BioProtoc.2898

Hamers-Casterman, C., Atarhouch, T., Muyldermans, S., Robinson, G., Hammers, C., Songa, E. B., Bendahman, N., & Hammers, R. (1993).

Naturally occurring antibodies devoid of light chains. *Nature*, *363*(6428), 446–448. https://doi.org/10.1038/363446a0

Harmansa, S., Alborelli, I., Bieli, D., Caussinus, E., & Affolter, M. (2017). A nanobody-based toolset to investigate the role of protein localization and dispersal in Drosophila. *ELife*, *6*. https://doi.org/10.7554/eLife.22549

Harmansa, S., Hamaratoglu, F., Affolter, M., & Caussinus, E. (2015). Dpp spreading is required for medial but not for lateral wing disc growth. *Nature*, *527*(7578), 317–322. https://doi.org/10.1038/nature15712

Harmsen, M. M., Ruuls, R. C., Nijman, I. J., Niewold, T. A., Frenken, L. G. J., & de Geus, B. (2000). Llama heavy-chain V regions consist of at least four distinct subfamilies revealing novel sequence features. *Molecular Immunology*, *37*(10), 579–590. https://doi.org/10.1016/S0161-5890(00)00081-X

Hausmann, G., Bänziger, C., & Basler, K. (2007). Helping Wingless take flight: how WNT proteins are secreted. *Nature Reviews Molecular Cell Biology*, *8*(4), 331–336. https://doi.org/10.1038/nrm2141

Havrylov, S., & Park, M. (2015). MS/MS-based strategies for proteomic profiling of invasive cell structures. *PROTEOMICS*, *15*(2–3), 272–286. https://doi.org/10.1002/pmic.201400220

Hayer, A., Stoeber, M., Bissig, C., & Helenius, A. (2010). Biogenesis of Caveolae: Stepwise Assembly of Large Caveolin and Cavin Complexes. *Traffic*, *11*(3), 361–382. https://doi.org/10.1111/j.1600-0854.2009.01023.x

Helma, J., Cardoso, M. C., Muyldermans, S., & Leonhardt, H. (2015). Nanobodies and recombinant binders in cell biology. *Journal of Cell Biology*, *209*(5), 633–644. https://doi.org/10.1083/jcb.201409074

Hoang, B., Moos, M., Vukicevic, S., & Luyten, F. P. (1996a). Primary Structure and Tissue Distribution of FRZB, a Novel Protein Related to Drosophila Frizzled, Suggest a Role in Skeletal Morphogenesis. *Journal of Biological Chemistry*, *271*(42), 26131–26137. https://doi.org/10.1074/jbc.271.42.26131

Hofmann, K. (2000). A superfamily of membrane-bound O -acyltransferases with implications for Wnt signaling. *Trends in Biochemical Sciences*, *25*(3), 111–112. https://doi.org/10.1016/S0968-0004(99)01539-X

Homma, Y., Hiragi, S., & Fukuda, M. (2021). Rab family of small GTPases: an updated view on their regulation and functions. *The FEBS Journal*, *288*(1), 36–55. https://doi.org/10.1111/febs.15453

Hopkins, C., Gibson, A., Stinchcombe, J., & Futter, C. (2000). *Chimeric molecules employing horseradish peroxidase as reporter enzyme for protein localization in the electron microscope* (pp. 35–45). https://doi.org/10.1016/S0076-6879(00)27265-0

Horton, E. R., Byron, A., Askari, J. A., Ng, D. H. J., Millon-Frémillon, A., Robertson, J., Koper, E. J., Paul, N. R., Warwood, S., Knight, D., Humphries, J. D., & Humphries, M. J. (2015). Definition of a consensus integrin adhesome and its dynamics during adhesion complex assembly and disassembly. *Nature Cell Biology*, *17*(12), 1577–1587. https://doi.org/10.1038/ncb3257

Houart, C., Caneparo, L., Heisenberg, C.-P., Barth, K. A., Take-Uchi, M., & Wilson, S. W. (2002). Establishment of the Telencephalon during Gastrulation by Local Antagonism of Wnt Signaling. *Neuron*, *35*(2), 255–265. https://doi.org/10.1016/S0896-6273(02)00751-1

Housley, M. P., Reischauer, S., Dieu, M., Raes, M., Stainier, D. Y. R., & Vanhollebeke, B. (2014). Translational profiling through biotinylation of tagged ribosomes in zebrafish. *Development*, *141*(20), 3988–3993. https://doi.org/10.1242/dev.111849

Hsieh, J.-C., Kodjabachian, L., Rebbert, M. L., Rattner, A., Smallwood, P. M., Samos, C. H., Nusse, R., Dawid, I. B., & Nathans, J. (1999). A new secreted protein that binds to Wnt proteins and inhibits their activites. *Nature*, *398*(6726), 431–436. https://doi.org/10.1038/18899

Hung, V., Zou, P., Rhee, H.-W., Udeshi, N. D., Cracan, V., Svinkina, T., Carr, S. A., Mootha, V. K., & Ting, A. Y. (2014). Proteomic Mapping of the Human Mitochondrial Intermembrane Space in Live Cells via Ratiometric APEX

Tagging. *Molecular Cell*, *55*(2), 332–341. https://doi.org/10.1016/j.molcel.2014.06.003

Kachkin, D. V., Khorolskaya, J. I., Ivanova, J. S., & Rubel, A. A. (2020). An Efficient Method for Isolation of Plasmid DNA for Transfection of Mammalian Cell Cultures. *Methods and Protocols*, *3*(4), 69. https://doi.org/10.3390/mps3040069

Karhemo, P.-R., Ravela, S., Laakso, M., Ritamo, I., Tatti, O., Mäkinen, S., Goodison, S., Stenman, U.-H., Hölttä, E., Hautaniemi, S., Valmu, L., Lehti, K., & Laakkonen, P. (2012). An optimized isolation of biotinylated cell surface proteins reveals novel players in cancer metastasis. *Journal of Proteomics*, *77*, 87–100. https://doi.org/10.1016/j.jprot.2012.07.009

Karp, N. A., Huber, W., Sadowski, P. G., Charles, P. D., Hester, S. V., & Lilley, K. S. (2010). Addressing Accuracy and Precision Issues in iTRAQ Quantitation. *Molecular & Cellular Proteomics*, *9*(9), 1885–1897. https://doi.org/10.1074/mcp.M900628-MCP200

Kawano, Y., & Kypta, R. (2003). Secreted antagonists of the Wnt signalling pathway. *Journal of Cell Science*, *116*(13), 2627–2634. https://doi.org/10.1242/jcs.00623

Kelley, L. A., Mezulis, S., Yates, C. M., Wass, M. N., & Sternberg, M. J. E. (2015). The Phyre2 web portal for protein modeling, prediction and analysis. *Nature Protocols*, *10*(6), 845–858. https://doi.org/10.1038/nprot.2015.053

Kicheva, A., Pantazis, P., Bollenbach, T., Kalaidzidis, Y., Bittig, T., Jülicher, F., & González-Gaitán, M. (2007). Kinetics of Morphogen Gradient Formation. *Science*, *315*(5811), 521–525. https://doi.org/10.1126/science.1135774

Kirsch, K. H., Georgescu, M.-M., Ishimaru, S., & Hanafusa, H. (1999). CMS: An adapter molecule involved in cytoskeletal rearrangements. *Proceedings of the National Academy of Sciences*, *96*(11), 6211–6216. https://doi.org/10.1073/pnas.96.11.6211

Koide, A., Bailey, C. W., Huang, X., & Koide, S. (1998). The fibronectin type III domain as a scaffold for novel binding proteins. *Journal of Molecular Biology*, *284*(4), 1141–1151. https://doi.org/10.1006/jmbi.1998.2238

Komekado, H., Yamamoto, H., Chiba, T., & Kikuchi, A. (2007). Glycosylation and palmitoylation of Wnt-3a are coupled to produce an active form of Wnt-3a. *Genes to Cells*, *12*(4), 521–534. https://doi.org/10.1111/j.1365-2443.2007.01068.x

Komiya, Y., & Habas, R. (2008). Wnt signal transduction pathways. *Organogenesis*, *4*(2), 68–75. https://doi.org/10.4161/org.4.2.5851

Korkut, C., Ataman, B., Ramachandran, P., Ashley, J., Barria, R., Gherbesi, N., & Budnik, V. (2009). Trans-Synaptic Transmission of Vesicular Wnt Signals through Evi/Wntless. *Cell*, *139*(2), 393–404. https://doi.org/10.1016/j.cell.2009.07.051

Kornberg, T. B., & Roy, S. (2014). Cytonemes as specialized signaling filopodia. *Development*, *141*(4), 729–736. https://doi.org/10.1242/dev.086223

Krause, M., Dent, E. W., Bear, J. E., Loureiro, J. J., & Gertler, F. B. (2003). Ena/VASP Proteins: Regulators of the Actin Cytoskeleton and Cell Migration. *Annual Review of Cell and Developmental Biology*, *19*(1), 541–564. https://doi.org/10.1146/annurev.cellbio.19.050103.103356

Kulyyassov, A., Shoaib, M., Pichugin, A., Kannouche, P., Ramanculov, E., Lipinski, M., & Ogryzko, V. (2011). PUB-MS: A Mass Spectrometry-based Method to Monitor Protein–Protein Proximity *in vivo*. *Journal of Proteome Research*, *10*(10), 4416–4427. https://doi.org/10.1021/pr200189p

Kuo, C.-L., Oyler, G. A., & Shoemaker, C. B. (2011). Accelerated Neuronal Cell Recovery from Botulinum Neurotoxin Intoxication by Targeted Ubiquitination. *PLoS ONE*, *6*(5), e20352. https://doi.org/10.1371/journal.pone.0020352

Kuo, J.-C., Han, X., Hsiao, C.-T., Yates III, J. R., & Waterman, C. M. (2011). Analysis of the myosin-II-responsive focal adhesion proteome reveals a role for β-Pix in negative regulation of focal adhesion maturation. *Nature Cell Biology*, *13*(4), 383–393. https://doi.org/10.1038/ncb2216

Lai, X., Wang, L., & Witzmann, F. A. (2013). Issues and Applications in Label-Free Quantitative Mass Spectrometry. *International Journal of Proteomics*, *2013*, 1–13. https://doi.org/10.1155/2013/756039

Lamaze, C., Tardif, N., Dewulf, M., Vassilopoulos, S., & Blouin, C. M. (2017). The caveolae dress code: structure and signaling. *Current Opinion in Cell Biology*, *47*, 117–125. https://doi.org/10.1016/j.ceb.2017.02.014

Lam, S. S., Martell, J. D., Kamer, K. J., Deerinck, T. J., Ellisman, M. H., Mootha, V. K., & Ting, A. Y. (2015). Directed evolution of APEX2 for electron microscopy and proximity labeling. *Nature Methods*, *12*(1), 51–54. https://doi.org/10.1038/nmeth.3179

Lecarpentier, Y., Schussler, O., Hébert, J.-L., & Vallée, A. (2019). Multiple Targets of the Canonical WNT/β-Catenin Signaling in Cancers. *Frontiers in Oncology*, *9*. https://doi.org/10.3389/fonc.2019.01248

Lehtonen, S., Zhao, F., & Lehtonen, E. (2002). CD2-associated protein directly interacts with the actin cytoskeleton. *American Journal of Physiology-Renal Physiology*, *283*(4), F734–F743. https://doi.org/10.1152/ajprenal.00312.2001

Leijnse, N., Oddershede, L. B., & Bendix, P. M. (2015). Helical buckling of actin inside filopodia generates traction. *Proceedings of the National Academy of Sciences*, *112*(1), 136–141. https://doi.org/10.1073/pnas.1411761112

Li, B., & Niswander, L. A. (2020). TMEM132A, a Novel Wnt Signaling Pathway Regulator Through Wntless (WLS) Interaction. *Frontiers in Cell and Developmental Biology*, *8*. https://doi.org/10.3389/fcell.2020.599890

Li, J., Mahajan, A., & Tsai, M.-D. (2006). Ankyrin Repeat: A Unique Motif Mediating Protein−Protein Interactions. *Biochemistry*, *45*(51), 15168–15178. https://doi.org/10.1021/bi062188q

Lin, H., Lin, H., Chiou, Y., Wu, C., Chiu, W., & Tang, M. (2018). Caveolin-1 down-regulation is required for Wnt5a-Frizzled 2 signalling in Ha-RasV12 - induced cell transformation. *Journal of Cellular and Molecular Medicine*, *22*(5), 2631–2643. https://doi.org/10.1111/jcmm.13531

Li, X., Wu, Y., Shen, C., Belenkaya, T. Y., Ray, L., & Lin, X. (2015). Drosophila p24 and Sec22 regulate Wingless trafficking in the early secretory pathway. *Biochemical and Biophysical Research Communications*, *463*(4), 483–489. https://doi.org/10.1016/j.bbrc.2015.04.151

Loughlin, F. E., Mansfield, R. E., Vaz, P. M., McGrath, A. P., Setiyaputra, S., Gamsjaeger, R., Chen, E. S., Morris, B. J., Guss, J. M., & Mackay, J. P. (2009). The zinc fingers of the SR-like protein ZRANB2 are single-stranded RNA-binding domains that recognize 5′ splice site-like sequences. *Proceedings of the National Academy of Sciences*, *106*(14), 5581–5586. https://doi.org/10.1073/pnas.0802466106

MacDonald, B. T., Tamai, K., & He, X. (2009). Wnt/β-Catenin Signaling: Components, Mechanisms, and Diseases. *Developmental Cell*, *17*(1), 9–26. https://doi.org/10.1016/j.devcel.2009.06.016

Markmiller, S., Soltanieh, S., Server, K. L., Mak, R., Jin, W., Fang, M. Y., Luo, E.-C., Krach, F., Yang, D., Sen, A., Fulzele, A., Wozniak, J. M., Gonzalez, D. J., Kankel, M. W., Gao, F.-B., Bennett, E. J., Lécuyer, E., & Yeo, G. W. (2018). Context-Dependent and Disease-Specific Diversity in Protein Interactions within Stress Granules. *Cell*, *172*(3), 590-604.e13. https://doi.org/10.1016/j.cell.2017.12.032

Martell, J. D., Deerinck, T. J., Sancak, Y., Poulos, T. L., Mootha, V. K., Sosinsky, G. E., Ellisman, M. H., & Ting, A. Y. (2012). Engineered ascorbate peroxidase as a genetically encoded reporter for electron microscopy. *Nature Biotechnology*, *30*(11), 1143–1148. https://doi.org/10.1038/nbt.2375

Masters, J. R. (2002). HeLa cells 50 years on: the good, the bad and the ugly. *Nature Reviews Cancer*, *2*(4), 315–319. https://doi.org/10.1038/nrc775

Mattes, B., Dang, Y., Greicius, G., Kaufmann, L. T., Prunsche, B., Rosenbauer, J., Stegmaier, J., Mikut, R., Özbek, S., Nienhaus, G. U., Schug, A., Virshup, D. M., & Scholpp, S. (2018). Wnt/PCP controls spreading of Wnt/β-catenin signals by cytonemes in vertebrates. *ELife*, *7*. https://doi.org/10.7554/eLife.36953

Mattes, B., & Scholpp, S. (2018). Emerging role of contact-mediated cell communication in tissue development and diseases. *Histochemistry and Cell Biology*, *150*(5), 431–442. https://doi.org/10.1007/s00418-018-1732-3

Mattila, P. K., & Lappalainen, P. (2008). Filopodia: molecular architecture and cellular functions. *Nature Reviews Molecular Cell Biology*, *9*(6), 446–454. https://doi.org/10.1038/nrm2406

McAllister, H. C., & Coon, M. J. (1966). Further Studies on the Properties of Liver Propionyl Coenzyme A Holocarboxylase Synthetase and the Specificity of Holocarboxylase Formation. *Journal of Biological Chemistry*, *241*(12), 2855–2861. https://doi.org/10.1016/S0021-9258(18)96542-7

Mehta, A. K., Majumdar, S. S., Alam, P., Gulati, N., & Brahmachari, V. (2009). Epigenetic regulation of cytomegalovirus major immediate-early promoter activity in transgenic mice. *Gene*, *428*(1–2), 20–24. https://doi.org/10.1016/j.gene.2008.09.033

Meyen, D., Tarbashevich, K., Banisch, T. U., Wittwer, C., Reichman-Fried, M., Maugis, B., Grimaldi, C., Messerschmidt, E.-M., & Raz, E. (2015). Dynamic filopodia are required for chemokine-dependent intracellular polarization during guided cell migration in vivo. *ELife*, *4*. https://doi.org/10.7554/eLife.05279

Mihara, E., Hirai, H., Yamamoto, H., Tamura-Kawakami, K., Matano, M., Kikuchi, A., Sato, T., & Takagi, J. (2016). Active and water-soluble form of lipidated Wnt protein is maintained by a serum glycoprotein afamin/α-albumin. *ELife*, *5*. https://doi.org/10.7554/eLife.11621

Mii, Y., & Taira, M. (2009). Secreted Frizzled-related proteins enhance the diffusion of Wnt ligands and expand their signalling range. *Development*, *136*(24), 4083–4088. https://doi.org/10.1242/dev.032524

Miller, J. R. (2002). The Wnts. In *Genome Biology* (Vol. 3, Issue 1). https://doi.org/10.1186/gb-2001-3-1-reviews3001

Mulligan, K. A., Fuerer, C., Ching, W., Fish, M., Willert, K., & Nusse, R. (2012). Secreted Wingless-interacting molecule (Swim) promotes long-range signaling by maintaining Wingless solubility. *Proceedings of the National Academy of Sciences*, *109*(2), 370–377. https://doi.org/10.1073/pnas.1119197109

Muntel, J., Boswell, S. A., Tang, S., Ahmed, S., Wapinski, I., Foley, G., Steen, H., & Springer, M. (2015). Abundance-based Classifier for the Prediction of

Mass Spectrometric Peptide Detectability Upon Enrichment (PPA). *Molecular & Cellular Proteomics*, *14*(2), 430–440. https://doi.org/10.1074/mcp.M114.044321

Muyldermans, S., Atarhouch, T., Saldanha, J., Barbosa, J. A. R. G., & Hamers, R. (1994). Sequence and structure of VH domain from naturally occurring camel heavy chain immunoglobulins lacking light chains. *"Protein Engineering, Design and Selection," 7*(9), 1129–1135. https://doi.org/10.1093/protein/7.9.1129

Nagy, V., & Watzele, M. (2006). FuGENE® 6 Transfection Reagent: minimizing reagent-dependent side effects as analyzed by gene-expression profiling and cytotoxicity assays. *Nature Methods*, *3*(5), iii–v. https://doi.org/10.1038/nmeth879

Neumann, S., Coudreuse, D. Y. M., Van Der Westhuyzen, D. R., Eckhardt, E. R. M., Korswagen, H. C., Schmitz, G., & Sprong, H. (2009). Mammalian Wnt3a is Released on Lipoprotein Particles. *Traffic*, *10*(3), 334–343. https://doi.org/10.1111/j.1600-0854.2008.00872.x

Nord, K., Gunneriusson, E., Ringdahl, J., Ståhl, S., Uhlén, M., & Nygren, P.-Å. (1997). Binding proteins selected from combinatorial libraries of an α-helical bacterial receptor domain. *Nature Biotechnology*, *15*(8), 772–777. https://doi.org/10.1038/nbt0897-772

Nusse, R., van Ooyen, A., Cox, D., Fung, Y. K. T., & Varmus, H. (1984). Mode of proviral activation of a putative mammary oncogene (int-1) on mouse chromosome 15. *Nature*, *307*(5947), 131–136. https://doi.org/10.1038/307131a0

Nüsslein-Volhard, C., & Wieschaus, E. (1980). Mutations affecting segment number and polarity in Drosophila. *Nature*, *287*(5785), 795–801. https://doi.org/10.1038/287795a0

Nwosu, Z. C., Ebert, M. P., Dooley, S., & Meyer, C. (2016). Caveolin-1 in the regulation of cell metabolism: a cancer perspective. *Molecular Cancer*, *15*(1), 71. https://doi.org/10.1186/s12943-016-0558-7

Nygaard, R., Yu, J., Kim, J., Ross, D. R., Parisi, G., Clarke, O. B., Virshup, D. M., & Mancia, F. (2021). Structural Basis of WLS/Evi-Mediated Wnt

Transport and Secretion. *Cell*, *184*(1), 194-206.e14. https://doi.org/10.1016/j.cell.2020.11.038

Ong, S.-E., & Mann, M. (2005). Mass spectrometry–based proteomics turns quantitative. *Nature Chemical Biology*, *1*(5), 252–262. https://doi.org/10.1038/nchembio736

Pani, A. M., & Goldstein, B. (2018). Direct visualization of a native Wnt in vivo reveals that a long-range Wnt gradient forms by extracellular dispersal. *ELife*, *7*. https://doi.org/10.7554/eLife.38325

Pappireddi, N., Martin, L., & Wühr, M. (2019). A Review on Quantitative Multiplexed Proteomics. *ChemBioChem*, *20*(10), 1210–1224. https://doi.org/10.1002/cbic.201800650

Parizek, P., Kummer, L., Rube, P., Prinz, A., Herberg, F. W., & Plückthun, A. (2012). Designed Ankyrin Repeat Proteins (DARPins) as Novel Isoform-Specific Intracellular Inhibitors of c-Jun N-Terminal Kinases. *ACS Chemical Biology*, *7*(8), 1356–1366. https://doi.org/10.1021/cb3001167

Pfeiffer, S., Ricardo, S., Manneville, J.-B., Alexandre, C., & Vincent, J.-P. (2002). Producing Cells Retain and Recycle Wingless in Drosophila Embryos. *Current Biology*, *12*(11), 957–962. https://doi.org/10.1016/S0960-9822(02)00867-9

Port, F., Hausmann, G., & Basler, K. (2011). A genome-wide RNA interference screen uncovers two p24 proteins as regulators of Wingless secretion. *EMBO Reports*, *12*(11), 1144–1152. https://doi.org/10.1038/embor.2011.165

Port, F., Kuster, M., Herr, P., Furger, E., Bänziger, C., Hausmann, G., & Basler, K. (2008). Wingless secretion promotes and requires retromer-dependent cycling of Wntless. *Nature Cell Biology*, *10*(2), 178–185. https://doi.org/10.1038/ncb1687

Pu, J., Guardia, C. M., Keren-Kaplan, T., & Bonifacino, J. S. (2016). Mechanisms and functions of lysosome positioning. *Journal of Cell Science*. https://doi.org/10.1242/jcs.196287

Ramírez-Weber, F.-A., & Kornberg, T. B. (1999). Cytonemes. *Cell*, *97*(5), 599–607. https://doi.org/10.1016/S0092-8674(00)80771-0

Ressurreição, M., Warrington, S., & Strutt, D. (2018). Rapid Disruption of Dishevelled Activity Uncovers an Intercellular Role in Maintenance of Prickle in Core Planar Polarity Protein Complexes. *Cell Reports*, *25*(6), 1415-1424.e6. https://doi.org/10.1016/j.celrep.2018.10.039

Rhee, H.-W., Zou, P., Udeshi, N. D., Martell, J. D., Mootha, V. K., Carr, S. A., & Ting, A. Y. (2013). Proteomic Mapping of Mitochondria in Living Cells via Spatially Restricted Enzymatic Tagging. *Science*, *339*(6125), 1328–1331. https://doi.org/10.1126/science.1230593

Riitano, G., Manganelli, V., Capozzi, A., Mattei, V., Recalchi, S., Martellucci, S., Longo, A., Misasi, R., Garofalo, T., & Sorice, M. (2020). LRP6 mediated signal transduction pathway triggered by tissue plasminogen activator acts through lipid rafts in neuroblastoma cells. *Journal of Cell Communication and Signaling*, *14*(3), 315–323. https://doi.org/10.1007/s12079-020-00551-w

Rios-Esteves, J., & Resh, M. D. (2013). Stearoyl CoA Desaturase Is Required to Produce Active, Lipid-Modified Wnt Proteins. *Cell Reports*, *4*(6), 1072–1081. https://doi.org/10.1016/j.celrep.2013.08.027

Rogers, S., & Scholpp, S. (2020). *Preserving Cytonemes for Immunocytochemistry of Cultured Adherent Cells* (pp. 183–190). https://doi.org/10.1007/7651_2020_305

Rojas, R., van Vlijmen, T., Mardones, G. A., Prabhu, Y., Rojas, A. L., Mohammed, S., Heck, A. J. R., Raposo, G., van der Sluijs, P., & Bonifacino, J. S. (2008). Regulation of retromer recruitment to endosomes by sequential action of Rab5 and Rab7. *The Journal of Cell Biology*, *183*(3), 513–526. https://doi.org/10.1083/jcb.200804048

Ross, P. L., Huang, Y. N., Marchese, J. N., Williamson, B., Parker, K., Hattan, S., Khainovski, N., Pillai, S., Dey, S., Daniels, S., Purkayastha, S., Juhasz, P., Martin, S., Bartlet-Jones, M., He, F., Jacobson, A., & Pappin, D. J. (2004). Multiplexed Protein Quantitation in Saccharomyces cerevisiae Using Amine-reactive Isobaric Tagging Reagents. *Molecular & Cellular*

Proteomics, *3*(12), 1154–1169. https://doi.org/10.1074/mcp.M400129-MCP200

Rothbauer, U., Zolghadr, K., Tillib, S., Nowak, D., Schermelleh, L., Gahl, A., Backmann, N., Conrath, K., Muyldermans, S., Cardoso, M. C., & Leonhardt, H. (2006). Targeting and tracing antigens in live cells with fluorescent nanobodies. *Nature Methods*, *3*(11), 887–889. https://doi.org/10.1038/nmeth953

Roubinet, C., Tsankova, A., Pham, T. T., Monnard, A., Caussinus, E., Affolter, M., & Cabernard, C. (2017). Spatio-temporally separated cortical flows and spindle geometry establish physical asymmetry in fly neural stem cells. *Nature Communications*, *8*(1), 1383. https://doi.org/10.1038/s41467-017-01391-w

Routledge, D., Rogers, S., Ono, Y., Brunt, L., Meniel, V., Tornillo, G., Ashktorab, H., Phesse, T. J., & Scholpp, S. (2022). The scaffolding protein flot2 promotes cytoneme-based transport of wnt3 in gastric cancer. *ELife*, *11*. https://doi.org/10.7554/eLife.77376

Routledge, D., & Scholpp, S. (2019). Mechanisms of intercellular wnt transport. In *Development (Cambridge)* (Vol. 146, Issue 10). Company of Biologists Ltd. https://doi.org/10.1242/dev.176073

Roux, K. J., Kim, D. I., Raida, M., & Burke, B. (2012). A promiscuous biotin ligase fusion protein identifies proximal and interacting proteins in mammalian cells. *Journal of Cell Biology*, *196*(6), 801–810. https://doi.org/10.1083/jcb.201112098

Ruzicka, L., Howe, D. G., Ramachandran, S., Toro, S., Van Slyke, C. E., Bradford, Y. M., Eagle, A., Fashena, D., Frazer, K., Kalita, P., Mani, P., Martin, R., Moxon, S. T., Paddock, H., Pich, C., Schaper, K., Shao, X., Singer, A., & Westerfield, M. (2019). The Zebrafish Information Network: new support for non-coding genes, richer Gene Ontology annotations and the Alliance of Genome Resources. *Nucleic Acids Research*, *47*(D1), D867–D873. https://doi.org/10.1093/nar/gky1090

Sagner, A., & Briscoe, J. (2017). Morphogen interpretation: concentration, time, competence, and signaling dynamics. *WIREs Developmental Biology*, *6*(4). https://doi.org/10.1002/wdev.271

Sakane, H., Yamamoto, H., & Kikuchi, A. (2010). LRP6 is internalized by Dkk1 to suppress its phosphorylation in the lipid raft and is recycled for reuse. *Journal of Cell Science*, *123*(3), 360–368. https://doi.org/10.1242/jcs.058008

Samavarchi-Tehrani, P., Samson, R., & Gingras, A.-C. (2020). Proximity Dependent Biotinylation: Key Enzymes and Adaptation to Proteomics Approaches. *Molecular & Cellular Proteomics*, *19*(5), 757–773. https://doi.org/10.1074/mcp.R120.001941

Sammar, M., Sieber, C., & Knaus, P. (2009). Biochemical and functional characterization of the Ror2/BRIb receptor complex. *Biochemical and Biophysical Research Communications*, *381*(1), 1–6. https://doi.org/10.1016/j.bbrc.2008.12.162

Sato, A., Yamamoto, H., Sakane, H., Koyama, H., & Kikuchi, A. (2010). Wnt5a regulates distinct signalling pathways by binding to Frizzled2. *The EMBO Journal*, *29*(1), 41–54. https://doi.org/10.1038/emboj.2009.322

Schiller, H. B., Friedel, C. C., Boulegue, C., & Fässler, R. (2011). Quantitative proteomics of the integrin adhesome show a myosin II-dependent recruitment of LIM domain proteins. *EMBO Reports*, *12*(3), 259–266. https://doi.org/10.1038/embor.2011.5

Selvaraj, C., Rudhra, O., Alothaim, A. S., Alkhanani, M., & Singh, S. K. (2022). *Structure and chemistry of enzymatic active sites that play a role in the switch and conformation mechanism* (pp. 59–83). https://doi.org/10.1016/bs.apcsb.2022.02.002

Shi, J., Ma, Y., Zhu, J., Chen, Y., Sun, Y., Yao, Y., Yang, Z., & Xie, J. (2018). A Review on Electroporation-Based Intracellular Delivery. *Molecules*, *23*(11), 3044. https://doi.org/10.3390/molecules23113044

Silhankova, M., Port, F., Harterink, M., Basler, K., & Korswagen, H. C. (2010). Wnt signalling requires MTM-6 and MTM-9 myotubularin lipid-phosphatase

function in Wnt-producing cells. *The EMBO Journal*, *29*(24), 4094–4105. https://doi.org/10.1038/emboj.2010.278

Sinha, A., & Mann, M. (2020). A beginner's guide to mass spectrometry–based proteomics. *The Biochemist*, *42*(5), 64–69. https://doi.org/10.1042/BIO20200057

Sonnett, M., Yeung, E., & Wühr, M. (2018). Accurate, Sensitive, and Precise Multiplexed Proteomics Using the Complement Reporter Ion Cluster. *Analytical Chemistry*, *90*(8), 5032–5039. https://doi.org/10.1021/acs.analchem.7b04713

Stadlmeier, M., Bogena, J., Wallner, M., Wühr, M., & Carell, T. (2018). A Sulfoxide-Based Isobaric Labelling Reagent for Accurate Quantitative Mass Spectrometry. *Angewandte Chemie International Edition*, *57*(11), 2958–2962. https://doi.org/10.1002/anie.201708867

Stanganello, E., Hagemann, A. I. H., Mattes, B., Sinner, C., Meyen, D., Weber, S., Schug, A., Raz, E., & Scholpp, S. (2015). Filopodia-based Wnt transport during vertebrate tissue patterning. *Nature Communications*, *6*(1), 5846. https://doi.org/10.1038/ncomms6846

Stanganello, E., & Scholpp, S. (2016). Role of cytonemes in Wnt transport. *Journal of Cell Science*. https://doi.org/10.1242/jcs.182469

Stuermer, C. A. O., Lang, D. M., Kirsch, F., Wiechers, M., Deininger, S.-O., & Plattner, H. (2001). Glycosylphosphatidyl Inositol-anchored Proteins and fyn Kinase Assemble in Noncaveolar Plasma Membrane Microdomains Defined by Reggie-1 and -2. *Molecular Biology of the Cell*, *12*(10), 3031–3045. https://doi.org/10.1091/mbc.12.10.3031

Sun, J., Yu, S., Zhang, X., Capac, C., Aligbe, O., Daudelin, T., Bonder, E. M., & Gao, N. (2017). Wntless-Sec12 complex on ER membrane regulates early Wnt secretory vesicle assembly and mature ligand export. *Journal of Cell Science*. https://doi.org/10.1242/jcs.200634

Surviladze, Z., Waller, A., Strouse, J. J., Bologa, C., Ursu, O., Salas, V., Parkinson, J. F., Phillips, G. K., Romero, E., Wandinger-Ness, A., Sklar, L. A., Schroeder, C., Simpson, D., Nöth, J., Wang, J., Golden, J., & Aubé, J.

(2010). A Potent and Selective Inhibitor of Cdc42 GTPase. *Probe Reports from the NIH Molecular Libraries Program*.

Takada, R., Satomi, Y., Kurata, T., Ueno, N., Norioka, S., Kondoh, H., Takao, T., & Takada, S. (2006). Monounsaturated Fatty Acid Modification of Wnt Protein: Its Role in Wnt Secretion. *Developmental Cell*, *11*(6), 791–801. https://doi.org/10.1016/j.devcel.2006.10.003

Tanaka, K., Kitagawa, Y., & Kadowaki, T. (2002). Drosophila Segment Polarity Gene Product Porcupine Stimulates the Posttranslational N-Glycosylation of Wingless in the Endoplasmic Reticulum. *Journal of Biological Chemistry*, *277*(15), 12816–12823. https://doi.org/10.1074/jbc.M200187200

Ting, L., Rad, R., Gygi, S. P., & Haas, W. (2011). MS3 eliminates ratio distortion in isobaric multiplexed quantitative proteomics. *Nature Methods*, *8*(11), 937–940. https://doi.org/10.1038/nmeth.1714

Tong, L. (2013). Structure and function of biotin-dependent carboxylases. *Cellular and Molecular Life Sciences*, *70*(5), 863–891. https://doi.org/10.1007/s00018-012-1096-0

Torres, V. A., Tapia, J. C., Rodriguez, D. A., Lladser, A., Arredondo, C., Leyton, L., & Quest, A. F. G. (2007). E-Cadherin Is Required for Caveolin-1-Mediated Down-Regulation of the Inhibitor of Apoptosis Protein Survivin via Reduced β-Catenin-Tcf/Lef-Dependent Transcription. *Molecular and Cellular Biology*, *27*(21), 7703–7717. https://doi.org/10.1128/MCB.01991-06

Torres, V. A., Tapia, J. C., Rodríguez, D. A., Párraga, M., Lisboa, P., Montoya, M., Leyton, L., & Quest, A. F. G. (2006). Caveolin-1 controls cell proliferation and cell death by suppressing expression of the inhibitor of apoptosis protein survivin. *Journal of Cell Science*, *119*(9), 1812–1823. https://doi.org/10.1242/jcs.02894

Tron, C. M., McNae, I. W., Nutley, M., Clarke, D. J., Cooper, A., Walkinshaw, M. D., Baxter, R. L., & Campopiano, D. J. (2009). Structural and Functional Studies of the Biotin Protein Ligase from Aquifex aeolicus Reveal a Critical Role for a Conserved Residue in Target Specificity. *Journal of Molecular Biology*, *387*(1), 129–146. https://doi.org/10.1016/j.jmb.2008.12.086

Tsien, R. Y. (1998). THE GREEN FLUORESCENT PROTEIN. *Annual Review of Biochemistry*, *67*(1), 509–544. https://doi.org/10.1146/annurev.biochem.67.1.509

Üren, A., Reichsman, F., Anest, V., Taylor, W. G., Muraiso, K., Bottaro, D. P., Cumberledge, S., & Rubin, J. S. (2000). Secreted Frizzled-related Protein-1 Binds Directly to Wingless and Is a Biphasic Modulator of Wnt Signaling. *Journal of Biological Chemistry*, *275*(6), 4374–4382. https://doi.org/10.1074/jbc.275.6.4374

Veitch, N. C. (2004). Horseradish peroxidase: a modern view of a classic enzyme. *Phytochemistry*, *65*(3), 249–259. https://doi.org/10.1016/j.phytochem.2003.10.022

Vu, K. B., Ghahroudi, M. A., Wyns, L., & Muyldermans, S. (1997). Comparison of llama VH sequences from conventional and heavy chain antibodies. *Molecular Immunology*, *34*(16–17), 1121–1131. https://doi.org/10.1016/S0161-5890(97)00146-6

Wenger, C. D., Lee, M. V., Hebert, A. S., McAlister, G. C., Phanstiel, D. H., Westphall, M. S., & Coon, J. J. (2011). Gas-phase purification enables accurate, multiplexed proteome quantification with isobaric tagging. *Nature Methods*, *8*(11), 933–935. https://doi.org/10.1038/nmeth.1716

Willert, K., Brown, J. D., Danenberg, E., Duncan, A. W., Weissman, I. L., Reya, T., Yates, J. R., & Nusse, R. (2003). Wnt proteins are lipid-modified and can act as stem cell growth factors. *Nature*, *423*(6938), 448–452. https://doi.org/10.1038/nature01611

Willert, K., & Nusse, R. (2012). Wnt Proteins. Cold Spring Harbor Perspectives in Biology, 4(9), a007864–a007864. https://doi.org/10.1101/cshperspect.a007864

Williams, L. J., Rasmussen, S. A., Flores, A., Kirby, R. S., & Edmonds, L. D. (2005). Decline in the Prevalence of Spina Bifida and Anencephaly by Race/Ethnicity: 1995–2002. *Pediatrics*, *116*(3), 580–586. https://doi.org/10.1542/peds.2005-0592

Wodarz, A., & Nusse, R. (1998). MECHANISMS OF WNT SIGNALING IN DEVELOPMENT. *Annual Review of Cell and Developmental Biology*, *14*(1), 59–88. https://doi.org/10.1146/annurev.cellbio.14.1.59

Wolf, L., & Boutros, M. (2023). The role of Evi/Wntless in exporting Wnt proteins. *Development*, *150*(3). https://doi.org/10.1242/dev.201352

Wörn, A., & Plückthun, A. (2001). Stability engineering of antibody single-chain Fv fragments. *Journal of Molecular Biology*, *305*(5), 989–1010. https://doi.org/10.1006/jmbi.2000.4265

Xavier, C. P., Melikova, M., Chuman, Y., Üren, A., Baljinnyam, B., & Rubin, J. S. (2014). Secreted Frizzled-related protein potentiation versus inhibition of Wnt3a/β-catenin signaling. *Cellular Signalling*, *26*(1), 94–101. https://doi.org/10.1016/j.cellsig.2013.09.016

Xiong, Z., Lo, H. P., McMahon, K.-A., Martel, N., Jones, A., Hill, M. M., Parton, R. G., & Hall, T. E. (2021). In vivo proteomic mapping through GFP-directed proximity-dependent biotin labelling in zebrafish. *ELife*, *10*. https://doi.org/10.7554/eLife.64631

Yamagishi, A., Masuda, M., Ohki, T., Onishi, H., & Mochizuki, N. (2004). A Novel Actin Bundling/Filopodium-forming Domain Conserved in Insulin Receptor Tyrosine Kinase Substrate p53 and Missing in Metastasis Protein. *Journal of Biological Chemistry*, *279*(15), 14929–14936. https://doi.org/10.1074/jbc.M309408200

Yamamoto, H., Komekado, H., & Kikuchi, A. (2006). Caveolin Is Necessary for Wnt-3a-Dependent Internalization of LRP6 and Accumulation of β-Catenin. *Developmental Cell*, *11*(2), 213–223. https://doi.org/10.1016/j.devcel.2006.07.003

Yamazaki, Y., Palmer, L., Alexandre, C., Kakugawa, S., Beckett, K., Gaugue, I., Palmer, R. H., & Vincent, J.-P. (2016). Godzilla-dependent transcytosis promotes Wingless signalling in Drosophila wing imaginal discs. *Nature Cell Biology*, *18*(4), 451–457. https://doi.org/10.1038/ncb3325

Yang, C., Czech, L., Gerboth, S., Kojima, S., Scita, G., & Svitkina, T. (2007). Novel Roles of Formin mDia2 in Lamellipodia and Filopodia Formation in

Motile Cells. *PLoS Biology*, *5*(11), e317. https://doi.org/10.1371/journal.pbio.0050317

Yang, P.-T., Lorenowicz, M. J., Silhankova, M., Coudreuse, D. Y. M., Betist, M. C., & Korswagen, H. C. (2008). Wnt Signaling Requires Retromer-Dependent Recycling of MIG-14/Wntless in Wnt-Producing Cells. *Developmental Cell*, *14*(1), 140–147. https://doi.org/10.1016/j.devcel.2007.12.004

Yang, Y., & Mlodzik, M. (2015). Wnt-Frizzled/Planar Cell Polarity Signaling: Cellular Orientation by Facing the Wind (Wnt). *Annual Review of Cell and Developmental Biology*, *31*(1), 623–646. https://doi.org/10.1146/annurev-cellbio-100814-125315

Young, K. H. (1998). Yeast Two-hybrid: So Many Interactions, (in) So Little Time…. *Biology of Reproduction*, *58*(2), 302–311. https://doi.org/10.1095/biolreprod58.2.302

Yuan, W., & Song, C. (2020). The Emerging Role of Rab5 in Membrane Receptor Trafficking and Signaling Pathways. *Biochemistry Research International*, *2020*, 1–10. https://doi.org/10.1155/2020/4186308

Yu, J., Chia, J., Canning, C. A., Jones, C. M., Bard, F. A., & Virshup, D. M. (2014). WLS Retrograde Transport to the Endoplasmic Reticulum during Wnt Secretion. *Developmental Cell*, *29*(3), 277–291. https://doi.org/10.1016/j.devcel.2014.03.016

Yu, S. R., Burkhardt, M., Nowak, M., Ries, J., Petrášek, Z., Scholpp, S., Schwille, P., & Brand, M. (2009). Fgf8 morphogen gradient forms by a source-sink mechanism with freely diffusing molecules. *Nature*, *461*(7263), 533–536. https://doi.org/10.1038/nature08391

Zhai, L., Chaturvedi, D., & Cumberledge, S. (2004). Drosophila Wnt-1 Undergoes a Hydrophobic Modification and Is Targeted to Lipid Rafts, a Process That Requires Porcupine. *Journal of Biological Chemistry*, *279*(32), 33220–33227. https://doi.org/10.1074/jbc.M403407200

Zhan, T., Rindtorff, N., & Boutros, M. (2017). Wnt signaling in cancer. *Oncogene*, *36*(11), 1461–1473. https://doi.org/10.1038/onc.2016.304

Zhao, C., Avilés, C., Abel, R. A., Almli, C. R., McQuillen, P., & Pleasure, S. J. (2005). Hippocampal and visuospatial learning defects in mice with a deletion of frizzled 9, a gene in the Williams syndrome deletion interval. *Development*, *132*(12), 2917–2927. https://doi.org/10.1242/dev.01871

Zheng, J., Fang, X., Wen, K., Li, J., Ma, Y., Liu, M., An, S., Li, J., Zalevsky, Z., & Gao, P. (2022). Large-field lattice structured illumination microscopy. *Optics Express*, *30*(15), 27951. https://doi.org/10.1364/OE.461615